Synthetic Studies of Photochemical Radical Generation from *N*-(acyloxy)pyridinium Salts

by

Edward John McClain

A dissertation submitted in partial fulfillment
of the requirements for the degree of
Doctor of Philosophy
(Chemistry)
in the University of Michigan
2021

Doctoral Committee:

Professor Corey R. J. Stephenson, Chair
Professor Melanie S. Sanford
Professor Max Shtein
Professor John P. Wolfe

Edward John McClain

emcclain@umich.edu

ORCID iD: 0000-0002-1390-6026

Dedication

For my grandparents – my unwavering role models who have always inspired me to be a better person and taught me the importance of love, patience, and family.

Acknowledgements

As my time at the University of Michigan is coming to an end, I find myself indebted to so many people whose mentorship, friendship, and support have helped me to reach this stepping-stone in my scientific career, and life.

I would like to thank my advisor, Corey Stephenson, who I could not have accomplished this feat without. During my visitation to Michigan, as a recruit my first question to Corey was "can I have a beer when we meet tomorrow?"…he said no. But, in spite of this brash comment, Corey still recruited me to his lab and has provided me excellent mentorship and steadfast support ever since. Since my first day in lab, Corey has always supported my intellectual endeavors and provided me numerous career development opportunities. During my time in the lab, Corey has given me the opportunity and support to provide talks and/or poster presentations just about any conference I could imagine, and these opportunities have always helped to energize and inspire my work in the lab. As a scientific advisor, Corey has demonstrated the value of patience, taught me the importance of hard work, and inspired me with creativity. Above all, over the year of 2020 and throughout the pandemic, Corey has always demonstrated that even though science is what brings our group together, the people are most important. And with this, Corey has demonstrated incredible patience and kindness throughout the pandemic supporting and encouraging each of us to take time away from work to maintain our mental health and helping us all to persevere through difficult times. And, especially for this, I will be forever thankful.

I would like to thank my committee members, Prof. John Wolfe, Prof. Melanie Sanford, and Prof. Max Shtein, for their support throughout my graduate studies. Without their insight and

generous feedback, I would not be where I am today. I would especially like to thank Melanie and her former graduate student James Bour for mentoring me through a rotation during my first year. This proved to be an invaluable experience. I would also like to thank Prof. Nathaniel Szymczak for his help and guidance throughout my graduate experience. In collaboration with Nate, I have had the opportunity to write a few grants, and each time Nate was omni present, helping to guide me along the way. In addition, Nate and his group have been very generous allowing me to use their UV/vis constantly throughout my studies.

I would like to thank the past and present members of the Stephenson group with whom I've worked. Dr. Markus Käräks, Dr. Irene Bosque, Dr. Xu Shu, and Dr. Dirk Alpers for their support and mentorship early in my graduate career. Thank you to Dr. Alexandra Sun who has been a fantastic co-worker, collaborator, and mentor throughout my time in the Stephenson group. The fragment coupling project was a pain, but with your enthusiasm and support we were able to scrape something together. Thank you to Dr. Tim Monos whose support and mentorship writing several grants and working on the EDA complex catalysis project has had a tremendous impact on my success. During my time in the Stephenson group, I have been extremely fortunate to work with a tight-knit group of students who were able to stick together for 3-4 years. To Dr. Kevin Romero, Dr. Gabe Magallanes, Dr. Taylor Sodano, Dr. Alexandra Sun, Dr. Rory C. McAtee, Dr. Daryl Staveness, Mr. Matthew Galliher, Mr. James Lester Collins III, Dr. Logan Combee, and Dr. Maddie Sowden; Thank you. Summer nights at Bills, conferences, winter Star Wars films, and coffee breaks are the lasting memories and experiences that have helped me persevere through graduate school. Worked sucked sometimes… but it always sucked a little less having you all as friends and lab mates to pass the days. To the current members of the Stephenson group: Anthony Allen, Cheng Yang, Efrey Noten, James Lester Collins III, Matthew Galliher, Bec Roldan, Alex

Harmata, Alan Wortman, Dr. Mike Supej, Dr. Jeong-Yu Son, Dr. Sahil Arora, Annika Tharp, Mami Horikawa, and Kason Glover; thank you for the continued support and enthusiasm. The pandemic has been a trying time on all, but the great group of students we have, have been able to push through with no loss of enthusiasm or effort. And to my mentees: Alyah Faith Chmiel, Xiaotong Wu, Alan Wortman, and Michaela Barry; Thank you for your hard work and high spirits.

Prior to the University of Michigan, I completed my undergraduate studies at West Virginia University. Thank you to Ms. Marylin Bowers whose support and encouragement throughout my time at WVU has helped me to succeed. Marylin was my guardian while away from home and her constant support and friendship helped me through difficult times. Her constant reminders to let loose helped me to not let college pass me by without a few nights to remember, or never remember? So Thank you Marylin, your friendship and guidance has meant the world to me. Thank you to Prof. Xiaodong "Michael" Shi, for taking a chance on me and providing me the opportunity to pursue undergraduate research in your lab. Mike Shi was the most encouraging and supportive mentor I have had the opportunity to work for, he knew I could attend a top graduate program, even when I did not believe in myself. Without his support and encouragement, I surely would not be in chemistry. Thank you to Prof. Brian Popp, who provided me a second opportunity for undergraduate studies at WVU. Brian was a phenomenal mentor who supported and encouraged me throughout my search for a graduate program and my final year at WVU. Finally, thank you to Trev, Zachey, Michael Block, and Michael Spencer for their support and friendship during our studies at WVU. Late nights in the CLC wouldn't have been the same without you all.

To my friends… Wes, Justin, Emily, Sam, Taylor, Lasky, Marc, Jessi, Nate, Matt, Figs, Brian, AC, Big Dave, Povse, Logan, Jesse, Colin, Twiz, Joe, Squiz, John, Dross, Phil, and anyone I have likely forgotten to list; Thank you.

To my family. My siblings Annie, Will, Callie, and CR; and my parents MaryAnne and Conan. Thank you for your unconditional love and support throughout graduate school. I've missed many family functions throughout my time at Michigan, but your love and support has been a constant, and no matter what happens I always know I have a loving and caring family there to support me.

And last… but certainly not least… Thank you to my loving, supportive, and all together amazing girlfriend Alyah Faith Chmiel. When I met you 3 years ago, I never could have imagined the life we have built together. Thank you for your unwavering support, love, and encouragement throughout graduate school. I truly could not have done this without you, and I look forward to repaying the favor during your time at UW-Madison. I love you and I cannot wait for our future together!

Table of Contents

List of Figures

List of Abbreviations

[O]	oxidant
°C	degree Celsius
Ac	acetyl
ACNO	methyl acridine-9-carboxylate *N*-oxide
AIBN	azobisisobutyronitrile
aq	aqueous
Ar	aryl
BEt_3	triethylborane
Bn	benzyl
Boc	tert-butoxycarbonyl
bpy	2,2‘-bipyridine
bpz	2,2‘-bipyrazine
Bu_3SnH	tributyltin hydride
CF_3	trifluoromethyl
CFL	compact fluorescent lightbulb
cm	centimeter
Cu	copper
CV	cyclic voltammetry
Cy	cyclohexyl
d	doublet

DCM	dichloromethane
dF(CF_3)ppy	2-(2,4-difluorophenyl)-5-(trifluoromethyl)pyridine
DFT	density functional theory
DMF	dimethylformamide
DMSO	dimethylsulfoxide
d.r.	diastereomeric ratio
dtbbpy	4,4'-di-tert-butyl-2,2'-bipyridine
EDA	electron donor-acceptor
EDG	electron donating group
EINO	ethyl isonicotinate *N*-oxide
equiv	equivalents
E_{red}	reduction potential
E_{ox}	oxidation potential
ESI	electrospray ionization
E^0	standart potential
Et	ethyl
$E_{1/2}$	half-wave potential
EWG	electron withdrawing group
Fac	facial
Fc	ferrocene
g	grams
h	hours
hν	light

Het	heteroarene
HOMO	highest occupied molecular orbital
HRMS	high resolution mass spectroscopy
HTE	high throughput experimentation
Hz	hertz
IR	infrared
Ir	iridium
ISC	intersystem crossing
J	coupling constant
L	liters
LED	light emitting diode
Li	lithium
LUMO	lowest occupied molecular orbital
M	molar concentration
m	multiplet
Me	methyl
MeCN	acetonitrile
Mes	mesityl
mg	milligrams
MHz	megahertz
min	minutes
mL	milliliters
MLCT	metal-to-ligand charge-transfer

mm	millimeters
mmol	millimoles
mol	moles
mol%	mole percent
MW	molecular weight
NHPI	N-hydroxy phthalimide
nm	nanometers
NMR	nuclear magnetic resonance
ns	nanosecond
O_2	oxygen
PC	photocatalyst
PCET	proton coupled electron transfer
Pd	palladium
PF_6	hexafluorophosphate anion
PFA	perfluoroalkoxy
Ph	phenyl
phen	1,10-phenanthroline
PNO	pyridine *N*-oxide
ppm	parts per million
ppy	2-phenylpyridine
PQCNO	methyl 2-phenylquinoline-4-carboxylate *N*-oxide
PQCN	methyl 2-phenylquinoline-4-carboxylate
ps	picoseconds

py or pyr	pyridine
q	quartet
rt	room temperature
Ru	ruthenium
s	singlet or second
SET	single electron transfer
SCE	saturated calomel electrode
t	triplet
TFA	trifluoroacetic acid
TFAA	trifluoroacetic anhydride
THF	tetrahydrofuran
TPPNO	triphenylpyridine *N*-oxide
TRIP	3,3′-Bis(2,4,6-triisopropylphenyl)-1,1′-binaphthyl-2,2′-diylhydrogenphosphate
UV	ultraviolet
V	volts
vis	visible
W	watt
δ	chemical shift in parts per million
λ_{max}	maximum wavelength
μL	microliters

Abstract

Energy supplied in the form of photons can interact with organic chromophores, enabling challenging bond formation and fragmentation reactions that could not otherwise be accessed. With an array of unique reactivity, photochemistry has the potential to revolutionize approaches to the synthesis of pharmaceutical and natural products targets alike. Over the past decade, coinciding with the emergence of photoredox catalysis, there has been a renewed interest in the study and development of photochemical methods for selective radical generation promoted by visible light. Importantly, these developments provide access to high energy radical intermediates under benign conditions, circumventing the need for hazardous, toxic reagents such as AIBN, tributyltin hydride, or UV light. Herein we describe the study of *N*-(acyloxy)pyridinium reagents as novel radical precursors, the development of new reactivity modes to leverage visible light for photochemical radical generation, and their application to aromatic C–H alkylation and perfluoroalkylation reactions.

Chapter 1 provides an overview of photochemical methods for radical generation. Starting with a brief synopsis of photochemistry and its application to organic synthesis, the proceeding sections cover recent developments in photoredox catalysis, EDA complex photochemistry, and photocleavable auxiliaries for photochemical radical generation, with specific attention directed to highlighting their applications for arene alkylation reactions.

Chapter 2 describes the development of a formal fragment coupling approach to the Minisci alkylation reaction. The developed reaction leverages a low cost, easily handled reagent mixture of heteroaromatic *N*-oxide with acyl chlorides for the *in-situ* generation of redox active esters.

Photochemical radical generation is enabled by a photoinduced electron transfer from employed polypyridyl iridium photosensitizer, leading to fragmentation of the redox active ester and subsequent decarboxylative radical generation. Reaction optimization, exploration of the scope of reactivity, adaptation of the reaction to flow processing, and demonstration of late-stage functionalization efforts are discussed.

Chapter 3 describes the development of a novel EDA complex, and its application as a catalyst for the radical trifluoromethylation of electron rich arenes. A historical overview of EDA complex photochemistry and its applications to organic synthesis is provided. Detailed studies of the designed EDA complex, reaction optimization, flow processing, and exploration of the scope of reactivity are each discussed.

Chapter 4 describes the discovery and development of methyl 2-phenylquinoline-4-carboxylate *N*-oxide (PQCNO) as an auxiliary for efficient photoinduced radical generation. Design, optimization, and study of the auxiliary, as well as application towards a photoinduced Minisci alkylation reaction are described.

Chapter 1 **Introduction**

*Portions of this chapter have been published in A. C. Sun, R. C. McAtee, E. J. McClain, C. R. J. Stephenson, Advancements in Visible Light-Enabled Radical C(sp^2)–H Alkylation of (Hetero)arenes. *Synthesis* **2019,** *51*, 1063–1072.; R. C. McAtee, E. J. McClain, C. R. J. Stephenson, Illuminating Photoredox Catalysis. *Trends Chem.* **2019,** *1,* 111-125.

1.1 A Brief Introduction to Photochemistry in Organic Synthesis

In 1912, following his seminal studies of organic photochemistry, Ciamician proclaimed that the use of the earth's most abundant and renewable source of energy (photons) was the way forward for a sustainable future.[1,2] And in the century to follow, the tremendous power of photochemistry was demonstrated through the development of novel modes of radical generation such as Norrish reactions[3] and complex structural rearrangements such as the meta-photocycloaddition reactions,[4] and further highlighted by their strategic applications to the synthesis of natural products such as grandisol, ginkgolide B, or (±)-modhephene.[5-7] Despite the ability of photoexcited states to undergo novel rearrangements and fragmentation reactions, for decades, the application of photochemical reactions to complex molecule synthesis has been under-utilized due to the belief that photochemical methods are inherently unselective and, thus, would lead to undesired, deleterious reactivity.[8] This misconception has likely arisen from early applications of high energy UV light to drive chemical transformations, which, in turn, led to deleterious reactivity that arose from uncontrolled excitations of common functional groups.

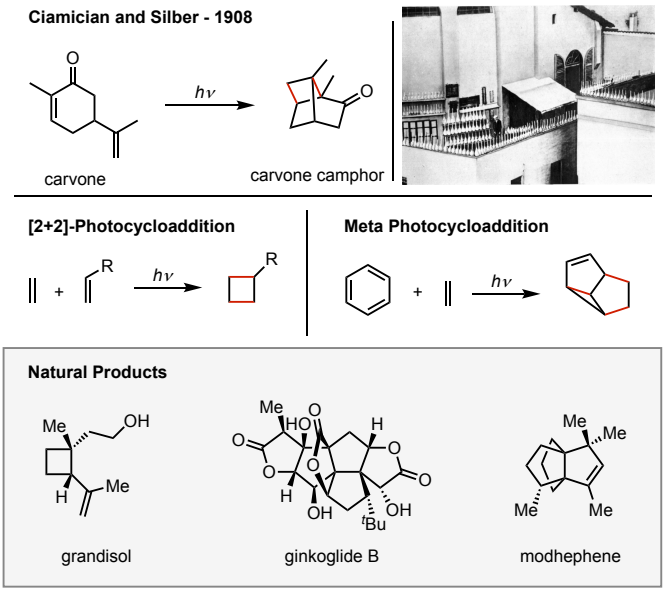

Figure 1. Photochemistry in Organic Synthesis

Contemporary applications of photochemistry in organic synthesis have overcome the selectivity issues of traditional UV photochemistry by employing designed molecular entities that harvest visible light to access reactive excited states. In this case, selectivity is imparted on the system by a red-shift of the light required for photoexcitation, delivering a reactivity paradigm where only the designed chromophore is effected by photon bombardment. The ensuing sections will outline principles of photoredox catalysis, electron donor-acceptor complexes, and photocleavable auxiliaries, and highlight their applications toward photochemical radical generation for arene alkylation and new developments for the Minisci alkylation reaction.

1.2 Photoredox Catalysis – Background and Applications

Over the past decade, photoredox catalysis has emerged as a state-of-the-art method for the generation of radical intermediates, facilitating their application organic synthesis by circumventing the use of hazardous, toxic reagents such as AIBN and tributyltin hydride.[9] The success and fast adaptation of photoredox catalysis is due to the selectivity provided by the

designed visible light absorbing photosensitizers that are used to convert energy supplied by photons to chemical potential energy. To achieve this energy conversion, upon absorption of a photon, transition metal based polypyridyl photosensitizers undergo efficient metal-to-ligand charge-transfer (MLCT) excitation, followed by intersystem crossing (ISC) to deliver a long-lived triplet excited state of the metal catalyst (τ = 557 ns for $[Ir(ppy)_2(dtbbpy)]PF_6$).[10] From the triplet excited state, the photosensitizers can engage with organic substrates through single electron-transfer (SET) events thereby undergoing either oxidative (or reductive) quenching of the excited state, returning the catalyst to the ground state.

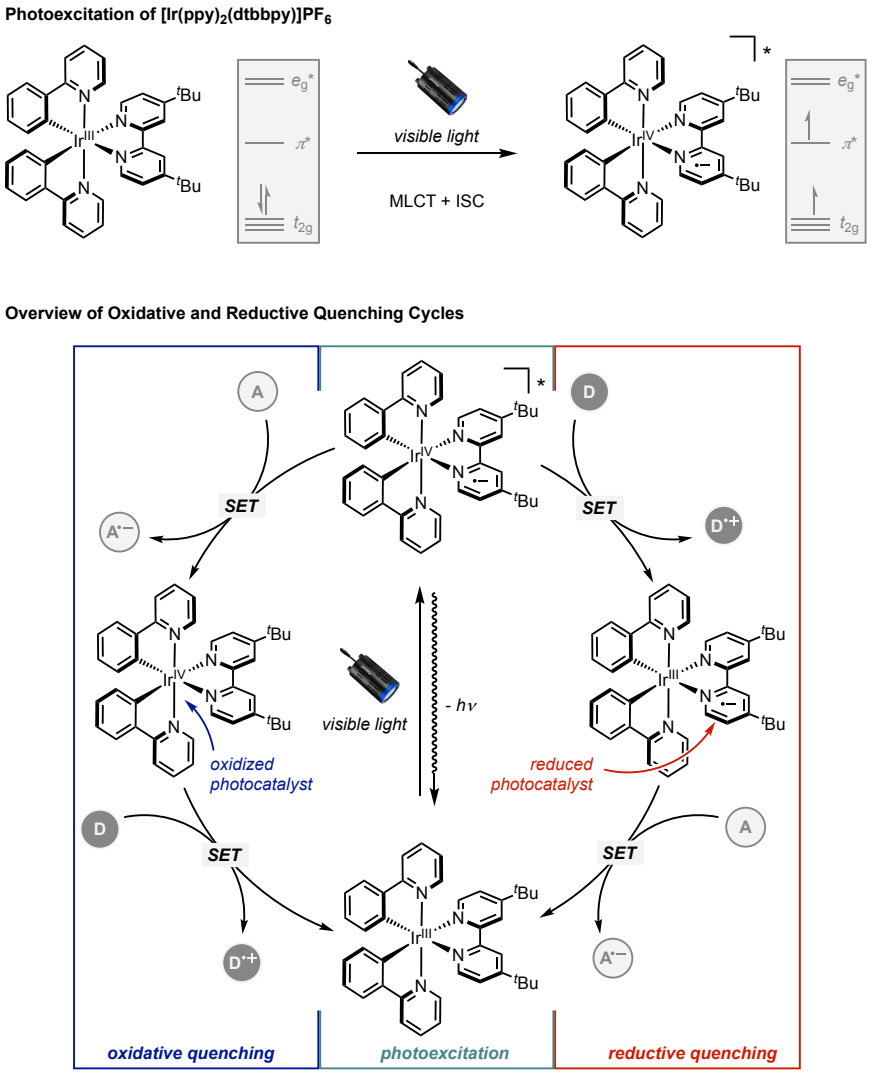

Figure 2. Overview of Excitation and Quenching for Polypyridyl Photosensitizers

The simplest and most efficient access to reactive radical intermediates is through the direct single electron oxidation/reduction of common chemical feed stocks, such as amines, carboxylic acids or alkyl halides. In 2011, MacMillan and coworkers reported a method for the preparation of benzylic amines from tertiary amines and electron deficient aryl nitrile derivatives in the presence of iridium photosensitizer $Ir(ppy)_3$.[11] The reaction is proposed to proceed through oxidation of the amine, followed by deprotonation of the α-position to generate the reactive α-amino radical intermediate. Subsequent trapping of the α-amino radical by the aryl nitrile, followed by extrusion of cyanide would deliver the desired benzylic amines. The reaction was demonstrated to tolerate a diverse array of both cyclic and acyclic amines, as well as electron deficient aryl nitriles. Following this report, in 2014, MacMillan and coworkers demonstrated the alkylation strategy was also amenable to the use of carboxylic acids as the radical precursor.[12] The decarboxylative alkylation was demonstrated to be effective using protected amino acid derivatives, and this decarboxylative radical generation could be extended to α-etheral acids.

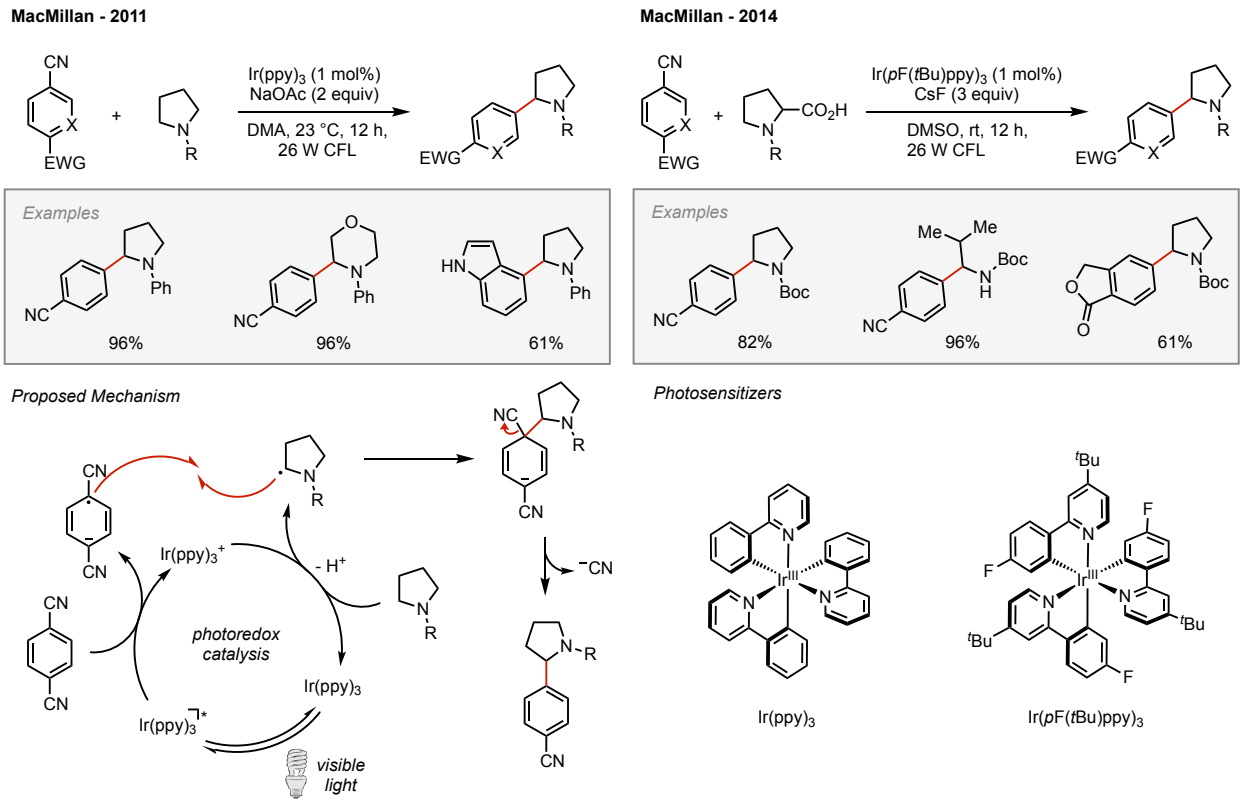

Figure 3. Alkylation of electron deficient aryl nitriles.

Alkyl and aryl boron reagents have recently been identified as diverse chemical feed stocks to serve as potential radical precursors. In this reaction paradigm, oxidative cleavage of the C–B bond releases a BX_3 (most commonly BF_3 or $B(OH)_3$) equivalent and generates a carbon centered radical. In 2016, Chen, Liu, and co-workers disclosed the C–H alkylation of N-heteroarenes with primary and secondary alkylboronic acids using the photocatalyst $Ru(bpy)_3Cl_2$ and acetoxybenziodoxole (BI-OAc) as a sacrificial oxidant.[13] The newly developed C–H alkylation reaction was demonstrated to tolerate a diverse set of substituted primary and secondary alkyl boronic acids. Pyridines, pyrimidines, and a purine riboside substrate were all efficiently functionalized. It should be noted that more electron-rich heteroarenes, including benzothiazole and benzimidazole, could also be successfully alkylated.

Potassium trifluoroborate salts serve as an attractive alternative to alkyl boronic acids, as alkyl trifluoroborates possess a filled p-orbital that delivers a more stable reagent, circumventing the decomposition pathways that often plague alkyl boronic acids and esters. In 2017, Molander and coworkers reported an arene C–H alkylation employing photoredox catalysis in conjunction with alkyl trifluoroborates as radical precursors in the presence of trifluoroactic acid and sacrificial oxidant potassium persulfate.[14] Under the optimized conditions, Molander and coworkers were able to demonstrate a broad scope of reactivity as pyridines, quinolines, indazoles, and quinazolines were all tolerated. Additionally, a diverse array of primary, secondary, and tertiary trifluoroborates were demonstrated to give good to excellent yields. Finally, to demonstrate the utility of the methods towards late-stage functionalization of potential drug leads, the authors were able to successfully alkylate comptothecin, an anti-cancer candidate, at the C-7 position.

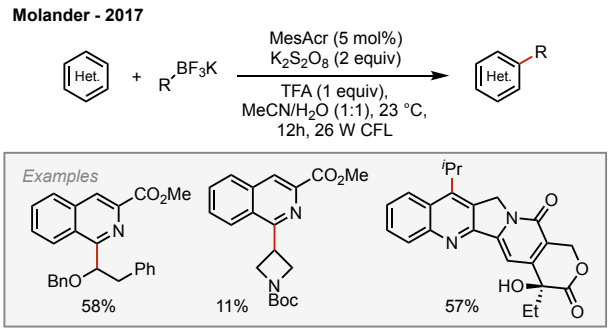

Figure 4. Minisci alkylation using potassium trifluoroborates.

Alkyl halides have also been demonstrated to serve alkyl radical precursors, albeit, under an opposite and complementary reactivity paradigm, as alkyl halides require a reduction event to generate the desired radical intermediates. In 2010, the Stephenson group demonstrated that efficient intra- and intermolecular alkylation of electron rich heteroarenes could be achieved when subjecting activated alkyl bromides to $Ru(bpy)_3Cl_2$ under irradiation with blue LEDs.[15,16] Indoles, azaindoles, and pyrroles were all amenable to reaction conditions. More recently, in 2018 Vertex

pharmaceuticals demonstrated the reductive dehalogenation of unactivated alkyl iodides, trapping the ensuing radical intermediates with (hetero)arenes delivered C–H alkylated products.[17]

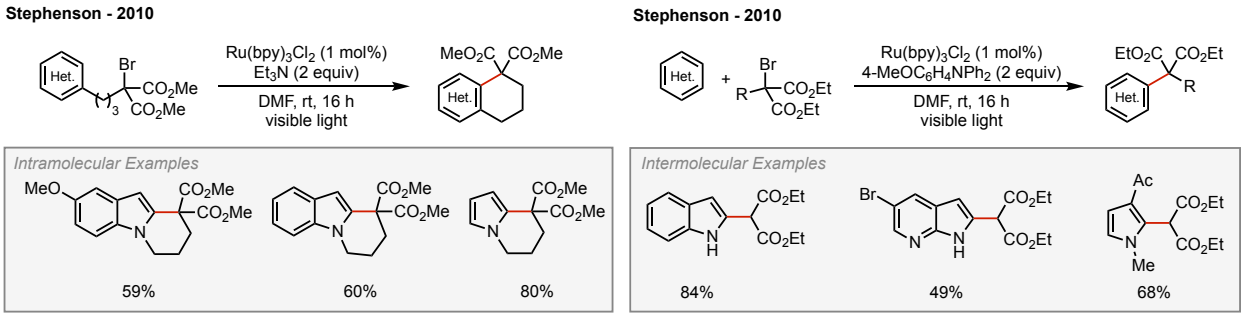

Figure 5. C–H alkylation via reductive dehalogenation

As an alternative to oxidative decarboxylation of carboxylic acids, the conversion of carboxylic acid derivatives to their corresponding redox active esters can provide access to a complementary reactivity paradigm enabling reductive decarboxylation for radical generation. In the context of photoredox catalysis, utilizing the reductive decomposition of redox active esters can allow for a redox neutral approach to aromatic C–H alkylation reactions. In addition, the conversion of carboxylic acids to their corresponding redox active esters can facilitate decarboxylation events that are otherwise inaccessible through direct oxidative decarboxylation of the free acid.

N-hydroxy phthalimide esters have emerged as a broadly useful class of redox active auxiliaries for reductive radical generation. First reported by Oda and Okada in 1991, single electron reduction of the *N*-hydroxy phthalimide ester by excited state $Ru(bpy)_3Cl_2$ induces a N–O bond fragmentation, ultimately releasing phthalimide, carbon dioxide, and an equivalent of a carbon centered radical.[18] Over the course of the past 5 years, photoredox catalysis has seen a resurgence in the application of *N*-hydroxy phthalimide esters, specifically, the redox active esters have been widely applied to radical C–H alkylation protocols.[19] In 2018 when Sherwood and coworkers disclosed a protocol that enabled the *in situ* generation of N-hydroxy phthalimide esters and their application to the Minisci alkylation, obviating the need for separate preparation and

isolation of the desired redox active esters.[20] Of particular note, in 2018 Phipps and coworkers reported an enantioselective C–H alkylation of heteroarenes that utilized the combination of a chiral Brønsted acid catalyst with photoredox catalysis.[21] Under the developed conditions, the use of a chiral phosphoric acid directed the addition of α-amino radicals to the 2-position of the heteroarene and delivered the corresponding entaino-enriched α-heterocyclic amines in good yields.

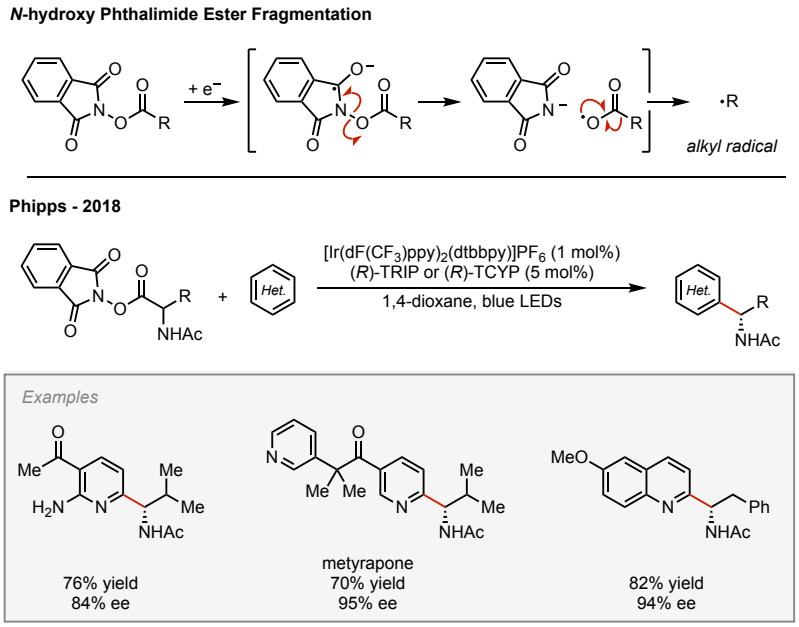

Figure 6. N-hydroxy phthalimide ester for C–H alkylation

Pioneering work from Sir Derek H. R. Barton's research group in the second half of the 20th century established *N*-(acyloxy) 2-thiopyridone as highly active radical precursors.[22] *N*-(acyloxy) 2-thiopyridones, commonly referred to as Barton esters, have been demonstrated to efficiently generate radical intermediates by either thermal initiation in the presence of AIBN, or upon irradiation with high power tungsten lamps. Barton esters are decarboxylative reductions, halogenations and rearrangements to the corresponding pyridyl thioethers. However, Barton esters are typically limited in the accessible scope of intermolecular functionalization's, as the desired

intermolecular trapping event must out compete rearrangement to the corresponding 2-pyridyl thioether ($k_{rxn}>>k_{rearrangement}$).[23]

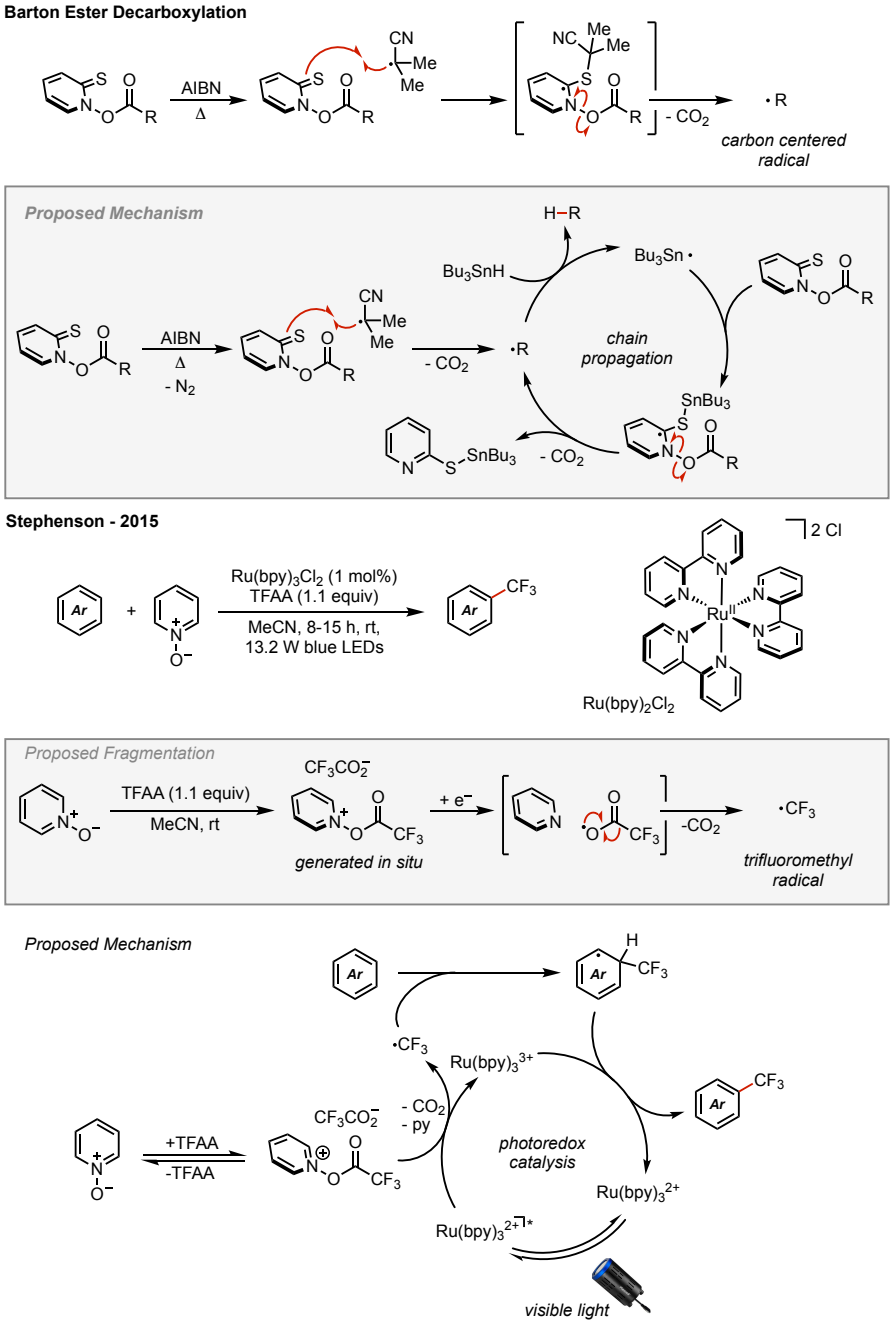

Figure 7. Pyridine N-oxide derived redox auxiliaries

In 2015, the Stephenson group reported the use of pyridine *N*-oxide as a low cost, easily handled redox auxiliary.[24] In the seminal report, Stephenson and coworkers demonstrated that *in*

situ acylation of pyridine *N*-oxide with trifluoroacetic anhydride generated an electron deficient *N*-(acyloxy)pyridinium species that, upon single electron reduction, decomposed to liberate pyridine, carbon dioxide and an equivalent of a trifluoromethyl radical. Trapping of the electron deficient trifluoromethyl radical with electron rich arenes provided access to a diverse array of C–H trifluoromethylated products. Notably, the unique decarboxylation of *N*-(trifluoroacetoxy)pyridiniums cannot be understated, as it circumvents issues that arise from direct oxidation of trifluoroacetic acid or the use of the corresponding *N*-(trifluoroacetoxy)phthalimide esters.[25] The direct oxidative decarboxylation of trifluoroacetic acid is inaccessible due the difficulty associated with its oxidation and the corresponding *N*-hydroxy phthalimide esters do not fragment to give the trifluoromethyl radical, but rather fragment to give the trifluoroacetate and the corresponding N-centered phthalimide radical.

1.3 Electron Donor-Acceptor Complexes in Synthetic Chemistry

Electron donor-acceptor (EDA) complexes are ground state associations of two or more molecules that give rise to a new electronic transition, referred to as a charge transfer band.[26] Since their discovery, EDA complexes have been extensively studied for their unique photochemical activity. Fundamental photophysical characterization of EDA complexes demonstrated that irradiation of the complex induces an electron transfer from the donor to the acceptor, giving rise to a radical ion pair.[27] However, early attempts to leverage the radical ion pair for synthetic chemistry were thwarted, as rapid back electron transfer led to deactivation potentially reactive intermediate. In the 1970s, pioneering studies by Kochi, among others, demonstrated that EDA complexes could be leveraged for photochemical radical generation if a readily fragmentable bond was incorporated into either donor or acceptor molecule.[28,29] In this reaction paradigm, the designed bond fragmentation occurs at a rate that is kinetically competitive with BET, thus

photoinduced electron transfer within the EDA complex invokes a bond fragmentation, liberating reactive radical intermediates that can be engaged for synthetically useful transformations.

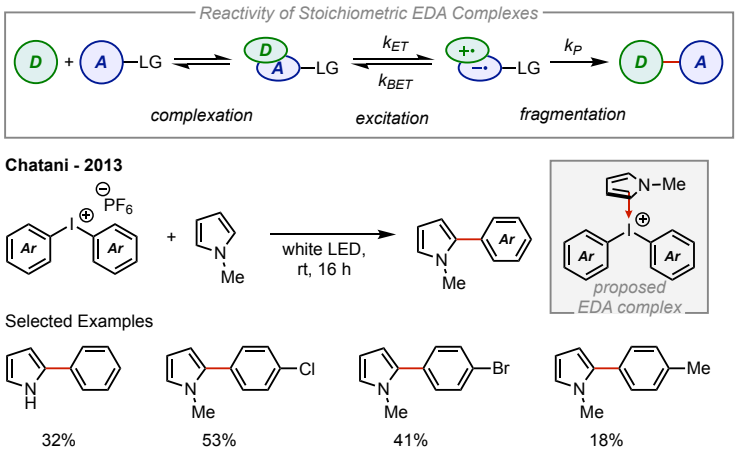

Figure 8. A) EDA complex reaction paradigm. B) Chatani EDA complex promoted C–H arylation

Over the past decade, there has been a renewed interest in EDA complex photochemistry as a mild and efficient means of photochemical radical generation. In general, synthetic applications of EDA complexes have focused on stoichiometric reactivity in which highly polarized substrates are employed and portions of both donor and acceptor are incorporated into the final product. The first modern examples of this reactivity were demonstrated by independent reports from the Chatani and Melchiorre groups in 2013.[30,31] Chatani and coworkers detailed the photochemical C–H arylation of pyrroles with di(aryl)iodonium reagents. Close examination of the reaction system demonstrated that exclusion of the iridium photocatalyst was observed to provide moderate yields of the desired C–H arylated products upon irradiation with white LEDs. From this observation, Chiatani and coworkers were able to identify the formation of a charge transfer complex between the electron rich pyrrole substrates and electron deficient di(aryl)iodonium acting as an acceptor. Following this report, a number of groups have demonstrated unique approaches to access arene C–H alkylation products via EDA complex photochemical radical generation. In 2015, the Melchiorre group demonstrated that indole substrates formed a charge transfer complex with

electron deficient alkyl bromides, and the complexation event was characterized by x-ray crystallography to be derived from a π-stacking event.[32] Irradiation of charge transfer complex with a 23 W CFL lamp provided access to the C–H alkylated indole products. Further investigation demonstrated that inclusion of a tethered nucleophile into the 3-positon of the indole framework allowed expedient access to pyrrolo- and furano-indolines. In 2019, Glorius and coworkers were able to further extend the indole-based approach to deaminative radical generation by using Katritzky salts.[33] This work allowed of extension of the scope of accessible alkyl substrates to encompass an array of fragments derived from amino acid precursors. Building on fundamentals developed by Kochi, Hong and coworkers have employed highly polarized pyridinium reagents as acceptors for EDA complex promoted radical generation.[34] Of particular note, Hong and coworkers demonstrated that sodium acetate is observed to form charge transfer complexes with *N*-amino pyridinium reagents.[35] Irradiation of the charge transfer complexes allowed for the radical 1,3-amino pyridylation of [1.1.1]-propellanes, incorporating both pieces of the bifunctional reagents into the final product.

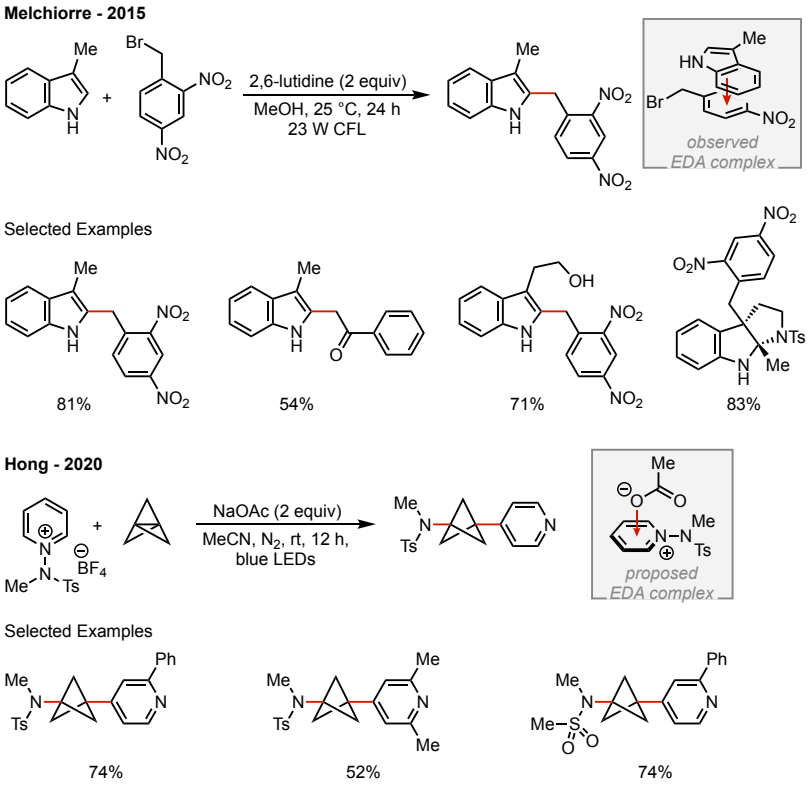

Figure 9. Recent examples of C–H alkylation enabled by EDA complex photochemistry

Radical perfluoroalkylation of arenes has become a focal point for synthetic applications of EDA photochemistry.[36] Perfluoroalkyl iodides are readily available reagents that possess highly polarized C–I bonds that in the presence of strong n-donor molecules, n→σ* complexation events have been documented, leading to EDA complexes capable of generating perfluoroalkyl radicals upon irradiation. In 2014, Melchiorre and coworkers were able to demonstrate that the enolates of α-cyanoarylacetates participated in the formation of an EDA complex with trifluoromethyl iodide, which was proposed to arise through an $n_C \rightarrow \sigma^*_{C\text{-}I}$ interaction.[37] Irradiation of the charge transfer complexes with 23 W CFL lamp provided access to the arene C–H trifluoromethylation products. In 2016, the Stephenson group demonstrated that *N*-(trifluoroacetoxy)pyridinium reagents formed charge transfer complexes with electron rich arenes through a proposed co-facial π-stacking event.[38] Irradiation of the complexes provided efficient access to arene C–H trifluoromethylation

products. However, due to the designed stoichiometric reaction, the scope of accessible trifluoromethylation reactions was limited by the identity of the donor substrate.

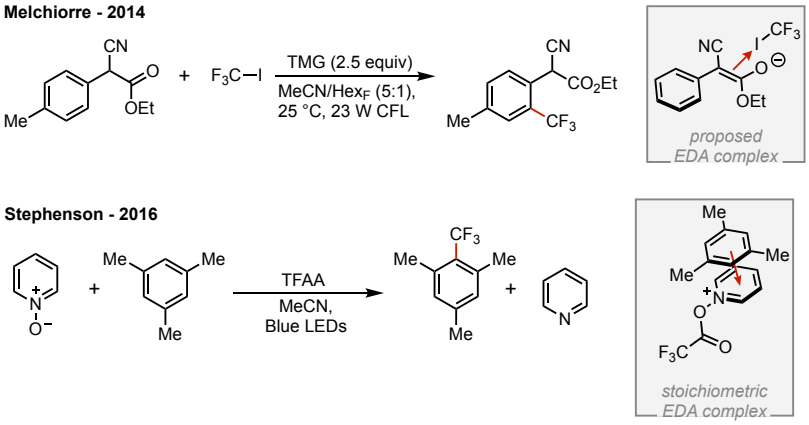

Figure 10. EDA complex promoted arene trifluoromethylation

1.4 Photocleavable Auxiliaries

Historically, the photochemical generation of radicals has been carried out through photolysis of ketones, *N*-(acyloxy)pyridones, or xanthates with high energy UV light.[39-41] Although these methods have found applications in synthetic chemistry, the widespread adoption of photochemical radical generation has been limited due to the propensity for uncontrolled, deleterious side reactions to arise under irradiation with UV light.[8] The design and implementation of visible light absorbing photocleavable auxiliaries represent an attractive alternative to highly used redox active esters. In principle, photocleavable auxiliaries should also be able to overcome limitations imposed by redox sensitive functionalities, as the photoinduced decomposition does not require an electron transfer event for radical generation.

An early example of a designed photocleavable auxiliary being applied for efficient photochemical radical generation was reported by Hasebe and Tsuchiya in 1984.[42] Their report detailed the use of benzophenone oxime esters for efficient photoinduced radical generation upon irradiation with a high-pressure mercury lamp equipped with a Pyrex filter. Under the developed

conditons, radical generation was proposed to arise via homolytic N–O bond cleavage in the excited triplet state, leading to efficient decarboxylation of the ester moiety. Hasebe and Tsuchiya were able to demonstrate a unique breadth of reactivity from the designed benzophenone oxime esters, as Minisci alkylation/arylation, as well as radical reduction reactions could all be accessed.[42-44] Recently, Glorius and coworkers have re-visited benzophenone oxime esters, demonstrating that radical generation can be accessed using blue light as the energy source in the presence of a suitable triplet sensitizer.[45]

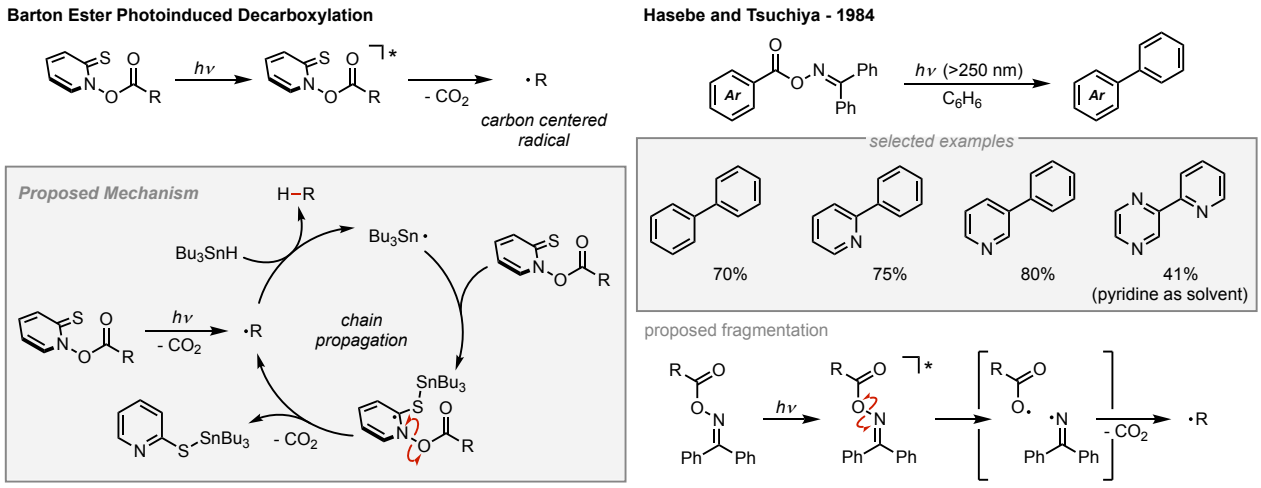

Figure 11. Early examples of designed photocleavable auxiliaries. Photoinduced fragmentation of Barton esters (left), Hasebe and Tsuchiya diphenyl oxime esters (left).

Barton esters were originally developed as potent radical chain carrying reagents. However, investigation of their photochemical reactivity revealed that the *N*-(acyloxy) 2-thiopyridones undergo an efficient photoinduced N–O bond fragmentation when irradiated with a 400W tungsten lamp, leading to the decarboxylative generation of radicals.[22] From the photoinduced decomposition, Barton and coworkers have demonstrated a myriad of reactivity that could be accessed, including radical reduction and Hundiecker halogenation reactions.[46,47] Although the photochemical decomposition provides an attractive alternative to thermal initiation with AIBN, kinetic limitations of Barton esters still remain, as the desired intermolecular

functionalization reactions need to out compete the trapping of the radical with the thiopyridone functionality. In spite of the kinetic limitations, Barton and coworkers were able to develop an efficient protocol for the Minisci alkylation, overcoming the kinetic restraints of the *N*-(acyloxy) 2-thiopyridones by using a large excess of the desired heterocyclic trap.[48]

A resurgence in studies focused on photochemical radical generation have led to new developments in the design and preparation of photocleavable auxiliaries. In 2017, Melchiorre and coworkers reported the excited state dissociation of 4-alkyl-1,4-dihydropyridines for efficient photoinduced radical generation.[49] Investigation of the proposed photoinduced fragmentation revealed toluene and bibenzyl could be isolated upon irradiation in the absence of a competent trap, demonstrating the dissociation was not reliant upon a SET event for radical generation. Further studies found that the 4-alkyl-1,4-dihydropyridines are potent excited state reductants. With an understanding of their excited state characteristics, Melchiorre and coworkers were able to leverage both the photoinduced decomposition and excited state reductant properties of 4-alkyl-1,4-dihydropyridines to access an array of nickel catalyzed reductive cross-coupling reactions, providing access to ketones and alkylated arene derivatives.

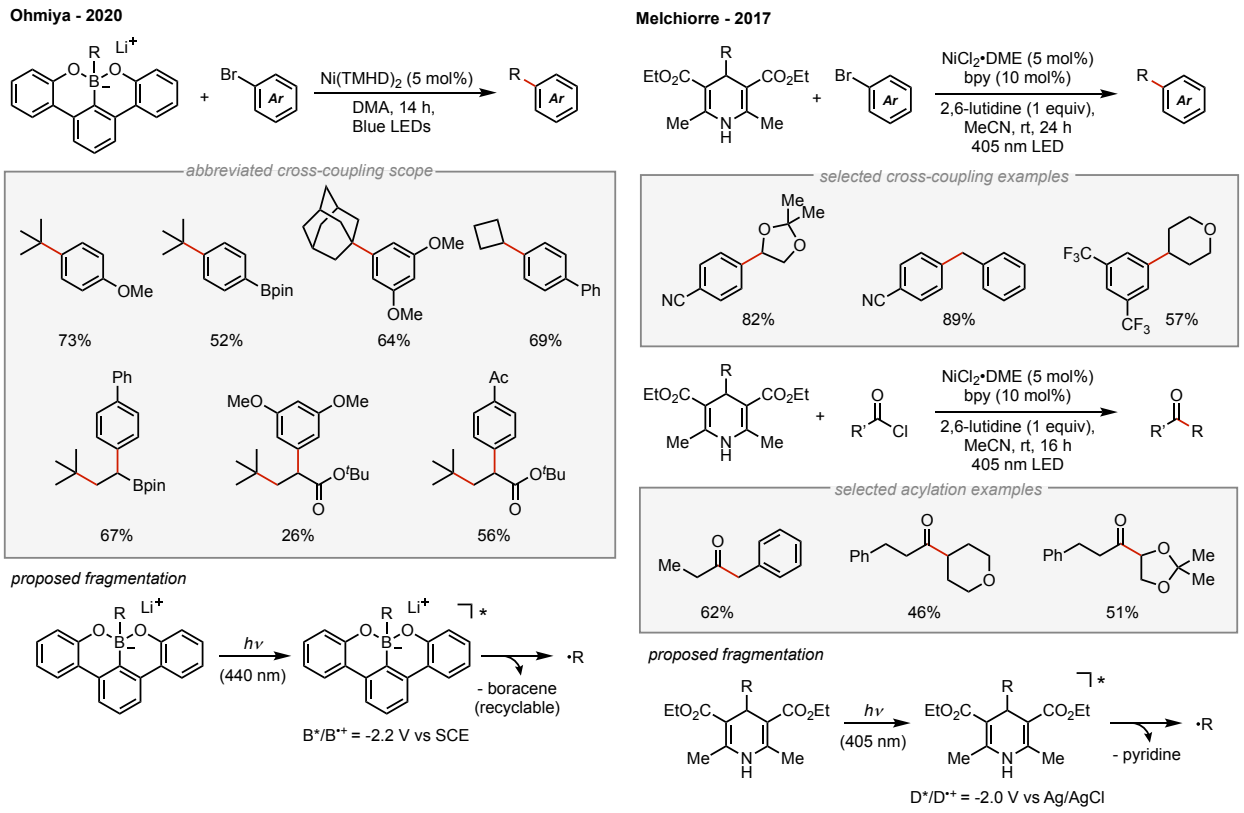

Figure 12. Modern developments of photocleavable auxiliaries. Ohmiya's boracene based alkyl borate (left) and Melchiorre's 4-alkyl-1,4-dihydropyridine (right).

In 2020, Ohmiya and colleagues reported boracene based alkyl borates as a new class of photocleavable auxiliaries for efficient photoinduced radical generation.[50] The borate salts were demonstrated to be bench stable reagents that could be efficiently prepared from boracene and alkyl lithium reagents. Characterization of the excited state properties showed that the boracene based alkyl borates are strong excited state reductants that undergo dissociation upon irradiation >370 nm light. Ohmiya and coworkers were able to use both excited state properties to access a variety of reductive nickel catalyzed cross-coupling reactions, demonstrating the ability to engage primary, secondary, and tertiary radicals for coupling to aryl halides and 3 component couplings to acrylate derivatives.

1.5 References

1. Ciamician, G. and Silber, P., Chemische Lichtwirkungen. *Ber. Dtsch. Chem. Ges.* **1908,** *41*, 1928−1935.
2. Giacomo Ciamician, The Photochemistry of the Future. *Science* **1912,** *36,* 385-394.
3. Oelgemöller, M.; Hoffman, N. Studies in Organic and Physical Photochemistry–An Interdisciplinary Approach. *Org. Biomol. Chem.* **2016,** *14,* 7392-7442.
4. Remy, R. and Bochet, C. G., Arene–Alkene Cycloaddition. *Chem. Rev.* **2016,** *116,* 9816–9849.
5. Poplata, S. and Bach, T. Enantioselective Intermolecular [2+2] Photocycloaddition Reaction of Cyclic Enones and Its Application in a Synthesis of (−)-Grandisol. *J. Am. Chem. Soc.* **2018,** *140,* 3228–3231.
6. Crimmins, M. T.; Pace, J. M.; Nantermet, P. G.; Kim-Meade, A. S.; Thomas, J. B.; Watterson, S. H.; Wagman, A. S. Total Synthesis of (±)-Ginkgolide B. *J. Am. Chem. Soc.* **1999**, *121,* 10249−10250.
7. Wender, P. A. and Dreyer, G. B. Synthetic studies on arene-olefin cycloadditions. 4. Total synthesis of (±)-modhephene. *J. Am. Chem. Soc.* **1982,** *104,* 5805–5807.
8. Kärkäs, M. D.; Porco, J. A.; Stephenson, C. R. J. Photochemical Approaches to Complex Chemotypes: Applications in Natural Product Synthesis. *Chem. Rev.* **2016,** *116,* 9683-9747.
9. Arias-Rotondoa, D. M.; McCusker, J. K. The photophysics of photoredox catalysis: a roadmap for catalyst design. *Chem. Soc. Rev.* **2016,** *45,* 5803-5820.
10. Prier, C. K.; Rankic, D. A.; MacMillan, D. W. C. Visible Light Photoredox Catalysis with Transition Metal Complexes: Applications in Organic Synthesis. *Chem. Rev.* **2013,** *113,* 5322−5363.

11. McNally, A.; Prier, C. K.; MacMillan, D. W. C. Discovery of an α-Amino C–H Arylation Reaction Using the Strategy of Accelerated Serendipity. *Science* **2011,** *334,* 1114-1117.

12. Zuo, Z.; MacMillan, D. W. C. Decarboxylative Arylation of α-Amino Acids via Photoredox Catalysis: A One-Step Conversion of Biomass to Drug Pharmacophore. *J. Am. Chem. Soc.* **2014,** *136,* 5257−5260.

13. Li, G.-X.; Morales-Rivera, C. A.; Wang, Y.; Gao, F.; He, G.; Liu, P.; Chen, G. Photoredox-mediated Minisci C–H alkylation of N-heteroarenes using boronic acids and hypervalent iodine. *Chem. Sci.* **2016,** *7*, 6407-6412.

14. Matsui, J. K.; Primer, D. N.; Molander, G. A. Metal-free C–H alkylation of heteroarenes with alkyltrifluoroborates: a general protocol for 1°, 2° and 3° alkylation. *Chem. Sci.* **2017,** *8*, 3512-3522.

15. Tucker, J. W.; Nguyen, J. D.; Narayanam, J. M. R.; Krabbe, S. W.; Stephenson, C. R. J. Tin-free radical cyclization reactions initiated by visible light photoredox catalysis. *Chem. Commun.* **2010,** *46*, 4985-4987.

16. Furst, L.; Matsuura, B. S.; Narayanam, J. M. R.; Tucker, J. W.; Stephenson, C. R. J. Visible Light-Mediated Intermolecular C−H Functionalization of Electron-Rich Heterocycles with Malonates. *Org. Lett.* **2010,** *12,* 3104–3107.

17. Bissonnette, N. B.; Boyd, M. J.; May, G. D.; Giroux, S.; Nuhant, P. C–H Functionalization of Heteroarenes Using Unactivated Alkyl Halides through Visible-Light Photoredox Catalysis under Basic Conditions. *J. Org. Chem.* **2018,** *83,* 10933–10940.

18. Okada, K.; Okamoto, K.; Morita, N.; Okubo, K.; Oda, M. Photosensitized decarboxylative Michael addition through N-(acyloxy)phthalimides via an electron-transfer mechanism. *J. Am. Chem. Soc.* **1991,** *113,* 9401–9402.

19. Parida, S. K.; Mandal, T.; Das, S.; Hota, S. K.; De Sarkar, S.; Murarka, S. Single Electron Transfer-Induced Redox Processes Involving N-(Acyloxy)phthalimides. *ACS Catal.* **2021,** *11,* 1640–1683.

20. Sherwood, T. C.; Li, N.; Yazdani, A. N.; Dhar, T. G. M. Organocatalyzed, Visible-Light Photoredox-Mediated, One-Pot Minisci Reaction Using Carboxylic Acids via N-(Acyloxy)phthalimides. *J. Org. Chem.* **2018,** *83*, 3000–3012.

21. Proctor, R. S. J.; Davis, H. J.; Phipps, R. J. Catalytic enantioselective Minisci-type addition to heteroarenes. *Science* **2018,** *360,* 419-422.

22. Barton, D. H. R.; Crich, D.; Motherwell, W. B. New and improved methods for the radical decarboxylation of acids. *J. Chem. Soc., Chem. Commun.* **1983,** 939-941.

23. Barton, D. H. R.; Bridon, D.; Fernandaz-Picot, I.; Zard, S. Z. The invention of radical reactions: Part XV. Some mechanistic aspects of the decarboxylative rearrangement of thiohydroxamic esters. *Tetrahedron* **1987,** *43,* 2733-2740.

24. Beatty, J. W.; Douglas, J. J.; Cole, K. P.; Stephenson, C. R. J. A scalable and operationally simple radical trifluoromethylation. *Nat. Commun.* **2015,** *6,* 7919.

25. Allen, L. J.; Cabrera, P. J.; Lee, M.; Sanford, M. S. *N*-Acyloxyphthalimides as Nitrogen Radical Precursors in the Visible Light Photocatalyzed Room Temperature C–H Amination of Arenes and Heteroarenes. *J. Am. Chem. Soc.* **2014,** *136,* 5607–5610.

26. Crisenza, G. E. M.; Mazzarella, D.; Melchiorre, P. Synthetic Methods Driven by the Photoactivity of Electron Donor–Acceptor Complexes. *J. Am. Chem. Soc.* **2020,** *142,* 5461–5476.

27. Hilinski, E. F.; Masnovi, J. M.; Amatore, C.; Kochi, J. K.; Rentzepis, P. M. Charge-Transfer Excitation of Electron Donor-Acceptor Complexes. Direct Observation of Ion

Pairs by Time Resolved (Picosecond) Spectroscopy. *J. Am. Chem. Soc.* **1983,** *105,* 6167−6168.

28. Bockman, T. M.; Lee, K. Y.; Kochi, J. K. Time-Resolved Spectroscopy and Charge-Transfer Photochemistry of Aromatic EDA Complexes with X-Pyridinium Cations. *J. Chem. Soc., Perkin Trans. 2* **1992,** 1581−1594.
29. Lee, K. Y.; Kochi, J. K. Charge-Transfer Structures of Aromatic EDA Complexes with *N*-Heteroatom-Substituted Pyridinium Cations. *J. Chem. Soc., Perkin Trans. 2* **1992,** 1011−1017.
30. Arceo, E.; Jurberg, I. D.; Álvarez-Fernandez, A.; Melchiorre, P. Photochemical activity of a key donor-acceptor complex can drive stereoselective catalytic α-alkylation of aldehydes. *Nat. Chem.* **2013**, *5*, 750−756.
31. Tobisu, M.; Furukawa, T.; Chatani, N. Visible Light-mediated Direct Arylation of Arenes and Heteroarenes Using Diaryliodonium Salts in the Presence and Absence of a Photocatalyst. *Chem. Lett.* **2013,** *42,* 1203−1205.
32. Kandukuri, S. R.; Bahamonde, A.; Chatterjee, I.; Jurberg, I. D.; Escudero-Adán, E. C.; Melchiorre, P. X-Ray Characterization of an Electron Donor–Acceptor Complex that Drives the Photochemical Alkylation of Indoles. *Angew. Chem. Int. Ed.* **2015,** *54,* 1485-1489.
33. James, M. J.; Strieth-Kalthoff, F.; Sandfort, F.; Klauck, F. J. R.; Wagener, F.; Glorius, F. Visible-Light-Mediated Charge Transfer Enables C−C Bond Formation with Traceless Acceptor Groups. Chem. Eur. J. 2019, 25, 8240-8244.
34. Jung, S.; Shin, S.; Park, S.; Hong, S. Visible-Light-Driven C4-Selective Alkylation of Pyridinium Derivatives with Alkyl Bromides. *J. Am. Chem. Soc.* **2020,** *142,* 11370–11375.

35. Shin, S.; Lee, S.; Choi, W.; Kim, N.; Hong, S. Visible-Light-Induced 1,3-Aminopyridylation of [1.1.1]Propellane with *N*-Aminopyridinium Salts. *Angew. Chem. Int. Ed.* **2021,** *60,* 7873–7879.

36. Postigo, A. Electron Donor-Acceptor Complexes in Perfluoroalkylation Reactions. *Eur. J. Org. Chem.* **2018,** 6391-6404.

37. Nappi, M.; Bergonzini, G.; Melchiorre, P. Metal-Free Photochemical Aromatic Perfluoroalkylation of α-Cyano Arylacetates. *Angew. Chem. Int. Ed.* **2014,** *53,* 4921-4925.

38. Beatty, J. W.; Douglas, J. J.; Miller, R.; McAtee, R. C.; Cole, K. P.; Stephenson, C. R. J. Photochemical Perfluoroalkylation with Pyridine N-Oxides: Mechanistic Insights and Performance on a Kilogram Scale. *Chem* **2016,** *1,* 456-472.

39. Oelgemöller, M.; Hoffman, N. Studies in Organic and Physical Photochemistry–An Interdisciplinary Approach. *Org. Biomol. Chem.* **2016,** *14,* 7392-7442.

40. Taylor, E. C.; Altland, H. W.; Kienzle, F.; McKillop, A. Thallium in Organic Synthesis. XLI. Synthesis of 1-Substituted 2-(1H)-Pyridones. New Synthesis of Unsymmetrical Biphenyls vis Photochemical Nitrogen–Oxygen Bond Clevage of 1-Aryloxy-2(1H)-pyridones. *J. Org. Chem.* **1976,** *41,* 24-27.

41. Zard, S. Z. On the Trail of Xanthates: Some New Chemistry for an Old Functional Group. *Angew. Chem., Int. Ed.* **1997,** *36,* 672-685.

42. Hasebe, M.; Kogawa, K.; Tsuchiya, T. Photochemical arylation by oxime esters in benzene and pyridine: simple synthesis of biaryl compounds. *Tet. Lett.* **1984,** *25,* 3887-3890.

43. Hasebe, M.; Tsuchiya, T. Photochemical generation of aliphatic radicals from benzophenone oxime esters: simple synthesis of alkylbenzenes and alkylpyridines. *Tet. Lett.* **1986,** *27,* 3239-3242.

44. Hasebe, M.; Tsuchiya, T. Photoreductive decarboxylation of carboxylic acids via their benzophenone oxime esters. *Tet. Lett.* **1987,** *28,* 6207-6210.

45. Patra, T.; Mukherjee, S.; Ma, J.; Strieth-Kalthoff, F.; Glorius, F. Visible-Light-Photosensitized Aryl and Alkyl Decarboxylative Functionalization Reactions. *Angew. Chem. Int. Ed.* **2019,** *58,* 10514–10520.

46. Barton, D. H. R.; Crich, D.; Motherwell, W. B. A practical alternative to the hunsdiecker reaction. *Tet. Lett.* **1983,** *24,* 4979–4982.

47. Barton, D. H. R.; Crich, D.; Motherwell, W. B. The invention of new radical chain reactions. Part VIII. Radical chemistry of thiohydroxamic esters; A new method for the generation of carbon radicals from carboxylic acids. *Tetrahedron* **1985,** *41,* 3901–3924.

48. Barton, D. H. R. Garcia, B.; Togo, H.; Zard, S. Z. Radical decarboxylative addition onto protonated heteroaromatic (and related) compounds. *Tet. Lett.* **1986,** *27,* 1327–1330.

49. Buzzetti, L.; Prieto, A.; Roy, S. R.; Melchiorre, P. Radical-Based C−C Bond-Forming Processes Enabled by the Photoexcitation of 4-Alkyl-1,4-dihydropyridines. *Angew. Chem. Int. Ed.* **2017**, *56,* 15039–15043.

50. Sato, Y.; Nakamura, K.; Sumida, Y.; Hashizume, D.; Hosoya, T.; Ohmiya, H. Generation of Alkyl Radical through Direct Excitation of Boracene-Based Alkylborate. *J. Am. Chem. Soc.* **2020,** *142,* 9938–9943.

Chapter 2 **Fragment Coupling Approach to the Minisci Alkylation**

2.1 Background

The incorporation of aliphatic chains or functional groups into *N*-heteroaromatic molecules can provide access to a myriad of functional motifs found throughout natural products, advanced materials, and pharmaceuticals.[1] In this regard, the development of new methods to accomplish the late-stage introduction of new substituents into complex molecules has become a focal point of contemporary research in organic chemistry.

The addition of a carbon centered radical to a heteroaromatic base resulting in the net C–H alkylation is commonly referred to as the Minisci reaction and has become a focal point for the late-stage diversification of heteroaromatic bases.[2,3] Developed by Italian chemist Francesco Minisci in the 1970s, initial reports employed silver (I) salts in the presence of strong persulfate oxidants and sulfuric acid in order to effect the alkylation of pyridine through decarboxylation of common carboxylic acids.[4] Contemporary studies of the Minisci alkylation have sought to

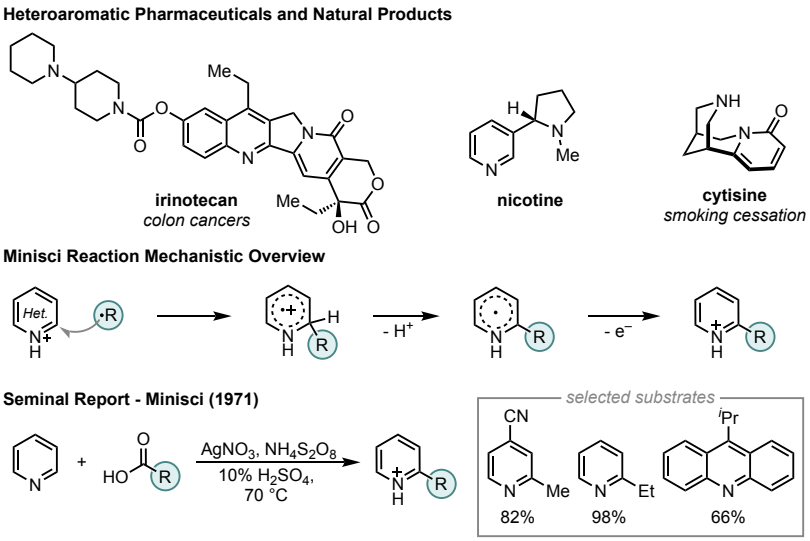

Figure 13. Overview of the Minisci reaction

establish mild conditions for the reaction, as such, methods employing photoredox catalysis to access radical intermediates have become commonplace.[5] In this regard, the use of reductively sensitive redox active auxiliaries in conjunction with photoredox catalysis provides a platform to access redox neutral Minisci reactions. In 2014 DiRocco and coworkers described the reductive decomposition of acetic peresters for the generation of radical intermediates.[6] The decomposition of acetic peresters was proposed to occur through a proton-coupled electron transfer event, leading to the production of acetate, acetone, and the desired radical intermediate. Ultimately, DiRocco *et al.* were able to leverage the reductive radical generation to access late-stage methylation of a number of known bioactive compounds such as caffeine, diflufenican, camptothecin, and varenicline. In 2018, Phipps and coworkers developed an enantioselective approach to the Minisci alkylation.[7] This report leveraged the reductive decomposition of N-hydroxy phthalimide esters for radical generation. Hydrogen bonding of the radical intermediate and protonated *N*-heteroaromatic base substrate to a chiral phosphoric acid catalyst allowed for control of the configuration of the newly formed stereocenter.

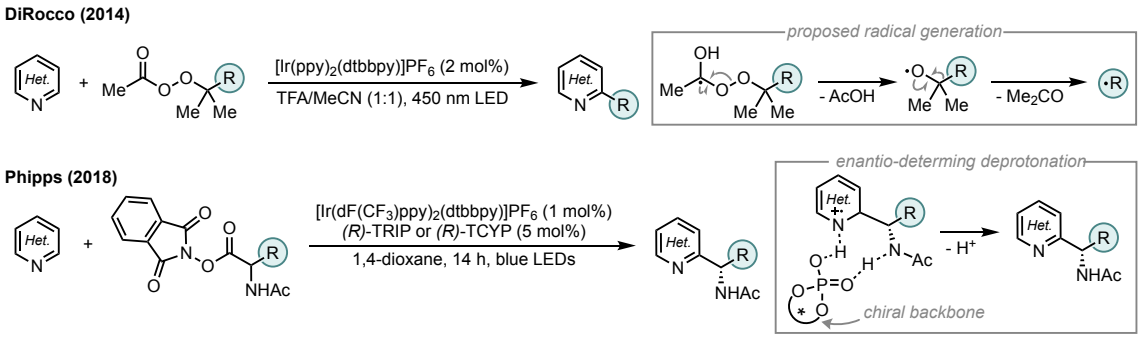

Figure 14. Recent advances in the Minisci alkylation employing photoredox catalysis

Since 2015, a focal point in our groups research has been the development of pyridine *N*-oxide and its derivatives as cheap, easily handled redox auxiliaries for decarboxylative radical generation.[8-10] *In situ* acylation of pyridine *N*-oxide with electrophilic acyl equivalents, such as acyl chlorides or trifluoroacetic anhydride, lead to the formation of electron deficient *N*-(acyloxy)pyridinium redox active esters. Single electron reduction of the electron deficient redox active esters induces a fast N–O bond fragmentation and decarboxylation, leading to the generation of reactive radical intermediates.[11] Our initial studies on this reactivity paradigm have focused on the generation of electrophilic trifluoromethyl and chlorodifluoromethyl radicals, and their intermolecular capture with electron rich aromatics. Herein, we discuss the development of divergent approach, leveraging N-(acyloxy)pyridinium reagents for the development of a formal fragment coupling approach to the Minisci alkylation reaction.

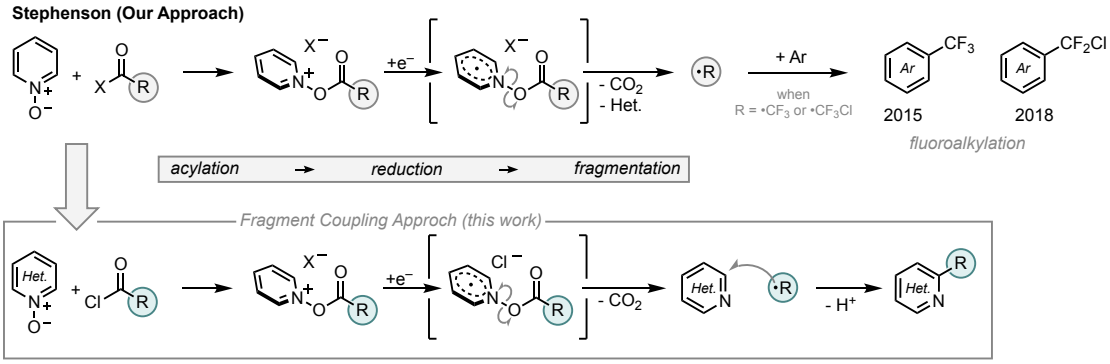

Figure 15. Pyridine N-oxides as radical precursors (top). Fragment coupling approach to the Minisci alkylation (bottom).

2.2 Results and Discussion

Pivaloyl chloride and 4-phenylpyridine *N*-oxide were chosen as model substrates for initial fragment coupling evaluation. Upon screening several solvents and photocatalysts, we discovered that a combination of acetonitrile and 1 mol % $[Ir(ppy)_2(dtbbpy)]PF_6$ furnished the desired 2-*tert*-butyl-4-phenylpyridine (**1**) product in 75% yield, as well as the 2,4-di-*tert*-butylated product in 5% yield. Under optimized conditions, the scope of the fragment coupling protocol was investigated. Successful ethyl (**2**) and methyl (**3**) addition to 4-phenylpyridine *N*-oxide was achieved, albeit at low to moderate yields, due to decreased radical stability and nucleophilicity.[12] Long chain, linear aliphatic radical intermediates provided modest yields of the desired fragment coupling product (4). In contrast, the benzylation (5) of 4-phenylpyridine *N*-oxide proceeded with significantly diminished yields. A predominant side reaction that was observed involved the formal decarbonylation of phenylacetyl chloride, yielding 73% formation of benzyl chloride. The protocol proved amenable to the coupling of 4-phenylpyridine with a wide range of secondary and tertiary cyclic alkanes (6-12), including the cyclohexyl (6) motif, which has been demonstrated to be a bioisostere of the phenyl functionality.[13] Furthermore, the fragment coupling protocol allowed access to the addition of polycyclic carbocycles, and heterocycles (13-20) in moderate yields. Notably, when evaluating nitrogen containing heterocycles, it was noticed that the 2,2,2-trichloroethyl carbamate (TCE) protecting group provided the best reactivity, although other protecting groups were also tolerated (16,17). Medicinally relevant fluorinated isosteres radical fragments were also amenable to the fragment coupling protocol (21-23), including the first example of incorporating the 1-fluorocyclopropane motif (22) onto a heterocyclic scaffold in one step from its carboxylic acid precursor. Overall, a variety of alkyl substrates, differing in size and

electronic properties, have been demonstrated to be successful coupling partners in this

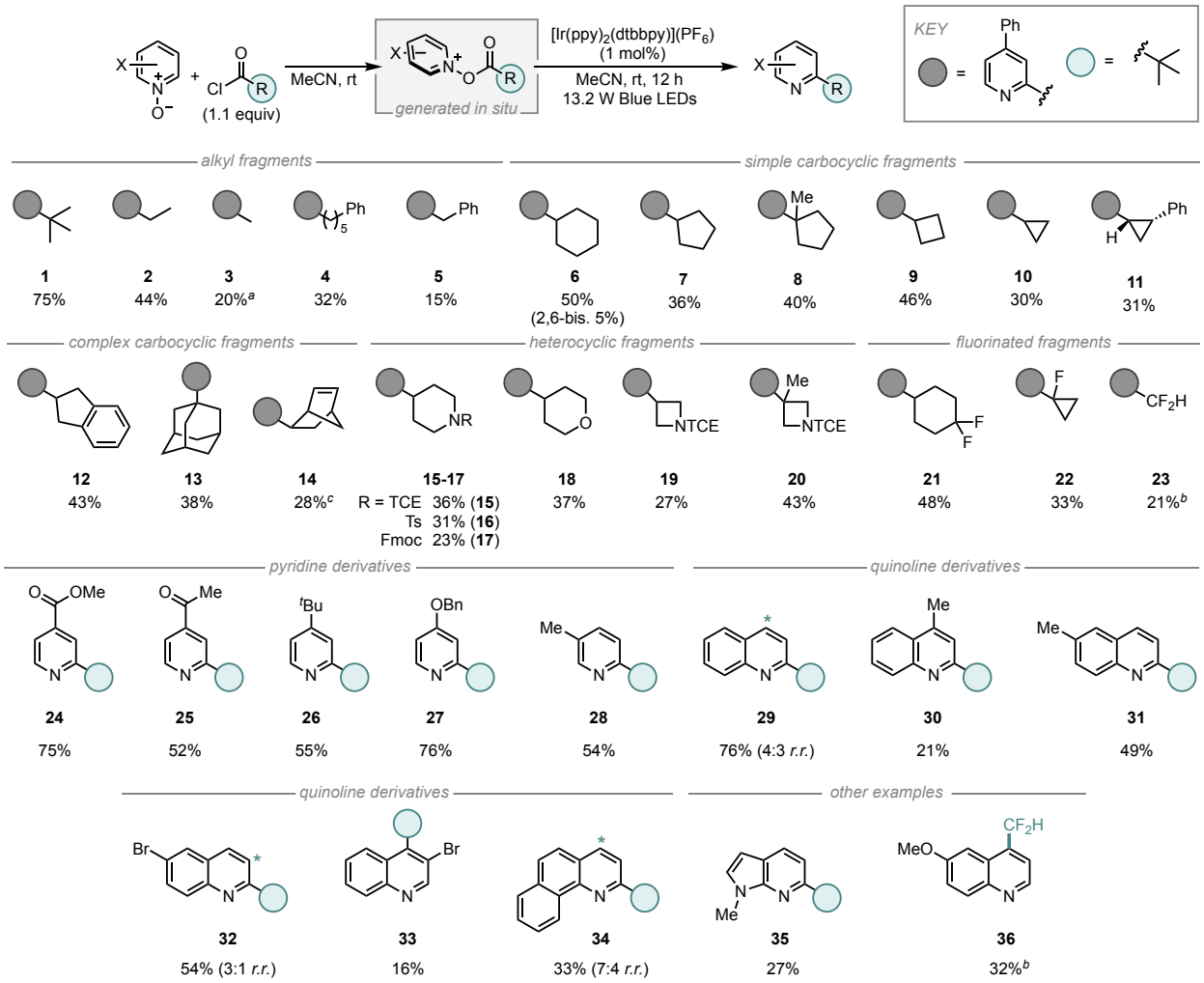

Figure 16. Scope of fragment coupling approach to the Minisci alkylation

transformation. An added benefit to this methodology entails the direct *in situ* formation of non-commercially available acid chloride reagents from the corresponding carboxylic acid (via oxalyl chloride and catalytic DMF), followed by addition of the heterocyclic N-oxide, without the need for any additional purification or isolation steps.

In the next phase of this study, we evaluated a variety of diverse and pharmaceutically relevant heterocyclic motifs. The addition of the *tert*-butyl radical to mildly electron-deficient pyridine *N*-oxide derivatives, such as ethyl isonicotinate *N*-oxide (24), as well as 4-acetylpyridine

N-oxide (25) proceeded in good yields (75% and 52% respectively). Pyridine *N*-oxide derivatives bearing 4-*tert*-butyl- and 4-benzyloxy substituents provided the corresponding products in good yields, 55% and 76% respectively. Alkyl substituents possessing benzylic C–H bonds were tolerated when employing 3- or 5- substituted derivatives (28). Quinoline *N*-oxide was successfully *tert*-butylated in 76% yield, leading to a 4:3 mixture of regioisomers (29). Several quinoline *N*-oxide derivatives containing methyl, methoxy, bromo-, and chloro- substituents, in addition to benzoquinoline, were alkylated in modest yields (30-34). The lower yields observed in the *tert*-butylation of lepidine *N*-oxide (30) can be attributed to competing deprotonation of the methyl substituent upon generation of the acylated complex, which results in displacement of pivalic acid and precludes reductive alkyl radical generation. 7-Azaindole, which can be considered as a bioisostere of the indole and purine motifs and constitutes an essential subunit of many pharmacophores,[14] could also be functionalized regioselectivity (35) using this protocol. Furthermore, difluoromethylation of 6-methoxyquinoline (36) exclusively resulted in functionalization at the 4-position. While a variety of pyridine and quinoline-based heterocyclic scaffolds could be accessed as coupling partners, functionalization of other five- and six-membered heterocyclic *N*-oxides, including benzylimidazole, quinoxaline, pyrimidine, and pyridazine N-oxide derivatives could not be achieved using this fragment coupling approach. As is evidenced by the significant recovery of *N*-oxide starting material, the observed lack of reactivity is suspected to be due to the diminished nucleophilicity of the *N*-oxide motif rather than inefficient radical addition.[15]

Next, we sought to gain an understanding of the underlying mechanism for the photochemical Minisci alkylation. Investigation of the photon dependence of the reaction revealed the quantum yield to be 1.7, indicating that an inefficient radical chain process is likely operating.[16]

Crossover experiments demonstrated the viability of both intramolecular and intermolecular radical capture occurring, subjecting two differentially acylated pyridine N-oxide derivatives to standard reaction conditions gave rise to a 1:1 mixture of cross-functionalized products.

Guided by our mechanistic studies, we sought to overcome the limitations imposed by the fragment coupling approach by accessing intermolecular alkylation reaction in the presence of pyridine *N*-oxide as a low-cost redox auxiliary. Moreover, the envisioned use of pyridine *N*-oxide as a sacrificial redox auxiliary would be an ideal platform for the alkylation of complex pharmacophore molecules. As transitioning away from simple heterocyclic substrates to more complicated, biologically relevant molecular scaffolds present further challenges, as both the selective formation of the *N*-oxide functionality and the ability to predict the nucleophilicity of the *N*-oxide increase in complexity. The intermolecular coupling concept came to fruition as subjection of quinoxaline to reaction conditions in the presence of excess pyridine *N*-oxide gave rise to the 2-*tert*-butyl product in good yield. Brimonidine, a drug molecule used for the treatment of rosacea and open-angle glaucoma, furnished the tert-butylated derivative in 11% yield (38). Finally, we were able to diversify the imidazopyridazine core structure (41) through the addition of *tert*-butyl (44% yield), methyl (16% yield) and difluoromethyl (13% yield) groups.[17]

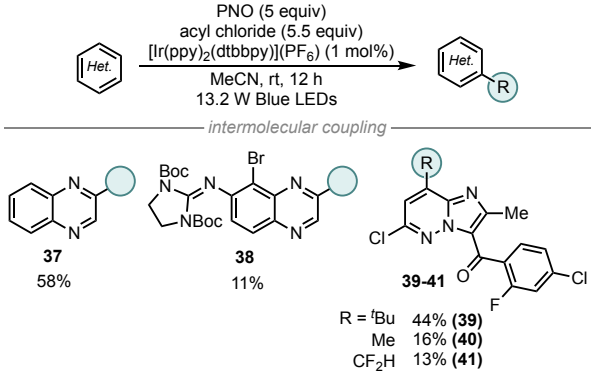

Figure 17. Scope of Intermolecular Alkylation.

Finally, we have demonstrated the capability to run this decarboxylative alkylation reaction on gram scale both in batch and in flow, suggesting that this methodology may translate beyond discovery scale. Using a 900 μL flow reactor, 1 gram of quinoline N-oxide was tert-butylated in an overall 71% yield (relative to 68 % yield on a 1 gram scale in batch), with a residence time of 2.25 min.

In conclusion, we have reported an operationally simple, visible light-mediated method for the decarboxylative alkylation of heterocyclic *N*-oxides. Most significantly, this protocol offers a platform for the reductive generation of alkyl radicals without the reliance on stoichiometric additives, harsh reagents, and sacrificial redox auxiliaries. We envision this methodology to be of significant utility and practicality for the diversification of heterocyclic scaffolds in a multitude of medicinal applications.

2.3 Experimental Procedures and Compound Characterization

Chemicals were either used as received or purified according to the procedures outlined in *Purification of Common Laboratory Chemicals*. Hygroscopic *N*-oxide substrates were dried on a high vaccuum line for 6 h at ambient temperature prior to use. Pyridine *N*-oxide was dried on a high vacuum line at 60 °C for 12 hours. Thin-layer chromatography (TLC) analysis of reaction mixtures was performed using Merck silica gel 60 F254 TLC plates and visualized by a dual short wave/long wave UV lamp. Column flash chromatography was performed using 230–400 mesh silica gel or via automated column chromatography.

Nuclear magnetic resonance (NMR) spectra were recorded using an internal deuterium lock on Varian MR400, Varian Inova 500 and Varian Vnmrs 700 spectrometers. Chemical shifts for ^{1}HNMR were reported as δ, parts per million, relative to the signal of $CHCl_3$ at 7.26 ppm. Chemical shifts for ^{13}CNMR were reported as δ, parts per million, relative to the center line signal

of the $CDCl_3$ triplet at 77.36 ppm. Multiplicities are reported using the following abbreviations: s = singlet, d = doublet, t = triplet, q = quartet, quint = quintet, m = multiplet, br = broad resonance, dd = doublet of doublet, dt = doublet of triplet, etc. High-resolution mass spectra (ESI) were recorded at the Mass Spectrometry Facility at the Department of Chemistry of the University of Michigan in Ann Arbor, MI, on a Micromass AutoSpec Ultima Magnetic Sector mass spectrometer using electrospray ionization (ESI), positive ion mode. IR spectra were recorded on a Perkin-Elmer Spectrum BX FT-IR spectrometer fitted with an ATR accessory. Actinometry and quantum yield measurements were performed with a Fluoromax-2 fluorimeter equipped with a 150W Xe arc lamp. UV-VIS measurements were obtained on a Shimadzu UV-1601 UV-VIS Spectrometer.

LED lights and the requisite power box and cables were purchased from Creative Lighting Solutions (http://www.creativelightings.com) with the following item codes: CL-FRS5050-12WP-12V (4.4 W blue LED light strip), CL-FRS5050WPDD-5M- 12V-BL (72 W LED strip), CL-PS94670-25W (25 W power supply), CL-PS16020-150W (150 W power supply), CL-PC6FT-PCW (power cord), CL-TERMBL-5P (terminal block). A reaction performed with a 24 W CFL placed 5 cm from the vial provided identical results. Unless stated otherwise, all reactions were run on a 0.8 mmol scale in a 2 dram vial equipped with stir bar and septum. The light apparatuses used to irradiate the reactions were constructed from test tube racks and wrapped with three 4.4 W blue LED strips. Reactions were run only in slots marked by an X in the picture below so as to keep a moderate distance from the light source (~2.5 cm). At this distance the temperature of the reactions did not exceed 35 ˚C.

Experimental light setup

General Experimental Procedures

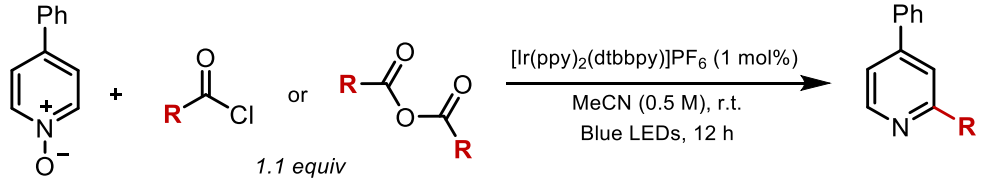

Procedure A. To a 2 dram vial equipped with a stir bar was added heterocyclic *N*-oxide (0.80 mmol, 1.0 equiv) and $[Ir(ppy)_2(dtbbpy)]PF_6$ (1.0 mol%). The combined materials were dissolved in MeCN (0.5 M, 1.6 mL) and stirred. Upon subsequent addition of the acid chloride or anhydride (0.88 mmol, 1.1 equiv), the resulting solution was stirred for 5 min. The vial was equipped with a screw-on cap with septum, and a 20 gauge needle was placed through the septum for the duration of the reaction. Three 4.4 W LED light strips (positioned 2.5 cm away) were turned on and the reaction was allowed to run for 12-15 hours before the light source was removed. Workup was performed by diluting the reaction with CH_2Cl_2 and washing with saturated $NaHCO_3$ (x1) and then brine (x1). The organic layer was dried over sodium sulfate before filtering and concentrating at 40 ˚C under reduced pressure. The crude residue can then be purified by column chromatography to afford the desired alkylation product(s).

Optimization: Trimethoxybenzene (0.80 mmol) was added as a stoichiometric internal standard upon completion of the reaction. A sample of the reaction was removed and diluted with $CDCl_3$ for NMR analysis.

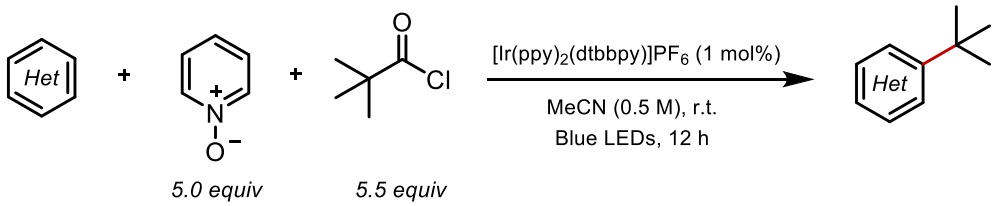

Procedure B. To a 2 dram vial equipped with a stir bar was added the heterocyclic substrate (0.8 mmol), pyridine *N*-oxide (1.6 mmol, 5.0 equiv), and $[Ir(ppy)_2(dtbbpy)]PF_6$ (1.0 mol%). The combined materials were dissolved in MeCN (0.5 M, 1.6 mL) and stirred. Upon subsequent addition of pivaloyl chloride (1.76 mmol, 5.5 equiv), the resulting solution was stirred for 5 min. The vial was equipped with a screw-on cap with septum, and a 25 gauge needle was placed through the septum for the duration of the reaction. Three 4.4 W LED light strips (positioned 2.5 cm away) were turned on and the reaction was allowed to run for 12-15 hours before the light source was removed. Workup was performed by diluting the reaction with CH_2Cl_2 and washing with saturated NaHCO3 (x1) and then brine (x1). The organic layer was dried over sodium sulfate before filtering and concentrating at 40 ˚C under reduced pressure. The crude residue can then be purified by column chromatography to afford the desired alkylation product(s).

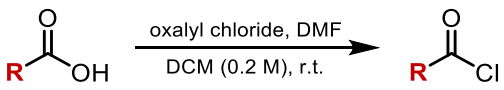

General procedure for acid chloride synthesis. To an oven-dried round bottom flask was added the carboxylic acid substrate (0.96 mmol, 1.0 equiv) and dichloromethane (0.2 M) under a nitrogen atmosphere. To the resulting stirred solution was added oxalyl chloride (1.15 mmol, 1.2 equiv)

and 2 drops of DMF. The mixture was stirred at room temperature until all gas evolution ceased (generally 1-5 hours), and reaction progress was monitored by 1H NMR spectroscopy. Product decomposition may be observed if the solution is stirred for over 5 hours. Upon reaching >99% conversion, the mixture was concentrated in vacuo to remove excess oxalyl chloride, and the crude acid chloride residue was used in the subsequent decarboxylation alkylation step without further purification.

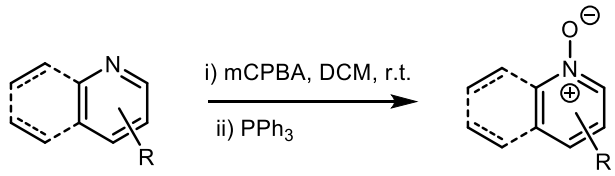

General heterocyclic *N*-oxide synthesis. This procedure was adapted from the work of Herzon and co-workers.[18] 3-Chloroperbenzoic acid (1.0 equiv, 60% w/w) was added in one portion to a solution of the heterocyclic substrate (1.0 equiv) in dichloromethane (0.2 M) at 24 °C. The reaction mixture was stirred for 12 h at 24 °C. PPh_3 (0.5 equiv) was added and the solution was stirred for another 4 h. The product mixture was concentrated to dryness and the residue obtained was purified by flash-column chromatography (eluting with ethyl acetate initially, grading to 10% methanol–ethyl acetate, linear gradient).

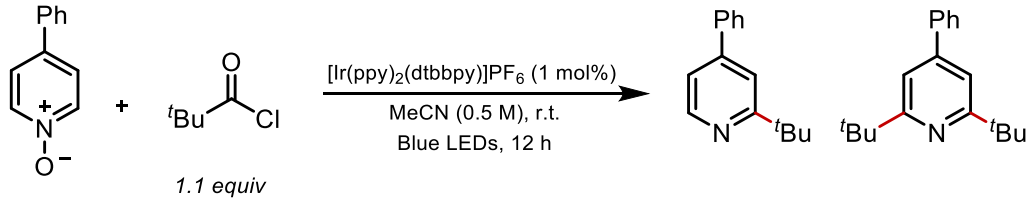

2-tert-butyl-4-phenylpyridine (1a) and 2,6-di-tert-butyl-4-phenylpyridine (1b)

The reaction was run according to General Procedure A and was purified by column chromatography (0% to 15% ethyl acetate in hexanes) to afford 2-tert-butyl-4-phenylpyridine (118 mg, 71%) and 2,6-di-tert-butyl-4-phenylpyridine (6 mg, 3%) as colorless oils. In addition, 4-

phenylpyridine (19 mg, 15%) was recovered. The acquired 1H and 13 CNMR spectra were identical to those reported in the literature.[19]

2-tert-butyl-4-phenylpyridine (1a): Rf = 0.75 (ethyl acetate/hexanes 1:4; UV). 1HNMR (CDCl3, 700 MHz): δ 8.61 (d, J = 5.1 Hz, 1H), 7.63 (d, J = 7.3 Hz, 2H), 7.54 (s, 1H), 7.48 (t, J = 7.6 Hz, 2H), 7.43 (t, J = 7.3 Hz, 1H), 7.30 (dd, J = 5.0, 1.5 Hz, 1H), 1.43 (s, 9H). 13C NMR (176 MHz, CDCl3): δ 170.13, 149.33, 148.95, 139.42, 129.31, 129.03, 127.41, 119.19, 117.52, 37.82, 30.58. HRMS (ESI) m/z [M + H]+ calcd for: C15H17N: 212.1434; found: 212.1435.

2,6-di-tert-butyl-4-phenylpyridine (1b): Rf = 0.88 (ethyl acetate/hexanes 1:4; UV). 1HNMR (CDCl3, 700 MHz): δ 7.64 – 7.59 (m, 2H), 7.47 (t, J = 7.7 Hz, 2H), 7.41 (d, J = 7.2 Hz, 1H), 7.29 (s, 2H), 1.40 (s, 18H). 13C NMR (176 MHz, CDCl3): δ 168.46, 149.01, 140.74, 129.19, 128.60, 127.61, 114.17, 38.10, 30.58. HRMS (ESI) m/z [M + H]+ calcd for: $C_{19}H_{25}N$: 268.2060; found: 268.2061. IR (neat): v = 2953, 2901, 2864, 1594, 1552, 1498, 1477, 1458, 1400, 1359, 1254, 1167, 1139, 1081.

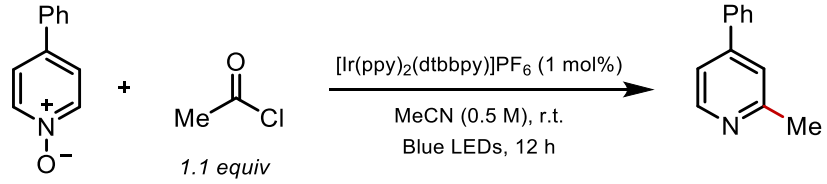

2-methyl-4-phenylpyridine (3)

The reaction was run according to General Procedure A and was purified by column chromatography (0% to 15% ethyl acetate in hexanes) to afford the title compound (27 mg, 20 %) in a mixture with 4-phenylpyridine (76 mg, 61%). Rf = 0.25 (ethyl acetate/hexanes 1:4; UV). ^{1}H

NMR (700 MHz, $CDCl_3$) δ 8.66 (d, *J* = 5.3 Hz, 2H), 8.54 (d, *J* = 5.1 Hz, 1H), 7.66 – 7.59 (m, *J* = 12.2, 7.8 Hz, 4H), 7.53 – 7.39 (m, 9H), 7.37 (s, 1H), 7.31 (d, *J* = 5.1 Hz, 1H), 2.62 (s, 3H). ^{13}C NMR (176 MHz, $CDCl_3$) δ 158.82, 150.23, 149.54, 148.69, 148.32, 138.42, 138.12, 129.10, 129.04, 129.02, 128.88, 126.99, 126.98, 121.63, 121.20, 118.86, 24.57. HRMS (ESI) m/z $[M + H]^+$ calcd for: $C_{12}H_{11}N$: 170.0964; found: 170.0963. The acquired ^1H and ^{13} CNMR spectral data corresponding to the mono-methylated product were identical to those reported in the literature.[20]

Note: 2-methyl-4-phenylpyridine and 4-phenylpyridine were inseparable by column chromatography and recrystallization. Attempts to selectivity oxidize 4-phenylpyridine using *m*-CPBA at low temperatures of 0°C and facilitate the isolation of the methylated product were also unsuccessful.

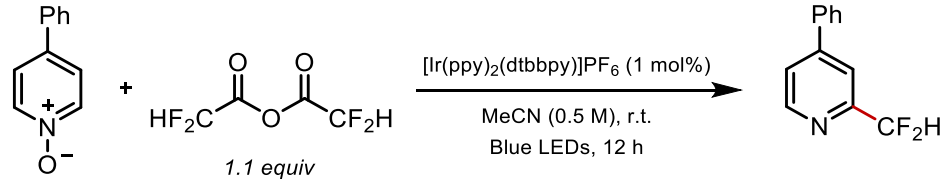

2-difluoromethyl-4-phenylpyridine (23)

The reaction was run according to General Procedure A and was purified by column chromatography (0% to 15% ethyl acetate in hexanes) to afford the title compound (34 mg, 21%) as a pale yellow oil and 4-phenylpyridine (78 mg, 63%). R_f = 0.69 (ethyl acetate/hexanes 1:4; UV). ^1H NMR (700 MHz, $CDCl_3$) δ 8.70 (d, *J* = 5.1 Hz, 1H), 7.86 (s, 1H), 7.71 – 7.59 (m, 3H), 7.57 – 7.46 (m, 3H), 6.70 (t, *J* = 55.5 Hz, 1H). ^{13}C NMR (176 MHz, $CDCl_3$) δ 153.76 (t, *J* = 25.5 Hz), 150.34, 150.31, 137.73, 129.93, 129.62, 127.43, 123.62, 118.41, 114.37 (t, *J* = 240.5 Hz). ^{19}F NMR (377 MHz, $CDCl_3$) δ -115.86 (d, *J* = 55.5 Hz). HRMS (ESI) m/z $[M + H]^+$ calcd for: $C_{12}H_9F_2N$: 206.0776; found: 206.0778. IR (neat): v = 3034, 1603, 1551, 1450, 1412, 1373, 1206, 1123, 1034.

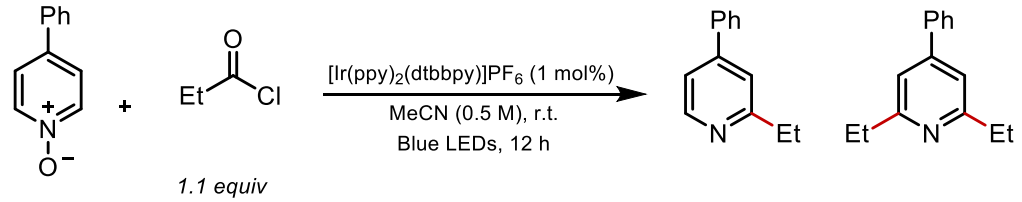

2-ethyl-4-phenylpyridine and 2,6-diethyl-4-phenylpyridine (2)

The reaction was run according to General Procedure A and was purified by column chromatography (0% to 15% ethyl acetate in hexanes) to afford 2-ethyl-4-phenylpyridine (65 mg, 44%) and 2,6-diethyl-4-phenylpyridine (10 mg, 6%) as colorless oils and 4-phenylpyridine (41 mg, 33%).

2-ethyl-4-phenylpyridine: R_f = 0.38 (ethyl acetate/hexanes 1:4; UV). ^{1}H NMR (700 MHz, $CDCl_3$) δ 8.57 (d, *J* = 5.1 Hz, 1H), 7.63 (d, *J* = 8.0 Hz, 2H), 7.48 (t, *J* = 7.5 Hz, 2H), 7.43 (t, *J* = 7.3 Hz, 1H), 7.38 (s, 1H), 7.32 (d, *J* = 5.1 Hz, 1H), 2.89 (q, *J* = 7.6 Hz, 2H), 1.36 (t, *J* = 7.6 Hz, 3H). ^{13}C NMR (176 MHz, $CDCl_3$) δ 164.36, 149.96, 149.16, 138.96, 129.37, 129.20, 127.39, 120.38, 119.42, 31.87, 14.35. HRMS (ESI) m/z $[M + H]^+$ calcd for: $C_{13}H_{13}N$: 184.1121; found: 184.1121. The acquired ^{1}H and ^{13} CNMR spectra were identical to those reported in the literature.[21]

2,6-diethyl-4-phenylpyridine: R_f = 0.57 (ethyl acetate/hexanes 1:4; UV). ^{1}H NMR (500 MHz, $CDCl_3$) δ 7.63 (d, *J* = 7.3 Hz, 2H), 7.49 – 7.41 (m, 3H), 7.19 (s, 2H), 2.87 (q, *J* = 7.6 Hz, 4H), 1.34 (t, *J* = 7.6 Hz, 6H). ^{13}C NMR (126 MHz, $CDCl_3$) δ 163.82, 149.59, 139.49, 129.28, 128.98, 127.43, 117.58, 31.98, 14.66. HRMS (ESI) m/z $[M + H]^+$ calcd for: $C_{15}H_{17}N$: 211.1361; found: 211.1353. IR (neat): v = 3060, 2966, 2925, 2850, 1698, 1598, 1554, 1498, 1461, 1406, 1197.

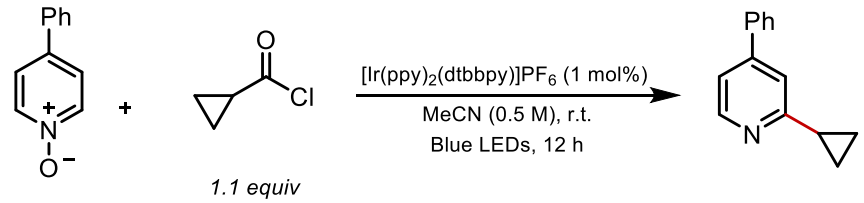

2-cyclopropyl-4-phenylpyridine (10)

The reaction was run according to General Procedure A and was purified by column chromatography (0% to 15% ethyl acetate in hexanes) to afford the title compound (47 mg, 30%) as a pale yellow oil and 4-phenylpyridine (50 mg, 40%). R_f = 0.68 (ethyl acetate/hexanes 1:4; UV). ^{1}HNMR ($CDCl_3$, 700 MHz): δ 8.48 (d, *J* = 5.1 Hz, 1H), 7.62 (d, *J* = 7.4 Hz, 2H), 7.47 (t, *J* = 7.6 Hz, 2H), 7.42 (t, *J* = 7.3 Hz, 1H), 7.34 (s, 1H), 7.24 (dd, *J* = 5.1, 1.6 Hz, 1H), 2.13 – 2.06 (m, 1H), 1.11 – 1.06 (m, 2H), 1.02 (ddd, *J* = 10.9, 6.6, 4.0 Hz, 2H). ^{13}C NMR (176 MHz, $CDCl_3$): δ 163.63, 149.98, 148.60, 138.95, 129.31, 129.12, 127.33, 119.65, 118.93, 17.63, 10.15. HRMS (ESI) m/z $[M + H]^+$ calcd for: $C_{14}H_{13}N$: 196.1121; found: 196.1121. The acquired ^{1}H and ^{13} CNMR spectra were identical to those reported in the literature.[22]

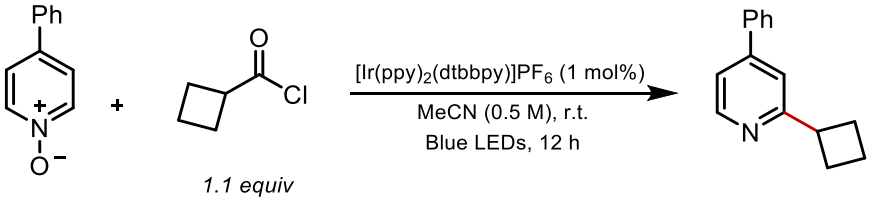

2-cyclobutyl-4-phenylpyridine (9)

The reaction was run according to General Procedure A and was purified by column chromatography (0% to 15% ethyl acetate in hexanes) to afford the title compound (70 mg, 42%) as a pale yellow oil and 4-phenylpyridine (43 mg, 35%). R_f = 0.62 (ethyl acetate/hexanes 1:4; UV).

^{1}H NMR (700 MHz, $CDCl_3$): δ 8.61 (d, *J* = 5.1 Hz, 1H), 7.63 (d, *J* = 7.5 Hz, 2H), 7.48 (t, *J* = 7.5 Hz, 2H), 7.43 (dd, *J* = 8.0, 6.5 Hz, 1H), 7.36 (s, 1H), 7.31 (d, *J* = 5.1 Hz, 1H), 3.74 (p, *J* = 8.8 Hz, 1H), 2.44 – 2.35 (m, 4H), 2.14 – 2.03 (m, 1H), 1.98 – 1.87 (m, 1H). ^{13}C NMR (176 MHz, $CDCl_3$) δ 165.52, 149.96, 148.92, 139.00, 129.32, 129.13, 127.35, 119.39, 119.26, 42.47, 28.78, 18.59. HRMS (ESI) m/z [M + H]$^+$ calcd for: $C_{15}H_{15}N$: 210.1277; found: 210.1279. IR (neat): v = 2935, 2864, 1594, 1545, 1499, 1472, 1399, 1243, 1182.

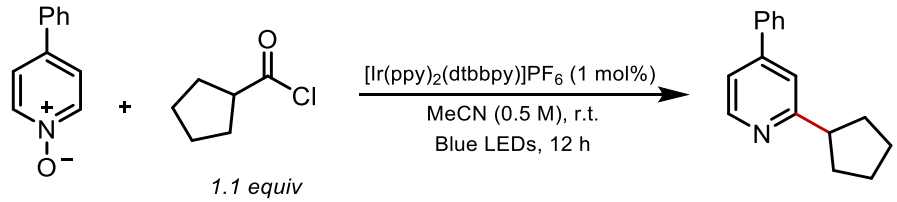

2-cyclopentyl-4-phenylpyridine (7)

The reaction was run according to General Procedure A and was purified by column chromatography (0% to 15% ethyl acetate in hexanes) to afford the title compound (70 mg, 39%) as a colorless oil and 4-phenylpyridine (50 mg, 40%). R_f = 0.68 (ethyl acetate/hexanes 1:4; UV). ^{1}H NMR (700 MHz, $CDCl_3$): δ 8.58 (d, *J* = 5.1 Hz, 1H), 7.63 (d, *J* = 7.5 Hz, 2H), 7.48 (t, *J* = 7.5 Hz, 2H), 7.43 (t, *J* = 7.3 Hz, 1H), 7.39 (s, 1H), 7.30 (d, *J* = 5.0 Hz, 1H), 3.30 – 3.18 (m, 1H), 2.17 – 2.08 (m, 2H), 1.90 – 1.80 (m, 4H), 1.73 – 1.70 (m, 2H). ^{13}C NMR (176 MHz, $CDCl_3$): δ 166.50, 149.91, 148.91, 139.07, 129.32, 129.10, 127.36, 120.04, 119.42, 48.43, 33.91, 26.19. HRMS (ESI) m/z [M + H]$^+$ calcd for: $C_{16}H_{17}N$: 224.1434; found: 224.1436. IR (neat): v = 2947, 2865, 1594, 1546, 1499, 1472, 1448, 1398, 1343, 1298, 1184.

2-(1-methylcyclohexyl)-4-phenylpyridine (8)

The reaction was run according to General Procedure A and was purified by column chromatography (0% to 15% ethyl acetate in hexanes) to afford the title compound (81 mg, 40%) as a pale yellow oil and 4-phenylpyridine (59 mg, 47%). R_f = 0.71 (ethyl acetate/hexanes 1:4; UV). ^{1}HNMR ($CDCl_3$, 700 MHz): δ 8.64 (d, *J* = 5.0 Hz, 1H), 7.65 – 7.61 (m, 2H), 7.53 (s, 1H), 7.49 (dd, *J* = 10.5, 4.7 Hz, 2H), 7.43 (t, *J* = 7.4 Hz, 1H), 7.29 (dd, *J* = 5.1, 1.6 Hz, 1H), 2.25 (d, *J* = 9.9 Hz, 2H), 1.64 – 1.59 (m, 4H), 1.48 – 1.42 (m, 4H), 1.28 (s, 3H). ^{13}C NMR (176 MHz, $CDCl_3$): δ 169.39, 149.59, 148.89, 139.52, 129.32, 129.01, 127.44, 119.02, 118.57, 41.24, 37.62, 37.54, 26.65, 23.15. HRMS (ESI) m/z $[M + H]^+$ calcd for: $C_{17}H_{19}N$: 252.1751; found: 252.1752. IR (neat): v = 2922, 2853, 1592, 1547, 1496, 1469, 1445, 1390, 1350.

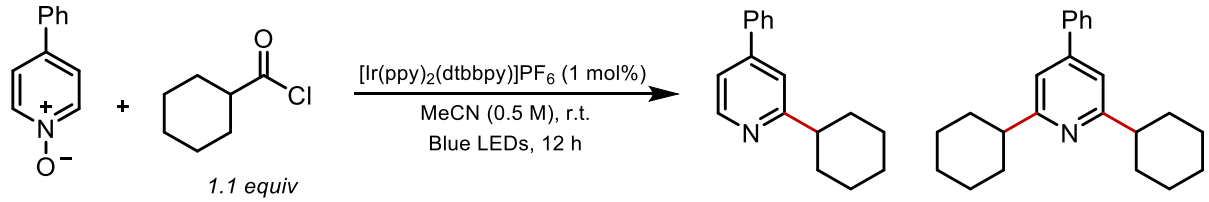

2-cyclohexyl-4-phenylpyridine and 2,6-dicyclohexyl-4-phenylpyridine (6)

The reaction was run according to General Procedure A and was purified by column chromatography (0% to 15% ethyl acetate in hexanes) to afford 2-cyclohexyl-4-phenylpyridine (94 mg, 50%) and 2,6-dicyclohexyl-4-phenylpyridine (10 mg, 5%) as colorless oils. In addition, 4-phenylpyridine (13 mg, 10%) was recovered. The acquired ^{1}H and ^{13} CNMR spectra were identical to those reported in the literature.[23]

2-cyclohexyl-4-phenylpyridine: R_f = 0.38 (ethyl acetate/hexanes 1:4; UV). ^{1}H NMR (700 MHz, $CDCl_3$): δ 8.57 (d, *J* = 5.1 Hz, 1H), 7.63 (dd, *J* = 5.2, 3.3 Hz, 2H), 7.48 (dd, *J* = 10.3, 4.7 Hz, 2H), 7.45 – 7.40 (m, 1H), 7.36 (s, 1H), 7.31 (dd, *J* = 5.1, 1.7 Hz, 1H), 2.77 (tt, *J* = 12.0, 3.4 Hz, 1H), 2.00 (dd, *J* = 13.5, 1.6 Hz, 2H), 1.91 – 1.84 (m, 2H), 1.80 – 1.73 (m, 1H), 1.59 (qd, *J* = 12.7, 3.3 Hz, 2H), 1.44 (qt, *J* = 13.0, 3.4 Hz, 2H), 1.36 – 1.27 (m, 1H). ^{13}C NMR (176 MHz, $CDCl_3$): δ 167.31, 149.77, 149.07, 139.07, 129.28, 129.08, 127.33, 119.47, 119.35, 47.01, 33.30, 26.93, 26.40. HRMS (ESI) m/z [M + H]$^+$ calcd for: $C_{17}H_{19}N$: 238.1590; found: 238.1592.

2,6-dicyclohexyl-4-phenylpyridine: R_f = 0.75 (ethyl acetate/hexanes 1:4; UV). ^{1}HNMR ($CDCl_3$, 700 MHz): δ 7.64 – 7.59 (m, 2H), 7.46 (t, *J* = 7.6 Hz, 2H), 7.40 (t, *J* = 7.4 Hz, 1H), 7.16 (s, 2H), 2.75 (tt, *J* = 11.9, 3.4 Hz, 2H), 2.02 – 2.01 (m, 4H), 1.88 – 1.83 (m, 4H), 1.78 – 1.74 (m, 2H), 1.54 (ddd, *J* = 24.8, 12.7, 3.1 Hz, 4H), 1.48 – 1.41 (m, 4H), 1.33 – 1.27 (m, 2H). ^{13}C NMR (176 MHz, $CDCl_3$): δ 166.60, 149.34, 139.98, 129.22, 128.81, 127.48, 116.33, 47.12, 33.56, 27.00, 26.56. HRMS (ESI) m/z [M + H]$^+$ calcd for: $C_{23}H_{29}N$: 320.2373; found: 320.2377. IR (neat): v = 3059, 2921, 2849, 1726, 1595, 1551, 1498, 1448, 1407, 1172.

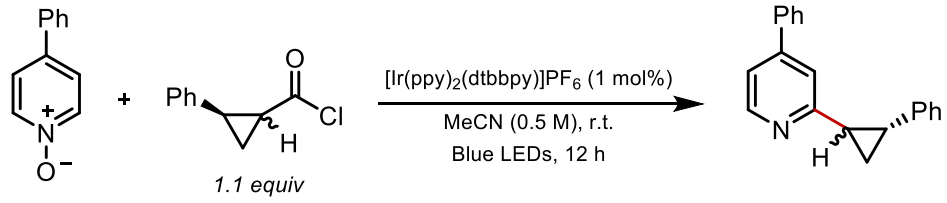

4-phenyl-2-(2-phenylcyclopropyl)pyridine (11)

The reaction was run according to General Procedure A and was purified by column chromatography (0% to 15% ethyl acetate in hexanes) to afford the title compound (67 mg, 31%) as a yellow oil and 4-phenylpyridine (51 mg, 41%). R_f = 0.50 (ethyl acetate/hexanes 1:4; UV). ^{1}HNMR ($CDCl_3$, 700 MHz): δ 8.54 (d, *J* = 5.1 Hz, 1H), 7.65 – 7.60 (m, 2H), 7.47 (t, *J* = 7.5 Hz,

2H), 7.45 – 7.39 (m, 2H), 7.32 – 7.27 (m, 3H), 7.21 – 7.17 (m, 3H), 2.62 – 2.55 (m, 1H), 2.38 – 2.33 (m, 1H), 1.86 – 1.81 (m, 1H), 1.51 (ddd, *J* = 8.6, 6.0, 4.8 Hz, 1H). ^{13}C NMR (176 MHz, $CDCl_3$): δ 161.95, 150.17, 148.69, 142.62, 138.80, 129.37, 129.22, 128.73, 127.35, 126.23, 126.17, 120.40, 119.20, 29.99, 28.52, 19.27. HRMS (ESI) m/z $[M + H]^+$ calcd for: $C_{20}H_{17}N$: 272.1438; found: 272.1437. IR (neat): v = 3025, 1949, 1594, 1545, 1496, 1473, 1457, 1415, 1371, 1191, 1076.

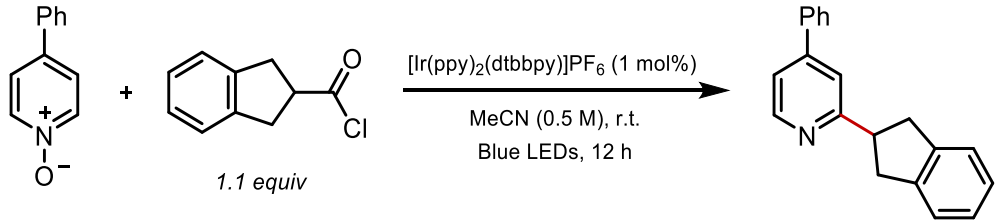

2-(2,3-dihydro-1H-inden-2-yl)-4-phenylpyridine (12)

The reaction was run according to General Procedure A and was purified by column chromatography (0% to 15% ethyl acetate in hexanes) to afford the title compound (93 mg, 43%) as a pale yellow solid and 4-phenylpyridine (44 mg, 35%). R_f = 0.50 (ethyl acetate/hexanes 1:4; UV). ^{1}HNMR ($CDCl_3$, 500 MHz): δ 8.62 (d, *J* = 5.1 Hz, 1H), 7.62 (d, *J* = 8.0 Hz, 2H), 7.50 – 7.45 (m, 3H), 7.43 (t, *J* = 7.3 Hz, 1H), 7.36 (dd, *J* = 5.1, 1.5 Hz, 1H), 7.28 – 7.26 (m, 2H), 7.21 – 7.17 (m, 2H), 3.95 (p, *J* = 8.8 Hz, 1H), 3.43 (dd, *J* = 15.7, 8.5 Hz, 2H), 3.35 (dd, *J* = 15.7, 9.1 Hz, 2H). ^{13}C NMR (176 MHz, $CDCl_3$): δ 165.14, 149.96, 149.16, 143.03, 138.84, 129.36, 129.23, 127.35, 126.78, 124.66, 119.96, 119.83, 47.85, 40.06. HRMS (ESI) m/z $[M + H]^+$ calcd for: $C_{20}H_{17}N$: 272.1437; found: 272.1434. IR (neat): v = 3036, 3019, 1596, 1543, 1471, 1401.

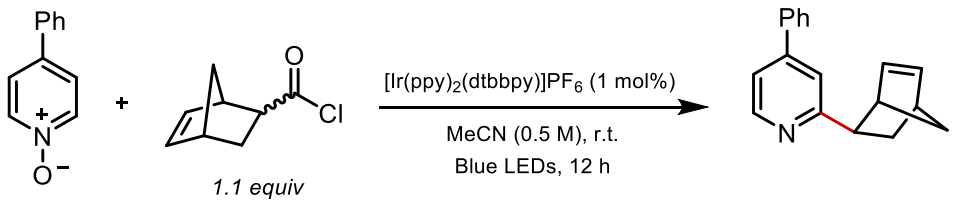

2-(bicyclo[2.2.1]hept-5-en-2-yl)-4-phenylpyridine (114)

The reaction was run according to General Procedure A and was purified by column chromatography (0% to 15% ethyl acetate in hexanes) to afford the title compound (55 mg, 28%) as a colorless oil and 4-phenylpyridine (59 mg, 48%). R_f = 0.53 (ethyl acetate/hexanes 1:4; UV). ^{1}HNMR ($CDCl_3$, 700 MHz): δ 8.58 (d, *J* = 5.1 Hz, 1H), 7.63 (d, *J* = 7.8 Hz, 2H), 7.48 (t, *J* = 7.5 Hz, 2H), 7.45 – 7.42 (m, 2H), 7.32 – 7.29 (m, 1H), 6.28 (dd, *J* = 5.4, 3.0 Hz, 1H), 6.22 (dd, *J* = 5.3, 2.8 Hz, 1H), 3.03 (d, *J* = 10.9 Hz, 2H), 2.90 (dd, *J* = 8.7, 4.5 Hz, 1H), 2.14 (dt, *J* = 11.7, 4.0 Hz, 1H), 1.81 (d, *J* = 8.3 Hz, 1H), 1.65 – 1.61 (m, 1H), 1.42 (d, *J* = 8.2 Hz, 1H). ^{13}C NMR (176 MHz, $CDCl_3$): δ 165.98, 149.71, 148.88, 139.11, 138.38, 137.33, 129.37, 129.16, 127.41, 120.92, 119.36, 49.03, 46.70, 46.00, 42.66, 32.59. HRMS (ESI) m/z $[M + H]^+$ calcd for: $C_{18}H_{17}N$: 248.1437; found: 248.1436. IR (neat): v = 3057, 2937, 2864, 1787, 1594, 1544, 1497, 1470, 1397, 1342, 1303, 1254, 1173.

2D NMR Data COSY, HSQC, HMBC, and NOESY experiments were employed to assign various resonances and confirm the structure of the resultant *endo*-product.

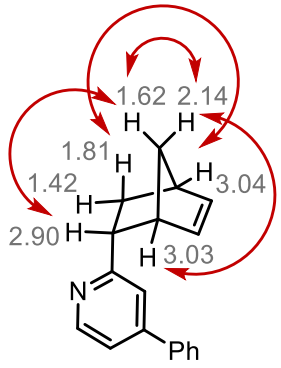

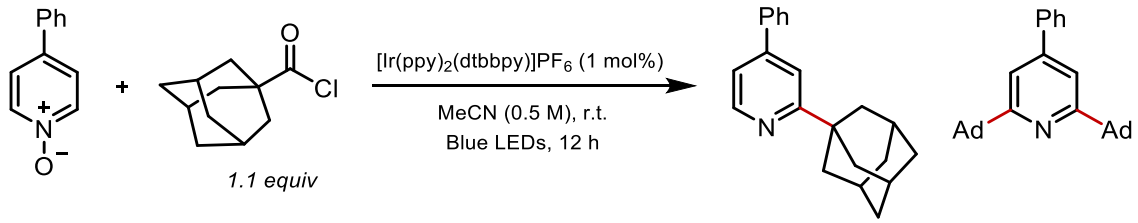

2-adamantyl-4-phenylpyridine and 2,6-diadamantyl-4-phenylpyridine (13)

The reaction was run according to General Procedure A and was purified by column chromatography (0% to 15% ethyl acetate in hexanes) to afford 2-adamantyl-4-phenylpyridine (97 mg, 42%) and 2,6-diadamantyl-4-phenylpyridine (41 mg, 12%) as white solids. In addition, 4-phenylpyridine (43 mg, 10%) was recovered.

2-adamantyl-4-phenylpyridine: R_f = 0.50 (ethyl acetate/hexanes 1:4; UV). ^{1}HNMR ($CDCl_3$, 700 MHz): δ 8.63 (d, *J* = 5.0 Hz, 1H), 7.63 (d, *J* = 7.3 Hz, 2H), 7.48 (dd, *J* = 9.2, 5.8 Hz, 3H), 7.42 (t, *J* = 7.3 Hz, 1H), 7.30 (dd, *J* = 5.0, 1.5 Hz, 1H), 2.14 (s, 3H), 2.07 (d, *J* = 2.2 Hz, 6H), 1.82 (d, *J* = 12.8 Hz, 6H). ^{13}C NMR (176 MHz, $CDCl_3$): δ 169.91, 149.50, 148.98, 139.50, 129.30, 129.01, 127.42, 119.25, 117.38, 42.32, 39.40, 37.15, 29.15. HRMS (ESI) m/z $[M + H]^+$ calcd for: $C_{21}H_{23}N$: 290.1903; found: 290.1905. IR (neat): v = 3056, 2899, 2846, 1591, 1547, 1467, 1450, 1392, 1320, 1101.

2,6-diadamantyl-4-phenylpyridine: R_f = 0.78 (ethyl acetate/hexanes 1:4; UV). ^{1}HNMR ($CDCl_3$, 700 MHz): δ 7.61 (d, *J* = 7.9 Hz, 2H), 7.45 (t, *J* = 7.6 Hz, 2H), 7.39 (t, *J* = 7.3 Hz, 1H), 7.21 (s, 2H), 2.13 (d, *J* = 19.2 Hz, 6H), 2.06 (d, *J* = 1.8 Hz, 12H), 1.79 (d, *J* = 12.1 Hz, 12H). ^{13}C NMR (176 MHz, $CDCl_3$): δ 168.29, 148.94, 140.84, 129.14, 128.51, 127.59, 114.09, 42.41, 39.70, 37.39, 29.31. HRMS (ESI) m/z $[M + H]^+$ calcd for: $C_{31}H_{37}N$: 424.2999; found: 424.2999. IR (neat): v = 3057, 2899, 2847, 1592, 1549, 1495, 1449, 1402, 1342, 1314, 1100.

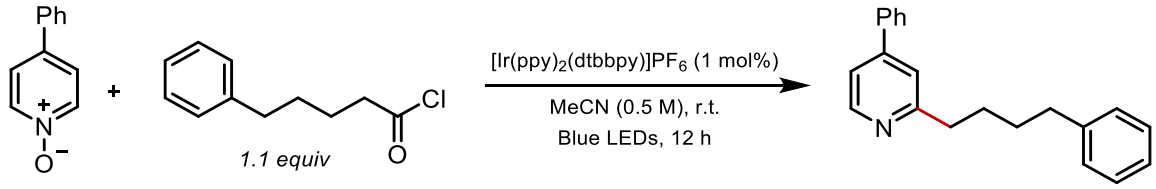

4-phenyl-2-(4-phenylbutyl)pyridine (4)

The reaction was run according to General Procedure A and was purified by column chromatography (0% to 15% ethyl acetate in hexanes) to afford the title compound (64 mg, 28%)

as a pale yellow oil and 4-phenylpyridine (51 mg, 41%). R_f = 0.39 (ethyl acetate/hexanes 1:4; UV). ^{1}HNMR ($CDCl_3$, 500 MHz): δ 8.57 (d, *J* = 5.1 Hz, 1H), 7.62 (d, *J* = 7.3 Hz, 2H), 7.51 – 7.39 (m, 3H), 7.36 – 7.29 (m, 2H), 7.34 – 7.26 (m, 2H), 7.20 – 7.14 (m, 3H), 2.88 (t, *J* = 7.7 Hz, 2H), 2.67 (t, *J* = 7.6 Hz, 2H), 1.88 – 1.78 (m, 2H), 1.76 – 1.70 (m, 2H). ^{13}C NMR (126 MHz, $CDCl_3$): δ 162.94, 149.89, 149.12, 142.81, 138.80, 129.35, 129.22, 128.74, 128.59, 127.36, 125.98, 121.02, 119.46, 38.63, 36.14, 31.54, 29.91. HRMS (ESI) m/z $[M + H]^+$ calcd for: $C_{21}H_{21}N$: 288.1747; found: 288.1746. IR (neat): v = 3024, 2926, 2855, 1596, 1546, 1495, 1473, 1452, 1399.

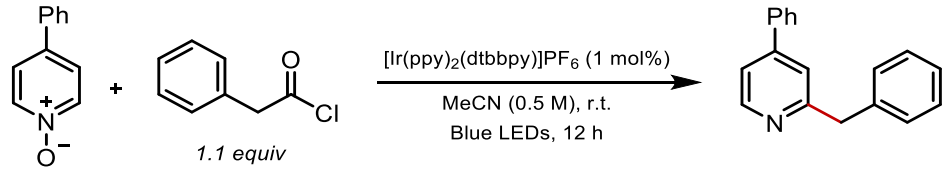

2-benzyl-4-phenylpyridine (5)

The reaction was run according to General Procedure A and was purified by column chromatography (0% to 15% ethyl acetate in hexanes) to afford the title compound (29 mg, 15%) as a pale yellow oil and 4-phenylpyridine (91 mg, 73%). R_f = 0.42 (ethyl acetate/hexanes 1:4; UV). ^{1}HNMR ($CDCl_3$, 500 MHz): δ 8.60 (d, *J* = 5.5 Hz, 1H), 7.57 (d, *J* = 7.1 Hz, 2H), 7.44 (dt, *J* = 14.0, 7.0 Hz, 3H), 7.34 - 7.31 (m, 6H), 7.23 (dd, *J* = 8.5, 4.3 Hz, 1H), 4.22 (s, 2H). ^{13}C NMR (126 MHz, $CDCl_3$): δ 161.80, 150.11, 149.37, 139.81, 138.72, 129.45, 129.36, 129.27, 128.96, 127.37, 126.76, 121.44, 119.76, 45.14. HRMS (ESI) m/z $[M + H]^+$ calcd for: $C_{18}H_{15}N$: 246.1277; found: 246.1279. The acquired ^{1}H and ^{13} CNMR spectra were identical to those reported in the literature.[19]

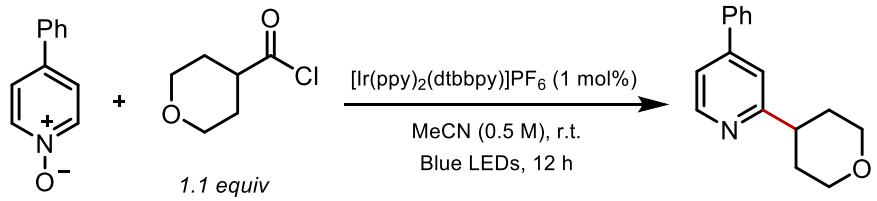

4-phenyl-2-(tetrahydro-2H-pyran-4-yl)pyridine (18)

The reaction was run according to General Procedure A and was purified by column chromatography (0% to 15% ethyl acetate in hexanes) to afford the title compound (71 mg, 37%) as a colorless oil and 4-phenylpyridine (55 mg, 44%). R_f = 0.64 (ethyl acetate/hexanes 1:4; UV). ^{1}H NMR (500 MHz, Chloroform-*d*) δ 8.59 (d, *J* = 5.1 Hz, 1H), 7.63 (dd, *J* = 7.4, 1.7 Hz, 2H), 7.52 – 7.41 (m, 3H), 7.38 (s, 1H), 7.35 (dd, *J* = 5.1, 1.7 Hz, 1H), 4.12 (dt, *J* = 11.3, 3.0 Hz, 2H), 3.58 (td, *J* = 11.4, 3.0 Hz, 2H), 3.02 (td, *J* = 11.1, 5.5 Hz, 1H), 2.02 – 1.92 (m, 4H). ^{13}C NMR (126 MHz, $CDCl_3$) δ 164.89, 149.65, 149.04, 138.55, 129.05, 128.93, 127.02, 119.61, 118.83, 68.14, 43.57, 32.53. HRMS (ESI) m/z $[M + H]^+$ calcd for: $C_{16}H_{17}NO$: 240.1383; found: 240.1384. IR (neat): v = 2947, 2839, 1937, 1594, 1546, 1472, 1443, 1384, 1357, 1237, 1124, 1084.

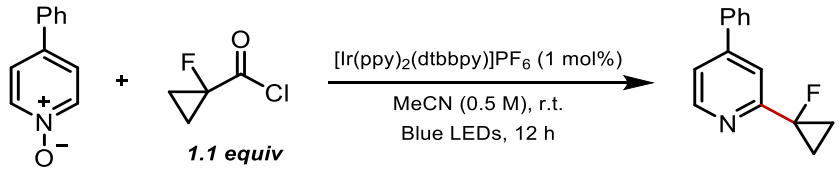

2-(1-fluorocyclopropyl)-4-phenylpyridine (22)

The reaction was run according to General Procedure A and was purified by column chromatography (0% to 15% ethyl acetate in hexanes) to afford the title compound (56 mg, 33%) as a colorless oil and 4-phenylpyridine (66 mg, 52%). R_f = 0.63 (ethyl acetate/hexanes 1:4; UV). ^{1}H NMR (500 MHz, $CDCl_3$) δ 8.51 (d, *J* = 5.1 Hz, 1H), 7.85 (s, 1H), 7.71 – 7.66 (m, 2H), 7.52 – 7.42 (m, 3H), 7.35 (dd, *J* = 5.2, 1.7 Hz, 1H), 1.54 – 1.47 (m, 4H). ^{13}C NMR (126 MHz, $CDCl_3$) δ 160.03,

159.83, 149.56, 148.77, 138.33, 129.05, 127.09, 119.56, 116.76, 80.29 (d, *J* = 214.1 Hz), 15.50, 15.41. ^{19}F NMR (470 MHz, $CDCl_3$) δ -193.55 (s). HRMS (ESI) m/z $[M + H]^+$ calcd for: $C_{14}H_{12}FN$: 214.1027; found: 214.1025. IR (neat): v = 3086, 3011, 2925, 1594, 1552, 1501, 1473, 1436, 1339, 1302, 1248, 1142, 1105.

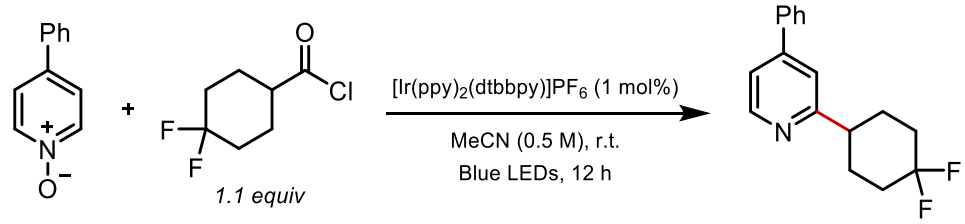

2-(4,4-difluorocyclohexyl)-4-phenylpyridine (21)

The reaction was run according to General Procedure A and was purified by column chromatography (0% to 15% ethyl acetate in hexanes) to afford the title compound (105 mg, 48%) as a colorless oil and 4-phenylpyridine (38 mg, 31%). R_f = 0.69 (ethyl acetate/hexanes 1:4; UV). ^{1}H NMR (500 MHz, Chloroform-*d*) δ 8.58 (d, *J* = 5.1 Hz, 1H), 7.62 (d, *J* = 7.5 Hz, 2H), 7.46 (dt, *J* = 24.1, 7.3 Hz, 3H), 7.40 – 7.32 (m, 2H), 2.90 – 2.85 (m, 1H), 2.31 – 2.18 (m, 2H), 2.14 – 2.04 (m, 2H), 2.04 – 1.92 (m, 3H), 1.90 – 1.84 (m, 1H). ^{13}C NMR (126 MHz, $CDCl_3$) δ 164.40, 149.60, 149.12, 138.42, 129.70, 128.99, 127.02, 123.13 (dd, *J* = 242.3, 239.7 Hz), 119.75, 118.88, 44.35, 33.77 (dd, *J* = 25.6, 22.8 Hz), 28.86 (d, *J* = 9.8 Hz). ^{19}F NMR (470 MHz, $CDCl_3$) δ -91.79 (d, *J* = 235.9 Hz), -101.70 (d, *J* = 236.5 Hz). HRMS (ESI) m/z $[M + H]^+$ calcd for: $C_{17}H_{17}F_2N$: 274.1402; found: 274.1400. IR (neat): v = 2936, 1723, 1595, 1547, 1472, 1447, 1372, 1269, 1097.

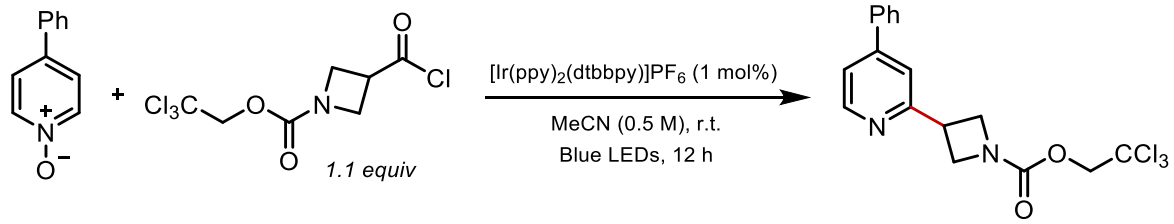

2,2,2-trichloroethyl 3-(4-phenylpyridin-2-yl)azetidine-1-carboxylate (19)

The reaction was run according to General Procedure A and was purified by column chromatography (20% to 50% ethyl acetate in hexanes) to afford the title compound (83 mg, 27%) as a colorless oil and 4-phenylpyridine (60 mg, 48%). R_f = 0.53 (ethyl acetate/hexanes 1:1; UV). ^{1}H NMR (500 MHz, Chloroform-*d*) δ 8.67 (d, *J* = 5.0 Hz, 1H), 7.62 (d, *J* = 7.0 Hz, 2H), 7.52 – 7.43 (m, 3H), 7.43 – 7.39 (m, 2H), 4.84 – 4.63 (m, 2H), 4.56 – 4.34 (m, 4H), 4.05 (tt, *J* = 8.8, 6.3 Hz, 1H). ^{13}C NMR (126 MHz, $CDCl_3$) δ 160.52, 154.35, 150.31, 149.23, 138.00, 129.19, 129.14, 127.00, 120.31, 119.89, 95.67, 74.55, 55.56, 54.91, 35.66. HRMS (ESI) m/z $[M + H]^+$ calcd for: $C_{17}H_{15}Cl_3N_2O_2$: 385.0272; found: 385.0274. IR (neat): v = 2951, 2884, 1718, 1596, 1547, 1401, 1349, 1126, 1059.

Note: See following page for synthesis of carboxylic acid starting material.

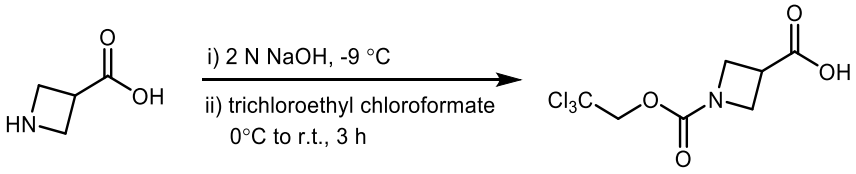

1-((2,2,2-trichloroethoxy)carbonyl)azetidine-3-carboxylic acid (19S)

Azetidine-3-carboxylic acid (1 g, 10 mmol) was placed in a round bottom flask equipped with a magnetic stir bar, dissolved in 15 mL of 2.0 N aqueous NaOH solution, and cooled to -10 ^{o}C. 2,2,2-Trichloroethyl chloroformate (1.4 mL, 11 mmol) was then added dropwise to the stirred solution at 0 ^{o}C. The mixture was stirred for 1 h at 0 ^{o}C and an additional 2 h at r.t. After the reaction, the mixture was extracted with diethyl ether (3 x 10 mL) and the aqueous phase was acidified to pH 2 with 2 N HCl. The aqueous phase was extracted with ethyl acetate (4 x 20 mL), and the combined ethyl acetate extracts were washed with brine, dried with Na_2SO_4, and concentrated

to yield the desired product (2.4 g, 87%) as a white solid. ^{1}H NMR (700 MHz, Chloroform-*d*) δ 10.63 (s, 1H), 4.71 (d, *J* = 11.4 Hz, 2H), 4.31 (d, *J* = 34.4 Hz, 4H), 3.51 (p, *J* = 7.5 Hz, 1H). ^{13}C NMR (176 MHz, $CDCl_3$) δ 176.67, 153.46, 94.73, 73.96, 51.15 (d, *J* = 111.6 Hz), 31.79. HRMS (ESI) m/z $[M + H]^+$ calcd for: $C_7H_8Cl_3NO_4$: 275.9592; found: 275.9597. IR (neat): v = 2967, 2901, 2632, 1724, 1699, 1425, 1413, 1338, 1279, 1235, 1126.

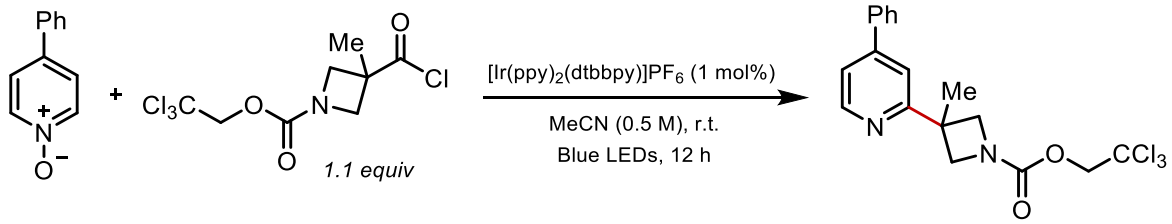

2,2,2-trichloroethyl 3-methyl-3-(4-phenylpyridin-2-yl)azetidine-1-carboxylate (20)

The reaction was run according to General Procedure A and was purified by column chromatography (20% to 50% ethyl acetate in hexanes) to afford the title compound (138 mg, 43%) as a colorless oil and 4-phenylpyridine (50 mg, 40%). R_f = 0.57 (ethyl acetate/hexanes 1:1; UV). ^{1}H NMR (500 MHz, Chloroform-*d*) δ 8.63 (d, *J* = 4.9, 1.1 Hz, 1H), 7.64 – 7.59 (m, 2H), 7.52 – 7.43 (m, 3H), 7.41 – 7.37 (m, 2H), 4.79 – 4.66 (m, 2H), 4.64 – 4.53 (m, 2H), 4.17 – 4.04 (m, 2H), 1.76 (s, 3H). ^{13}C NMR (126 MHz, $CDCl_3$) δ 164.68, 154.58, 149.73, 149.76, 149.34, 138.23, 129.17, 127.05, 119.87, 117.63, 95.71, 74.59 – 74.46 (m), 61.25, 60.50, 40.57, 27.31. HRMS (ESI) m/z $[M + H]^+$ calcd for: $C_{18}H_{17}Cl_3N_2O_2$: 399.0428; found: 399.0436. IR (neat): v = 2965, 2876, 1727, 1595, 1541, 1447, 1418, 1362, 1194, 1152, 1109.

Note: See following page for synthesis of carboxylic acid starting material.

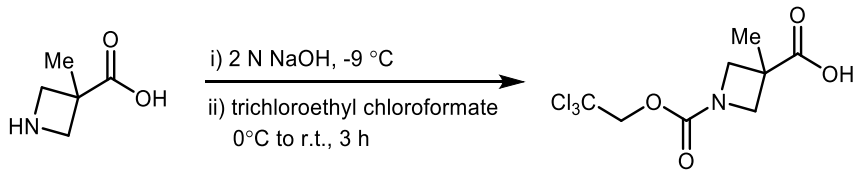

3-methyl-1-((2,2,2-trichloroethoxy)carbonyl)azetidine-3-carboxylic acid (20S)

3-Methylazetidine-3-carboxylic acid (0.5 g, 4.34 mmol) was placed in a round bottom flask equipped with a magnetic stir bar, dissolved in 6.5 mL of 2.0 N aqueous NaOH solution, and cooled to -9 ^{o}C. 2,2,2-Trichloroethyl chloroformate (0.6 mL, 4.77 mmol) was then added dropwise to the stirred solution at 0 ^{o}C. The mixture was stirred for 1 h at 0 ^{o}C and an additional 2 h at r.t. After the reaction, the mixture was extracted with diethyl ether (3 x 10 mL) and the aqueous phase was acidified to pH 2 with 2 N HCl. The aqueous phase was extracted with ethyl acetate (4 x 20 mL), and the combined ethyl acetate extracts were washed with brine, dried with Na_2SO_4, and concentrated to yield the desired product (1.1 g, 84%) as a white solid. ^{1}H NMR (700 MHz, Chloroform-*d*) δ 10.31 (s, 1H), 4.71 (d, *J* = 13.7 Hz, 2H), 4.43 (d, *J* = 42.7 Hz, 2H), 3.88 (d, *J* = 33.7 Hz, 2H), 1.62 (s, 3H). ^{13}C NMR (176 MHz, $CDCl_3$) δ 178.96, 153.68, 94.80, 73.95, 57.76 (d, *J* = 119.2 Hz), 38.61, 21.62. HRMS (ESI) m/z $[M + H]^+$ calcd for: $C_8H_{10}Cl_3NO_4$: 289.9752; found: 289.9748. IR (neat): v = 2968, 2895, 2582, 1723, 1964, 1466, 1434, 1414, 1358, 1317, 1302, 1227, 1187, 1139.

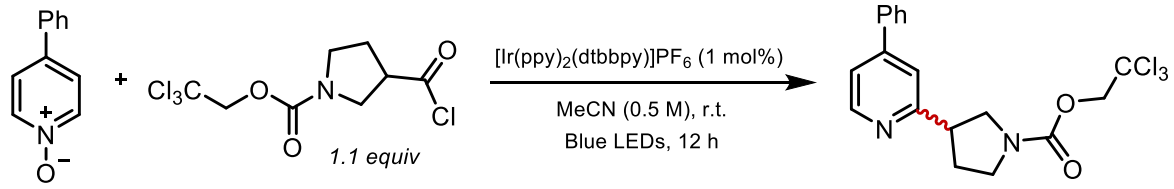

2,2,2-trichloroethyl 1-(4-phenylpyridin-2-yl)pyrrolidine-3-carboxylate

The reaction was run according to General Procedure A and was purified by column chromatography (10% acetone in dichloromethane) to afford the title compound (42 mg, 13%)

as a colorless oil and 4-phenylpyridine (77 mg, 62%). R_f = 0.65 (10% acetone/dichloromethane; UV). ^{1}H NMR (500 MHz, Chloroform-*d*) (50:50 mixture of rotamers) δ 8.63 – 8.58 (m, 1H), 7.62 (d, *J* = 7.5 Hz, 2H), 7.57 – 7.42 (m, 3H), 7.42 – 7.36 (m, 2H), 4.85 – 4.70 (m, 2H), 4.00 (ddd, *J* = 18.3, 10.9, 7.8 Hz, 1H), 3.86 – 3.70 (m, 2H), 3.70 – 3.52 (m, 2H), 2.43 – 2.27 (m, 2H). ^{13}C NMR (126 MHz, $CDCl_3$) (50:50 mixture of rotamers) δ 160.79, 160.61, 152.89, 152.86, 150.00, 149.97, 149.94, 149.22, 149.17, 138.13, 129.13, 127.02, 120.22, 120.16, 120.10, 120.01, 119.95, 95.86, 95.78, 74.86, 74.83, 51.62, 51.23, 46.48, 46.19, 45.99, 45.35, 32.14, 31.48. HRMS (ESI) m/z [M + H]$^+$ calcd for: $C_{18}H_{17}Cl_3N_2O_2$: 289.9748; found: 289.9748. IR (neat): v = 2949, 2881, 1713, 1595, 1547, 1473, 1410, 1352, 1333, 1174, 1122, 1057.

Note: See following page for synthesis of carboxylic acid starting material.

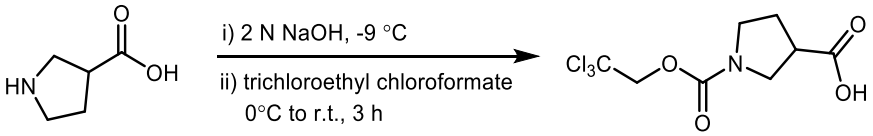

1-((2,2,2-trichloroethoxy)carbonyl)pyrrolidine-3-carboxylic acid

Pyrrolidine-3-carboxylic acid (1 g, 8.7 mmol) was placed in a round bottom flask equipped with a magnetic stir bar, dissolved in 13 mL of 2.0 N aqueous NaOH solution, and cooled to -9 ^{o}C. 2,2,2-Trichloroethyl chloroformate (1.2 mL, 9.57 mmol) was then added dropwise to the stirred solution at 0 ^{o}C. The mixture was stirred for 1 h at 0 ^{o}C and an additional 2 h at r.t. After the reaction, the mixture was extracted with diethyl ether (3 x 10 mL) and the aqueous phase was acidified to pH 2 with 2 N HCl. The aqueous phase was extracted with ethyl acetate (4 x 20 mL), and the combined ethyl acetate extracts were washed with brine, dried with Na_2SO_4, and concentrated to yield the desired product (2.3 g, 90%) as a white solid. ^{1}H NMR (700 MHz, Chloroform-*d*) δ 10.37 (s, 1H), 4.80 – 4.69 (m, 2H), 3.76 (dd, *J* = 21.7, 6.9 Hz, 2H), 3.69 – 3.48 (m,

2H), 3.17 (dp, *J* = 22.1, 7.5 Hz, 1H), 2.25 (tt, *J* = 14.2, 7.2 Hz, 2H). ^{13}C NMR (176 MHz, $CDCl_3$) δ 177.58, 177.48, 152.15, 152.09, 94.95, 94.92, 74.31, 47.73, 47.16, 45.10, 44.62, 42.26, 41.46, 28.08, 27.40. HRMS (ESI) m/z $[M + H]^+$ calcd for: $C_8H_{10}Cl_3NO_4$: 275.9592; found: 275.9597. IR (neat): v = 3184, 2899, 1721, 1696, 1450, 1426, 1367, 1345, 1295, 1282, 1245, 1198, 1131.

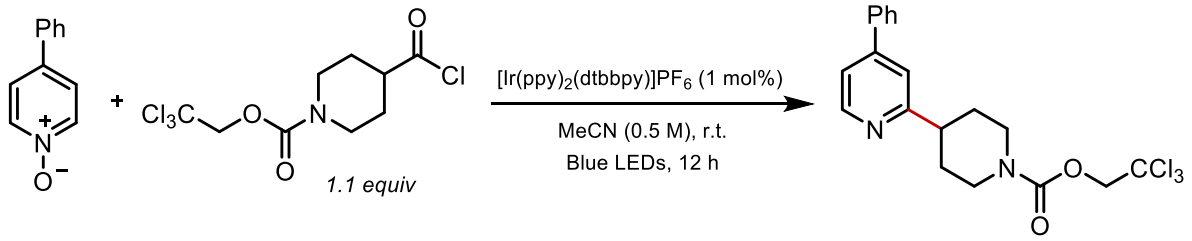

2,2,2-trichloroethyl 4-(4-phenylpyridin-2-yl)piperidine-1-carboxylate (15)

The reaction was run according to General Procedure A and was purified by column chromatography (20% to 50% ethyl acetate in hexanes) to afford the title compound (331 mg, 36%) as a colorless oil and 4-phenylpyridine (52 mg, 42%). R_f = 0.55 (ethyl acetate/hexanes 1:1; UV). ^{1}H NMR (500 MHz, Chloroform-*d*) δ 8.58 (d, *J* = 5.3 Hz, 1H), 7.64 – 7.59 (m, 2H), 7.46 (dt, *J* = 23.5, 7.4 Hz, 4H), 7.36 (d, *J* = 3.8 Hz, 2H), 4.77 (s, 2H), 4.45 – 4.35 (m, 3H), 3.07 (t, *J* = 13.2 Hz, 1H), 2.99 (td, *J* = 12.0, 6.1 Hz, 2H), 2.08 – 2.01 (m, 3H), 1.87 (qd, *J* = 12.7, 4.3 Hz, 3H). ^{13}C NMR (126 MHz, $CDCl_3$) δ 164.33, 153.39, 149.72 (d, *J* = 6.0 Hz), 149.16, 138.39, 129.09, 129.03, 127.01, 119.79 (d, *J* = 10.4 Hz), 119.01 (d, *J* = 10.3 Hz), 95.75, 75.21 – 75.01 (m), 44.62 (d, *J* = 15.6 Hz), 44.36, 31.59 (d, *J* = 26.1 Hz). HRMS (ESI) m/z $[M + H]^+$ calcd for: $C_{19}H_{19}Cl_3N_2O_2$: 413.0585; found: 413.0589. IR (neat): v = 2747, 1706, 1594, 1548, 1468 1428, 1273, 1213, 1125.

Note: See following page for synthesis of carboxylic acid starting material.

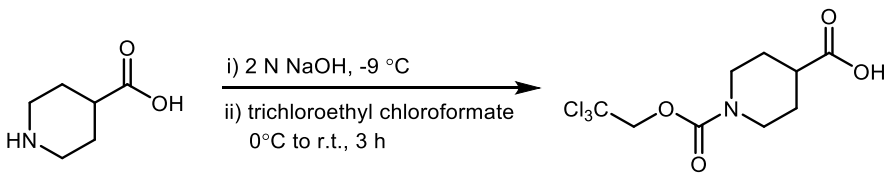

1-((2,2,2-trichloroethoxy)carbonyl)piperidine-4-carboxylic acid (15S)

Piperidine-4-carboxylic acid (1 g, 7.0 mmol) was placed in a round bottom flask equipped with a magnetic stir bar, dissolved in 10 mL of 2.0 N aqueous NaOH solution, and cooled to -9 ºC. 2,2,2-Trichloroethyl chloroformate (1 mL, 7.7 mmol) was then added dropwise to the stirred solution at 0 ºC. The mixture was stirred for 1 h at 0 ºC and an additional 2 h at r.t. After the reaction, the mixture was extracted with diethyl ether (3 x 10 mL) and the aqueous phase was acidified to pH 2 with 2 N HCl. The aqueous phase was extracted with ethyl acetate (4 x 20 mL), and the combined ethyl acetate extracts were washed with brine, dried with Na_2SO_4, and concentrated to yield the desired product (2.0 g, 93%) as a white solid. ^{1}H NMR (700 MHz, Chloroform-*d*) δ 10.61 (s, 1H), 4.75 (d, *J* = 12.2 Hz, 2H), 4.21 – 4.05 (m, 2H), 3.18 – 2.92 (m, 2H), 2.58 (tt, *J* = 10.6, 4.0 Hz, 1H), 1.97 (d, *J* = 10.3 Hz, 2H), 1.73 (qd, *J* = 11.1, 4.2 Hz, 2H). ^{13}C NMR (176 MHz, $CDCl_3$) δ 180.43, 153.72, 95.98, 75.46, 43.79 (d, *J* = 18.9 Hz), 40.80, 27.91 (d, *J* = 41.1 Hz). HRMS (ESI) m/z [M + H]$^+$ calcd for: $C_9H_{12}Cl_3NO_4$: 303.9905; found: 303.9909. IR (neat): v = 3209, 2861, 1725, 1686, 1445, 1428, 1365, 1389, 1242, 1171, 1129.

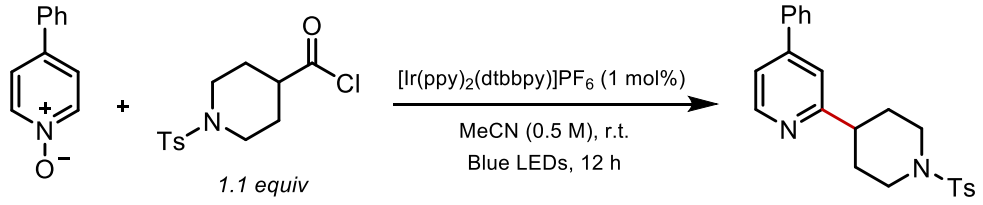

4-phenyl-2-(1-tosylpiperidin-4-yl)pyridine (16)

The reaction was run according to General Procedure A and was purified by column chromatography (20% to 50% ethyl acetate in hexanes) to afford the title compound (314 mg, 31%) as a colorless oil and 4-phenylpyridine (60 mg, 48%). R_f = 0.51 (ethyl acetate/hexanes 1:1; UV). ^{1}H NMR (500 MHz, Chloroform-*d*) δ 8.55 (d, *J* = 5.1 Hz, 1H), 7.69 (d, *J* = 7.9 Hz, 2H), 7.61 – 7.58 (m, 2H), 7.51 – 7.41 (m, 3H), 7.37 – 7.33 (m, 3H), 7.31 (s, 1H), 4.00 – 3.90 (m, 2H), 2.69 (tt, *J*

= 12.0, 3.9 Hz, 1H), 2.48 – 2.37 (m, 5H), 2.11 – 1.91 (m, 4H). ^{13}C NMR (126 MHz, $CDCl_3$) δ 164.07, 149.65 (d, *J* = 4.9 Hz), 149.13, 143.45, 138.34, 133.34, 129.63 (d, *J* = 8.3 Hz), 129.08, 127.73 (d, *J* = 7.2 Hz), 126.99, 119.83 (d, *J* = 9.3 Hz), 118.76 (d, *J* = 9.3 Hz), 46.52, 46.49, 43.65, 31.17, 21.53 (d, *J* = 7.2 Hz). HRMS (ESI) m/z $[M + H]^+$ calcd for: $C_{23}H_{24}N_2O_2S$: 393.1631; found: 393.1634. IR (neat): v = 2918, 2855, 1702, 1592, 1468, 1443, 1274, 1216, 1158, 1130, 1092.

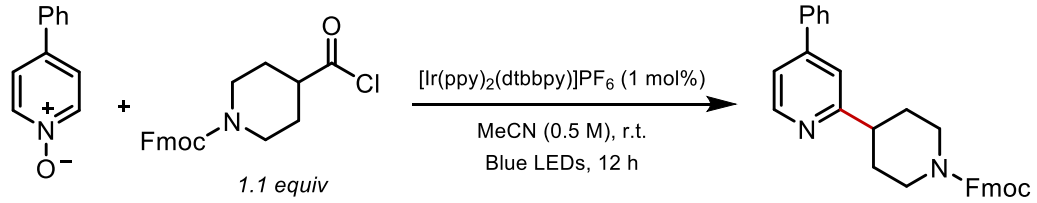

(9H-fluoren-9-yl)methyl 4-(4-phenylpyridin-2-yl)piperidine-1-carboxylate (17)

The reaction was run according to General Procedure A and was purified by column chromatography (20% to 50% ethyl acetate in hexanes) to afford the title compound (85 mg, 23%) as a colorless oil and 4-phenylpyridine (73 mg, 59%). R_f = 0.54 (ethyl acetate/hexanes 1:1; UV). ^{1}H NMR (500 MHz, Chloroform-*d*) δ 8.59 (d, *J* = 5.1 Hz, 1H), 7.76 (d, *J* = 7.5 Hz, 2H), 7.67 – 7.54 (m, 4H), 7.55 – 7.42 (m, 3H), 7.42 – 7.35 (m, 4H), 7.32 (t, *J* = 7.4 Hz, 2H), 4.44 (t, *J* = 4.5 Hz, 3H), 4.27 (t, *J* = 6.9 Hz, 2H), 2.96 (ddt, *J* = 12.2, 7.5, 3.7 Hz, 3H), 2.00 (d, *J* = 13.1 Hz, 2H), 1.79 (s, 2H). ^{13}C NMR (126 MHz, $CDCl_3$) δ 164.61, 155.21, 149.71, 149.69, 149.13, 144.13, 141.33, 138.46, 129.09, 129.01, 127.63, 127.03, 125.03, 119.95, 119.76, 119.01, 67.27, 47.42, 44.54, 44.37, 31.66. HRMS (ESI) m/z $[M + H]^+$ calcd for: $C_{31}H_{28}N_2O_2$: 461.2331; found: 461.2332. IR (neat): v = 3037, 2919, 2796, 2751, 1702, 1595, 1546, 1491, 1475, 1444, 1366, 1335, 1267, 1131.

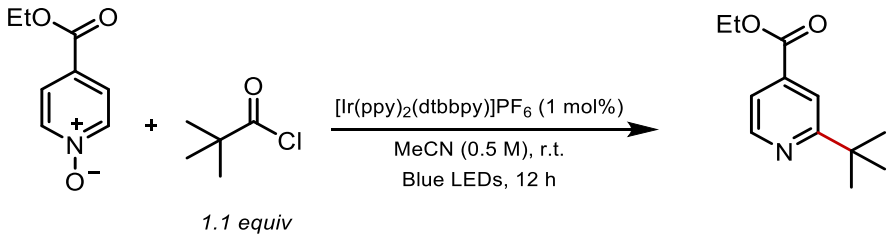

Ethyl 2-(*tert*-butyl)isonicotinate (24)

The reaction was run according to General Procedure A and the *N*-oxide substrate was prepared according to a reported procedure.[24] The crude product was purified by column chromatography (0% to 15% ethyl acetate in hexanes) to afford the title compound (124 mg, 75%) as a colorless oil. R_f = 0.71 (ethyl acetate/hexanes 1:4; UV). ^{1}H NMR (500 MHz, $CDCl_3$) δ 8.70 (d, *J* = 5.0 Hz, 1H), 7.89 (d, *J* = 1.5 Hz, 1H), 7.63 (dd, *J* = 4.9, 1.5 Hz, 1H), 4.41 (q, *J* = 7.2 Hz, 2H), 1.44 – 1.38 (m, 12H). ^{13}C NMR (126 MHz, $CDCl_3$) δ 170.52, 165.70, 149.29, 137.83, 119.80, 118.38, 61.61, 37.65, 30.09, 14.22. HRMS (ESI) m/z $[M + H]^+$ calcd for: $C_{12}H_{17}NO_2$: 208.1332; found: 208.1332. The acquired ^{1}H and ^{13} CNMR spectra were identical to those reported in the literature.[25]

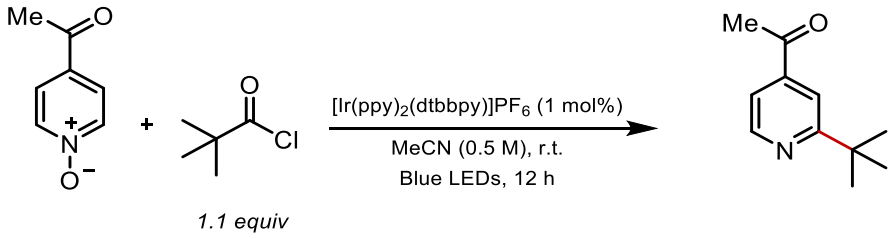

2-*tert*-butyl-4-acetylpyridine (25)

The reaction was run according to General Procedure A and the *N*-oxide substrate was prepared according to a reported procedure.[18] The crude product was purified by column chromatography (0% to 15% ethyl acetate in hexanes) to afford the title compound (74 mg, 52%) as a colorless oil. R_f = 0.5 (ethyl acetate/hexanes 1:4; UV). ^{1}H NMR (500 MHz, $CDCl_3$) δ 8.74 (d, *J* = 5.0 Hz, 1H), 7.77 (s, 1H), 7.55 – 7.48 (m, 1H), 2.62 (s, 3H), 1.39 (s, 9H). ^{13}C NMR (126

MHz, $CDCl_3$) δ 198.35, 171.30, 150.06, 143.55, 118.81, 116.79, 38.07, 30.45, 27.09. HRMS (ESI) m/z $[M + H]^+$ calcd for: $C_{11}H_{15}NO$: 178.1226; found: 178.1225. IR (neat): v = 2959, 2867, 1694, 1594, 1557, 1480, 1398, 1357, 1287, 1232, 1140, 1092.

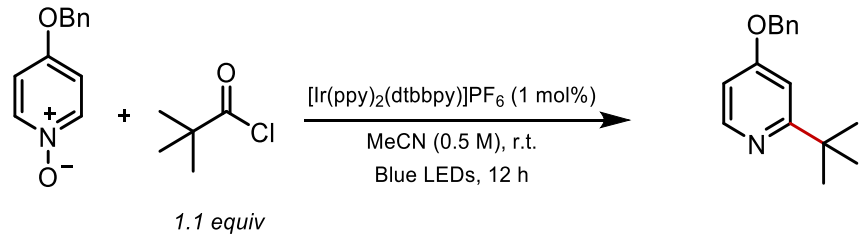

1.1 equiv

2-*tert*-butyl-4-benzyloxypyridine (27)

The reaction was run according to General Procedure A and the *N*-oxide substrate was prepared according to a reported procedure.[26] The crude product was purified by column chromatography (0% to 15% ethyl acetate in hexanes) to afford the title compound (147 mg, 76%) as a colorless oil. R_f = 0.45 (ethyl acetate/hexanes 1:4; UV). ^1H NMR (700 MHz, $CDCl_3$) δ 8.41 (d, *J* = 5.6 Hz, 1H), 7.47 – 7.31 (m, 5H), 6.93 (s, 1H), 6.72 – 6.67 (m, 1H), 5.09 (s, 2H), 1.34 (s, 9H). ^{13}C NMR (176 MHz, $CDCl_3$) δ 171.44, 165.44, 150.32, 136.22, 129.03, 128.65, 127.93, 107.20, 106.89, 70.01, 37.66, 30.41. HRMS (ESI) m/z $[M + H]^+$ calcd for: $C_{16}H_{19}NO$: 242.1539; found: 242.1541. IR (neat): v = 2954, 1701, 1592, 1560, 1495, 1478, 1453, 1416, 1378, 1361, 1290, 1227, 1205, 1129.

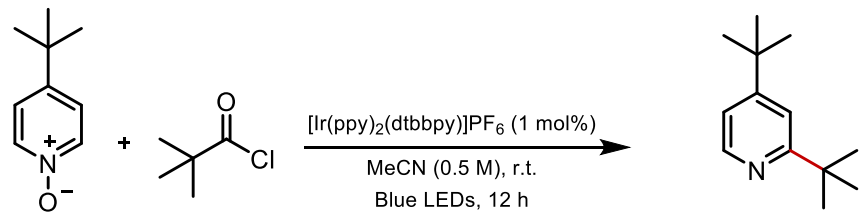

1.1 equiv

2,4-di-*tert*-butylpyridine (26)

The reaction was run according to General Procedure A on a 0.5 mmol scale and the *N*-oxide substrate was prepared according to a reported procedure.[18] The crude product was purified by column chromatography (0% to 30% ethyl acetate in hexanes) to afford the title compound (53 mg, 55%) as a colorless oil. R_f = 0.56 (ethyl acetate/hexanes 1:4; UV). ^{1}H NMR (700 MHz, $CDCl_3$) δ 8.47 (d, *J* = 5.6 Hz, 1H), 7.32 (d, *J* = 1.4 Hz, 1H), 7.08 (dd, *J* = 5.6, 1,4 Hz, 1H), 1.37 (s, 9H) 1.31 (s, 9H). ^{13}C NMR (176 MHz, $CDCl_3$) δ 168.98, 159.86, 148.32, 117.75, 115.68, 37.39, 34.74, 30.61, 30.28. HRMS (ESI) m/z $[M + H]^+$ calcd for: $C_{13}H_{21}N$: 192.1747; found: 192.1747. IR (neat): v = 2960, 2869, 1810, 1767, 1743, 1597, 1551, 1481, 1461, 1396, 1364, 1296, 1255, 1192, 1153, 1094, 1042, 1006, 940.

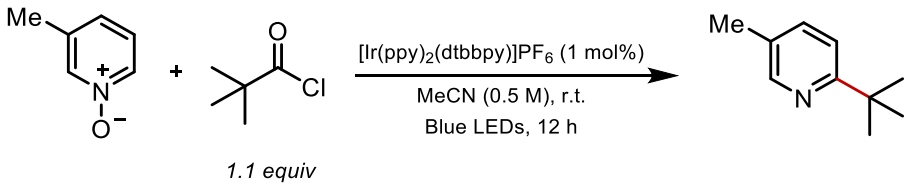

2-(*tert*-butyl)-5-methylpyridine- (28)

The reaction was run according to General Procedure A on a 0.5 mmol scale and the *N*-oxide substrate was purchased from ArkPharm and distilled under vacuum prior to use. Following the reaction, triethylamine (69 uL, 50.6 mg, 0.5 mmol) was added to the crude reaction mixture, and the crude reaction mixture was filtered through Celite. The mixture was then purified by column chromatography (0% to 60% ethyl acetate in hexanes) to afford the title compound (40 mg, 54%) as a colorless oil. R_f = 0.61 (ethyl acetate/hexanes 1:4; UV). ^{1}H NMR (700 MHz, $CDCl_3$) δ 8.40 (d, *J* = 2.3 Hz, 1H), 7.41 (dd, *J* = 8.2, 2.2 Hz, 1H), 7.23 (d, *J* = 8.1 Hz, 1H), 2.29 (s, 3H), 1.35 (s, 9H). ^{13}C NMR (176 MHz, $CDCl_3$) δ166.68, 149.25, 137.13, 130.10, 118.90, 30.59, 27.53, 18.30. HRMS (ESI) m/z $[M + H]^+$ calcd for: $C_{10}H_{16}N$: 150.1277; found: 150.1278. IR (neat): v = 2956, 2924, 2853, 1729, 1510, 1462, 1366, 1259, 1121, 1087, 1018, 909.

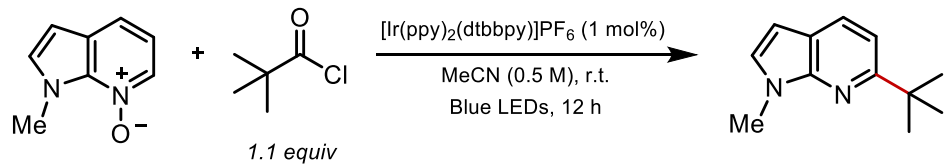

6-(*tert*-butyl)-1-methyl-1H-pyrrolo[2,3-*b*]pyridine (35)

The reaction was run according to General Procedure A and the *N*-oxide substrate was prepared according to a reported procedure.[27] The crude product was purified by column chromatography (0% to 15% ethyl acetate in hexanes) to afford the title compound (41 mg, 27%) as a colorless oil. R_f = 0.56 (ethyl acetate/hexanes 1:4; UV). ^{1}H NMR (500 MHz, $CDCl_3$) δ 8.27 (d, *J* = 5.0 Hz, 1H), 7.15 (d, *J* = 3.5 Hz, 1H), 6.97 (d, *J* = 5.1 Hz, 1H), 6.64 (d, *J* = 3.5 Hz, 1H), 3.89 (s, 3H), 1.49 (s, 9H). ^{13}C NMR (126 MHz, $CDCl_3$) δ 152.65, 148.31, 143.04, 127.25, 118.15, 112.03, 100.37, 35.81, 31.45, 30.28. HRMS (ESI) m/z $[M + H]^+$ calcd for: $C_{12}H_{16}N_2$: 189.1386; found: 189.1382. IR (neat): v = 2961, 1782, 1742, 1682, 1552, 1455, 1363, 1317, 1253.

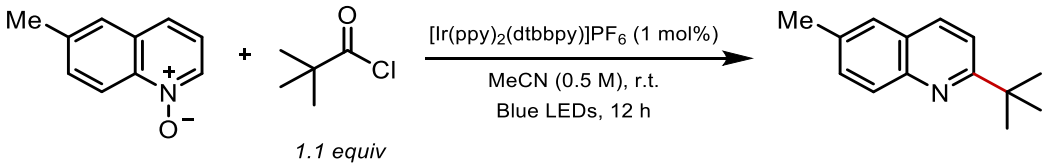

2-(*tert*-butyl)-6-methylquinoline- (31)

The reaction was run according to General Procedure A on a 0.5 mmol scale and the *N*-oxide substrate was prepared according to a reported procedure.[18] The crude product was purified by column chromatography (0% to 20% ethyl acetate in hexanes) to afford the title compound (49 mg, 49%) as a colorless oil. R_f = 0.64 (ethyl acetate/hexanes 1:4; UV). ^{1}H NMR (700 MHz, $CDCl_3$) δ 8.03 (d, *J* = 8.61 Hz, 1H), 7.60 (d, *J* = 9.2 Hz, 1H), 7.53- 7.49 (m, 2H), 7.36 (dd, *J* = 8.0 Hz, 1H), 2.81 (s, 3H), 1.47 (s, 9H). ^{13}C NMR (176 MHz, $CDCl_3$) δ167.76, 146.11, 137.37,

135.93, 128.96, 126.16, 125.28, 125.07, 117.71, 38.40, 30.20, 17.71.HRMS (ESI) m/z $[M + H]^+$ calcd for: $C_{14}H_{17}N$: 200.1434; found: 200.1435. IR (neat): v = 2954, 2923, 2864, 1616, 1599, 1568, 1501, 1460, 1427, 1362, 1310, 1276, 1147.

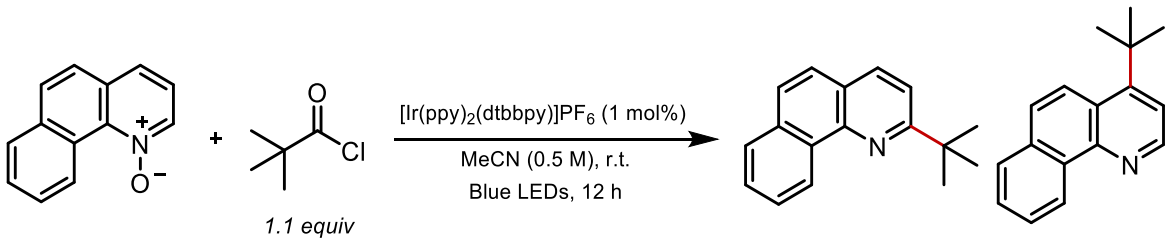

2-*tert*-butylbenzoquinoline (34a) and 4-*tert*-butylbenzoquinoline (34b)

The reaction was run according to General Procedure A and the *N*-oxide substrate was prepared according to a reported procedure.[18] The crude product was purified by column chromatography (0% to 15% ethyl acetate in hexanes) to afford 2-*tert*-butylbenzoquinoline (68 mg, 36%) and 4-*tert*-butylbenzoquinoline (19 mg, 10%) as colorless oils.

2-*tert*-butylbenzoquinoline (34a): R_f = 0.88 (ethyl acetate/hexanes 1:4; UV). ^{1}H NMR (700 MHz, $CDCl_3$) δ 9.40 (d, *J* = 8.1 Hz, 1H), 8.10 (d, *J* = 8.3 Hz, 1H), 7.88 (d, *J* = 7.8 Hz, 1H), 7.75 (d, *J* = 8.7 Hz, 1H), 7.73 – 7.68 (m, 1H), 7.69 – 7.64 (m, *J* = 10.5, 5.0 Hz, 2H), 7.62 (d, *J* = 8.3 Hz, 1H), 1.55 (s, 9H). ^{13}C NMR (176 MHz, $CDCl_3$) δ 168.35, 145.42, 136.07, 134.00, 132.25, 128.07, 127.95, 126.97, 126.97, 125.43, 124.94, 124.32, 118.56, 38.72, 30.77. HRMS (ESI) m/z $[M + H]^+$ calcd for: $C_{17}H_{17}N$: 236.1434; found: 236.1435. IR (neat): v = 2960, 1594, 1561, 1496, 1476, 1389, 1359, 1144, 1129.

4-*tert*-butylbenzoquinoline (34b): R_f = 0.67 (ethyl acetate/hexanes 1:4; UV). ^{1}H NMR (500 MHz, $CDCl_3$) δ 9.35 (d, *J* = 8.1 Hz, 1H), 8.90 (d, *J* = 4.8 Hz, 1H), 8.34 (d, *J* = 9.4 Hz, 1H), 7.89 (d, *J* = 7.5 Hz, 1H), 7.80 (d, *J* = 9.4 Hz, 1H), 7.74 – 7.65 (m, 2H), 7.51 (d, *J* = 4.8 Hz, 1H), 1.66 (s, 9H). ^{13}C NMR (126 MHz, $CDCl_3$) δ 155.97, 148.81, 147.87, 132.86, 132.79, 128.31, 127.58, 127.14, 126.23, 125.47, 125.37, 124.27, 119.24, 36.42, 31.76. HRMS (ESI) m/z $[M + H]^+$ calcd for: $C_{17}H_{17}N$:

236.1434; found: 236.1435. IR (neat): v = 2956, 2873, 1755, 1621, 1564, 1514, 1443, 1397, 1368, 1266, 1154, 1108.

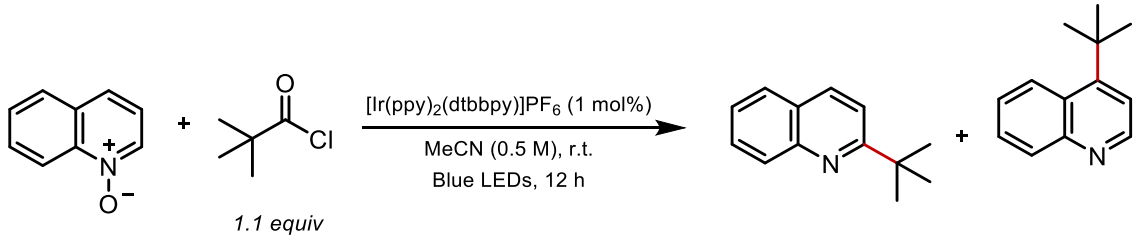

2-(tert-butyl)quinoline (29a) and 4-(tert-butyl)quinoline (29b)

The reaction was run according to General Procedure A and was purified by column chromatography (0% to 15% ethyl acetate in hexanes) to afford 2-(*tert*-butyl)quinoline (64 mg, 43%) and 4-(*tert*-butyl)quinoline (49 mg, 33%) as colorless oils. The acquired ^{1}H and ^{13} CNMR spectra were identical to those reported in the literature.[28]

2-(tert-butyl)quinoline (29a): R_f = 0.71 (ethyl acetate/hexanes 1:4; UV). ^{1}H NMR (700 MHz, $CDCl_3$): δ 8.09 – 8.04 (m, 2H), 7.76 (dd, *J* = 8.1, 1.4 Hz, 1H), 7.66 (ddd, *J* = 8.4, 6.9, 1.4 Hz, 1H), 7.52 (d, *J* = 8.7 Hz, 1H), 7.47 (ddd, *J* = 8.0, 6.9, 1.2 Hz, 1H), 1.47 (s, 9H). ^{13}C NMR (176 MHz, $CDCl_3$): δ 169.22, 147.42, 135.80, 129.41, 128.93, 127.18, 126.42, 125.58, 118.19, 38.11, 30.17, 30.13. HRMS (ESI) m/z $[M + H]^+$ calcd for: $C_{13}H_{15}N$: 186.1277; found: 186.1274.

4-(tert-butyl)quinoline (29b): R_f = 0.56 (ethyl acetate/hexanes 1:4; UV). ^{1}HNMR ($CDCl_3$, 700 MHz): δ 8.81 (d, *J* = 4.7 Hz, 1H), 8.41 (dd, *J* = 8.7, 1.3 Hz, 1H), 8.14 (dd, *J* = 8.4, 1.4 Hz, 1H), 7.67 (ddd, *J* = 8.2, 6.8, 1.3 Hz, 1H), 7.56 – 7.50 (m, 1H), 7.35 (d, *J* = 4.7 Hz, 1H), 1.62 (s, 9H). ^{13}C NMR (176 MHz, $CDCl_3$): δ 155.68, 150.21, 149.44, 131.14, 128.06, 127.08, 126.45, 125.10, 118.10, 36.10, 31.23. HRMS (ESI) m/z $[M + H]^+$ calcd for: $C_{13}H_{15}N$: 186.1277; found: 186.1274.

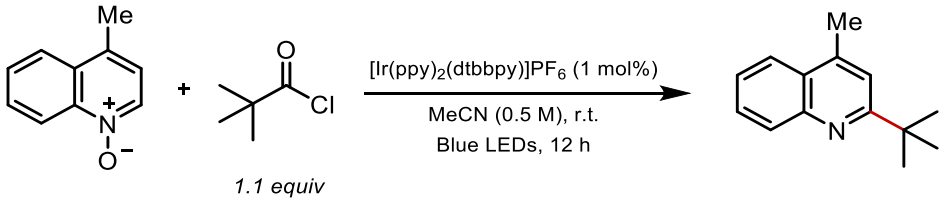

2-(*tert*-butyl)lepidine (30)

The reaction was run according to General Procedure A on a 0.5 mmol scale and the *N*-oxide substrate was prepared according to a reported procedure.[18] The crude product was purified by column chromatography (0% to 20% ethyl acetate in hexanes) to afford the title compound (21 mg, 21%) as a colorless oil. The reaction of lepidine N-oxide immediately discolors to a dark purple upon the addition of acyl chloride, this is believed to be due to a competing decomposition pathway. R_f = 0.68 (ethyl acetate/hexanes 1:4; UV). ^{1}H NMR (700 MHz, $CDCl_3$) δ 8.06 (d, *J* = 7.8 Hz, *1H*), 7.94 (d, *J* = 8.2 Hz, 1H), 7.66 (t, *J* = 6.9 Hz, 1H), 7.49 (t, *J* = 6.9 Hz, 1H), 7.35 (s, 1H), 2.69 (s, 3H), 1.46 (s, 9H). ^{13}C NMR (176 MHz, $CDCl_3$) δ 169.07, 147.43, 143.72, 130.09, 128.81, 126.67, 125.51, 123.52, 119.04, 38.06, 30.27, 19.12. HRMS (ESI) m/z $[M + H]^+$ calcd for: $C_{14}H_{17}N$: 200.1434; found: 200.1436. IR (neat): v = 3061, 2955, 2863, 1601, 1558, 1506, 1480, 1411, 1392, 1363, 1334, 1270, 1246, 1228, 1153, 1107, 1023, 932, 862, 810, 755, 709.

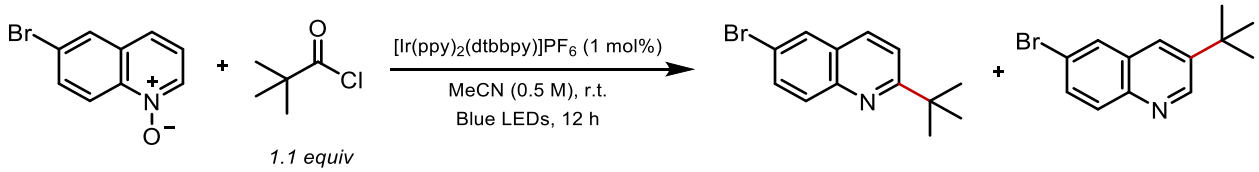

2-(*tert*-butyl)-6-bromoquinoline (32a) and 3-(*tert*-butyl)-6-bromoquinoline (32b)

The reaction was run according to General Procedure A on a 0.5 mmol scale and the *N*-oxide substrate was prepared according to a reported procedure.[18] The crude product was purified by column chromatography (0% to 30% ethyl acetate in hexanes) to afford 2-(*tert*-butyl)-6-

bromoquinoline (43 mg, 33%) as a yellow oil and 3-(*tert*-butyl)-6-bromoquinoline (14 mg, 11%) as a colorless oil.

2-(*tert*-butyl)-6-bromoquinoline (32a)

R_f = 0.64 (ethyl acetate/hexanes 1:4; UV). ^{1}H NMR (700 MHz, $CDCl_3$) 7.98 (d, *J* = 8.8 Hz, 1H), 7.92 (d, *J* = 8.9 Hz, 1H), 7.92 (d, *J* = 2.1 Hz, 1H) 7.72 (dd, *J* = 9.0, 2.0 Hz, 1H), 7.54 (d, *J* = 8.7 Hz, 1H), 1.45 (s, 9H). ^{13}C NMR (126 MHz, $CDCl_3$) δ 170.11, 146.36, 135.19, 132.68, 131.56, 129.58, 127.92, 119.61, 119.43, 38.58, 30.38. HRMS (ESI) m/z $[M + H]^+$ calcd for: $C_{13}H_{14}BrN$: 264.0382; found: 264.0385. IR (neat): v = 2958, 2865, 1594, 1550, 1487, 1458, 1363, 1301, 11889, 1104, 1059.

3-(*tert*-butyl)-6-bromoquinoline (32b)

R_f = 0.24 (ethyl acetate/hexanes 1:4; UV). ^{1}H NMR (700 MHz, $CDCl_3$) δ 8.81 (d, *J* = 4.7 Hz, 1H), 8.56 (s, 1H), 8.00 (d, *J* = 8.9 Hz, 1H), 7.74 (d, *J* = 9.0 Hz, 1H), 7.37 (d, J = 4.8 Hz, 1H), 1.61 (s, 9H) ppm. ^{13}C NMR (176 MHz, $CDCl_3$) δ 155.15, 150.72, 148.21, 132.94, 131.74, 128.97, 128.40, 119.49, 119.02, 36.26, 31.40 ppm. HRMS (ESI) m/z $[M + H]^+$ calcd for: $C_{13}H_{14}BrN$: 264.0382; found: 264.0384. IR (neat): v = 2965, 2215, 1600, 1581, 1492, 1365, 1333, 1259, 1179, 1068, 997.

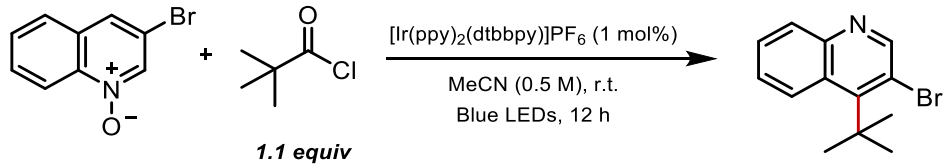

4-(*tert*-butyl)-3-bromoquinoline (33)

The reaction was run according to General Procedure A on a 0.5 mmol scale and the *N*-oxide substrate was prepared according to a reported procedure.[18] The crude product was purified by column chromatography (0% to 30% ethyl acetate in hexanes) to afford the title compound (27 mg, 20%) as a colorless oil. R_f = 0.75 (ethyl acetate/hexanes 1:4; UV). ^{1}H NMR (700 MHz,

$CDCl_3$) δ 8.35 (s,1H), 8.02 (d, *J* = 8.4 Hz, 1H), 7.70 - 7.65 (m, 2H), 7.50 (t, *J* = 7.0 Hz, 1H) 1.64 (s, 9H). ^{13}C NMR (176 MHz, $CDCl_3$) δ 163.96, 145.29, 141.54, 129.59, 129.53, 127.80, 126.96, 126.13, 116.57, 40.38, 29.16. HRMS (ESI) m/z $[M + H]^+$ calcd for: $C_{13}H_{14}BrN$: 264.0382; found: 264.0370. IR (neat): v = 2954, 2927, 2868, 1587, 1480, 1459, 1397, 1363, 1321, 1300, 1200, 1152, 1133, 1110, 961.

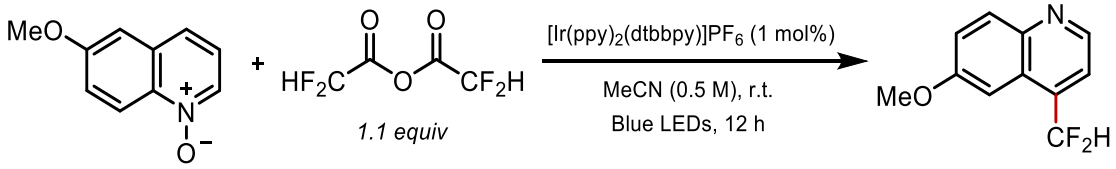

4-(difluoromethyl)-6-methoxyquinoline (36)

The reaction was run according to General Procedure A and the *N*-oxide substrate was prepared according to a reported procedure.[18] The crude product was purified by column chromatography (0% to 15% ethyl acetate in hexanes) to afford the title compound (54 mg, 32%) as a colorless oil. R_f = 0.63 (ethyl acetate/hexanes 1:4; UV). ^1H NMR (500 MHz, $CDCl_3$) δ 8.86 (d, *J* = 4.4 Hz, 1H), 8.09 (d, *J* = 9.2 Hz, 1H), 7.54 (d, *J* = 4.4 Hz, 1H), 7.44 (dd, *J* = 9.3, 2.7 Hz, 1H), 7.31 (dt, *J* = 2.6, 1.4 Hz, 1H), 7.09 (t, *J* = 54.6 Hz, 1H), 3.97 (s, 3H). ^{13}C NMR (126 MHz, $CDCl_3$) δ 158.54, 147.23, 144.88, 136.22 (t, *J* = 3.2 Hz), 131.77, 125.29 (t, *J* = 3.0 Hz), 122.64, 118.38 (t, *J* = 7.8 Hz), 113.74 (t, *J* = 240.1 Hz), 101.21, 55.61. ^{19}F NMR (471 MHz, $CDCl_3$) δ -115.32 (d, *J* = 54.7 Hz). HRMS (ESI) m/z $[M + H]^+$ calcd for: $C_{11}H_9F_2NO$: 210.0725; found: 210.0725. IR (neat): v = 2937, 1921, 1678, 1622, 1508, 1479, 1358, 1308, 1245, 1229, 1108, 1081, 1026.

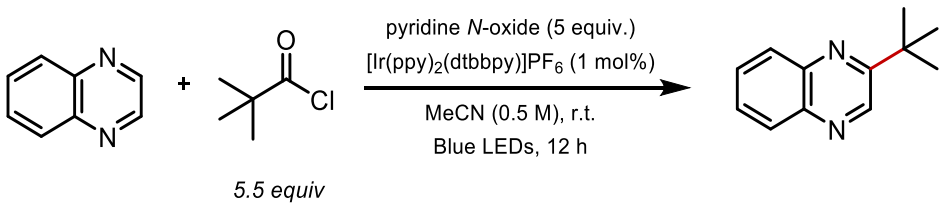

2-(*tert*-butyl)-quinoxaline (37)

The reaction was run according to General Procedure B on a 0.5 mmol scale and was purified by column chromatography (5% to 80% ethyl acetate in hexanes) to afford the title compound (68 mg, 73%) as a light yellow oil. Rf = 0.56 (ethyl acetate/hexanes 1:4; UV). ^{1}H NMR (700 MHz, $CDCl_3$) δ 8.99 (s, 1H), 8.06 (d, *J* = 5.7 Hz, 1H), 8.05 (d, J = 5.6 Hz, 1H), 7.73 (t, *J* = 7.0 Hz, 1H), 7.70 (t, J = 7.0 Hz, 1H) 1.52 (s, 9H). ^{13}C NMR (176 MHz, $CDCl_3$) δ 163.65, 143.40, 141.56, 140.72, 129.60, 129.24, 128.86, 128.84, 37.21, 29.71 ppm. HRMS (ESI) m/z $[M]^+$ calcd for: $C_{12}H_{15}N_2$: 186.1157; found: 186.1162. IR (neat): v = 3025, 2963, 2669, 1596, 1546, 1495, 1464, 1409, 1366, 1273, 1226, 1203, 1128, 1074, 1023, 995.

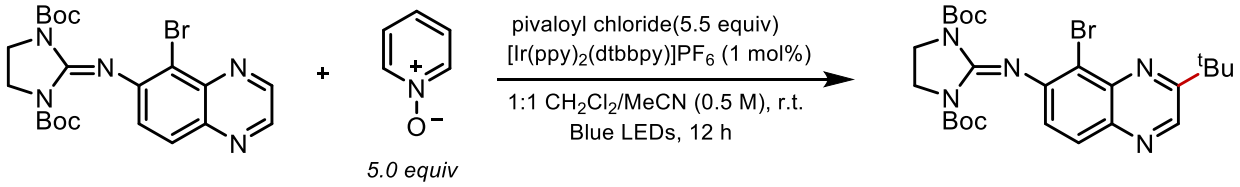

2-*tert*-butyl-4-acetylpyridine (38)

The reaction was run according to General Procedure B using 1:1 dichloromethane/MeCN (0.5 M) as the reaction solvent. The crude material was purified by column chromatography (10% to 30% ethyl acetate in hexanes) to afford the title compound (48 mg, 11%) as a yellow solid. R_f = 0.58 (ethyl acetate/hexanes 1:4; UV). ^{1}H NMR (500 MHz, $CDCl_3$) δ 8.97 (s, 1H), 7.87 – 7.79 (m, 1H), 7.49 – 7.41 (m, 1H), 3.90 – 3.85 (m, 4H), 1.48 (s, 9H), 1.30 (s, 18H). ^{13}C NMR (126 MHz, $CDCl_3$) δ 161.46, 149.92, 143.04, 139.61, 138.93, 127.97, 127.21, 126.60, 126.32, 83.10, 42.71, 29.75, 27.88, 27.85. HRMS (ESI) m/z $[M + H]^+$ calcd for: $C_{25}H_{34}BrN_5O_4$: 548.1867; found: 548.1874. IR (neat): v = 2978, 1805, 1737, 1710, 1666, 1603, 1471, 1368, 1310, 1252, 1235, 1149, 1107.

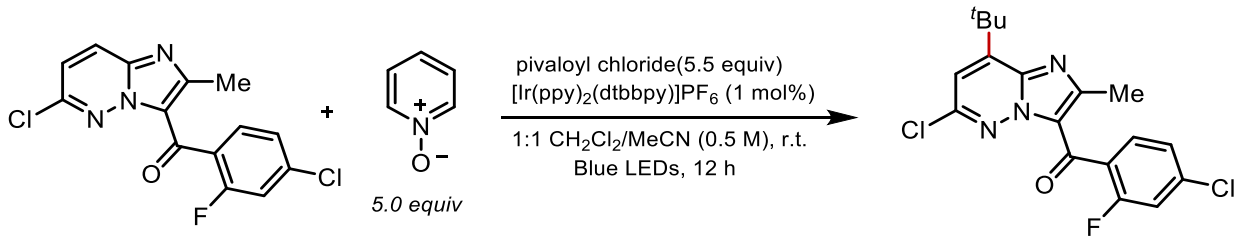

(8-(tert-butyl)-6-chloro-2-methylimidazo[1,2-b]pyridazin-3-yl)(4-chloro-2-fluorophenyl)methanone (39)

The reaction was run according to General Procedure B on a 0.5 mmol scale using 1:1 dichloromethane/MeCN (0.5 M) as the reaction solvent. The crude material was purified by column chromatography (0% to 30% ethyl acetate in hexanes) to afford the title compound (84 mg, 44%) as a white solid. R_f = 0.59 (ethyl acetate/hexanes 1:4; UV). ^{1}H NMR (700 MHz, $CDCl_3$) δ 7.60 (t, *J* = 7.8 Hz, 1H), 7.29 (d, *J* = 6.5 Hz, 1H), 7.12 (d, *J* = 10.1 Hz, 1H), 6.98 (s, 1H), 2.66 (s, 3H), 1.58 (s, 9H). ^{13}C NMR (176 MHz, $CDCl_3$) δ 180.57, 161.37, 159.92, 151.55, 150.69, 147.13, 139.08, 139.02, 138.79, 131.54, 131.51, 127.25, 127.17, 125.40, 125.38, 125.09, 117.43, 116.73, 116.58, 36.44, 29.13, 16.81. ^{19}F NMR (377 MHz, $CDCl_3$) δ -112.42 (dd, *J* = 10.1, 7.5 Hz). HRMS (ESI) m/z [M + H]+ calcd for: $C_{18}H_{17}Cl_2FN_3O$: 380.0727; found: 380.0731. IR (neat): v = 3091, 2959, 1636, 1604, 1573, 1539, 1506, 1480, 1410, 1376, 1345, 1316, 1290, 1257, 1242, 1210, 1161, 1118, 1077, 1052, 995.

(6-chloro-2,8-dimethylimidazo[1,2-*b*]pyridazin-3-yl)(4-chloro-2-fluorophenyl)methanone (40)

The reaction was run according to General Procedure B using 1:1 dichloromethane/MeCN (0.5 M) as the reaction solvent. The crude material was purified by column chromatography (0% to 30% ethyl acetate in hexanes) to afford the title compound (43 mg, 16%) as a white solid. R_f = 0.56 (ethyl acetate/hexanes 1:4; UV). ^{1}H NMR (500 MHz, $CDCl_3$) δ 7.62 (t, *J* = 7.9 Hz, 1H), 7.30 (dd, *J* = 8.4, 1.8 Hz, 1H), 7.12 (dd, *J* = 10.0, 1.9 Hz, 1H), 7.02 (d, *J* = 1.5 Hz, 1H), 2.69 (s, 3H), 2.67 (s, 3H). ^{13}C NMR (126 MHz, $CDCl_3$) δ 180.15, 160.37 (d, *J* = 255.1 Hz), 152.00, 146.58, 139.55, 138.99 (d, *J* = 10.6 Hz), 138.47, 131.26 (d, *J* = 3.7 Hz), 126.59 (d, *J* = 13.9 Hz), 125.66, 125.13 (d, *J* = 3.4 Hz), 120.75, 116.35 (d, *J* = 25.7 Hz), 16.65, 16.25. ^{19}F NMR (377 MHz, $CDCl_3$) δ -112.41 (dd, *J* = 10.2, 7.5 Hz). HRMS (ESI) m/z $[M + H]^+$ calcd for: $C_{15}H_{10}Cl_2FN_3O$: 338.0258; found: 338.0263. IR (neat): v = 2051, 2922, 1636, 1606, 1553, 1503, 1480, 1400, 1379, 1347, 1290, 1224, 1136, 1078.

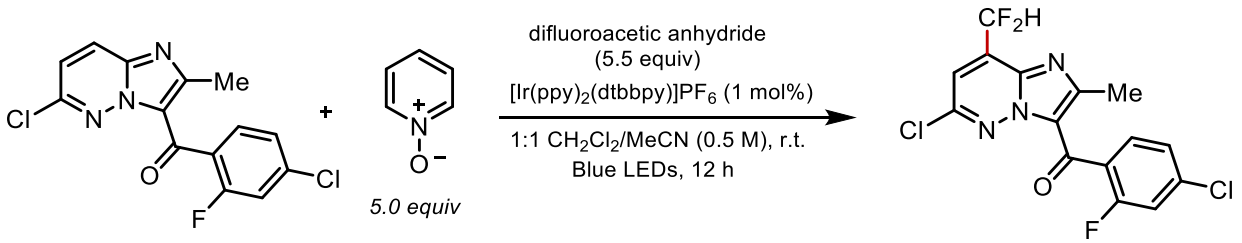

(4-chloro-2-fluorophenyl)(6-chloro-8-(difluoromethyl)-2-methylimidazo[1,2-*b*]pyridazin-3-yl)methanone (41)

The reaction was run according to General Procedure B using 1:1 dichloromethane/MeCN (0.5 M) as the reaction solvent. The crude material was purified by column chromatography (0% to 30% ethyl acetate in hexanes) to afford the title compound (39 mg, 13%) as a white solid. R_f = 0.61 (ethyl acetate/hexanes 1:4; UV). ^{1}H NMR (500 MHz, $CDCl_3$) δ 8.21 (s, 1H), 7.69 – 7.62 (m, 1H), 7.32 (d, *J* = 8.3 Hz, 1H), 7.14 (d, *J* = 10.0 Hz, 1H), 6.84 (t, *J* = 54.1 Hz, 1H), 2.73 (s, 3H). ^{19}F NMR (471 MHz, $CDCl_3$) δ -112.50 (t, *J* = 8.7 Hz), -117.65 (d, *J* = 54.3 Hz). ^{13}C NMR (126 MHz, $CDCl_3$) δ 179.82, 161.18, 159.73, 153.40, 146.64, 139.62 (d, *J* = 10.6 Hz), 135.33, 131.95 – 130.86

(m, 2C), 126.38 – 125.53 (m), 125.35 (d, J = 3.4 Hz), 117.58 (t, J = 6.2 Hz), 116.47 (d, J = 25.5 Hz), 109.15 (t, J = 242.0 Hz). 16.23. HRMS (ESI) m/z $[M + H]^+$ calcd for: $C_{11}H_{15}NO$: 374.0069; found: 374.0071. IR (neat): v = 3432, 3100, 2921, 1634, 1609, 1572, 1503, 1480, 1417, 1316, 1146, 1087, 1048.

Equipment and Procedure for Batch and Flow Processing

A. Equipment and Setup

Figures S2-S4 represent the specific equipment and setup used while performing the decarboxylative *tert*-butylation of quinoline *N*-oxide in continuous flow. This setup was used for both small (200 μmol) and large (6.9 mmol) scale reactions.

The LED assembly was obtained from Luxeon StarLEDs (Model No.: SP-02-V4, consisting of a series of seven LXML-PR02-A900 Royal Blue Luxeon Rebel ES LEDs mounted to a SinkPad-II base; http://www.luxeonstar.com/royal-blue-447.5nm-sinkpad-ii-40mm-7-led-round-led-1030mw) and was adhered to a heat sink to dissipate heat from the LED (Luxeon, 60 mm round x 45 mm high alpha heat sink; http://www.luxeonstar.com/60mm-round-3.9-degree-cw-alpha-heat-sink). This was powered with a Costway DC power supply (Model No.: EP20570-110V), with both constant current (0-5 A) and constant voltage (0-30 V) capabilities. The light source was operated at 700 mA (unless otherwise noted); the manufacturer lists this as the optimal operating current. Material was pumped through the system with an IPC-04 Ismatec peristaltic pump (Model No.: ISM930C, 4 channel pump) with a range of 32.2 μL/min up to 3.2 mL/min. Material was flowed through Teflon PFA tubing (0.030” inner diameter, 1/16” outer diameter)

which was obtained from IDEX Health & Science (Part No.: 1514L; https://www.idex-hs.com/fluidic-connections/dupontr-pfa-tubing-natural-1-16-od-x-030-id-x-50ft.html).

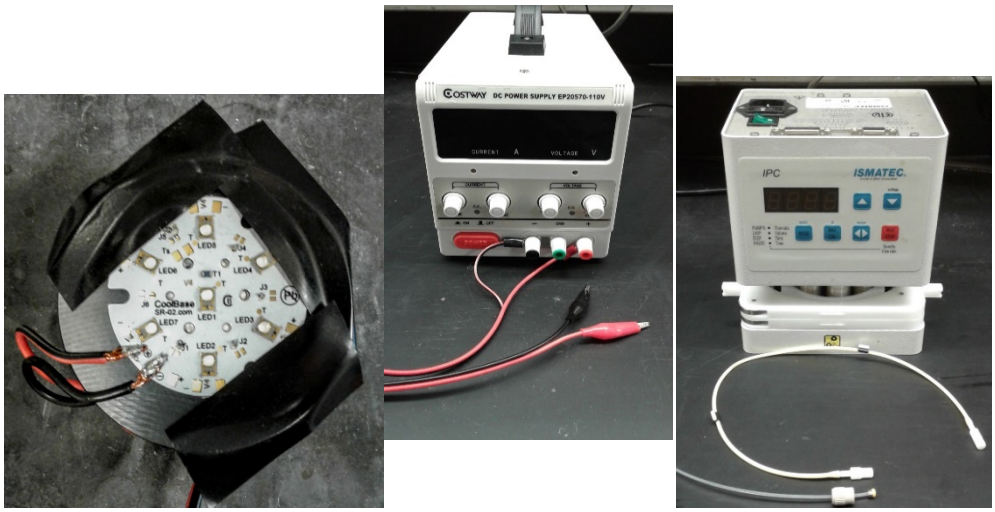

Continuous Flow Processing Equipment. (Left: Luxeon SP-02-V4 Royal Blue LED mounted to heat sink; Middle: Ismatec peristaltic pump; Right: Costway DC controller).

Depicts the setup for the gram-scale continuous flow reaction. Beyond the peristaltic pump, the tubing was wrapped around two 18x150 mm borosilicate test tubes and secured in place with tape, generating a 900 µL internal volume reactor. Aluminum foil was taped around the tubing at the points outside of the intended irradiation window as this would define the "reaction vessel". The reaction vessel itself was suspended 1 cm above and below the two light pucks. A back pressure regulator of 20 psi (obtained from IDEX Health & Science; Part No. P-791) was fitted in between the reactor and the collection flask to control the release of carbon dioxide after the mixture has left the reactor. Finally, the end of the tubing was threaded through a rubber septum which was fitted onto a collection flask with a 20 gauge needle for the dissipation of any pressure build-up from the generation of gaseous byproducts. During each run, a cardboard box lined with aluminum foil (not depicted) was placed over the light source and reaction vessel to minimize irradiation of

the starting material vessel or the collection vessel. To get an estimate of the reaction mixture temperature, a thermometer was placed inside one of the borosilicate test tubes. As the light source tends to generate heat even when attached to the heat sink, a stream of compressed air was blown between the LEDs and the tubing to keep the temperature near room temperature. The light source was turned on at least a few minutes before each run to ensure the reaction vessel equilibrated to the steady state temperature (generally 32-35 °C).

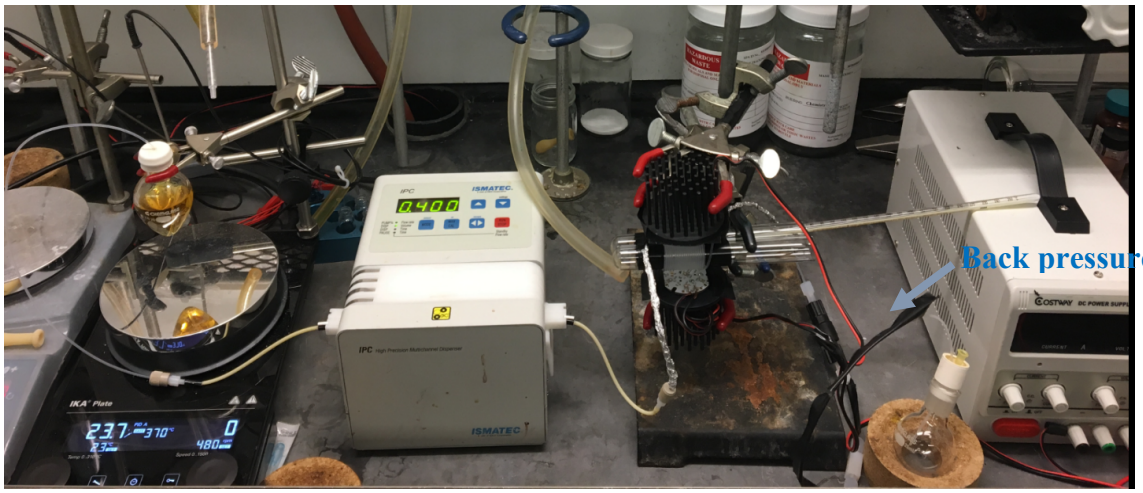

Full Apparatus (direction of flow is from left to right).

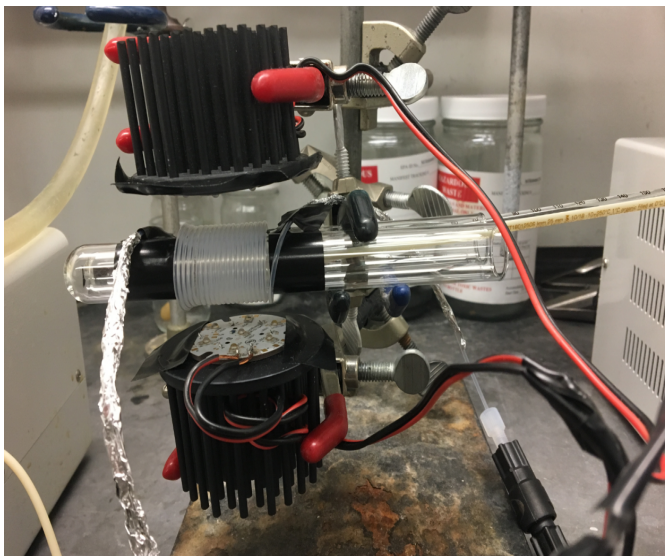

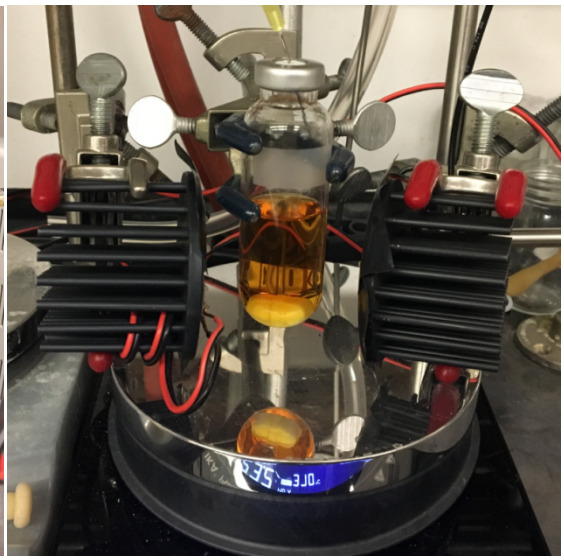

Continuous Flow and Batch Reaction Vessels. (Left: Side view of continuous flow reaction vessel; Right: Gram-scale batch reaction vessel with light sources 1 cm apart on either side of vial)

For the large-scale batch reactions (ca. 1 g, 6.9 mmol of quinoline *N*-oxide), the reaction setup mimicked the flow apparatus. Thus, the reaction vessel was placed in between two light pucks (1 cm distance on each side) and cooled with a stream of compressed air. A 20 gauge needle was inserted into the septum cap to allow for release of carbon dioxide.

B. Optimization of Flow Conditions on Small Scale (200 μmol)

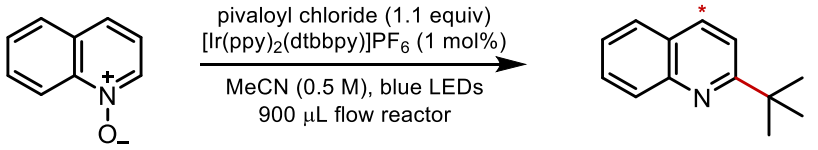

Batch yield: 72% (3:4)

Flow rate (mL/min)	***Residence time (min)***	***^{1}H NMR yield (%)***
0.10	9.0	66 (3:4)
0.25	3.6	70 (3:4)
0.40	**2.25**	**71 (3:4)**
0.50	1.8	66 (3:4)
0.75	1.2	65 (3:4)
1.00	0.9	66 (3:4)

Optimization of Continuous Flow Conditions on Small Scale

General Optimization Procedure. To a 2 dram vial equipped with a stir bar was added anhydrous quinoline *N*-oxide (0.20 mmol, 1.0 equiv), which had been pre-dried on a high vacuum line for 6 h at ambient temperature. Upon addition of $[Ir(ppy)_2(dtbbpy)]PF_6$ (1.0 mol%), the combined materials were dissolved in MeCN (0.5 M) and stirred. Upon subsequent addition of pivaloyl

chloride (0.22 mmol, 1.1 equiv), the resulting solution was stirred for 5 min. The vial was equipped with a septum, through which the reactor tubing had been threaded. The reaction mixture was then flowed through the flow apparatus (see Section A) at various flow rates. Trimethoxybenzene (0.20 mmol) was added as a stoichiometric internal standard upon completion of the reaction. A sample of the reaction was removed and diluted with $CDCl_3$ for ^1H NMR analysis.

C. Gram-scale Flow and Batch Reactions

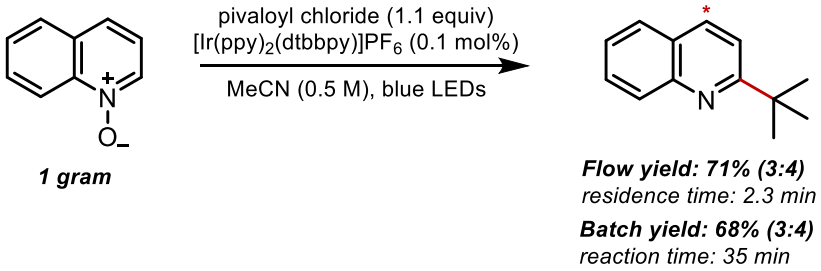

General Gram-Scale Flow Procedure. To a 2 dram vial equipped with a stir bar was added anhydrous quinoline *N*-oxide (6.9 mmol, 1.0 g), which had been pre-dried on a high vacuum line for 6 h at ambient temperature. Upon addition of $[Ir(ppy)_2(dtbbpy)]PF_6$ (0.1 mol%), the combined materials were dissolved in MeCN (0.5 M) and stirred. Pivaloyl chloride (7.59 mmol, 1.1 equiv) was added and the resulting solution was stirred for 5 min. The vial was equipped with a septum, through which the reactor tubing had been threaded. The reaction mixture was then flowed through the flow apparatus (see Section A) at a flow rate of 400 µL/min, providing a residence time of 2.3 min. Workup was performed by diluting the reaction with CH_2Cl_2 and washing with saturated $NaHCO_3$ (x1) and then brine (x1). The organic layer was dried over sodium sulfate before filtering and concentrating at 40 ˚C under reduced pressure. The crude residue was then purified by column chromatography (gradient of 10% ethyl acetate/hexanes to 20% ethyl acetate/hexanes)

to afford a 3:4 mixture of 2-*tert*-butyl quinoline and 4-*tert*-butyl quinoline (overall yield: 0.91 g, 71%). For full characterization of products, see page 69.

General Gram-Scale Batch Procedure. To a 20 mL microwave vial equipped with a stir bar was added anhydrous quinoline N-oxide (6.9 mmol, 1.0 g), which had been pre-dried on a high vacuum line for 6 h at ambient temperature. Upon addition of $[Ir(ppy)_2(dtbbpy)]PF_6$ (0.1 mol%), the combined materials were dissolved in MeCN (0.5 M) and stirred. Pivaloyl chloride (7.59 mmol, 1.1 equiv) was added and the resulting solution was stirred for 5 min. The vial was sealed with a septum cap, through which was inserted a 20 gauge needle. The reaction mixture was stirred and irradiated for 35 min. Upon completion of the reaction, workup was performed by diluting the reaction with CH_2Cl_2 and washing with saturated $NaHCO_3$ (x1) and then brine (x1). The organic layer was dried over sodium sulfate before filtering and concentrating at 40 ˚C under reduced pressure. The crude residue was then purified by column chromatography (gradient of 10% ethyl acetate/hexanes to 20% ethyl acetate/hexanes) to afford a 3:4 mixture of 2-*tert*-butyl quinoline and 4-*tert*-butyl quinoline (overall yield: 0.87 g, 68%). For full characterization of products, see page 69.

Preliminary Optimization Data

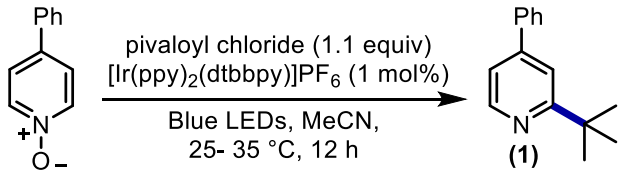

Entry[a]	Alteration from standard	Yield (%)[b]
1	**None**	**71%, 75%[c]**
2	$Ru(bpy)_3(PF_6)_2$	57%
3	$Ir(ppy)_3$	23%
4	$[Ir(dF(CF_3)ppy)_2(dtbbpy)]PF_6$	67%
5	DCM as solvent	57%
6	DMF as solvent	70%
7	0.1 mol% $[Ir(ppy)_2(dttbpy)]PF_6$	60%
8	0.08 M concentration	64%
9	2.0 equiv. pivaloyl chloride	65%

[a] Reactions run on a 0.4 mmol scale with 1.1 equiv of pivaloyl chloride, using 13.2 W blue LEDs. [b] Determined by ^1H NMR spectroscopy with trimethoxybenzene as the internal standard. [c] Isolated yield.

Additional Control Reactions

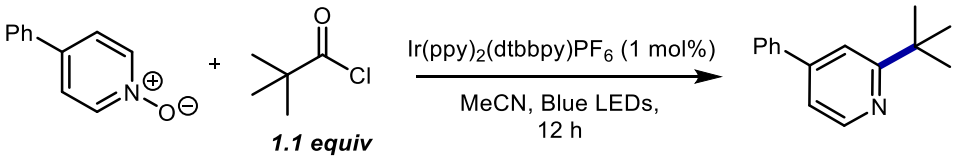

Entry[a]	Alteration from standard	Yield (%)[b]
1	reaction time: 15 min	71
2	pre-sparged reaction with N_2	71
3	No LED lights	0
4	No photocatalyst	0
5	0.25 M concentration	70

[a] Reactions run on a 0.4 mmol scale with 1.1 equiv of pivaloyl chloride, using 13.2 W blue LEDs. [b] Determined by ^{1}H NMR spectroscopy with trimethoxybenzene as the internal standard.

Lewis Acid Additive Screens

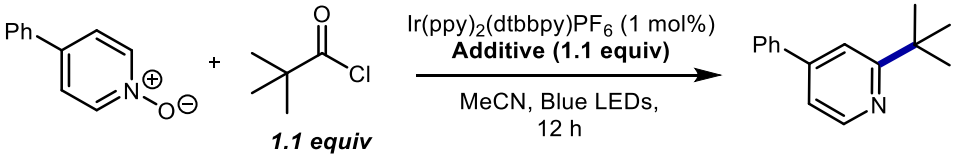

Entry[a]	Additive (1.1 equiv)	Yield (%)[b]
1	$BF_3 \bullet OEt_2$	<10
2	$B(OH)_3$	42
3	TMSCl	62
4	LiCl	64
5	HCl in dioxane	3

[a] Reactions run on a 0.4 mmol scale with 1.1 equiv of pivaloyl chloride, using 13.2 W blue LEDs. [b] Determined by ^{1}H NMR spectroscopy with trimethoxybenzene as the internal standard.

Additional Solvent Screens

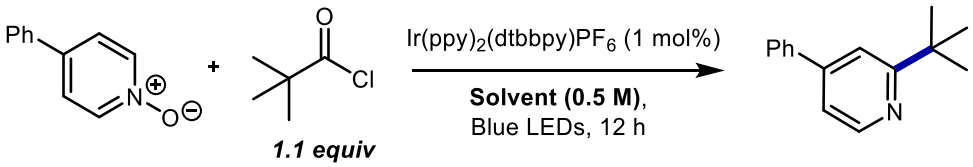

Entry[a]	Solvent (0.5 M)	Yield (%)[b]
1	$MeNO_2$	66
2	DMA	15
3	Chloroform	<10
4	DME	6
5	*t*-Amyl alcohol	33
6	MeCN/DME (1:1)	53
7	$MeNO_2$/DME (1:1)	12
8	MeCN/*t*-BuOH (1:1)	51
9	$MeNO_2$/*t*-BuOH (1:1)	15
10	MeCN/CyOH (1:1)	52
11	$MeNO_2$/CyOH (1:1)	0

[a] Reactions run on a 0.4 mmol scale with 1.1 equiv of pivaloyl chloride, using 13.2 W blue LEDs. [b] Determined by ^{1}H NMR spectroscopy with trimethoxybenzene as the internal standard.

Unsuccessful substrates

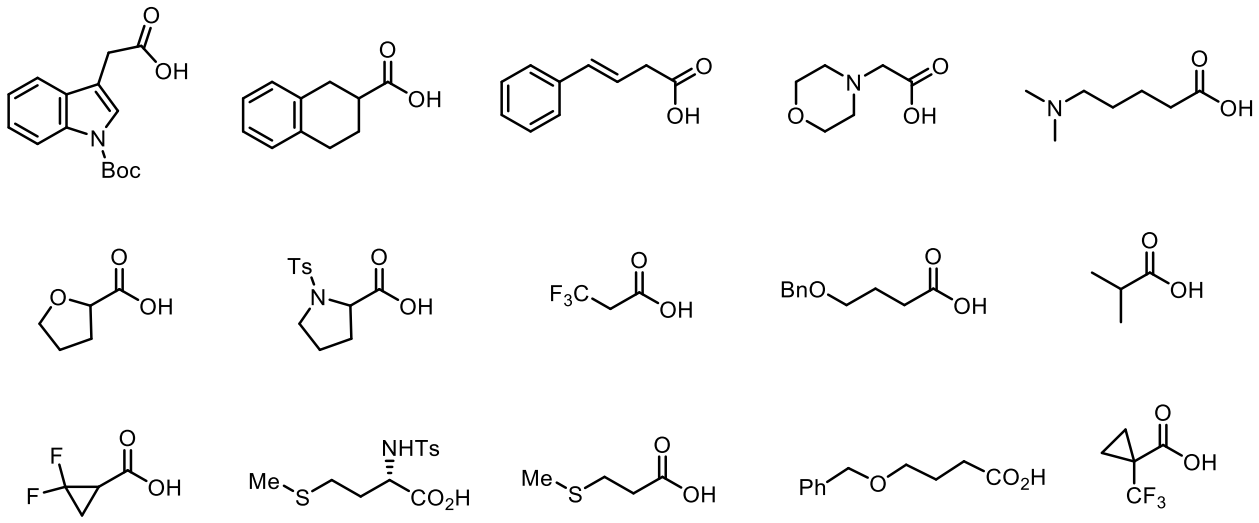

The carboxylic acid substrates listed above failed to provide alkylation products in sufficient quantities under the optimized conditions (General Procedure A), with 4-phenylpyridine N-oxide as a coupling partner.

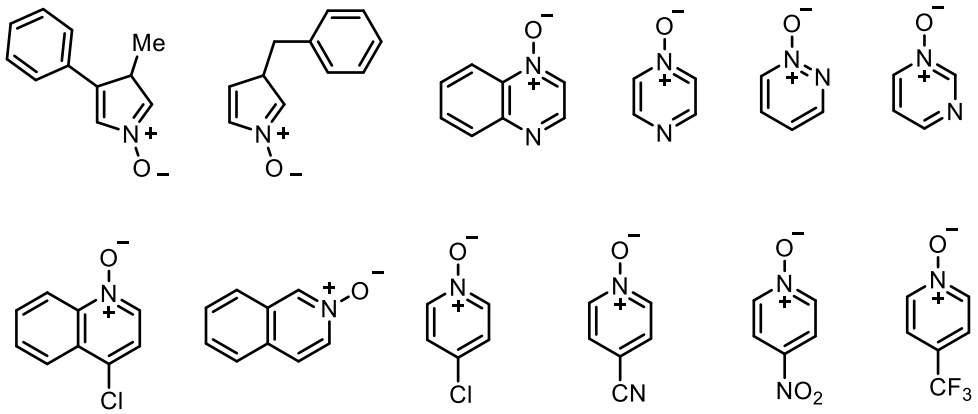

The heterocyclic N-oxide substrates listed above failed to provide alkylation products in sufficient quantities under the optimized conditions (General Procedure A), using pivaloyl chloride as a coupling partner, due to either failed acylation or solubility issues.

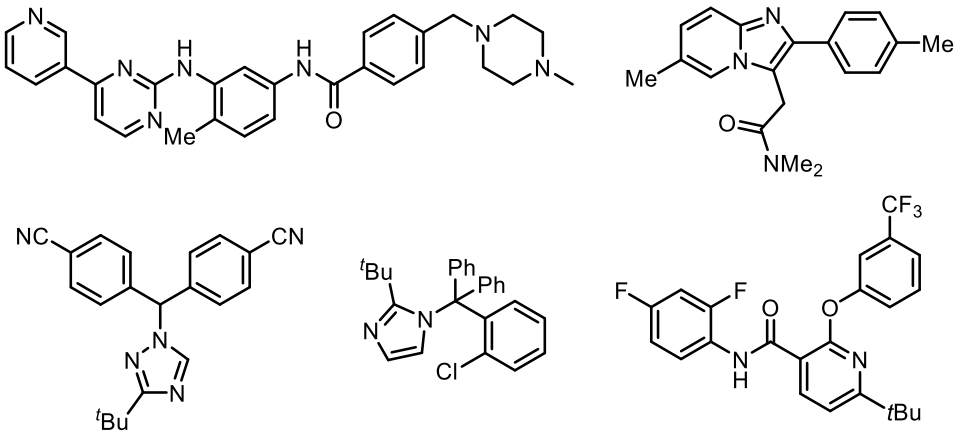

The heterocyclic substrates listed above failed to provide alkylation products in sufficient quantities under the optimized conditions (General Procedure B), using pivaloyl chloride as a coupling partner and pyridine N-oxide as a redox auxiliary.

Electrochemical Measurements

As discussed in a previous report[9] by our group, the measurement of reduction potentials for the *N*-(acyloxy)pyridinium salts reported in this manuscript cannot be accurately performed through cyclic voltammetry analysis. The observed signal using cyclic voltammetry is found to have variations in shape and peak potential from run to run, and the peak shape is dependent upon sweep rate. Therefore, differential pulse voltammetry (DPV) was performed to obtain the reduction potentials of the various pyridine N-oxide/acid chloride combinations, and reproducible potentials were obtained through these methods. Measurements were performed with a model CHI660C multi-potentiostat from CH Instruments. Measurements were performed with a glassy carbon working electrode, Pt auxiliary electrode, Ag/AgCl reference electrode, Bu_4NPF_6 electrolyte (0.1 M in MeCN), and analyte (pyridine-N-oxide/pivaloyl chloride, 1:1, 0.01 M) with the following settings: Incr E (V) = 0.001, Amplitude (V) = 0.005, Pulse Width (sec) = 0.05, Sampling Width (sec) = 0.01, Pulse Period (sec) = 0.5, Quiet Time (sec) = 2, Sensitivity (A/V) = 1 e^{-5}. All voltammograms are reported/displayed after conversion to voltage vs. SCE, where:

$$V_{SCE} = V_{Ag/AgCl} \quad 0.05\ V$$

Onset potentials are estimated based on the intersection of the baseline and onset slope (shown).

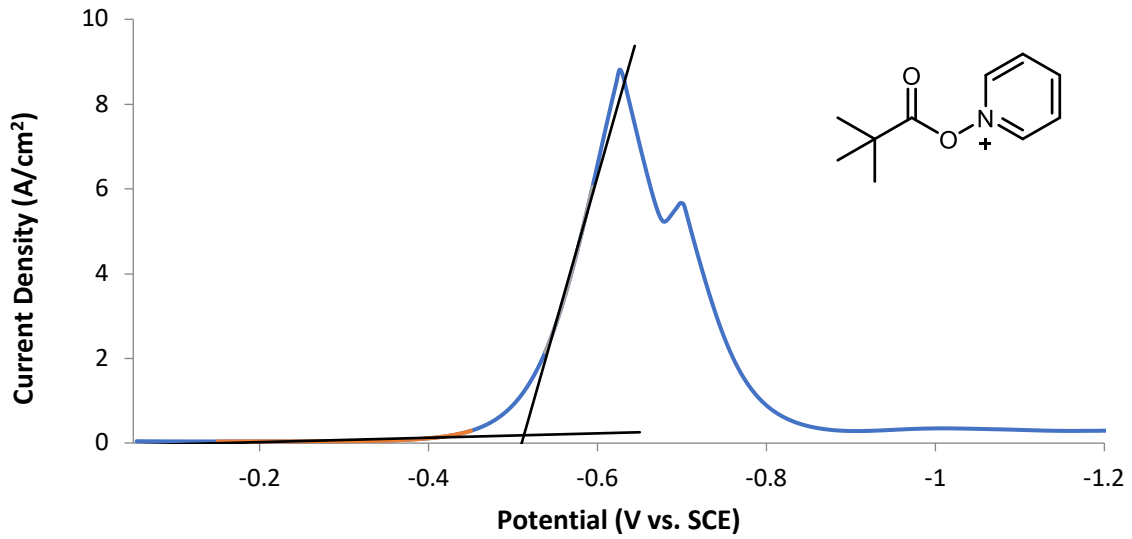

DPV of the pivaloyl chloride/pyridine *N*-oxide adduct. Onset reduction potential is observed at –0.51 V vs. SCE. Peak reduction potential is observed at –0.63 V vs. SCE.

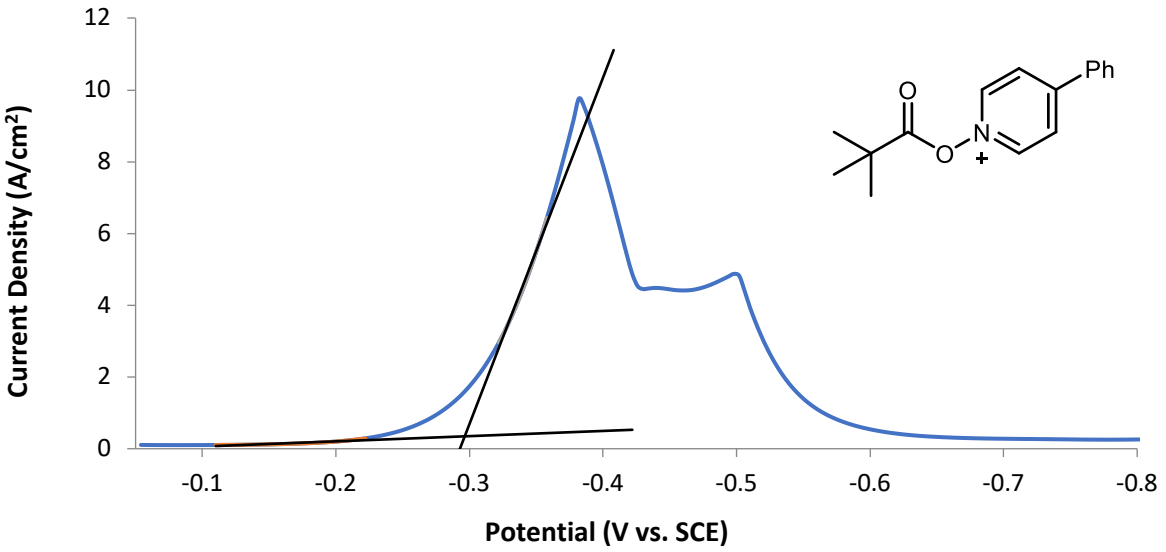

DPV of the pivaloyl chloride/4-phenylpyridine *N*-oxide adduct. Onset reduction potential is observed at –0.29 V vs. SCE. Peak reduction potential is observed at –0.38 V vs. SCE.

Quantum Yield Measurements

This experiment closely followed the procedure reported by Cismesia and Yoon.[16] The only modification was the use of a 0.1 cm path length cuvette for the UV/Vis data during the calculation of the photon flux, a modification made during recent investigations into our photochemical radical trifluoromethylation chemistry.[9]

The light source employed was a 150 W Xenon Arc lamp within a Fluoromax-2 Fluorimeter. UV/Vis data was collected on a Shimadzu UV-1601 UV-Vis Spectrometer. The photon flux of this specific fluorimeter had previously been determined within the group to be 5.46×10^{-9} einstein/s at 436 nm (1 einstein = 1 mol photons). The experiment was repeated as is detailed in the Supplementary Information of our recent report[8] to obtain a photon flux of

$5.55x10^{-9}$ einstein/s at 436 nm; this value was used in the following calculations. Specific details for the experimental determination of the quantum yield for the *tert*-butylation of quinoline *N*-oxide are provided below:

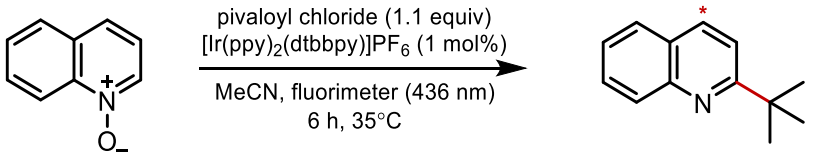

Isolated Yield: 26% (3:4)
Quantum Yield: 1.7

Procedure for Quantum Yield Calculation. In a dark room, anhydrous quinoline N-oxide (0.8 mmol) was added to a dry quartz cuvette (1 cm path length) equipped with a stir bar. Upon addition of $[Ir(ppy)_2(dtbbpy)]PF_6$ (1 mol%), the combined materials were dissolved in MeCN (2 mL) and stirred. Pivaloyl chloride (0.88 mmol) was added and the resulting solution was capped, sealed, and stirred for 5 min. Light exclusion was achieved by wrapping the cuvette in aluminum foil until the reaction was placed in the fluorimeter. The sample holder was pre-equilibrated to 35 °C, and the reaction sample was allowed to equilibrate to this temperature over 10 minutes. The sample was stirred and irradiated at 436 nm with a 10 nm slit width for 21600 (6 h). After irradiation, workup was performed by diluting the reaction with CH_2Cl_2 and washing with saturated $NaHCO_3$ (x1) and then brine (x1). The organic layer was dried over sodium sulfate before filtering and concentrating at 40 ˚C under reduced pressure. The crude residue was then purified by column chromatography (gradient of 10% ethyl acetate/hexanes to 20% ethyl acetate/hexanes) to afford a 3:4 mixture of 2-*tert*-butylquinoline and 4-*tert*-butylquinoline, with an overall yield of 26% (0.204 mmol).

The quantum yield was calculated as follows (Equations 1 and 2), where flux = photon flux; t = time of irradiation (s); f = fraction of light absorbed = $1 - 10^{-A}$, where A = absorbance. As seen in the aforementioned reports, the absorbance of the system is substantial (>3), leading to

an f value of approximately 1. For the purposes of this calculation, f is assumed to be equal to 1, implying that all light was absorbed.

$$\text{Quantum Yield} = = \frac{\text{mol product}}{\text{flux} \cdot t \cdot f} \quad (1)$$

$$= \frac{204 \text{ mol}}{(5.55 \times 10^{-9} \text{ einstein/s}) \cdot (21600 \text{ s}) \cdot (1)} = 1.7 \quad (2)$$

2.5 References

1. Vitaku, E.; Smith, D. T.; Njardarson, J. T. Analysis of the Structural Diversity, Substitution Patterns, and Frequency of Nitrogen Heterocycles among U.S. FDA Approved Pharmaceuticals. *J. Med. Chem.* **2014,** *57,* 10257–10274.

10257.

2. Matthew A. J. Ducton. Minisci reactions: Versatile CH-functionalizations for medicinal chemists. *Med. Chem. Commun.* **2011**, *2*, 1135-1161.

3. Proctor, R. S. J.; Phipps, R. J. Recent Advances in Minisci-Type Reactions. *Angew. Chem. Int. Ed.* **2019,** *58,* 13666–13699.

4. Minisci, F.; Bernardi, R.; Bertini, F.; Galli, R.; Perchinummo, M. Nucleophilic character of alkyl radicals—VI : A new convenient selective alkylation of heteroaromatic bases. *Tetrahedron* **1971,** *27,* 3575-3579.

5. Sun, A. C.; McAtee, R. C.; McClain, E. J.; Stephenson, C. R. J. Advancements in Visible Light-Enabled Radical C(sp^2)–H Alkylation of (Hetero)arenes. *Synthesis* **2019,** *51*, 1063–1072.

6. DiRocco, D. A.; Dykstra, K.; Krska, S.; Vachal, P.; Conway, D. V.; Tudge, M. Late-Stage Functionalization of Biologically Active Heterocycles Through Photoredox Catalysis. *Angew. Chem., Int. Ed.* **2014,** *53,* 4802-4806.

7. Proctor, R. S. J.; Davis, H. J.; Phipps, R. J. Catalytic enantioselective Minisci-type addition to heteroarenes. *Science* **2018**, *360,* 419.

8. Beatty, J. W.; Douglas, J. J.; Cole, K. P.; Stephenson, C. R. J. A scalable and operationally simple radical trifluoromethylation. *Nat. Commun.* **2015,** *6,* 7919.

9. Beatty, J. W.; Douglas, J. J.; Miller, R.; McAtee, R. C.; Cole, K. P.; Stephenson, C. R. J. Photochemical Perfluoroalkylation with Pyridine *N*-Oxides: Mechanistic Insights and Performance on a Kilogram Scale. *Chem* **2016,** *1,* 456-472.

10. McAtee, R. C. Beatty, J. W.; McAtee, C. C.; Stephenson, C. R. J. Radical Chlorodifluoromethylation: Providing a Motif for (Hetero)arene Diversification. *Org. Lett.* **2018,** *20,* 3491–3495.

11. Lorance, E. D.; Kramer, W. H.; Gould, I. R. Barrierless Electron Transfer Bond Fragmentation Reactions. *J. Am. Chem. Soc.* **2004,** *126,* 14071–14078.

12. De Vleeschouwer, F.; Van Speybroeck, V.; Waroquier, M.; Geerlings, P.; De Proft, F. Electrophilicity and Nucleophilicity Index for Radicals. *Org. Lett.* **2007,** *9,* 2721-2724.

13. Gunaydin, H.; Bartberger, M. D. Stacking with No Planarity? *ACS Med. Chem. Lett.* **2016**, *7*, 341-344.

14. Popowycz, F.; Routier, S.; Joseph, B.; Merour, J.-Y. Synthesis and reactivity of 7-azaindole (1H-pyrrolo[2,3-b]pyridine). *Tetrahedron* **2007,** *63,* 1031-1064.

15. Baidya, M.; Brotzel, F.; Mayr, H. Nucleophilicities and Lewis basicities of imidazoles, benzimidazoles, and benzotriazoles. *Org. Biomol. Chem.* **2010,** *8,* 1929-1935.

16. Cismesiaa, M. A.; Yoon, T. P. Characterizing chain processes in visible light photoredox catalysis. *Chem. Sci.* **2015,** *6,* 5426-5434.

17. Douglas, J. J.; Cole, K. P.; Stephenson, C. R. J. Photoredox Catalysis in a Complex Pharmaceutical Setting: Toward the Preparation of JAK2 Inhibitor LY2784544. *J. Org. Chem.* **2014,** *79,* 11631-11643.

18. Ma, X.; Dang, H.; Rose, J. A.; Rablen, P.; Herzon, S. B. Hydroheteroarylation of Unactivated Alkenes Using N-Methoxyheteroarenium Salts. *J. Am. Chem. Soc.* **2017,** *139,* 5998-6007.

19. Brackow, J., Wanner, K. T. Direct synthesis of 4,4-disubstituted *N*-silyl-1,4-dihydropyridines. *Tetrahedron* **2006**, *62*, 2395-2404.

20. Panda, S.; Coffin, A.; Nguyen, Q. N.; Tantillo, D. J.; Ready, J. M. Synthesis and Utility of Dihydropyridine Boronic Esters. *Angew. Chem. Int. Ed.* **2016,** *55,* 2205-2209.

21. Jo, W.; Kim, J.; Choi, S.; Cho, S. H. C−H Coupling Reactions Directed by Sulfoxides: Teaching an Old Functional Group New Tricks. *Angew. Chem., Int. Ed.* **2016**, *55*, 9842-9846.

22. Wei, Y.; Yoshikai, N. Modular Pyridine Synthesis from Oximes and Enals through Synergistic Copper/Iminium Catalysis. *J. Am. Chem. Soc.* **2013,** *135,* 3756-3759.

23. Fang, L.; Chen, L.; Yu, J.; Wang, L. Benzoyl Peroxide Promoted Radical ortho-Alkylation of Nitrogen Heteroaromatics with Simple Alkanes and Alcohols. *Eur. J. Org. Chem.* **2015**, *9*, 1910-1914.

24. Sevov, C. S.; Brooner, R. E. M.; Chenard, E.; Assary, R. S.; Moore, J. S.; Rodriguez-Lopez, J.; Sanford, M. S. Evolutionary Design of Low Molecular Weight Organic Anolyte Materials for Applications in Nonaqueous Redox Flow Batteries. *J. Am. Chem. Soc.* **2015**, *137*, 14465-14472.

25. Galloway, J. D.; Mai, D. N.; Baxter, R. D. Silver-Catalyzed Minisci Reactions Using Selectfluor as a Mild Oxidant. *Org. Lett.* **2017**, *19*, 5772-5775.

26. Ichihara, Y.; Fujimara, R.; Tsuneki, H.; Wada, T.; Okamoto, K.; Gouda, H.; Hirono, S.; Sugimoto, K.; Matsuya, Y.; Sasaoka, T.; Toyooka, N. Rational design and synthesis of 4-substituted 2-pyridin-2-ylamides with inhibitory effects on SH2 domain-containing inositol 5′-phosphatase 2 (SHIP2). *Eur. J. Med. Chem.* **2013**, *62*, 649-660.

27. Huestis, M.P.; Fagnou, K. Site-Selective Azaindole Arylation at the Azine and Azole Rings via N-Oxide Activation. *Org. Lett.* **2009**, *11*, 1357-1360.

28. Matsui, J. K.; Primer, D. N.; Molander, G. A. Metal-free C–H alkylation of heteroarenes with alkyltrifluoroborates: a general protocol for 1°, 2° and 3° alkylation. *Chem. Sci.* **2017,** *8*, 3512-3522.

Chapter 3 **Leveraging Electron Donor-Acceptor Complexes in Catalysis**

3.1 Electron Donor-Acceptor Complexes in Synthetic Chemistry

Electron donor-acceptor (EDA) complexes are ground state aggregates that are characterized by the formation of a red-shifted transition referred to as a charge transfer band.[1] Photoexcitation of this transition induces an electron transfer event that produces a radical ion pair. These radical ion pairs typically return to the ground state via a rapid back electron transfer event, leaving little opportunity for either radical ion component to engage in productive reactivity.[2,3] To overcome these challenges, EDA complexes employed in synthesis are designed to incorporate a labile bond that fragments upon photoexcitation at a rate competitive with back electron transfer.[4-8] The rapid bond scission event decomposes one component of the contact ion pair, facilitating the otherwise improbable cage escape and thus enabling potential downstream radical reactivity. Pioneering studies by Kochi and coworkers exemplify this reactivity paradigm, as EDA complexes derived from pyridinium salts were demonstrated to undergo rapid fragmentation of the N–X bond upon photoexcitation, facilitating the nitration and fluorination of the aromatic donor molecules.[9,10] Despite the long-standing interest in the stoichiometric photoinduced reactivity of charge transfer complexes, reaction manifolds that implement EDA complexes as catalytic intermediates remain

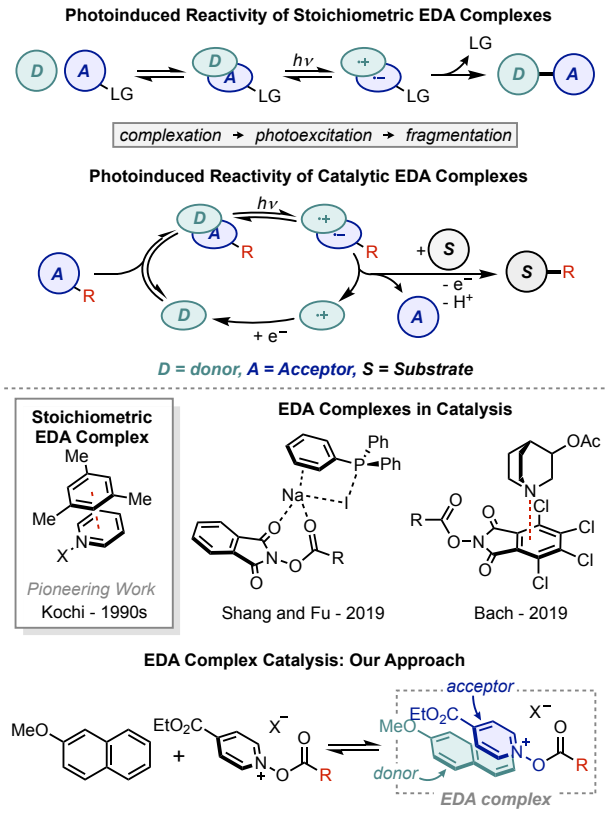

Figure 18. Synthetic applications of EDA complexes, background information.

severely underexplored.[4] The development of EDA complex catalysis represents an important advancement in this field, as it will expand the scope of reactivity by decoupling the complexation and photogeneration of radicals from substrate choice/functionalization (Figure 18). In 2013, Melchiorre and co-workers demonstrated that organocatalysis paired with photoinduced EDA complex reactivity could achieve the asymmetric α-alkylation of aldehydes.[11] This reactivity was enabled by the formation of a highly polarized, electron rich enamine as a catalytic intermediate that could associate with electron deficient nitrobenzyl bromides and α-bromoacetophenones (Figure 18). Subsequent efforts have further demonstrated the utility of coupling organocatalysis with EDA complex photochemistry.[12-15]

In 2019, Shang and Fu reported a strategy for EDA complex catalysis that utilized the combination of triphenylphosphine with sodium iodide as a catalyst species.[16-18] Photoexcitaiton

of the charge-transfer complexes formed from the triphenylphosphine/sodium iodide catalyst species with *N*-hydroxyphthalimide redox auxiliaries, Katritzky's *N*-alkyl pyridinium salts, or Togni's reagent promoted alkylation or trifluoromethylation reactions, respectively (Figure 18). The same year, Bach and Bosque showed that 3-acetoxyquinuclidine could function as a catalyst in the presence of tetrachlorophthalamide redox active esters, delivering amino- and hydro-decarboxylation as well as cyclization and dimerization reactions upon irradiation of the EDA complex (Figure 18).[19]

In 2015, our group reported the application of trifluoroacetic anhydride and pyridine *N*-oxide as a cheap, readily available, easily handled reagent combination for the radical trifluoromethylation of electron-rich (hetero)arenes.[20,21] During this study, it was discovered that a background trifluoromethylation reaction was occurring in the absence of a photocatalyst. Subsequent UV/vis studies revealed that the reaction was promoted by a stoichiometric EDA complex between the aromatic substrate (donor) and *N*-(trifluoroacetoxy)pyridinium (acceptor). We saw this as an opportunity to develop a generalized catalytic reaction manifold predicated on the formation and photoexcitation of an EDA complex as a catalytic intermediate. The application of an exogenous donor catalyst allows for the formation of a highly modular EDA complex, imparting the ability to tune the charge transfer band energy for selective photoexcitation events. Additionally, this reaction design delivers the radical intermediate through an EDA complex derived from a π-stacking interaction,[3] providing complementary reactivity to perfluoroalkylation methods that employ nitrogenous bases for the formation of an EDA complex,[22-26] while allowing for more diverse, less polarized radical fragments to be accessed.

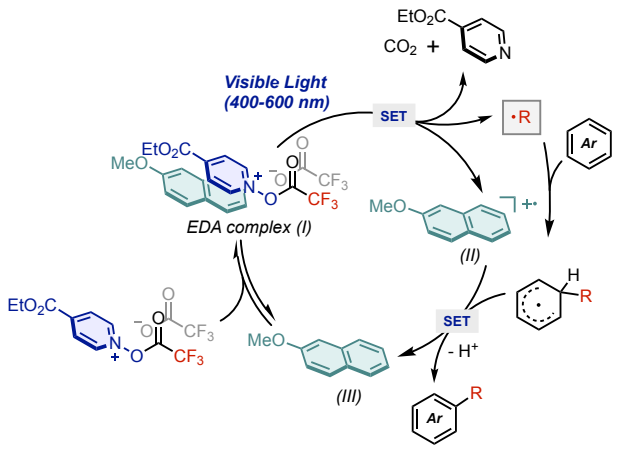

Figure 19. Plausible mechanism for EDA complex catalysis

Upon realization of a π-stacking interaction that delivers the desired EDA complex (I), we envisioned that a catalytic manifold may be accessible as the reversible π-stacking interaction allows for facile entry into the catalytic cycle. Photoexcitation of the EDA complex (I) induces an electron transfer event that produces 2-methoxynaphthalene radical cation (II) and liberates an equivalent of the reactive radical intermediate. In the presence of an arene, the radical can be efficiently trapped. Subsequent oxidation and deprotonation of the radical addition adduct produces the desired C−H trifluoromethylated product and regenerates 2-methoxynaphthalene (III) to turn over the catalytic cycle (Figure 19). Previous determination of the quantum yield the $Ru(bpy)_3Cl_2$ catalyzed trifluoromethylation reaction was determined to be 0.87, lending support to the catalytic activity of 2-methoxynaphthalene being responsible for the trifluoromethylation.[20,21]

3.2 Results and Discussion

Initial investigations into the development of a catalytic manifold focused on the optimization of the charge-transfer complex that will serve as a catalytic intermediate. Preliminary studies revealed that donors with extended π-systems (i.e. naphthalene) provided more absorbing EDA complexes, while the incorporation of an electron donating substituent increased observed

reactivity of the EDA complex. EDA complexes are characterized by Mulliken's theory of charge transfer, a postulate that relates the energy of the charge transfer band (E_{CT}) for the complex to the difference between the donor ionization energy (IE) and acceptor electron affinity (EA).[27-28] Studies of the acceptor revealed ethyl isonicotinate *N*-oxide exhibited the formation of an EDA complex with anisole that provided a charge transfer band with a maximum absorbance at 369 nm. Altering the donor arene in acetonitrile led to the formation of new, red-shifted charge transfer bands. As is predicted by Mulliken theory, E_{CT} decreased as the IE of the donor decreased (Figure 3B). Importantly, more red-shifted charge transfer bands allow for highly selective excitation of the desired transition, a facet controllable through the choice of donor catalyst and light source (Figure 3). For instance, in the presence of 2-methoxynaphthalene or pyrene as donor catalysts, optimal yields were obtained when applying blue light irradiation (456 nm). However, irradiation with either violet (390 nm) or green (525 nm) light negatively impacted reactivity (Figure 20C).

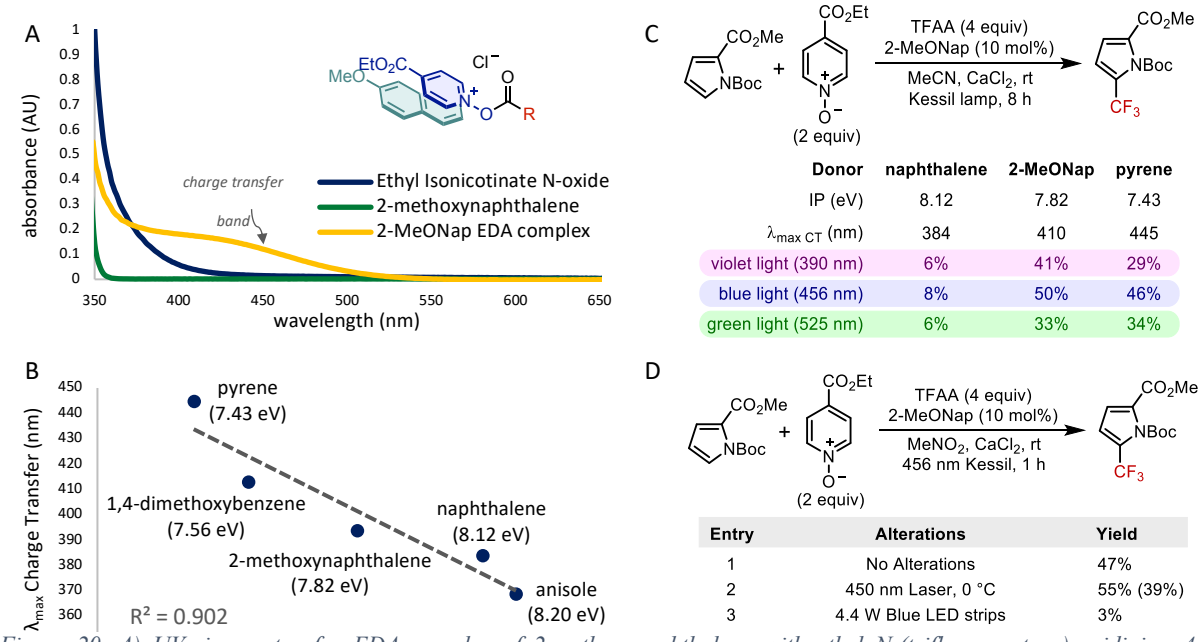

Figure 20. A) UV-vis spectra for EDA complex of 2-methoxynaphthalene with ethyl N-(trifluoroacetoxy)pyridinium-4-carboxylate. B) Mulliken correlation of arene donors with ethyl N-(trifluoroacetoxy)pyridinium-4-carboxylate in acetonitrile. C) Effect of irradiation wavelength on reactivity of EDA complexes. ^{19}F NMR yields with $PhCF_3$ as internal standard. D) Optimization of reaction conditions. ^{19}F NMR yields with $PhCF_3$ as internal standard (Isolated yield).

Further studies of the EDA complex demonstrated that the absorbance of the charge transfer band increased with the polarity of the solvent and concentration, as the complex showed peak absorbance properties in nitromethane at or above 0.6 M. Interestingly, it was found that the addition of an inorganic salt, such as calcium chloride, had a modest impact on the absorbance of the complex, as the addition of 1 equivalent of calcium chloride in nitromethane delivered the strongest absorbance for the CT band (Figure S15). It is believed that the Lewis acidic metal plays a dual role in increasing the absorptivity of the EDA complex, by both modifying the acceptor through coordination and by acting as an electrolyte, thereby increasing the ionic strength of the solution. Analysis of the complex using Job's method[29] demonstrated that the most absorbing species is a 4:1 complex of 2-methoxynaphthalene donor to ethyl *N*-(trifluoroacetoxy)pyridinium-4-carboxylate acceptor in nitromethane (Figure 21). Precedence for EDA complexes that deviate from a 1:1 stoichiometry is found in Kochi's work, in which it was demonstrated that pyrene and pyridine *N*-oxide in the presence of Lewis acid boron trifluoride form 2:1:1 complexes.[30] It should be noted that while our observations support a 4:1 donor:acceptor stoichiometry, many states could exist in solution at any given time, and it is unclear which of these is the most reactive form of the EDA complex under the reaction conditions.

Applying knowledge gained from the aforementioned studies of the EDA complex, investigation of the trifluoromethylation reaction revealed that optimal yields (55% 3a) were obtained in the presence of 10 mol% 2-methoxynaphthalene donor, calcium chloride (1 equiv), ethyl isonicotinate *N*-oxide (2 equiv) and an excess of trifluoroacetic anhydride (4 equiv) under irradiation from a 450 nm laser diode (Figure 3D). Notably, this result is on par with the yield

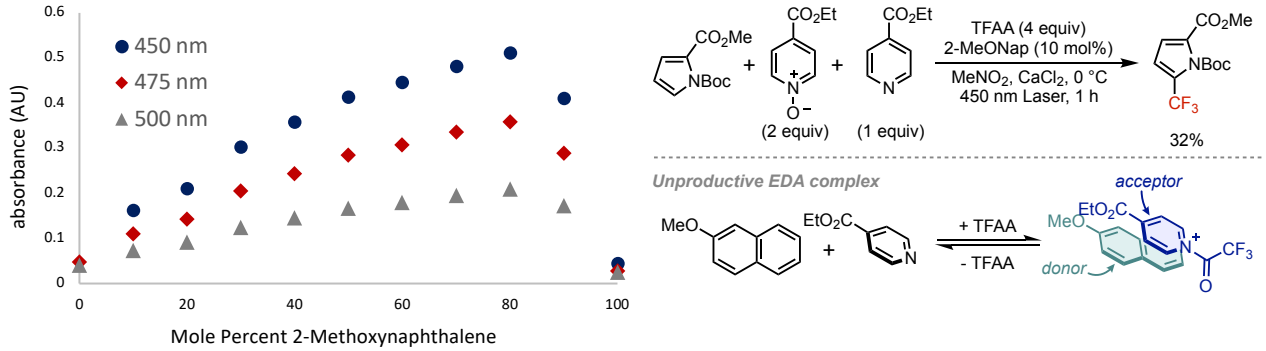

Figure 21. Job plot of 2-methoxynaphthalene (donor) with ethyl N-(trifluoroacetoxy)pyridinium-4-carboxylate (acceptor). (●) Absorbance at 450 nm. (♦) Absorbance at 475 nm. (▲) Absorbance at 500 nm. Right – Reaction inhibition by ethyl isonicotinate.

obtained when carrying out the radical trifluoromethylation under $Ru(bpy)_3Cl_2$ catalyzed conditions.[20,21] Increasing the loadings of ethyl isonicotinate *N*-oxide/TFAA did not lead to increased yields of the C–H trifluoromethylation products, but instead resulted in the production of the trifluoroacetylated side product, which arises from nucleophilic trapping of the electrophilic ethyl *N*-(trifluoroacetoxy)pyridinium-4-carboxylate intermediate. A second addition of 2 equiv. of ethyl isonicotinate *N*-oxide and 4 equiv. TFAA reagent mixture in nitromethane, followed by irradiation for an additional hour, did not improve the reaction yield. We hypothesized that under reaction conditions the production of ethyl isonicotinate caused the reaction to stall. To test this hypothesis, we carried out the reaction in the presence of 1 equivalent of ethyl isonicotinate. Indeed, the addition of ethyl isonicotinate has a deleterious effect on the reaction outcome (Figure 21). And further investigations revealed that an unproductive EDA complex forms with ethyl *N*-(trifluoroacetyl)pyridinium-4-carboxylate that is produced under reaction conditions following decarboxylation. It is hypothesized that this complex sequesters donor catalyst away from the designed EDA complex, and absorbs photons that would otherwise be absorbed by the key catalytic intermediate.

Exploration of the scope of the trifluoromethylation reaction demonstrated that *N*-protecting groups had an influence on the reactivity, as *N*-Boc protected methyl pyrrole-2-

carboxylate gave the highest yield (55%, 3a). While *N*-mesyl (3c) and *N*-tosyl (3d) protecting groups had a significant deleterious impact on the reaction. *N*-Boc pyrrole (3g) proceeded in 41% yield with a 3 to 1 mixture of mono to bis trifluoromethylation. *N*-Boc 2-acetylpyrrole (3f)

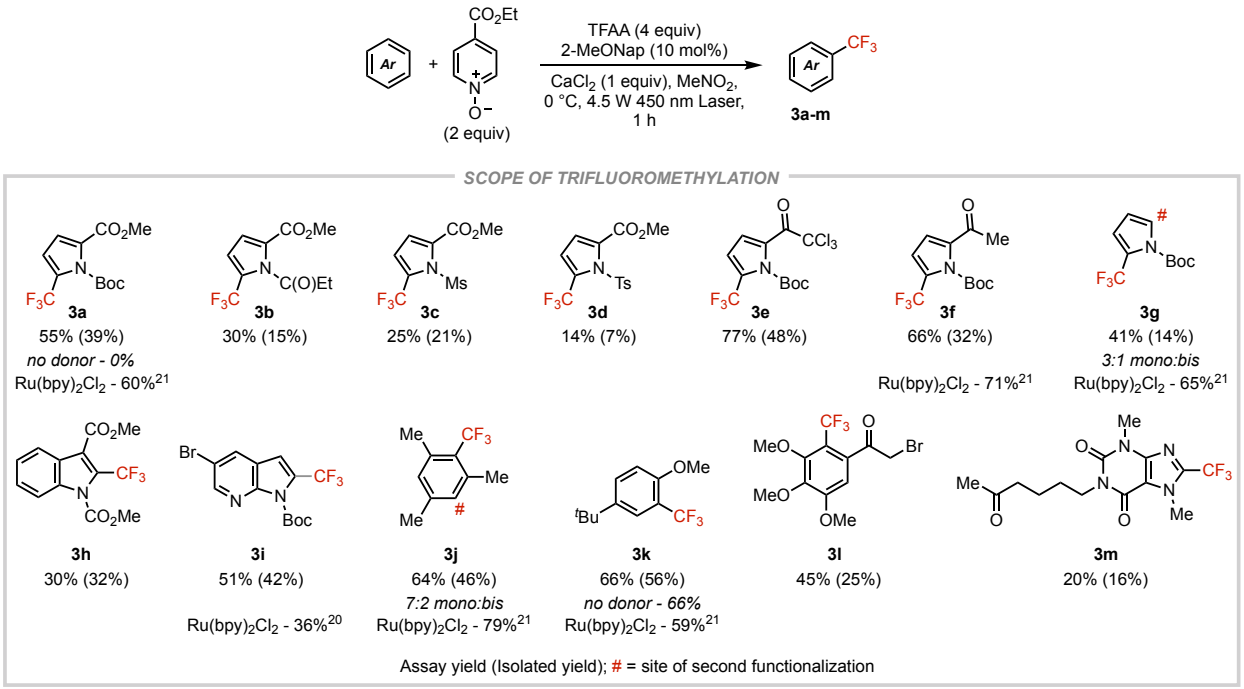

Figure 22. Scope of EDA complex catalyzed radical trifluoromethylation. Standard conditions: Arene (0.2 mmol, 1equiv), EINO (2 equiv), TFAA (4 equiv), 2-methoxynaphthalene (10 mol%), calcium chloride (1 equiv), nitromethane (0.25 mL, 0.8 M), 0 °C, 450 nm Laser

proceeded in good yield providing 66% of the trifluoromethylated product. *N*-Boc 2-(trichloro)acetylpyrrole (3e) and α-bromoacetophenone (3l) also provided the trifluoromethylated products in good yields, notably retaining the α-halogenation. Substituted benzene derivatives were effective substrates for the trifluoromethylation reaction, providing the trifluoromethylated aromatics in good yields (3j-3l). Finally, moderately complex indole (3h) and *N*-Boc-5-bromo-7-azaindole (3i) provided the trifluoromethylated products in modest yield as single-isomers.

Given the low costs of reagents and access to process friendly materials the reported EDA complex catalyzed trifluoromethylation may be an attractive reaction for process chemists, as such, we sought to explore the scalability of the reaction. Initial scale-up efforts failed, as in the presence

of calcium chloride the reactions became opaque and gelatinous. UV/vis studies revealed that calcium chloride could be exchanged for lithium chloride, delivering a heterogeneous, free-flowing reaction mixture and positively impacting the absorptivity of the EDA complex. Applying this knowledge to scale up efforts, methyl *N*-Boc pyrrole-2-carboxylate was effectively trifluoromethylated on a 2 mmol scale in a plug-flow reactor delivering 1.19 g (46%) of the desired product, notably, this is a 10-fold increase in scale relative to the batch reactions (Figure 23).

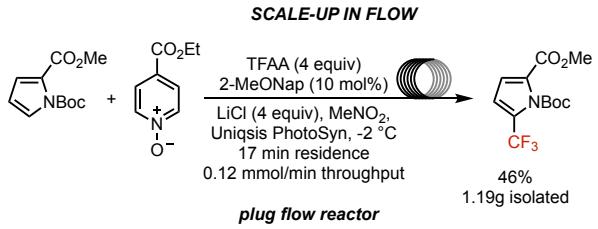

Figure 23. Flow scale-up of EDA complex trifluoromethylation

EDA complexes have been extensively studied for their ability to promote radical perfluoroalkylation reactions.[31] However, these reaction manifolds are predicated on the ability of *n*-donors to favorably interact with the polarized C–I bond of perfluoroalkyl iodides for complexation. However, this approach prevents unified applicability across perfluoroalkylation and alkylation reaction manifolds, as less polarized alkyl iodides do not form EDA complexes. Under our EDA complex catalysis conditions, *in situ* generation of ethyl *N*-(pivaloyloxy)pyridinium-4-carboxylate in the presence of 2-methoxynaphthalene delivered the desired EDA complex (IV) that displayed a broad absorbance from 380-495 nm assigned as the CT band. Subjecting this species to the reaction conditions in the presence of 1 equivalent of quinoxaline furnished the desired 2-(*tert*-butyl)quinoxaline (4a) in 57% yield (Figure 24). Attempts to further optimize for the Minisci alkylation were unsuccessful, as alkylation ethyl isonicotinate derived acceptor was competitive with that of quinoxaline. Extension of the EDA complex catalyzed Minisci alkylation allowed for the alkylation of more complex heterocycles.

Subjecting 3-chloro-6-phenyl pyridazine to the reaction conditions provided *tert*-butyl addition product 4b in 24% yield. Addition of the *tert*-butyl substituent to the imidazopyridine core structure of Gandotinib was carried out to provide structure 4c in 24% yield. A brief exploration of diverse radical fragments revealed that cyclohexyl, cyclopropyl, and benzyl radical fragments were efficiently generated and provided synthetically useful yields of the alkylated quinoxaline products (4d-f).

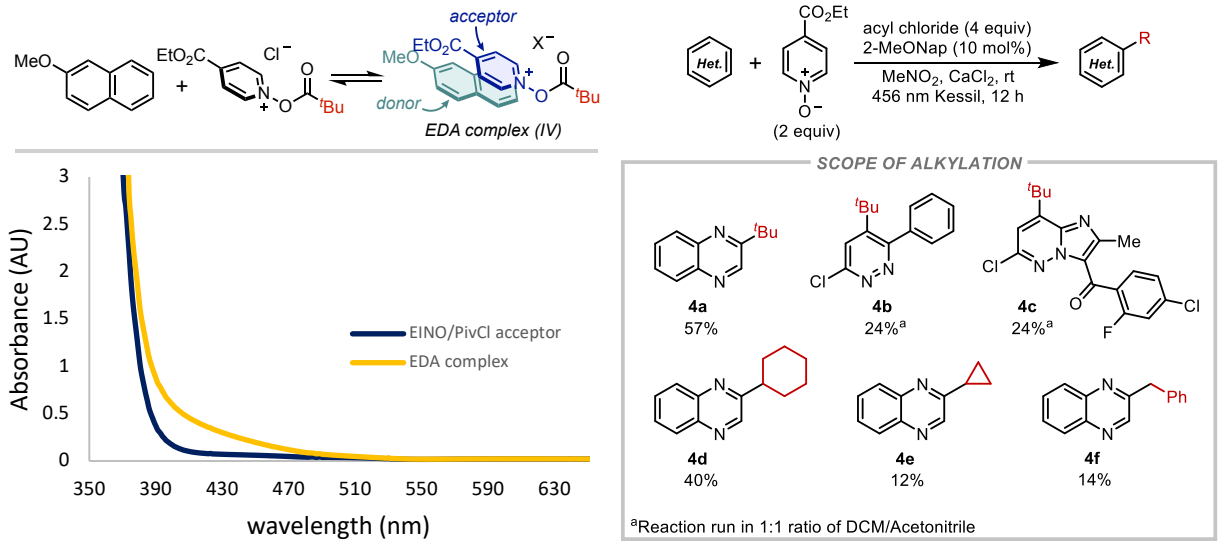

Figure 24. UV-vis of N-(pivaloxy)pyridinium EDA complex (left). Scope of EDA complex catalyzed Minisci alkylation (right).

We have developed a photochemical protocol that leverages an EDA complex as a catalytic intermediate to promote the C–H trifluoromethylation and alkylation of (hetero)arenes. The catalytic reaction is enabled by the selective donor-acceptor complexation between ethyl *N*-(acyloxy)pyridinium-4-carboxylate salts and an exogenous donor, 2-methoxynaphthalene, which undergoes photo-chemical degradation to reveal the reactive radical intermediates. Study of the EDA complex revealed that the addition of inorganic salts, calcium chloride and lithium chloride, enhanced the absorptivity of the complex. This information allowed for the EDA complex promoted trifluoromethylation of methyl *N*-Boc pyrrole-2-carobylate to be carried out on multigram scale in flow.

3.3 Outlook and Future Directions

The development of alkylation and perfluoroalkylation catalyzed by a designed EDA complex provides a novel reactivity paradigm that is significantly under-explored.[4] In this regard, future studies for EDA catalysis can extend from this seminal work in one of two major directions, 1) demonstration of new radical based transformations from the developed catalyst system or 2) development of new catalyst systems focused on accessing reactivity enabled by an oxidation event. On the basis of the above statement, two such ideas are highlighted below.

Aryl Transfer Reaction. A focal point of research in our group over the past decade has been the development radical aryl transfer reactions.[32-34] In this regard, applying the developed EDA catalysis conditions, aryl transfer reactivity could be accessed through use of 1,1-diaryl pentenol substrates.[35] In this reaction paradigm, the aryl transfer product would be furnished through a 1,5-radical cyclization, followed by an oxidation to yield the acetophenone product. Oxidation of the ketyl radical would be the chain carrying process in this reaction, as electron transfer to the *N*-(acyloxy)pyridinium would result in the production of a second equivalent of a radical intermediate while concomitantly delivering the desired acetophenone.

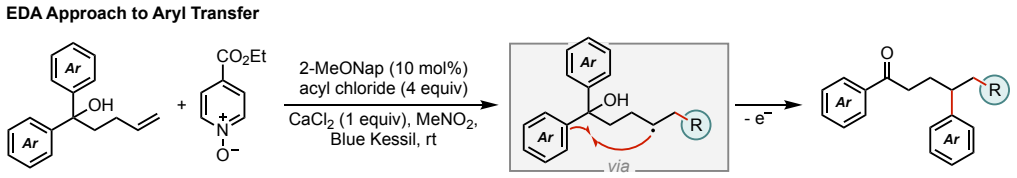

Figure 25. Proposed EDA complex catalyzed aryl transfer reaction.

Biaryl Coupling. To this point, the majority of approaches to leverage EDA complexes in catalysis have focused on the reductive decomposition of an auxiliary for radical generation, with little development in the way of accessing oxidative reactivity.[4,18,19] A potential avenue to access

EDA complex catalysis under an oxidative reaction paradigm is the development of biaryl coupling from aryl borate reagents. Oxidation of aryl borate reagents has been documented to lead to reductive elimination products.[36] The application of *N*-methyl pyridinium reagents as acceptors should allow for the formation of an EDA complex with the aryl borate substrate, and subsequent irradiation would lead to an electron transfer, and ultimately to the formation of the desired biaryl products. Preliminary studies revealed that exposing sodium tetraphenyl borate to methyl viologen dichloride in acetonitrile led to efficient formation of the desired biphenyl product upon irradiation with a 390 nm lamp. Although this reaction is stoichiometric in acceptor, it serves as a proof of concept demonstrating the biaryl products can be accessed through EDA complex promoted reactivity.

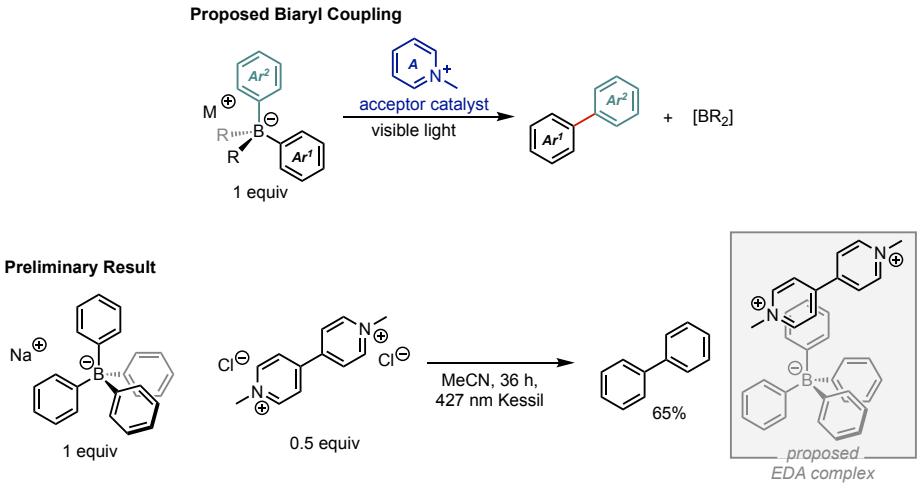

Figure 26. EDA complex catalyzed biaryl coupling

3.4 Experimental Procedures and Compound Characterization

General Information:

All chemicals were used as received unless otherwise noted. Reactions were monitored by TLC and visualized with a dual short wave/long wave UV lamp. Column flash chromatography was performed using 230-400 mesh silica gel or via automated column chromatography. Preparative

TLC purifications were run on silica plates of 1000 μm thickness. NMR spectra were recorded on Varian MR400, Varian Inova 500, Varian Vnmrs 500, or Varian Vnmrs 700 spectrometers. Chemical shifts for ^{1}H NMR were reported as δ, parts per million, relative to the signal of $CHCl_3$ at 7.26 ppm. Chemical shifts for ^{13}C NMR were reported as δ, parts per million, relative to the center line signal of the $CDCl_3$ triplet at 77.16 ppm. Chemical shifts for ^{19}F NMR were reported as δ, parts per million, relative to the signal of a trifluorotoluene internal standard at -63.72 ppm. Reaction optimization experiments (donor screening, N-oxide screening, and substrate screening) were quantitatively analyzed by ^{19}F NMR with a relaxation delay of 1s, while later optimization experiments and all internal standard yields were quantified by ^{19}F NMR with a 5s relaxation delay. The abbreviations s, br. s, d, dd, br. d, ddd, t, q, br. q, qi, m, and br. m stand for the resonance multiplicity singlet, broad singlet, doublet, doublet of doublets, broad doublet, doublet of doublet of doublets, triplet, quartet, broad quartet, quintet, multiplet and broad multiplet, respectively. IR spectra were recorded on a Perkin-Elmer Spectrum BX FT-IR spectrometer fitted with an ATR accessory. Mass Spectra were recorded at the Mass Spectrometry Facility at the Department of Chemistry of the University of Michigan in Ann Arbor, MI on an Agilent Q-TOF HPCL-MS with ESI high resolution mass spectrometer. Fluorescence, actinometry, and quantum yield measurements were performed with a Fluoromax-2 fluorimeter equipped with a 150W Xe arc lamp. UV-VIS measurements were obtained on a Shimadzu UV-1601 UV/VIS Spectrometer or a Varian Cary-50 spectrophotometer. $MeNO_2$ was distilled over $CaCl_2$ prior to usage and was stored in individual desiccators in between reactions. TFAA was freshly distilled in a Hickman still at 55 °C under an atmosphere of argon. Ethyl isonicotinate was distilled under vacuum in a short path distillation apparatus prior to use.

LED and laser irradiation sources:

• LED ribbons and the requisite power box and cables were purchased from Creative Lighting Solutions (http://www.creativelightings.com) with the following item codes: CL-FRS5050-12WP-12V (4.4W blue LED light strip), CL-PS94670-25W (25 W power supply), CL-PC6FT-PCW (power cord), CL-TERMBL-5P (terminal block). Green and Purple (near UV) were purchased under the same product code.

• 450 nm NUBM 6W Laser was purchased from DTR's laser shop (https://sites.google.com/site/dtrlpf/, accessed July 9, 2018) and includes 450 nm Laser diode with 12mm copper module and H2 lens, an aluminium radiator heat sink (20x27x50mm), a DC voltage controller (Costway EP20570-110V). The laser apparatus was assembled using a chemglass vial adapter (CG1318), and a 24/40 septa (CG302228), a fan (Westpointe Electrical GVF4-RP), and electrical tape. Laser was aligned and operated using Eagle Pair 190-540 nm OD5 laser safety goggles in alignment with OSEA, ANSI and University of Michigan Laser Safety Standards. 60% of laser accidents occur when aligning the laser beam with the target. Take precaution to eliminate reflective surfaces when designing a reactor.

Reaction Procedures

Reaction Procedure A: Blue LED, ambient temperature

Reactions were run on a 0.1-1.0 mmol scale in a 1 or 2 dram vial quipped with stir bar and cap (parafilmed shut). Three 4.4W BLUE LED ribbons were wrapped in a U shape around the demarcated reaction positions (x). At this distance the standing air temperature (no fan used) was measured at 30-35°C after about 1 hour of irradiation.

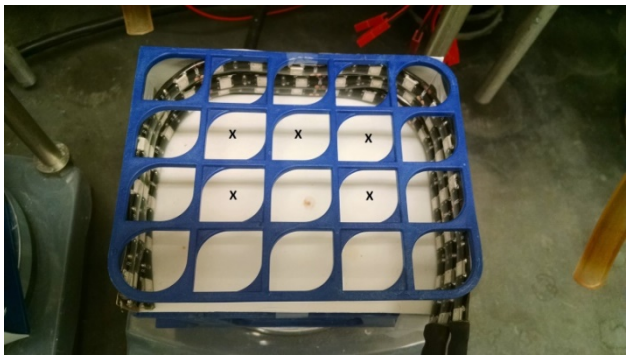

Reaction Procedure B: Green LED, 13°C

Reactions were run on a 0.1-1.0 mmol scale in a 1 or 2-dram vial quipped with stir bar and cap (parafilmed shut). Three 4.4W Green LED ribbons were wrapped in a circle around the reaction with the reaction about 1-2 inches from the outside of the jacked beaker. At this distance the internal bath temperature did not 13 °C. Programming lower temperatures resulted in ice formation on the outside of the beaker prohibiting direct LED irradiation of the reactions.

Reaction Procedure C: 450 nm Laser irradiated EDA trifluoromethylation reaction.

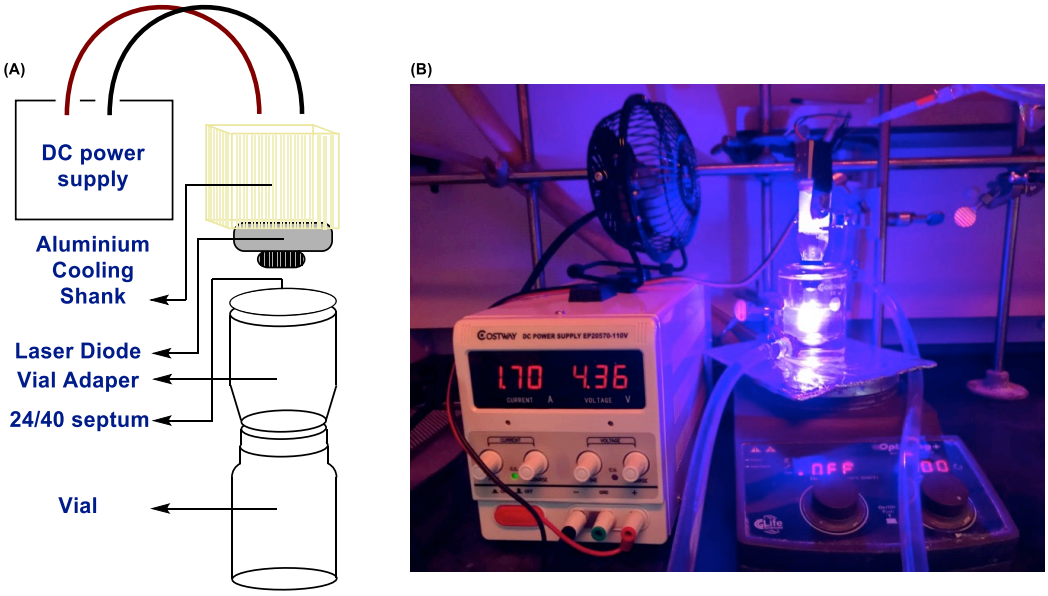

Laser set-up protocol: A dummy vial was placed on the laser set up and the laser was strapped into place using electrical tape against the septum - vial adapter holster. The laser was powered to 0.2 amperes to test the placement of the light. At this current input it is safe to look at without protection (<500 mW of light power). The laser beam was adjusted by hand to ensure the laser path intersected the center of the vial. Electrical tape ensured stability of the laser mount on the vial adapter. Once all was set, the electrical tape was reinforced with a layer of parafilm around the adapter body. The laser device was attached to a three-prong clamp, and with the dummy vial attached with a piece of cardboard below, the laser was set to 1.7 A current input. **SAFETY: DO NOT LOOK AT THIS EVEN WITH BLUE LIGHT PROECTION. THE INCIDENT LIGHT OFF THE CARDBOARD/VIAL IS SUFFICIENTLY BRIGHT TO IRRITATE THE EYES.** Stabilize the laser swiftly at 1.70A, and then turn off the power. Do this swiftly as prolonged exposure of the cardboard to the laser at high power will result in burning.

Reaction set-up protocol: To a 1-dram vial with stir bar, neat arene or heteroarene substrate (0.2 mmol) was measured on the bench top. To this was added ethyl isonicotinate *N*-oxide crystals (0.4

mmol, 67 mg, 2 equiv), 2-methoxynaphthalene (0.02 mmol, 3.1 mg, 0.1 equiv), and $CaCl_2$ (0.2 mmol, 22.2 mg, 1 equiv). The neat mixture of solids was diluted in $MeNO_2$ (250 µL, 0.8 M with respect to arene substrate), followed by the addition of TFAA (0.8 mmol, 113 µL, 4 equiv). The vial was attached to the vial adapter mounting the laser, and the reaction solution was dipped into the methanol bath cooled by a jacketed beaker to 0°C. The reaction was allowed to pre-stir at this temperature for 5 minutes prior to initiating irradiation. The reaction was irradiated at 1.70-1.71 amperes for 1 hour while stirring at 700 rpm. Following this irradiation period, the laser was shut off, and the reaction was quenched with an equal volume addition (125 µL) of MeOH at 0°C. Substrate purification is detailed below.

Photon Flux Measurements:

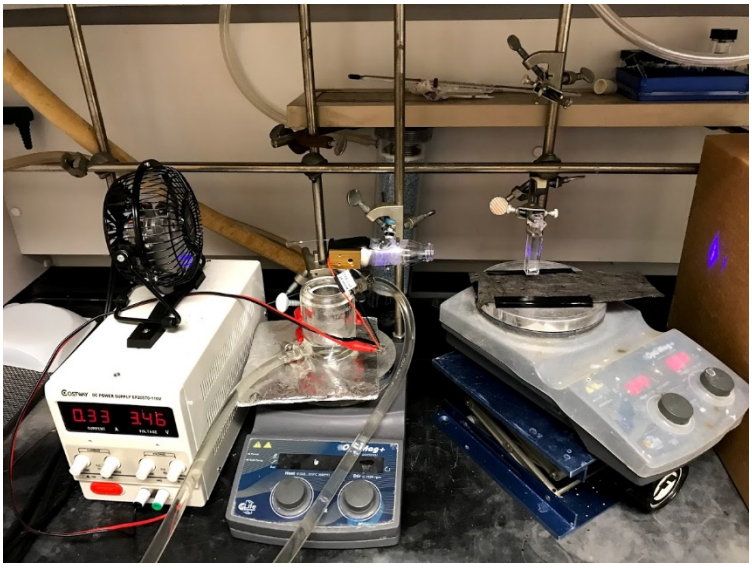

Flux Experiment Set-up

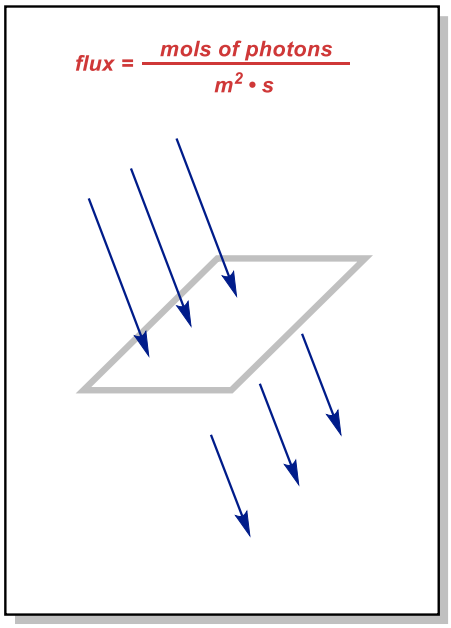

LED Ribbons (4.4 W) = 9.8 x 10^{-8} E/s

0.65 W, 450 nm Laser Diode = 2.9 x 10^{-6} E/s

2.5 W, 450 nm Laser Diode = 5.4 x 10^{-6} E/s

Calculated with Ferrioxylate Actinometer

Standard Sample preparation : 0.05 M stock solution: To a 100 mL volumetric flask, 0.281 mL of concentrated H_2SO_4 was added to 90 mL of deionized water. Then the remainder of volume was filled with deionized water to the 100 mL graduation mark.

0.15 M potassium ferrioxolate solution: This solution was prepared by dissolving solid $K_3FeC_2O_4 \cdot 3H_2O$ (1.842 g, 3.75 mmol) in 20 mL of 0.05 M H_2SO_4 (*aq*) solution. The remainder of the 25 mL volume was then filled with 0.05 M H_2SO_4 (*aq*) after ensuring the ferrioxylate had fully dissolved. This solution was stored in an amber bottle and kept in the dark except for the brief time it was in use.

Developer solution: 225 g of sodium acetate trihydrate was dissolved in 1 liter of 0.5 M sulfuric acid. 10 g of 1,10-phenantroline was added to this solution. This was stored in a 1 L clear glass bottle, but stored in the dark when not in use.

Experimental Procedure: Prior to running the experiment, 5x3 2 dram amber vials were filled with 5x0.9 mL with a 1 mL repeater pipette and capped. The laser was aligned and pre-set to the desired input current by irradiating an empty cuvette to ensure the beam was not reflecting off the stir bar, or stir plate below. After alignment the laser was turned off. In the dark, to a 1 mL quartz cuvette was charged with 3x0.9 mL of the 0.15 M potassium ferrioxolate solution. This was stirred at 700 rpm for 1 minute prior to extracting 10 μL and adding it to a vial of developer solution. To being the reaction, an object used to block the laser beam was placed in between the laser and the stirring reaction. Then the laser was turned on and allowed to settle on the desired light output (this takes 10-15 seconds, often over-shoots the programmed amperage). Then the barrier was removed and the reaction began. 10 μL aliquots were extracted and added to individual vials of developer solution. Each light setting was repeated three times.

Data Analysis:

To calculate the photon flux, first determine the number of Fe^{2+} ions produced in the reaction:

$$moles\ Fe^{2+} = \frac{\Delta A_{510\ nm} V_1 V_3}{\varepsilon_{510\ nm} l V_2}$$

Δ A = difference in absorbance at 510 nm between sample and t_0 time point

l = pathlength of cuvette (1 cm)

$\varepsilon_{510\ nm}$ = Extinction coefficient of $Fe(phen)_3$ complex at 510 nm (11,100 M^{-1} cm^{-1})

V_1 = total volume of irradiated solution (3x0.9 mL = 2.7 mL)

V_2 = volume of aliquot extracted from V_1 (0.01 mL)

V_3 = volume that V_2 is diluted to (5x0.9 mL = 4.5 mL)

Photon flux is then determined as:

$$photon\ flux = \frac{moles\ of\ Fe^{2+}}{\emptyset_{405\,nm} \bullet t \bullet F}$$

$\emptyset_{450}$ = 0.93

t = time evolved (seconds)

F = mean fraction of light absorbed by the ferrioxalate solution (F = 0.986)

0.71 A 450 nm Laser Irradiation:

Flux = 2.98×10^{-6} mol photons/second

	Samples (A_{510})						
time of irr (seconds)	**1**	**2**	**3**	**mean**	**std dev**	**rel dev**	**dA**
0	0.266846	0.280273	0.265259	0.270793	0.008248	3%	0
15	0.466064	omit	0.450806	0.458435	0.010789	2%	0.187642
30	0.727173	0.701782	0.671997	0.700317	0.027617	4%	0.429525
45	0.86731	0.907837	0.85437	0.876506	0.027894	3%	0.605713
60	omit	0.949219	0.994507	0.971863	0.032023	3%	0.70107
75	1.005737	1.236328	1.178955	1.14034	0.120047	11%	0.869547

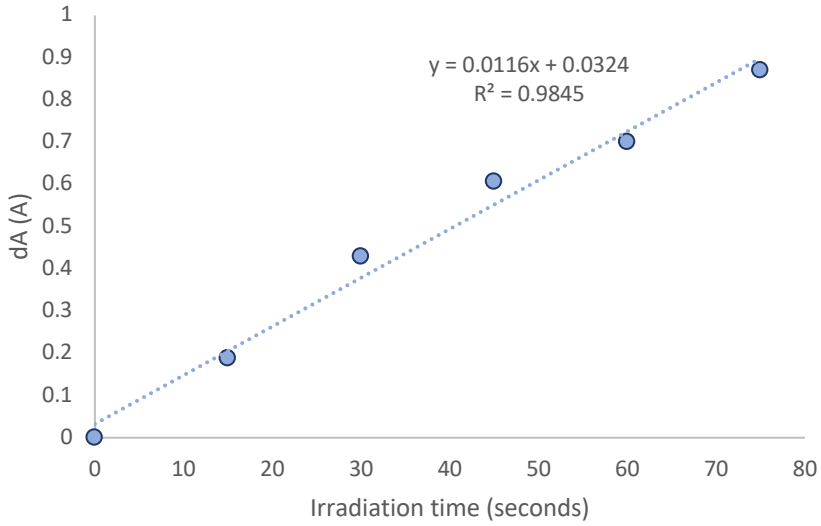

Photon flux using 0.71A 450 nm Laser irradiation

1.70 A 450 nm Laser Irradiation:

Flux = 5.44 x 10^{-6} mol photon/second

	Samples (A_{510})						
time of irr (seconds)	1	2	3	mean	std dev	rel dev	dA
0	0.285889	0.281006	0.293945	0.286946667	1%	0.022771	0
10	0.79895	0.791016	0.757202	0.782389333	2%	0.028337	0.495443
20	1.216553	1.107666	1.074097	1.132772	7%	0.065744	0.845825
30	1.06311	1.392578	0.775879	1.077189	31 %	0.286478	0.790242

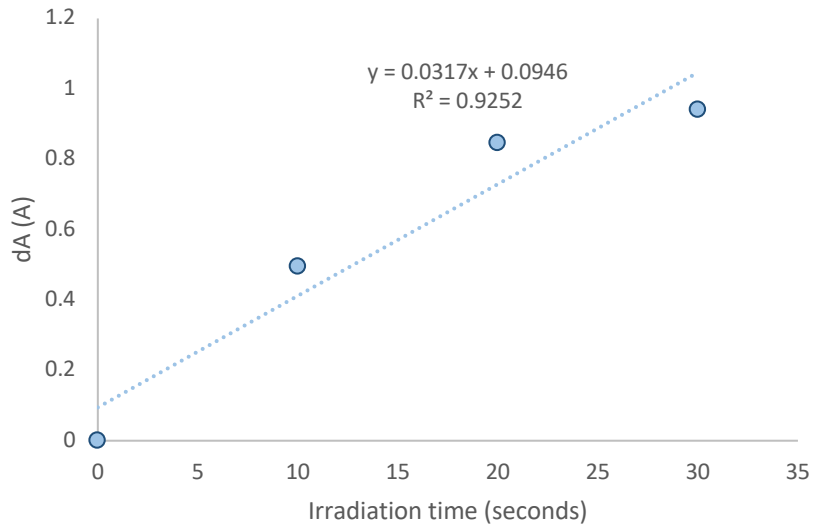

Photon Flux time using 1.70 A 450 nm laser irradiation

Creative Lighting Ribbon, 4.4 W Blue

Flux = 1.62 x 10-8 mol photons/second/ribbon

For 3 ribbons = 2.92 x 10-7 photons/second

Two of the sides of the vial were taped off with black electrical tape to ensure a single path length of 1 cm.

The ribbon was cut into 6 individual units each containing 3 LEDs. Electrical tape was used to only expose 2 of the units, and the results have been scaled to account for the whole ribbon, and multiple ribbons used for the reactor. Ferroxylate actinometry does not measure Green irradiation (515 nm), thus the magnitude of the photo flux for both creative lighting ribbon designs are hypothesized to be within the same order of magnitude (~100 weaker than the laser flux).

	Samples (A_{510})						
time of irr (seconds)	**1**	**2**	**3**	**mean**	**std dev**	**rel dev**	**dA**
0	0.363892	0.332397	0.306396	0.334228	0.028792	9%	0
90	0.403076	0.369385	0.338257	0.370239	0.032418	9%	0.036011
180	0.435913	0.395752	0.337769	0.389811	0.049341	13%	0.055583
270	0.454712	0.431641	0.406128	0.430827	0.024302	6%	0.096599
360	0.505737	0.504761	0.429443	0.47998	0.043769	9%	0.145752

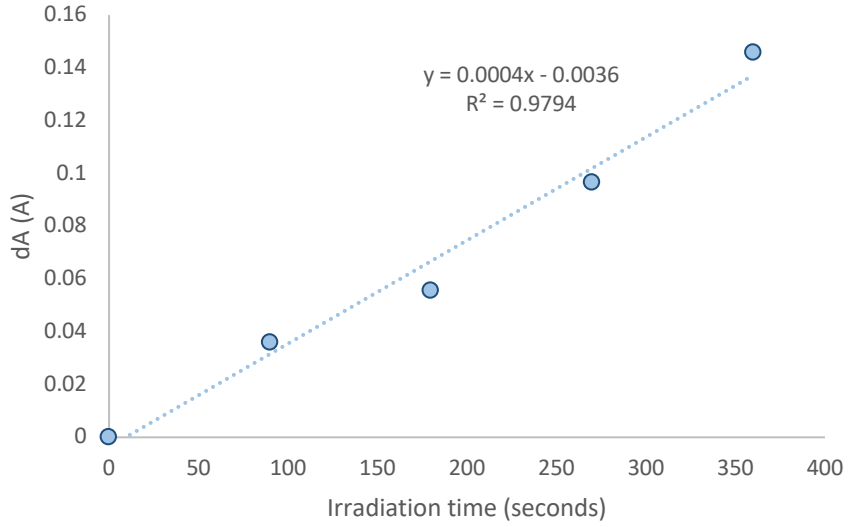

Procedure for reaction in Uniqsis Photosyn Flow Reactor

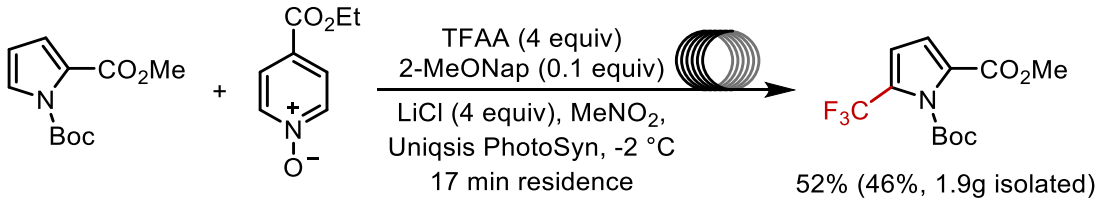

Flow reactor: Uniqsis Photosyn reactor 455 nm irradiation, cold coil reactor base with a 10 mL PFA coil.

Reactor set-up: The Uniqsis Photosyn reactor was connected to an ethylene glycol/water chiller that cooled the reaction loop to -2 °C. The LEDs of the Photosyn reactor were cooled by a constant flow of water. Material was pumped through the system with an IPC-04 Ismatec peristaltic pump (Model No.: ISM930C, 4 channel pump) with a range of 32.2 µL/min up to 3.2 mL/min.

Prior to running the reaction, the reactor loop was primed by first flowing 3 mL of nitromethane, followed closely by flowing 3 mL of neat TFAA through the reactor. This was done to rid the tubing of any water that may have been in the system.

To a flame dried 4-dram vial equipped with a stir bar was weighed methyl N-Boc pyrrole-2-carboxylate (2 g, 8.9 mmol, 1 equiv). To this was added ethyl isonicotintae N-oxide (2 equiv, 17.8 mmol, 2.97 g), 2-methoxynaphthalene (0.1 equiv, 0.89 mmol, 140 mg) and lithium chloride (4 equiv, 35.5 mmol, 1.5 g). The mixture of solvents was then taken up in nitromethane (11 mL), sonicated for a minute to ensure mixing, and cooled to 0 °C in an ice bath. TFAA (4 equiv, 35.5 mmol, 7.5 g, 5 mL) was then added slowly to the cooled, stirred mixture immediately prior to starting the flow reaction. **Caution!** The acylation with TFAA is exothermic and reacts vigorously, care should be taken so that TFAA is added slowly. The receiving flask for the flow reaction was a 100 mL round bottom containing 50 mL of a saturated sodium bicarbonate solution, and this

solution was cooled in an ice bath. At the conclusion of the reaction, 25 μL of benzotrifluoride was added and the reaction yield was determined by ^{19}F NMR (52%).

The crude reaction material was taken up in to 10 mL of water and extracted with DCM (3 x 10 mL). The combined organic extracts were washed with sat. sodium bicarbonate (1 x 10 mL) and sat. NaCl solution (1 x 10 mL). The combined organic extracts were dried over sodium sulfate. The crude material was purified by column chromatography on a Biotage Selekt automatic column system, gradient from 0-10% ethyl acetate in hexanes. Methyl N-Boc 5-(trifluoromethyl)pyrrole-2-carboxylate was isolated as a colorless oil (1.19 g, 46%).

Reaction Screening Experiments:

Reaction screen 1: Finding a Good Donor

For the reactions in MeCN: To a 1-dram vial with stir bar, neat arene or heteroarene substrate (0.1 mmol) was measured on the bench top. To this neat substrate, pyridine *N*-oxide (0.20 mmol, 19.0 mg, 1 equiv) was added along with the specified donor (0.01 mmol, 0.1 equiv). The neat mixture of solids was diluted in MeCN (250 μL, 0.4 M with respect to arene substrate) followed by the addition of TFAA (0.4 mmol, 56 μL, 4 equiv). The vial was flushed with nitrogen, capped and parafilmed shut, and placed in reactor described in Reaction procedure A. The reaction was irradiated at 12 hours while stirring at 700 rpm. Following this irradiation period, the LEDs were shut off, and the reaction was quenched with an equal volume addition (250 μL) of MeOH at room temperature. 12.3 μL (1 equiv) of 1,1,1-trifluorotoluene was added to the reaction mixture, and a sample was of this solution was analyzed by ^{1}H and ^{19}F NMR.

Reaction in $MeNO_2$: To a 1-dram vial with stir bar, neat arene or heteroarene substrate (0.1 mmol) was measured on the bench top. To this neat substrate, 4-Phenyl pyridine *N*-oxide (0.20 mmol,

34.2 mg, 1 equiv) was added. The neat mixture of solids was diluted in $MeNO_2$ (500 µL, 0.2 M with respect to arene substrate) followed by the addition of TFAA (0.4 mmol, 56 µL, 4 equiv). The vial was flushed with nitrogen, capped and parafilmed shut, and placed in reactor described in Reaction procedure A. The reaction was irradiated at 12 hours while stirring at 700 rpm. Following this irradiation period, the LEDs were shut off, and the reaction was quenched with an equal volume addition (500 µL) of MeOH at room temperature. 12.3 µL (1 equiv) of 1,1,1-trifluorotoluene was added to the reaction mixture, and a sample was of this solution was analyzed by ^{1}H and ^{19}F NMR.

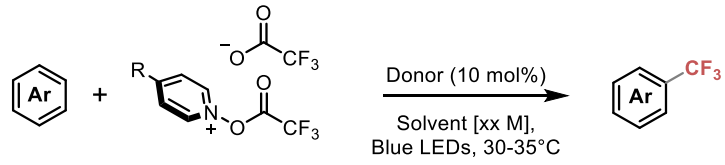

D	IP(eV)	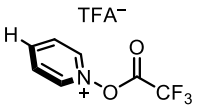 MeCN [0.4 M]	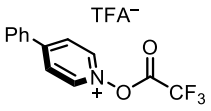 $MeNO_2$ [0.2 M]
Naphthalene	8.12	1	10
1,3,5-trimethoxybenzene	7.96	1	0
hexamethylbenzene	7.85	5	12
N-trifluoroacetylcarbazole	--	2	--
2-Methoxynaphthalene	7.8	8	28
N-methylcarbazole	7.57	6	0
4-bromophenyl-diphenylamine	--	18	15
triphenylamine	6.86	18	10

Reaction Screen 2: Finding an optimal PNO reagent and arene substrate:

To a 1-dram vial with stir bar, neat arene or heteroarene substrate (0.1 mmol) was measured on the bench top. To this neat substrate, pyridine *N*-oxide (0.20 mmol, 1 equiv) derivative was added along with 2-methoxynaphthalene (0.01 mmol, 1.5 mg, 0.1 equiv). The neat mixture of solids was

diluted in $MeNO_2$ (125 µL, 0.2 M with respect to arene substrate) followed by the addition of TFAA (0.4 mmol, 56 µL, 4 equiv). The vial was flushed with nitrogen, capped and parafilmed shut, and placed in reactor described in Reaction procedure B. The reaction was irradiated at 12 hours while stirring at 700 rpm. Following this irradiation period, the LEDs were shut off, and the reaction was quenched with an equal volume addition (125 µL) of MeOH at room temperature. 12.3 µL (1 equiv) of 1,1,1-trifluorotoluene was added to the reaction mixture, and a sample was of this solution was analyzed by ^{1}H and ^{19}F NMR.

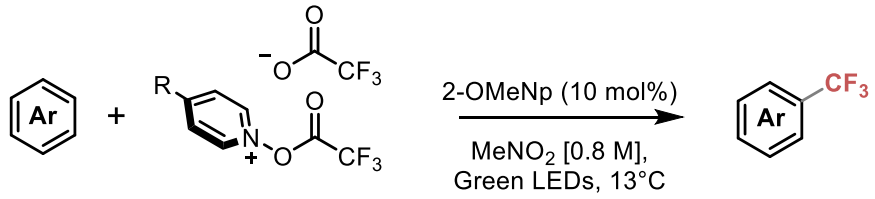

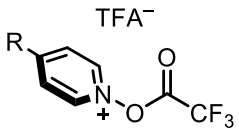		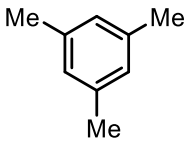	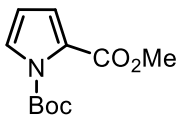
R = H	0 (***0***)	0 (***0***)	0 (***0***)
R = Ph	0 (***0***)	18 (***10****)	5 (***0***)
R = CO_2Et	5 (***0***)	38 (***0***)	50 (***0***)
R = CN	5 (***0***)	12 (***0***)	10 (***0***)

(+)-2-OMeNp
(–)-2-OMeNp
**** with Blue LEDs***

Reaction Screen 3: Reassessing Donors

To a flame dried 1-dram vial with stir bar was weighed methyl N-Boc pyrrole-2-carboxylate (0.1 mmol, 23 mg, 1 equiv). To this was added ethyl isonicotinate *N*-oxide (0.4 mmol, 67 mg, 2 equiv) along with the specified donor (0.01 mmol, 0.1 equiv) and calcium chloride (0.21 mmol, 11.1 mg, 1 equiv). The mixture of solids was evacuated and backfilled with nitrogen 5 times , then the solids were taken up in $MeNO_2$ (125 µL) followed by the addition of TFAA (0.4 mmol, 56 µL, 4 equiv). The vial was flushed with nitrogen, capped, electrical film placed over the septa, and parafilmed shut, and placed 5 cm away from a single Kessil lamp. The reaction was irradiated for 12 hours while stirring at 700 rpm. Following this irradiation period, the Kessil lamp was shut off, and the reaction was quenched with an equal volume addition (125 µL) of MeOH at room temperature. 12.3 µL (1 equiv) of 1,1,1-trifluorotoluene was added to the reaction mixture, and a sample was of this solution was analyzed by ^{1}H and ^{19}F NMR.

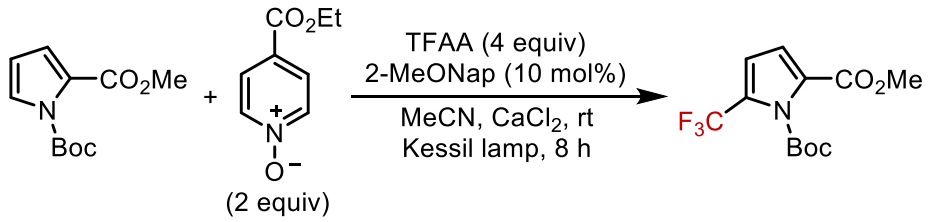

Donor	naphthalene	2-MeONap	pyrene
IP (eV)	8.12	7.82	7.43
$\lambda_{max\ CT}$ (nm)	384	410	445
violet light (390 nm)	6%	41%	29%
blue light (456 nm)	8%	50%	46%
green light (525 nm)	6%	33%	34%

Reaction Screen 4: Solvent, Tempearature and Additive Screening

To a 1-dram vial with stir bar, neat arene or heteroarene substrate (0.1 mmol) was measured on the bench top. To this neat substrate, ethyl isonicotinate *N*-oxide crystals (0.2 mmol, 33 mg, 2 equiv) was added along the specified donor (0.01 mmol, 0.1 equiv). The neat mixture of solids

was diluted in $MeNO_2$ (125 µL, 0.2 M with respect to arene substrate) followed by the addition of TFAA (0.4 mmol, 56 µL, 4 equiv). The vial was flushed with nitrogen, capped and parafilmed shut, and placed in reactor described in Reaction procedure A or C. The reaction was irradiated for the indicated time while stirring at 700 rpm. Following this irradiation period, the light source was shut off, and the reaction was quenched with an equal volume addition (125 µL) of MeOH at room temperature. 12.3 µL (1 equiv) of 1,1,1-trifluorotoluene was added to the reaction mixture, and a sample was of this solution was analyzed by ^{1}H and ^{19}F NMR.

Entry	Reaction Procedure	Time (min)	Temp. (°C)	Solvent	Yield[a]
1	A	900	rt	$MeNO_2$	22[b]
2	A	900	"	$MeNO_2$	6[c]
6	C - 0.70 A, 450 nm laser	60	"	$MeNO_2$	26
7	C - 1.70 A, 450 nm laser	"	"	$MeNO_2$	43
8	C - 5.00 A, 450 nm laser	"	"	$MeNO_2$	5
9	C - 1.70 A, 450 nm laser	"	"	MeCN	33
10	C - 1.70 A, 450 nm laser	"	"	Propylene carbonate	13
11	"	"	0	$MeNO_2$[d,e]	55
12	"	"	–15	$MeNO_2$[d]	47
13	"	"	22	$MeNO_2$[d]	42
14	"	"	–40	MeCN	22
15	"	"	0	MeCN	24
16	"	"	rt	DMF	18
17	"	"	"	THF	12
18	"	"	"	DMSO	0
19	"	"	"	DMA	0
20	"	"	"	EtOAc	22
21	"	"	"	TFE	0

22	“	“	“	HFIP	0
23	“	“	“	DCE	0
24	“	“	“	$MeNO_2$ + HFIP (1:1)	9
25	“	“	“	Cyclohexane	9
26	“	“	“	TFT:$MeNO_2$ (1:1)	42
27	“	“	“	TFT:$MeNO_2$ (2:1)	35
28	“	“	“	TFT:$MeNO_2$ (5:1)	20
29	“	“	“	TFT:$MeNO_2$ (1:2)	24

[a] ^{19}F-NMR yield standardized to 1,1,1-trifluorotoluene

[b] Reaction degassed by sparging.

[c] reaction exposed to O_2 for entirety of run

[d] run with 1 equiv of $CaCl_2$ as desiccant in reaction

[e] average of 4 reactions

Reaction Screen 5: Screen of Blue Light Sources

To a flame dried 1-dram vial with stir bar was weighed methyl N-Boc pyrrole-2-carboxylate (0.1 mmol, 23 mg, 1 equiv). To this was added ethyl isonicotinate *N*-oxide (0.2 mmol, 33 mg, 2 equiv) was added along the specified donor (0.01 mmol, 0.1 equiv), and calcium chloride (0.1 mmol, 11.1 mg, 1 equiv). The mixture of solids was evacuated and backfilled with nitrogen 5 times, then the solids were taken up in $MeNO_2$ (125 µL) followed by the addition of TFAA (0.4 mmol, 56 µL, 4 equiv). The vial was flushed with nitrogen, capped, electrical film placed over the septa, and parafilmed shut, and placed 5 cm away from a single Kessil lamp. The reaction was irradiated while stirring at 700 rpm. Following this irradiation period, the light source was shut off, and the reaction was quenched with an equal volume addition (125 µL) of MeOH at room temperature. 12.3 µL (1 equiv) of 1,1,1-trifluorotoluene was added to the reaction mixture, and a sample was of this solution was analyzed by ^{1}H and ^{19}F NMR.

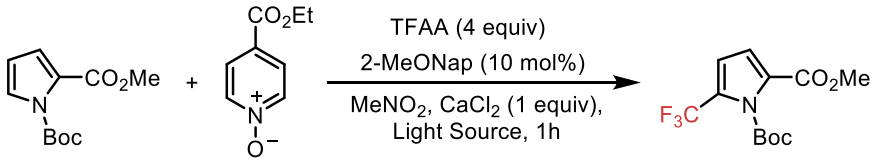

Entry	Light Source	Time	Yield*
1	Blue LED Strips	1 h	3%
2	Blue Laser 450 nm (0 °C)	1 h	38%
3	Kessil-427 nm	1 h	37%
4	Kessil-456 nm	1 h	39%
5	SynLED photoreactor	1 h	32%
6	Kessil-456 nm	8 h	48%

* Determined by ^{19}F NMR with $PhCF_3$ as an internal standard

We understood these results to indicate that the increased photon flux of the light source positively impacted the trifluoromethylation reaction until the reaction manifold is saturated with photons. At which point, excess photons do not impact the reactivity.

Reaction Screen 6: Equivalents of PNO, TFAA, and 2-MeONap

To a flame dried 1-dram vial with stir bar was weighed methyl N-Boc pyrrole-2-carboxylate (0.1 mmol, 23 mg, 1 equiv). To this was added ethyl isonicotinate *N*-oxide (0.2 mmol, 33 mg, 2 equiv) was added along the specified donor (0.01 mmol, 0.1 equiv) and calcium chloride (0.1mmol, 11.1 mg, 1 equiv). The mixture of solids was evacuated and backfilled with nitrogen 5 times, then the solids were taken up in $MeNO_2$ (125 µL) followed by the addition of TFAA (0.4 mmol, 56 µL, 4 equiv). The vial was flushed with nitrogen, capped, electrical film placed over the septa, and parafilmed shut, and placed 5 cm away from a single Kessil lamp. The reaction was irradiated for 8-12 hours while stirring at 700 rpm. Following this irradiation period, the light source was shut off, and the reaction was quenched with an equal volume addition (125 µL) of MeOH at room

temperature. 12.3 µL (1 equiv) of 1,1,1-trifluorotoluene was added to the reaction mixture, and a sample was of this solution was analyzed by ^{1}H and ^{19}F NMR.

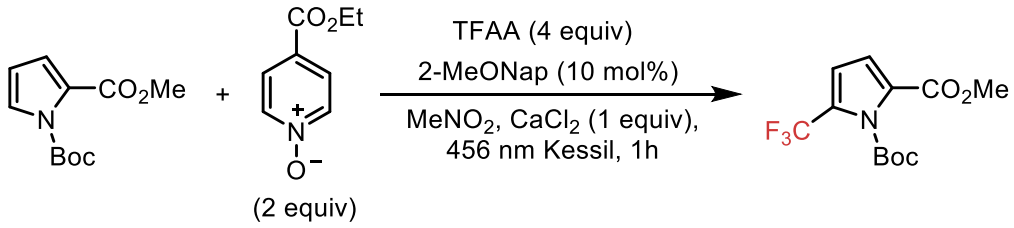

Entry	Alteration	Time	Yield*
1	2 eq PNO, 4 eq TFAA	1 h	52%
2	4 eq PNO, 8 eq TFAA	1 h	60%
3	8 eq PNO, 16 eq TFAA	1 h	52%
4	20 mol% 2-MeONap	1 h	49%
5	50 mol% MeONap	1 h	56%
6	2x (2 eq PNO, 4 eq TFAA)	1 h	53%

* Determined by ^{19}F NMR with $PhCF_3$ as an internal standard

Entries 1-3 demonstrate that the addition of excess TFAA/PNO reagent mixture have little to no positive influence on the formation of trifluoromethylated product. The increased loadings of TFAA/PNO reagent mixture also led to an increase in observed Friedel crafts like trifluoroacylation product. Entries 4 and 5 demonstrate that increasing the loading of donor catalyst has no impact on the efficiency of the reaction. Entry 6 demonstrates that two successive additions of TFAA/PNO reagent mixture does not positively impact the reaction, likely suggesting that the catalyst has become inactivated through functionalization.

Reaction Screen 7: Inorganic salt additives

To a flame dried 1-dram vial with stir bar was weighed methyl N-Boc pyrrole-2-carboxylate (0.1 mmol, 23 mg, 1 equiv). To this was added ethyl isonicotinate *N*-oxide (0.2 mmol, 33 mg, 2 equiv) was added along the specified donor (0.01 mmol, 0.1 equiv) and inorganic salt (0.1 mmol, 1 equiv). The mixture of solids was evacuated and backfilled with nitrogen 5 times, then the solids were taken up in $MeNO_2$ (125 µL) followed by the addition of TFAA (0.4 mmol, 56 µL, 4 equiv). The vial was flushed with nitrogen, capped, electrical film placed over the septa, and parafilmed shut, and placed 5 cm away from a single Kessil lamp. The reaction was irradiated for 8-12 hours while stirring at 700 rpm. Following this irradiation period, the light source was shut off, and the reaction was quenched with an equal volume addition (125 µL) of MeOH at room temperature. 12.3 µL (1 equiv) of 1,1,1-trifluorotoluene was added to the reaction mixture, and a sample was of this solution was analyzed by ^{1}H and ^{19}F NMR.

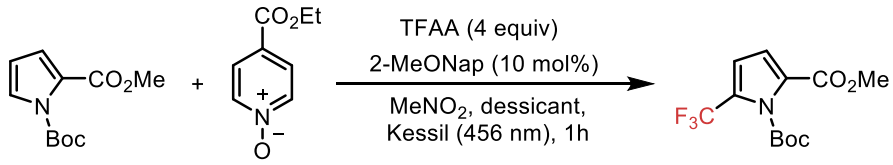

Entry	Dessicant	Time	Yield*
1	$CaCl_2$ (1 equiv)	1 h	38%
2	$MgSO_4$ (1 equiv)	1 h	37%
3	$NaSO_4$ (1 equiv)	1 h	27%
4	LiCl (3 equiv)	1 h	37%
5	$TBAPF_6$ (1 equiv)	1 h	39%

* Determined by ^{19}F NMR with $PhCF_3$ as an internal standard

We understood these results to demonstrate that inorganic salt additives positively impact the reaction by increasing the ionic strength of the solution. However, the influence of Lewis acidic metals binding to ethyl isonicotinate N-oxide, thereby increasing its ability to act as an acceptor molecule cannot be ruled out.

Reaction in the presence of ethyl isonicotinate

To a flame dried 1-dram vial with stir bar was weighed methyl N-Boc pyrrole-2-carboxylate (0.1 mmol, 23 mg, 1 equiv). To this was added ethyl isonicotinate *N*-oxide crystals (0.2 mmol, 33 mg, 2 equiv) was added along the specified donor (0.01 mmol, 0.1 equiv) and calcium chloride (0.1mmol, 1 equiv). The solids were taken up in $MeNO_2$ (125 µL) followed by the addition of ethyl isonicotinate (1 equiv, 15 µL), and TFAA (0.4 mmol, 56 µL, 4 equiv). The reaction was then run according to procedure C. The reaction was irradiated for 1 hour while stirring at 700 rpm. Following this irradiation period, the light source was shut off, and the reaction was quenched with an equal volume addition (125 µL) of MeOH at room temperature. 12.3 µL (1 equiv) of 1,1,1-trifluorotoluene was added to the reaction mixture, and a sample was of this solution was analyzed by ^{1}H and ^{19}F NMR.

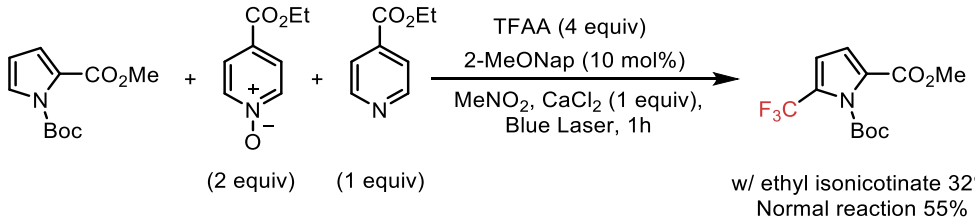

UV/vis of *N*-(trifluoroacetyl)pyridinium EDA complex: To a flame dried 1-dram vial was weighed 0.6 mmol (95 mg, 1 equiv) of 2-methoxynaphthalene, and this was taken up in 3 mL of acetonitrile. The mixture was then sonicated until the arene was completely dissolved. To this solution was added ethyl isonicotinate (1 equiv, 0.6 mmol, 90 µL), the vial was capped and shaken vigorously. The solution was then transferred to a quartz cuvette and 169 µL of TFAA was added, the cuvette was capped and shaken 5 times to ensure mixing, the solution became a pale yellow in color but remained clear. A UV/vis spectrum of the EDA complex was then obtained.

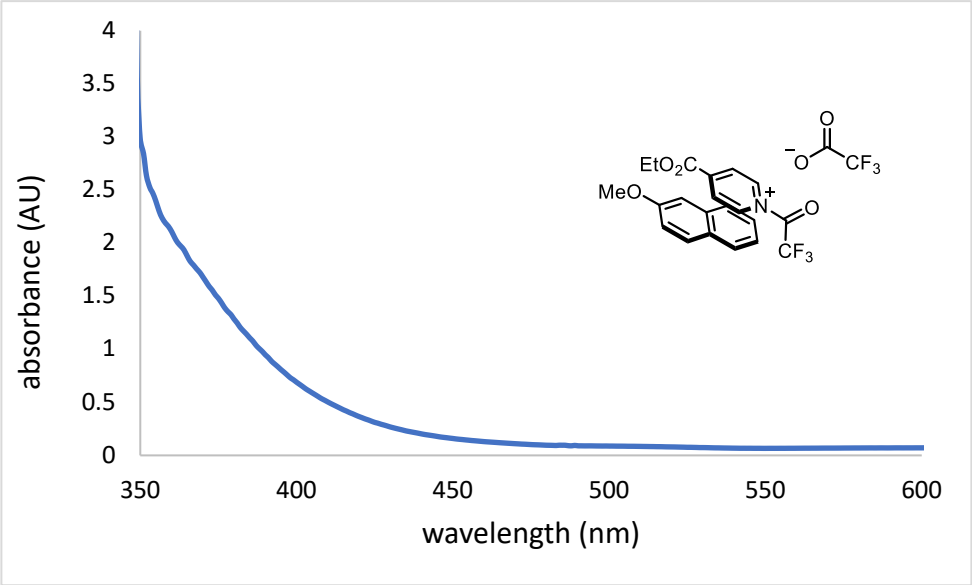

UV/vis spectra of *N*-(trifluoroacetyl)pyridinium EDA complex at 0.2 M.

Abbreviated scope of reactivity when run with 456 nm Kessil lamp

Following Reaction Procedure D. Substrate (0.200 mmol, 1 equiv) was weighed into a 1 dram vial equipped with a stirbar. To this was added ethyl isonicotinate *N*-oxide (66.8 mg, 2 equiv), 2-methoxynaphthalene (3.16 mg, 0.1 equiv), and $CaCl_2$ (22.2 mg, 1 equiv). The solids were evacuated and backfilled 5 times with nitrogen. Then 250 µL of $MeNO_2$ was added, followed by TFAA (113 µL, 4 equiv). The vial was then sealed with electrical tape and parafilm, placed in front of a 456 nm Kessil lamp and irradiated for 1 hour ambient temperature. At the conclusion of the reaction period, the reactions were quenched with 250 µL of methanol and 25 µL of benzotrifluoride was added. Reaction yield determined by ^{19}F NMR.

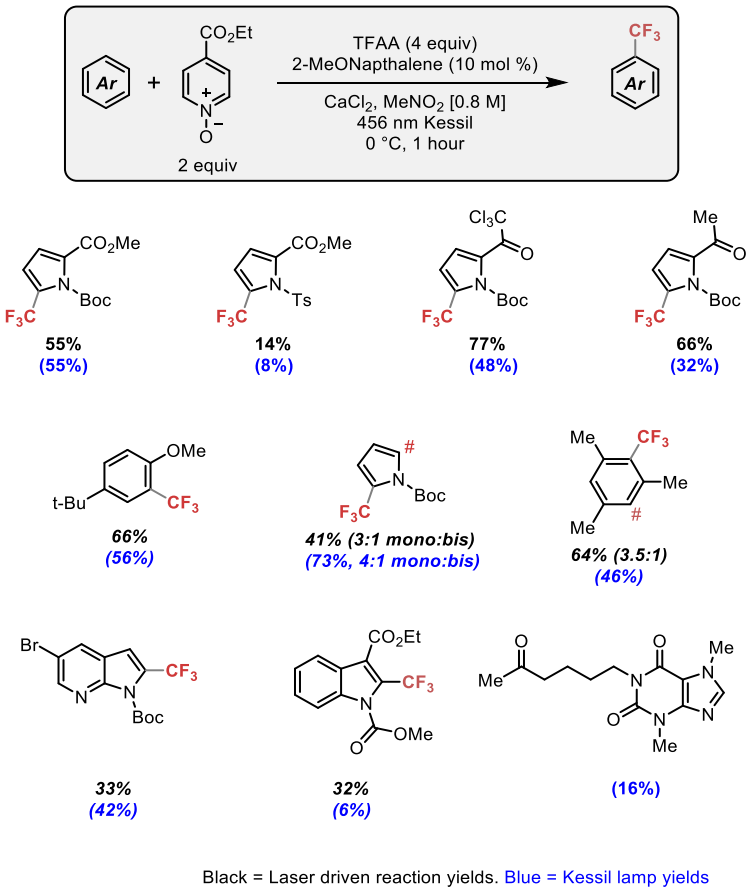

Black = Laser driven reaction yields. Blue = Kessil lamp yields

Section 4: Mulliken Correlation with various donors.

Experimental Procedure: UV-vis spectrum of free arene and the EDA complex with ethyl N-(trifluoroacetoxy)pyridinium-4-carboxylate was obtained.

Preparation of ethyl isonicotinate N-oxide stock solution: To a flame dried 4-dram vial was weighed 502 mg of ethyl isonicotinate N-oxide. To this was added 5 mL of acetonitrile, and the mixture was sonicated until ethyl isonicotinate N-oxide had completely dissolved in solution. This solution was then used for the preparation of UV-vis samples below.

UV/vis of free arene donor: To a flame dried 1-dram vial was weighed 0.3 mmol (1 equiv) of the free arene. The arene was then taken up in 3 mL of acetonitrile and transferred to a quartz cuvette. A UV/vis spectrum was obtained.

UV/vis of EDA complex: To a flame dried 1-dram vial was weighed 0.3 mmol (1 equiv) of arene donor, and this was taken up in 2.5 mL of acetonitrile. The mixture was then sonicated until the arene was completely dissolved. To this solution was added 0.5 mL of a 0.6 M solution of ethyl isonicotinate *N*-oxide in acetonitrile, the vial was capped and shaken vigorously. The solution was then transferred to a quartz cuvette and 84 μL of TFAA was added, the cuvette was capped and shaken 5 times to ensure mixing. A UV/vis spectrum of the sample was obtained on a Varian Cary-50 spectrophotometer.

Processing of UV/vis data. Spectra of the arene donor, ethyl *N*-(trifluoroacetoxy)pyridinium-4-carboxylate, and EDA complexes in acetonitrile, and these spectra were plotted in Microsoft excel. To reveal the contribution of the charge-transfer band to the overall absorbance of the UV/vis spectrum, the absorbance for the free donor arene and ethyl *N*-(trifluoroacetoxy)pyridinium-4-carboxylate was subtracted from the spectra of the EDA complex. After processing this data, the λ_{maxCT} was determined using OrginPro 2019 peak deconvolution to determine the maximum, and this point was plotted against the ionization energy for the donor.

Findings:

- CT bands could be clearly resolved after background subtraction.
- As predicted by Mulliken theory, the λ_{maxCT} is linearly correlated with the ionization potential of the donor arene. However, trends in ionization potential deviate slightly as more conjugated arenes are used (i.e. benzene vs naphthalene), and these deviations in the ionization potential trends lead to slight deviations from perfect linearity for the energy of the charge transfer band of the EDA complexes.
- More conjugated arenes (naphthalene's and pyrene) delivered the most absorbing CT bands.

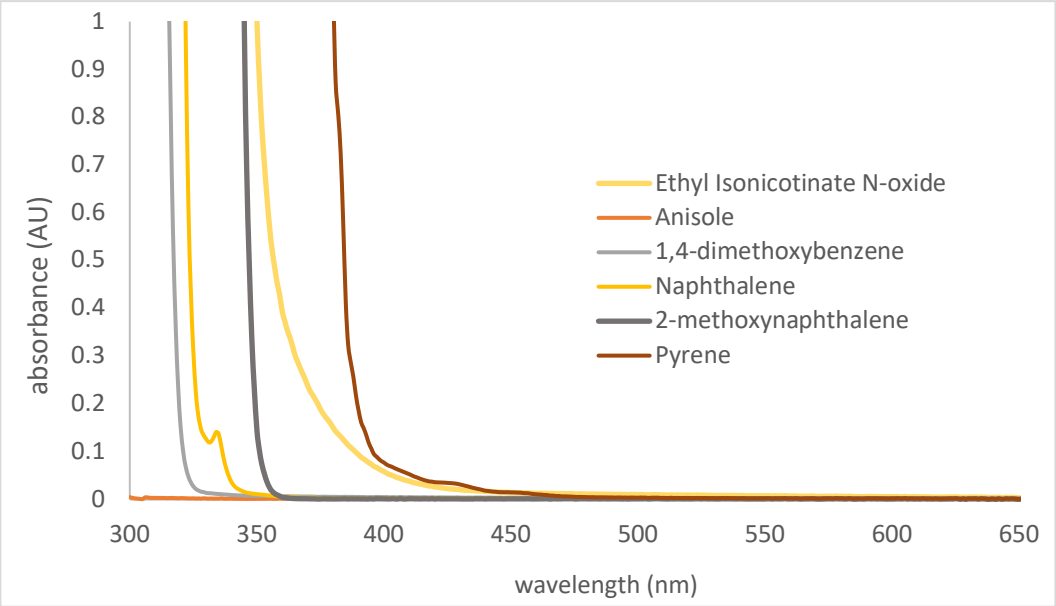

Figure S2. UV-vis spectra of arene donors at 0.2 M.

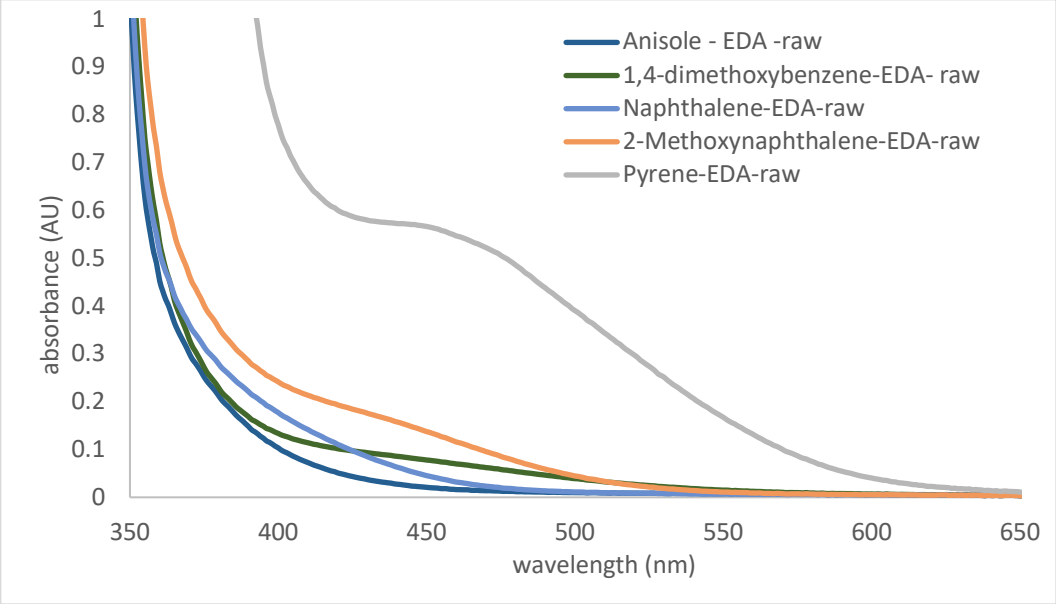

Figure S3. UV-vis spectra of EDA complexes at 0.2 M

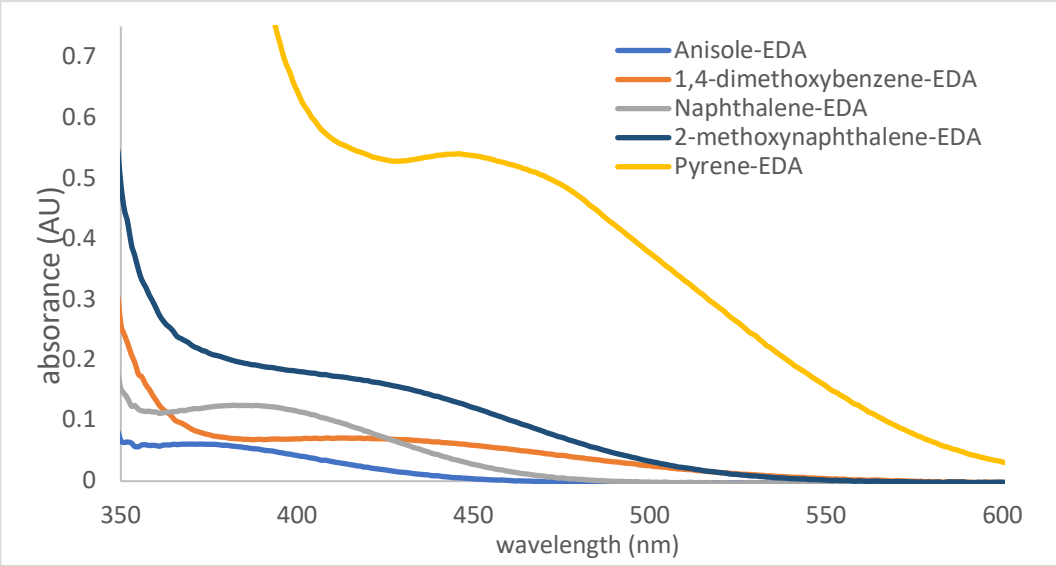

Figure S4. UV-vis spectra of EDA complexes at 0.2 M, background subtracted.

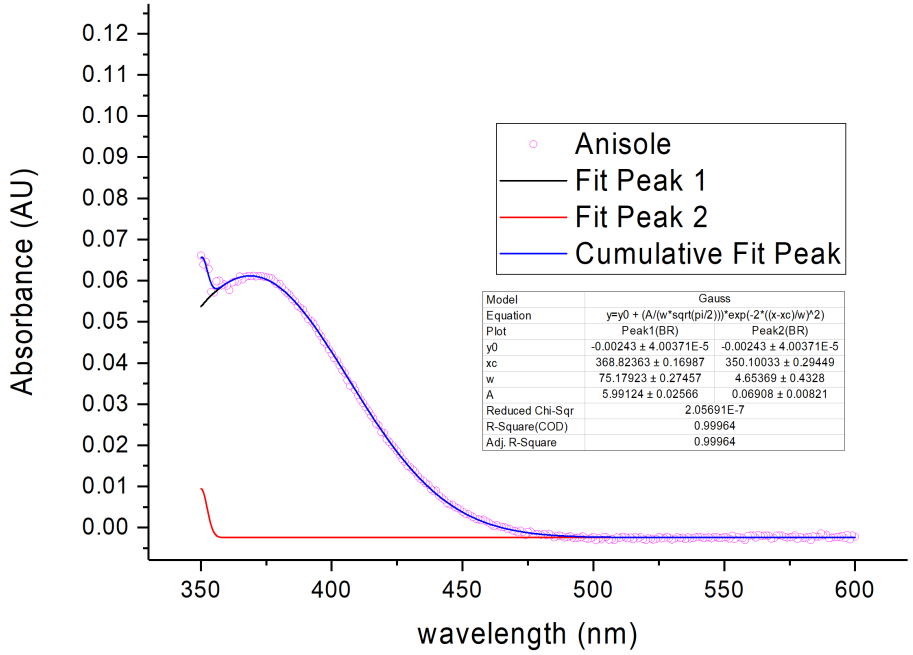

Model	Gauss	
Equation	y=y0 + (A/(w*sqrt(pi/2)))*exp(-2*((x-xc)/w)^2)	
Plot	Peak1(BR)	Peak2(BR)
y0	-0.00243 ± 4.00371E-5	-0.00243 ± 4.00371E-5
xc	368.82363 ± 0.16987	350.10033 ± 0.29449
w	75.17923 ± 0.27457	4.65369 ± 0.4328
A	5.99124 ± 0.02566	0.06908 ± 0.00821
Reduced Chi-Sqr	2.05691E-7	
R-Square(COD)	0.99964	
Adj. R-Square	0.99964	

Figure S5. OriginPro Peak deconvolution fit of CT band for Anisole EDA complex

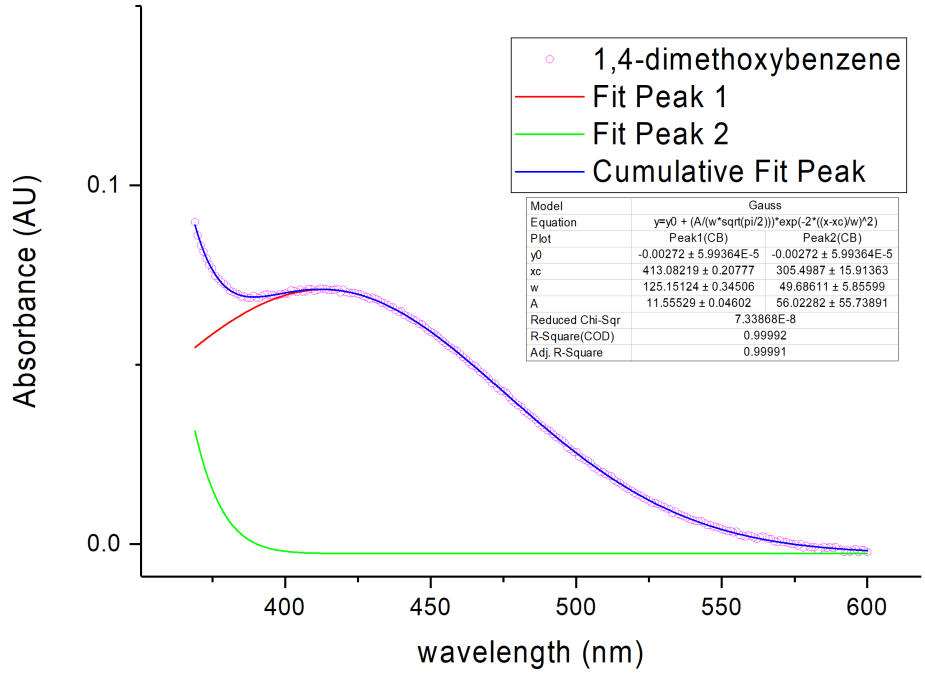

Model	Gauss	
Equation	y=y0 + (A/(w*sqrt(pi/2)))*exp(-2*((x-xc)/w)^2)	
Plot	Peak1(CB)	Peak2(CB)
y0	-0.00272 ± 5.99364E-5	-0.00272 ± 5.99364E-5
xc	413.08219 ± 0.20777	305.4987 ± 15.91363
w	125.15124 ± 0.34506	49.68611 ± 5.85599
A	11.55529 ± 0.04602	56.02282 ± 55.73891
Reduced Chi-Sqr	7.33868E-8	
R-Square(COD)	0.99992	
Adj. R-Square	0.99991	

Figure S6. OriginPro Peak deconvolution fit of CT band for 1,4-dimethoxybenzene EDA complex

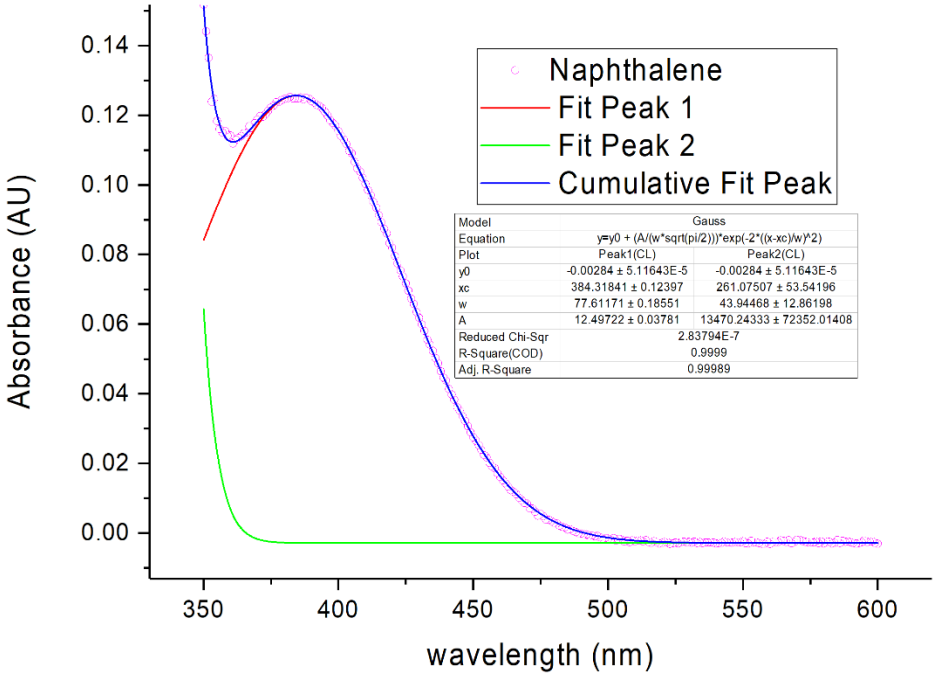

Model	Gauss	
Equation	y=y0 + (A/(w*sqrt(pi/2)))*exp(-2*((x-xc)/w)^2)	
Plot	Peak1(CL)	Peak2(CL)
y0	-0.00284 ± 5.11643E-5	-0.00284 ± 5.11643E-5
xc	384.31841 ± 0.12397	261.07507 ± 53.54196
w	77.61171 ± 0.18551	43.94468 ± 12.86198
A	12.49722 ± 0.03781	13470.24333 ± 72352.01408
Reduced Chi-Sqr	2.83794E-7	
R-Square(COD)	0.9999	
Adj. R-Square	0.99989	

Figure S7. OriginPro Peak deconvolution fit of CT band for Naphthalene EDA complex.

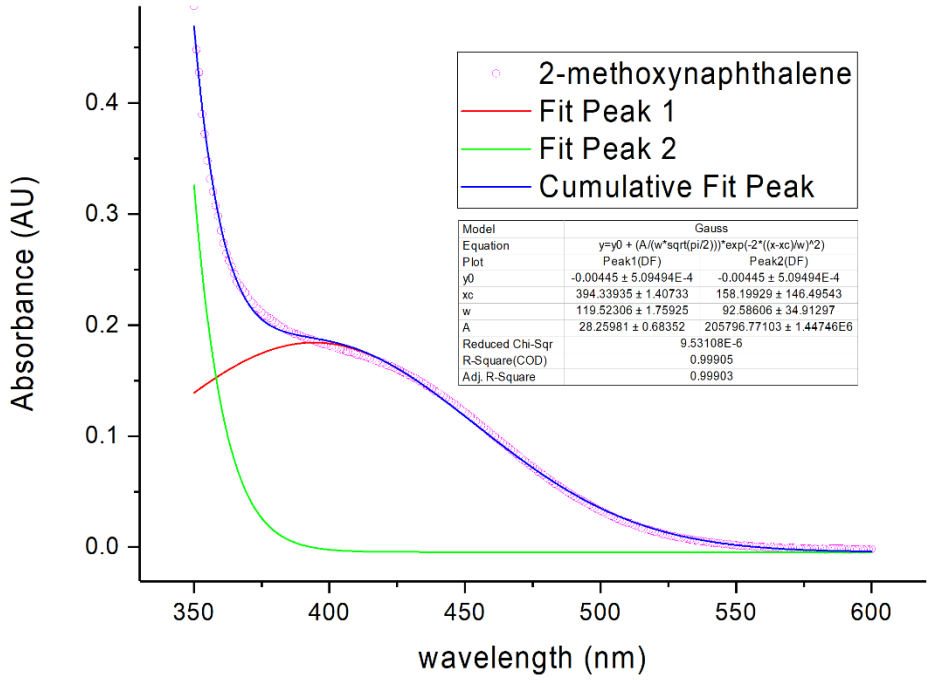

Model	Gauss	
Equation	y=y0 + (A/(w*sqrt(pi/2)))*exp(-2*((x-xc)/w)^2)	
Plot	Peak1(DF)	Peak2(DF)
y0	-0.00445 ± 5.09494E-4	-0.00445 ± 5.09494E-4
xc	394.33935 ± 1.40733	158.19929 ± 146.49543
w	119.52306 ± 1.75925	92.58606 ± 34.91297
A	28.25981 ± 0.68352	205796.77103 ± 1.44746E6
Reduced Chi-Sqr	9.53108E-6	
R-Square(COD)	0.99905	
Adj. R-Square	0.99903	

Figure S8. OriginPro Peak deconvolution fit of CT band for 2-methoxynaphthalene EDA complex.

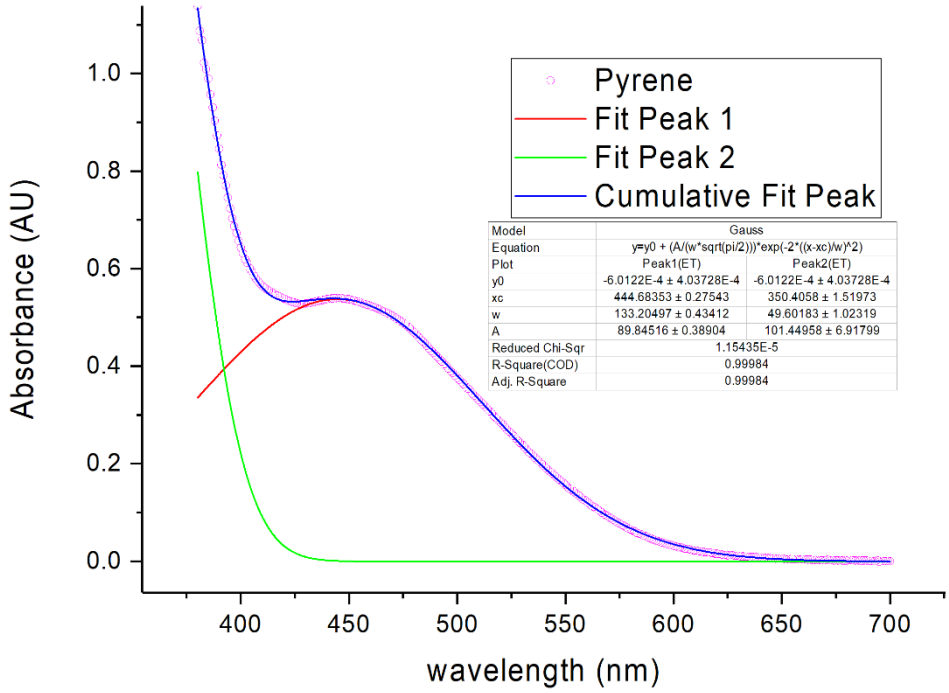

Figure S9. OriginPro Peak deconvolution fit of CT band for Pyrene EDA complex.

Section 5: UV-vis studies of EDA complex I

EDA complex absorption as a function of solvent polarity

To a 3 mL (1 cm path length) cuvette, the following masses were measured of the ethyl isonicotinate *N*-oxide (83.6 mg, 0.500 mmol) and 2-Methoxynaphthalene (79.1 mg, 0.500 mmol). The solids were then diluted in the specified solvent (2.5 mL, 0.4 M in ethyl isonicotinate *N*-oxide or 2-Methoxynaphthalene), followed by the addition of 141 µL of TFAA (1.00 mmmol, 2 equiv). UV/Vis spectra were recorded on a Shimadzu UV-1601 UV-VOS spectrometer with a Peltier temperature controller, set to 23°C. Prior to analyzing each sample, the cuvette was equilibrated in the temperature-controlled chamber for 3 minutes. The absorbance values were benchmarked against the solvent dipole moment (µ).

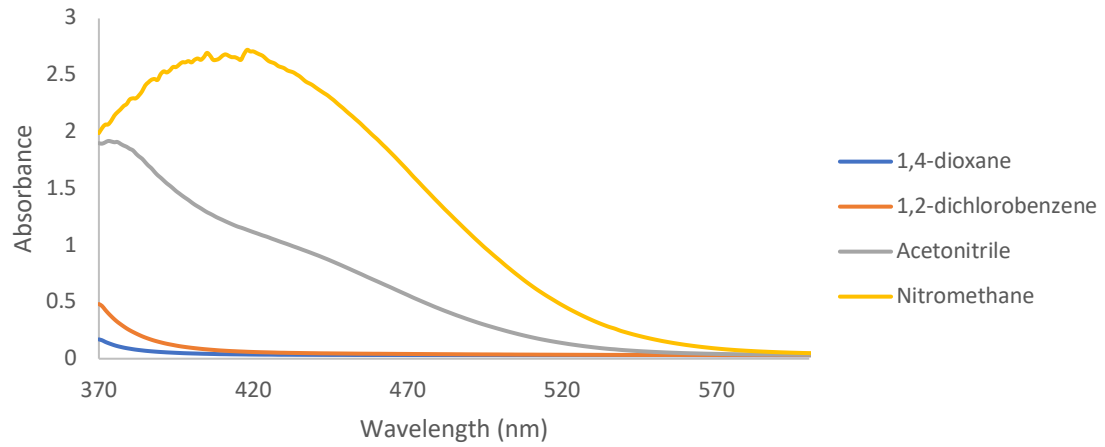

Figure S10. UV-vis spectra of EDA complex I in various solvents.

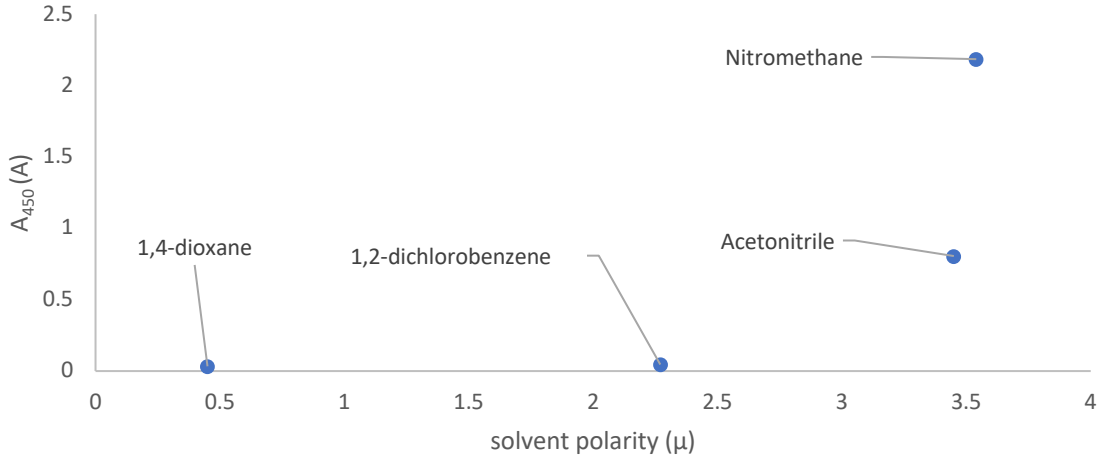

Figure S11. EDA complex I absorbance at 450 nm vs solvent dipole moment (μ).

EDA complex absorbance as a function of concentration.

A stock solution amounting to 10 mL of a 1 M solution of both ethyl isonicotinate *N*-oxide and 2-methoxynaphthalene was prepared in $MeNO_2$.

To a clean 3 mL (1 cm path length) cuvette, the following volumes were measured of the PNO/2-OMeNp, TFAA and void volume in $MeNO_2$. UV/Vis spectra were recorded on a Shimadzu UV-1601 UV-VOS spectrometer with a Peltier temperature controller, set to 23°C. Prior to analyzing each sample, the cuvette was equilibrated in the temperature-controlled chamber for 3 minutes.

Concentration of Accepter (or Donor) [M]	Volume of stock solution (µL)	TFAA volume (µL)	$MeNO_2$ void volume (mL)
0.05	125	17	2.375
0.1	250	35	2.250
0.12	300	42	2.200
0.14	350	49	2.150
0.16	400	56	2.100
0.2	500	70	2.000
0.5	1250	176	1.250
0.8	2000	281	0.500
1.0	2500	352	0.000

Concentration of Accepter (or Donor) [M]	Adjusted concentration for TFAA volume)	Recorded Absorbance @ 450 nm
0.05	0.05	0.0068
0.1	0.10	0.0283
0.12	0.12	0.0441
0.14	0.14	0.0621
0.16	0.16	0.0813
0.2	0.19	0.9745
0.5	0.47	3.578
0.8	0.72	3.574
1	0.88	3.574

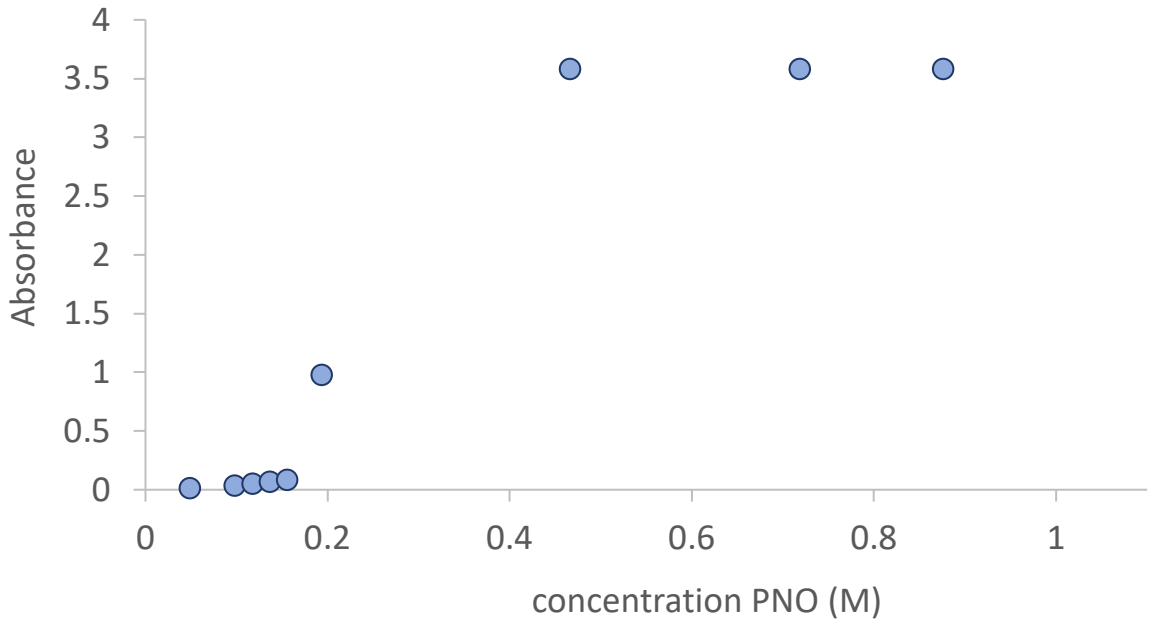

Figure S12. EDA complex I absorbance at 450 nm vs concentration of the EDA complex.

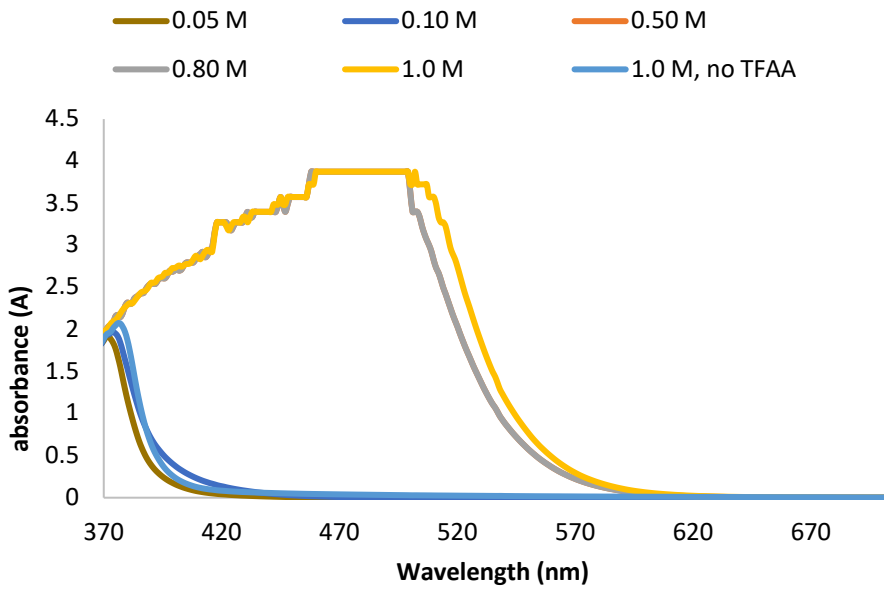

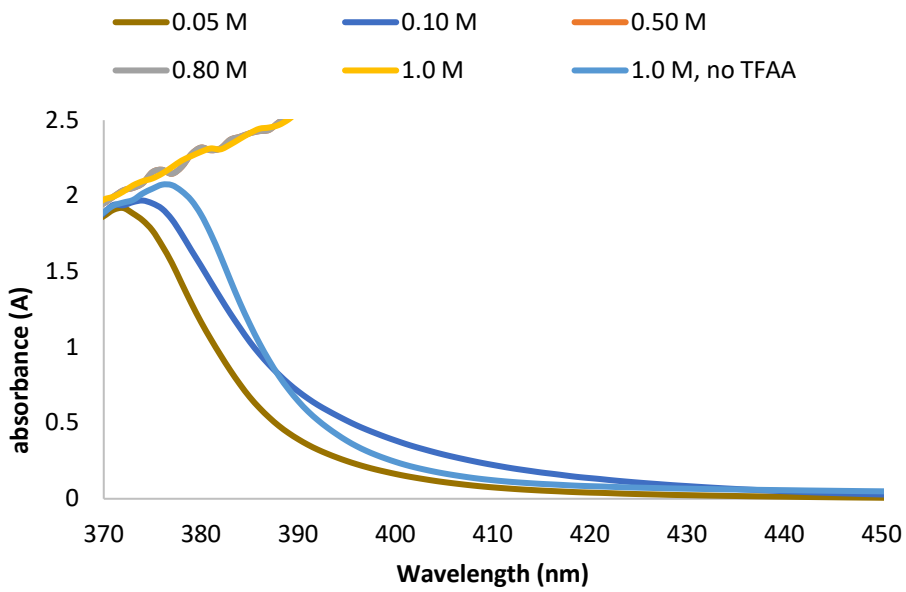

Figure S13. UV-vis of EDA complex I at various concentrations.

Investigation of effect of Lewis acid on absorbance of EDA complex I

Plot of calcium chloride equivalents vs absorbance of EDA complex 1: To a flame dried 1-dram vial was weighed 2-methoxynaphthalene (1 equiv, 0.3 mmol, 47.5 mg) and ethyl isonicotinate *N*-oxide (1 equiv, 0.3 mmol, 50 mg). To the solids was added 3 mL of sparged nitromethane and the mixture was sonicated for about 1 minute. To this mixture was added 85 µL of TFAA, the vial was shaken vigorously, and then the solution was immediately transferred to a 3 mL quartz cuvette. A UV/vis spectrum of the sample was obtained on a Varian Cary-50 spectrophotometer. Following acquisition of the UV/vis spectrum, 1 equivalent (0.3 mmol, 33.3 mg) of calcium chloride was added to the sample, the sample was shaken vigorously, and a UV/vis spectrum of the sample was obtained. This process was repeated 3 times to give data EDA complex I absorbance in the presence of 1, 2, and 3 equivalents of calcium chloride, respectively. The data was processed using Microsoft excel.

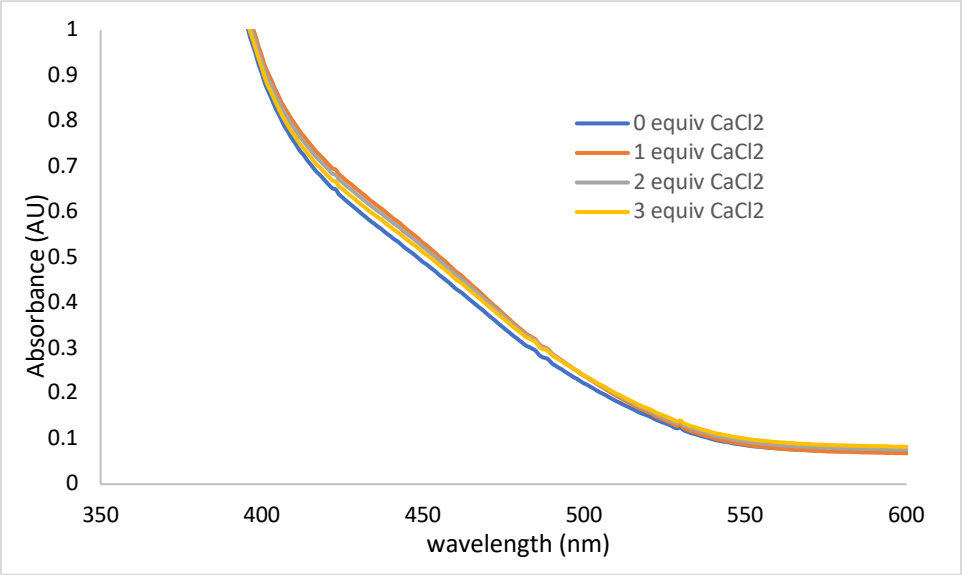

Figure S14. UV/vis spectrum of EDA complex I in the presence of calcium chloride.

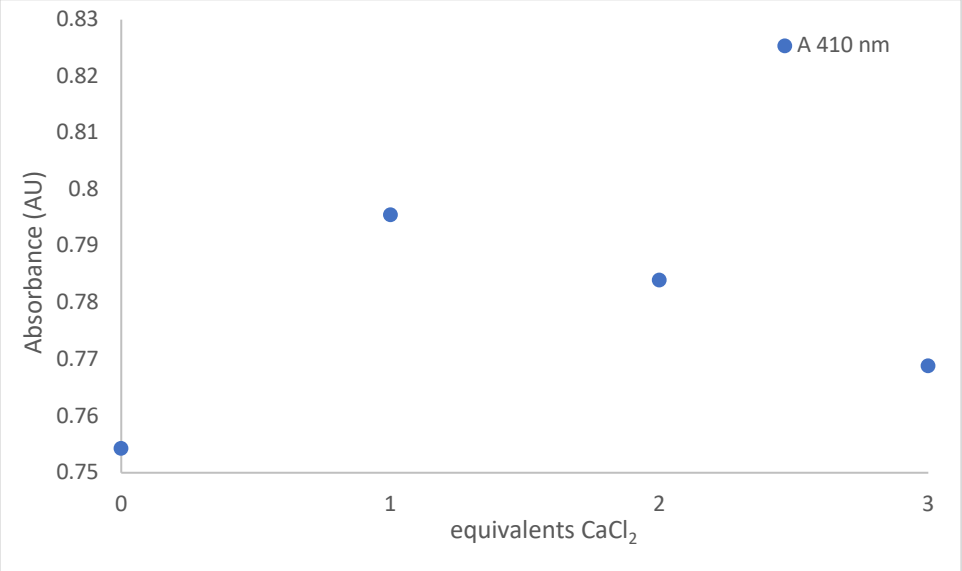

Figure S15. Absorbance of EDA complex I at 410 nm as a function of calcium chloride additive.

Plot of lithium chloride equivalents vs absorbance of EDA complex 1: To a flame dried 1-dram vial was weighed 2-methoxynaphthalene (1 equiv, 0.3 mmol, 47.5 mg) and ethyl isonicotinate *N*-oxide (1 equiv, 0.3 mmol, 50 mg). To the solids was added 3 mL of sparged nitromethane and the mixture was sonicated for about 1 minute. To this mixture was added 85 µL of TFAA, the vial was

shaken vigorously, and then the solution was immediately transferred to a 3 mL quartz cuvette. A UV/vis spectrum of the sample was obtained on a Varian Cary-50 spectrophotometer. Following acquisition of the UV/vis spectrum, 1 equivalent (0.3 mmol, 13 mg) of lithium chloride was added to the sample, the sample was shaken vigorously, and a UV/vis spectrum of the sample was obtained. This process was repeated 5 more times to give data EDA complex I absorbance in the presence of 1, 2, 3, 4, 5, and 10 equivalents of lithium chloride, respectively. The data was processed using Microsoft excel.

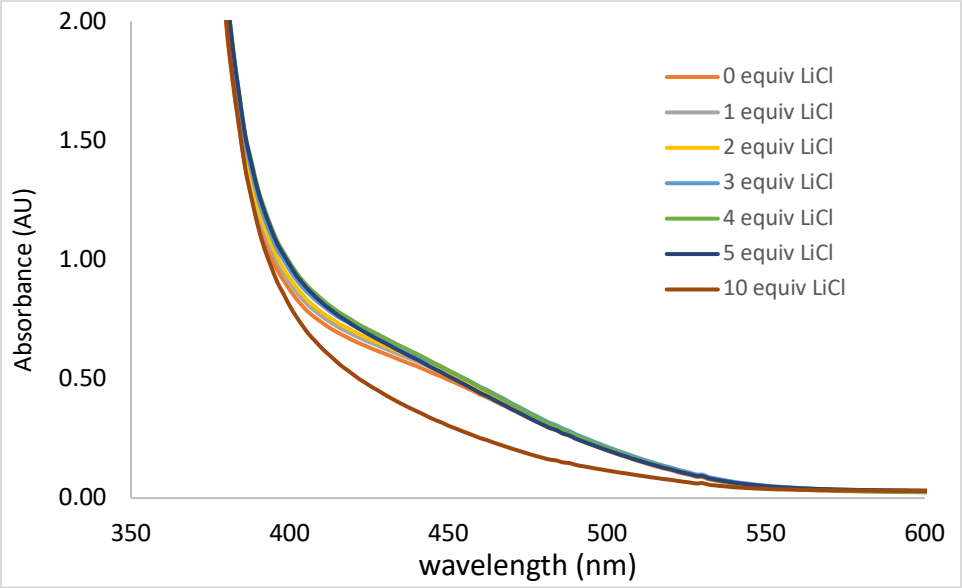

Figure S16. UV/vis spectrum of EDA complex I in the presence of lithium chloride in $MeNO_2$.

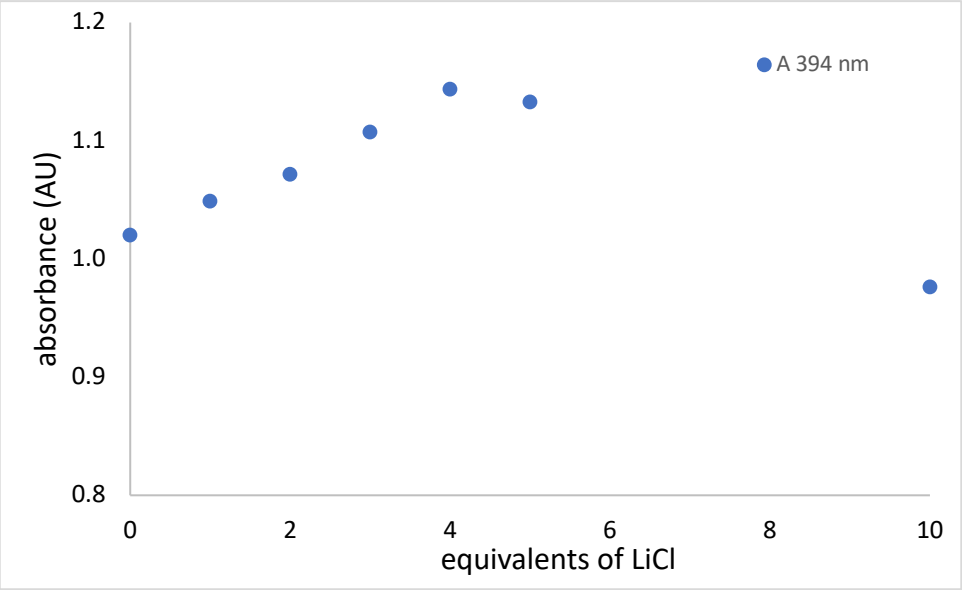

Figure S17. Absorbance of EDA complex I vs equivalents of lithium chloride in $MeNO_2$.

Plot of lithium chloride equivalents vs absorbance of EDA complex 1: To a flame dried 1-dram vial was weighed 2-methoxynaphthalene (1 equiv, 0.3 mmol, 47.5 mg) and ethyl isonicotinate *N*-oxide (1 equiv, 0.3 mmol, 50 mg). To the solids was added 3 mL of sparged acetonitrile and the mixture was sonicated for about 1 minute. To this mixture was added 85 µL of TFAA, the vial was shaken vigorously, and then the solution was immediately transferred to a 3 mL quartz cuvette. A UV/vis spectrum of the sample was obtained on a Varian Cary-50 spectrophotometer. Following acquisition of the UV/vis spectrum, 1 equivalent (0.3 mmol, 13 mg) of lithium chloride was added to the sample, the sample was shaken vigorously, and a UV/vis spectrum of the sample was obtained. This process was repeated 5 times to give data EDA complex I absorbance in the presence of 1, 2, 3, 4, and 5 equivalents of lithium chloride, respectively. The data was processed using Microsoft excel.

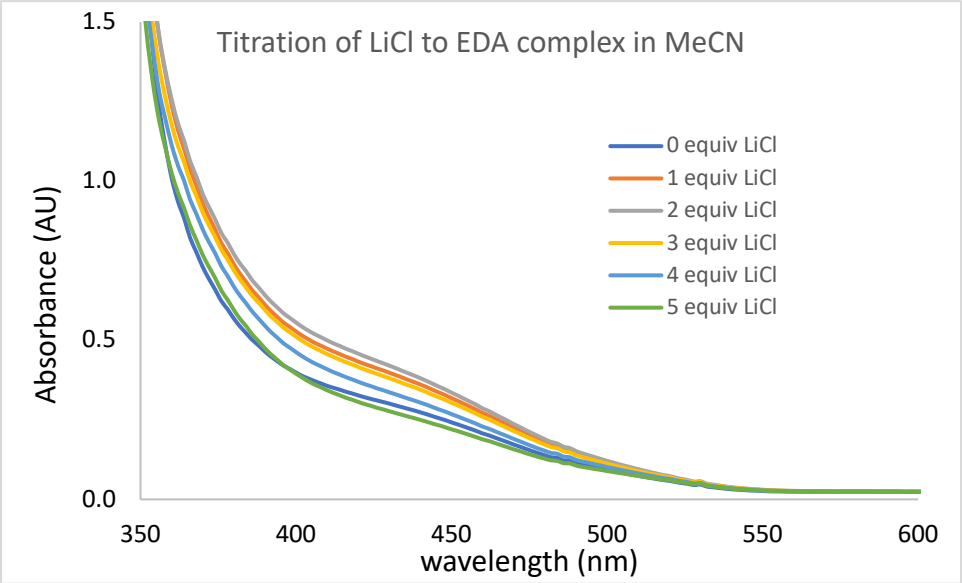

Figure S18. UV-vis spectrum of EDA complex I in the presence of lithium chloride in MeCN.

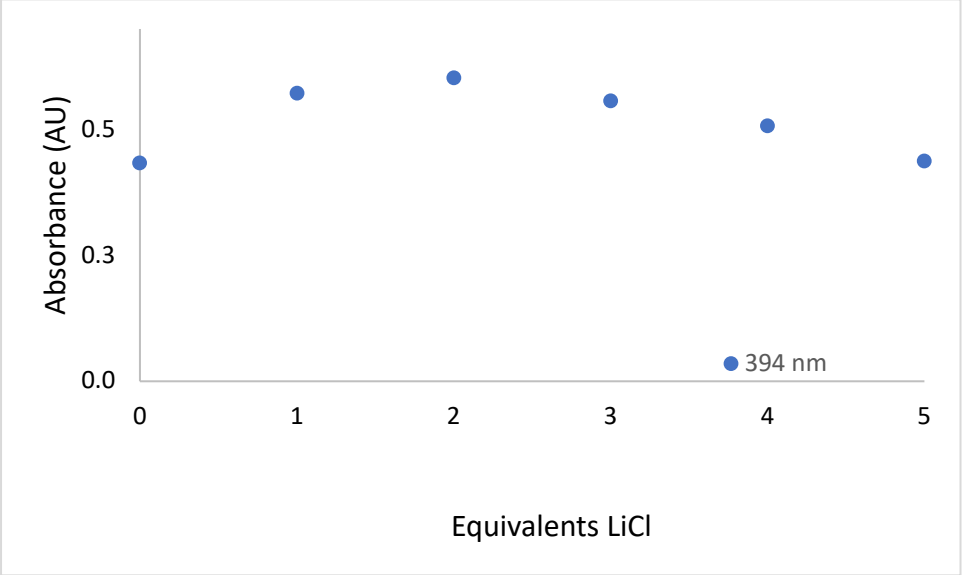

Figure S19. Absorbance of EDA complex I vs equivalents of lithium chloride in MeCN.

Plot of tetrabutylammonium hexafluorophosphate equivalents vs absorbance of EDA complex 1: To a flame dried 1-dram vial was weighed 2-methoxynaphthalene (1 equiv, 0.6 mmol, 95 mg) and ethyl isonicotinate *N*-oxide (1 equiv, 0.6 mmol, 100 mg). To the solids was added 3 mL of sparged acetonitrile and the mixture was sonicated for about 1 minute. To this mixture was

added 169 µL of TFAA, the vial was shaken vigorously, and then the solution was immediately transferred to a 3 mL quartz cuvette. A UV/vis spectrum of the sample was obtained on a Varian Cary-50 spectrophotometer. Following acquisition of the UV/vis spectrum, 1 equivalent (0.6 mmol, 232.5 mg) of lithium chloride was added to the sample, the sample was shaken vigorously, and a UV/vis spectrum of the sample was obtained. This process was repeated 5 times to give data EDA complex I absorbance in the presence of 1, 2, 3, 5, and 10 equivalents of tetrabutylammonium hexafluorophosphate, respectively. The data was processed using Microsoft excel.

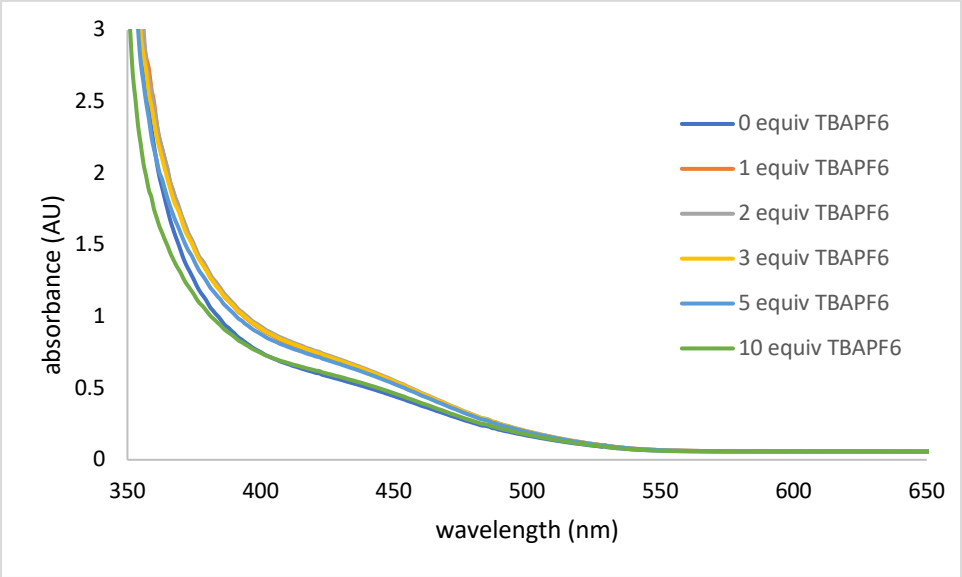

Figure S20. UV-vis spectrum of EDA complex I in the presence of Bu_4NPF_6 in MeCN.

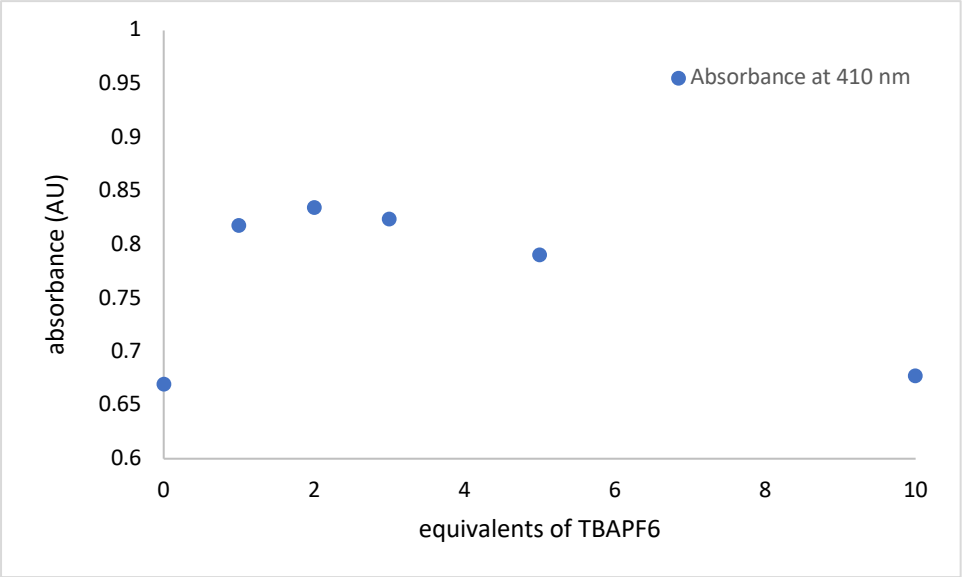

Figure S21. Absorbance of EDA complex I vs equivalents of Bu_4NPF_6 in MeCN.

Discussion: Job plots for the effect of inorganic salts on the absorbance of EDA complex 1 demonstrate the addition of an inorganic salt positively influences the overall absorptivity of the EDA complex. The positive influence of the non-coordinating tetrabutylammonium hexafluorophosphate salt on the absorptivity of the EDA complex suggests that the role of the inorganic salt additives function by increasing the ionic strength of the solution. However, the role of coordination of Lewis acidic ions to ethyl isonicotinate N-oxide, thereby increasing its ability to act as an acceptor, cannot be ruled out.

Section 6: Job Plot Experiments:

Job Plot of EDA complex 1: Two separate 0.5 M stock solutions of ethyl isonicotinate *N*-oxide and 2-methoxynaphthalene in $MeNO_2$ were prepared in flame dried 4-dram vials.

2-methoxynaphthalene stock solution: 5 mmol (791 mg) of 2-methoxynaphthalene was weighed into a flame dried 4-dram vial. To this was added 10 mL of sparged nitromethane. This mixture was sonicated for 2 mins to ensure mixing.

Ethyl isonicotinate *N*-oxide stock solution: 5 mmol (836 mg) of ethyl isonicotinate *N*-oxide was weighed into a flame dried 4-dram vial. To this was added 10 mL of sparged $MeNO_2$. This mixture was sonicated for 2 mins to ensure mixing.

Preparation of samples: To a flame dried 1-dram vial was added ethyl isonicotinate *N*-oxide stock solution, 2-methoxynaphthalene stock solution, and 1.63 mL of sparged $MeNO_2$. This mixture was sonicated for ~ 30 seconds. Immediately prior to transferring the solution to a cuvette, 169 µL of TFAA was added, and the mixture was shaken vigorously. The solutions were then transferred by pipette to a 3 mL (1 cm path length) cuvette. UV/Vis spectra were recorded on a Varian Cary-50 spectrophotometer.

ethyl isonicotinate *N*-oxide			**2-methoxynaphthalene**			**TFAA**	**Void**	**Total**
						volume	volume	
mmol	ratio	volume (µL)	mmol	ratio	volume (µL)	(µL)	(µL)	volume (µL)
0	0	0	0.6	1	1200	169	1630	2999
0.06	0.1	120	0.54	0.9	1080	169	1630	2999
0.12	0.2	240	0.48	0.8	960	169	1630	2999
0.18	0.3	360	0.42	0.7	840	169	1630	2999
0.24	0.4	480	0.36	0.6	720	169	1630	2999
0.3	0.5	600	0.3	0.5	600	169	1630	2999
0.36	0.6	720	0.24	0.4	480	169	1630	2999
0.42	0.7	840	0.18	0.3	360	169	1630	2999
0.48	0.8	960	0.12	0.2	240	169	1630	2999
0.54	0.9	1080	0.06	0.1	120	169	1630	2999
0.6	1	1200	0	0	0	169	1630	2999

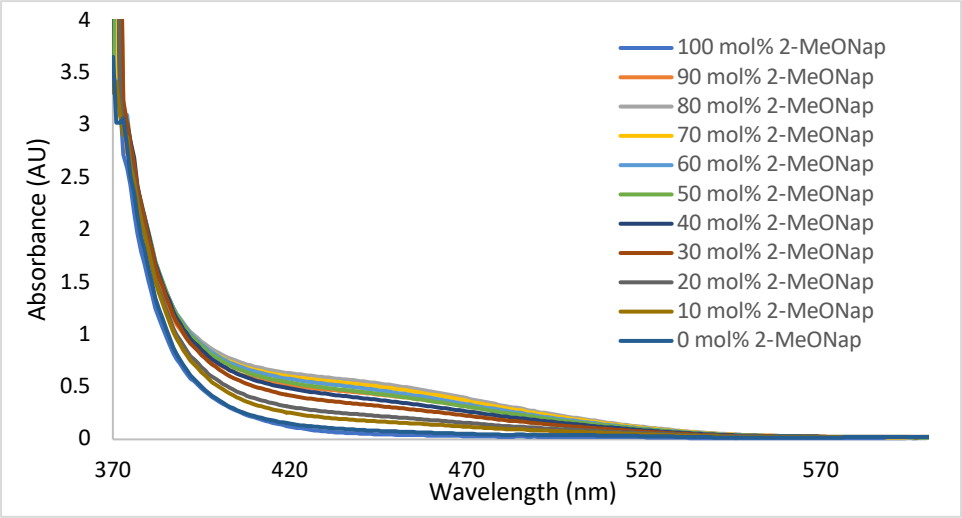

Figure S22. UV/vis EDA complex 1 at 0.2 M with continuous variation of 2-methoxynaphthalene and ethyl isonicotinate *N*-oxide components.

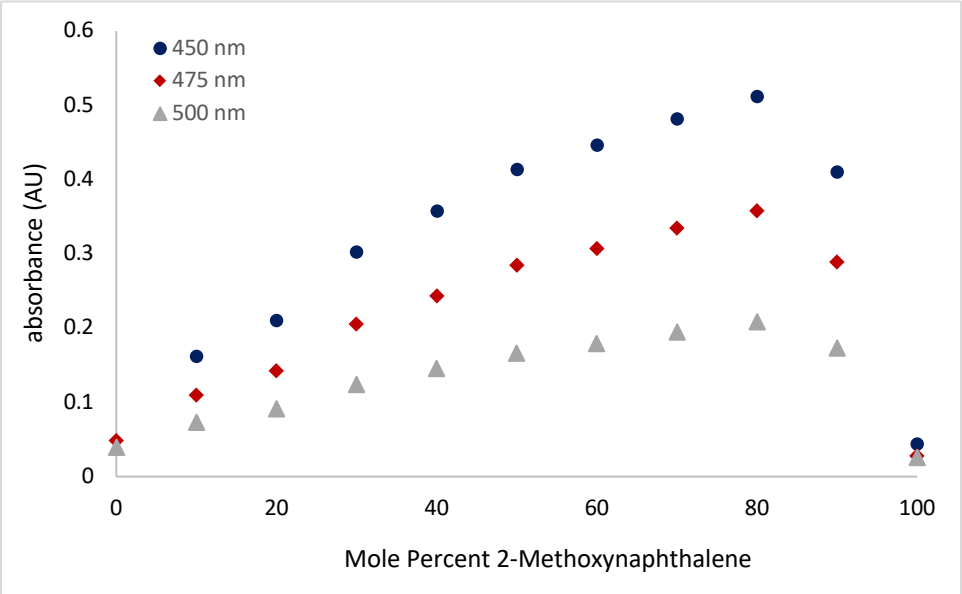

Figure S23. Job plot EDA complex 1 at 0.2 M concentration. (●) Plot of absorbance at 450 nm. (♦) Plot of absorbance at 475 nm. (▲) Plot of absorbance at 500 nm.

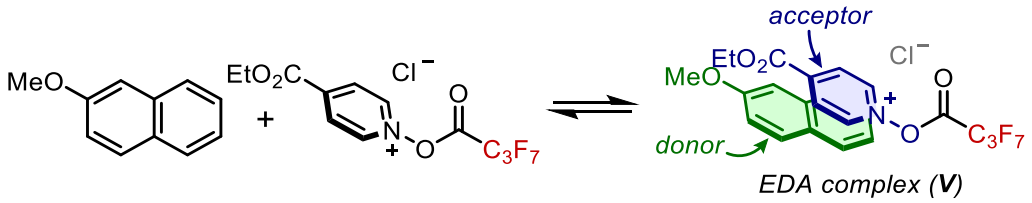

Job Plot of EDA complex V. Two separate 0.5 M stock solutions of ethyl isonicotinate *N*-oxide and 2-methoxynaphthalene in nitromethane were prepared in flame dried 4-dram vials.

2-methoxynaphthalene stock solution: 5 mmol (791 mg) of 2-methoxynaphthalene was weighed into a flame dried 4-dram vial. To this was added 10 mL of sparged nitromethane. This mixture was sonicated for 2 mins to ensure mixing.

Ethyl *N*-(heptafluorobutyroxy)pyridinium-4-carboxylate stock solution: 5 mmol (836 mg) of ethyl isonicotinate *N*-oxide was weighed into a flame dried 4-dram vial. To this was added 10 mL of sparged nitromethane. This mixture was sonicated for 2 mins to ensure mixing. The mixture was cooled in an ice bath, and 1.49 mL of perfluorobutyrl chloride was added slowly to the solution. The mixture was again sonicated for ~ 30 seconds.

Preparation of samples: To a flame dried 1-dram vial was added Ethyl *N*-(heptafluorobutyroxy)pyridinium-4-carboxylate stock solution, 2-methoxynaphthalene stock solution, and 1.80 mL of sparged nitromethane. This mixture was sonicated for ~ 30 seconds. Immediately prior to transferring the solution to a cuvette. The solutions were then transferred by pipette to a 3 mL (1 cm path length) cuvette. UV/Vis spectra were recorded on a Varian Cary-50 spectrophotometer.

Ethyl *N*-(heptafluorobutyroxy)pyridinium-4-carboxylate			2-methoxynaphthalene			Void	Total
mmol	ratio	volume (μL)	mmol	ratio	volume (μL)	volume (μL)	volume (μL)
0	0	0	0.6	1	1200	1800	3000
0.06	0.1	120	0.54	0.9	1080	1800	3000
0.12	0.2	240	0.48	0.8	960	1800	3000
0.18	0.3	360	0.42	0.7	840	1800	3000
0.24	0.4	480	0.36	0.6	720	1800	3000
0.3	0.5	600	0.3	0.5	600	1800	3000
0.36	0.6	720	0.24	0.4	480	1800	3000
0.42	0.7	840	0.18	0.3	360	1800	3000
0.48	0.8	960	0.12	0.2	240	1800	3000
0.54	0.9	1080	0.06	0.1	120	1800	3000
0.6	1	1200	0	0	0	1800	3000

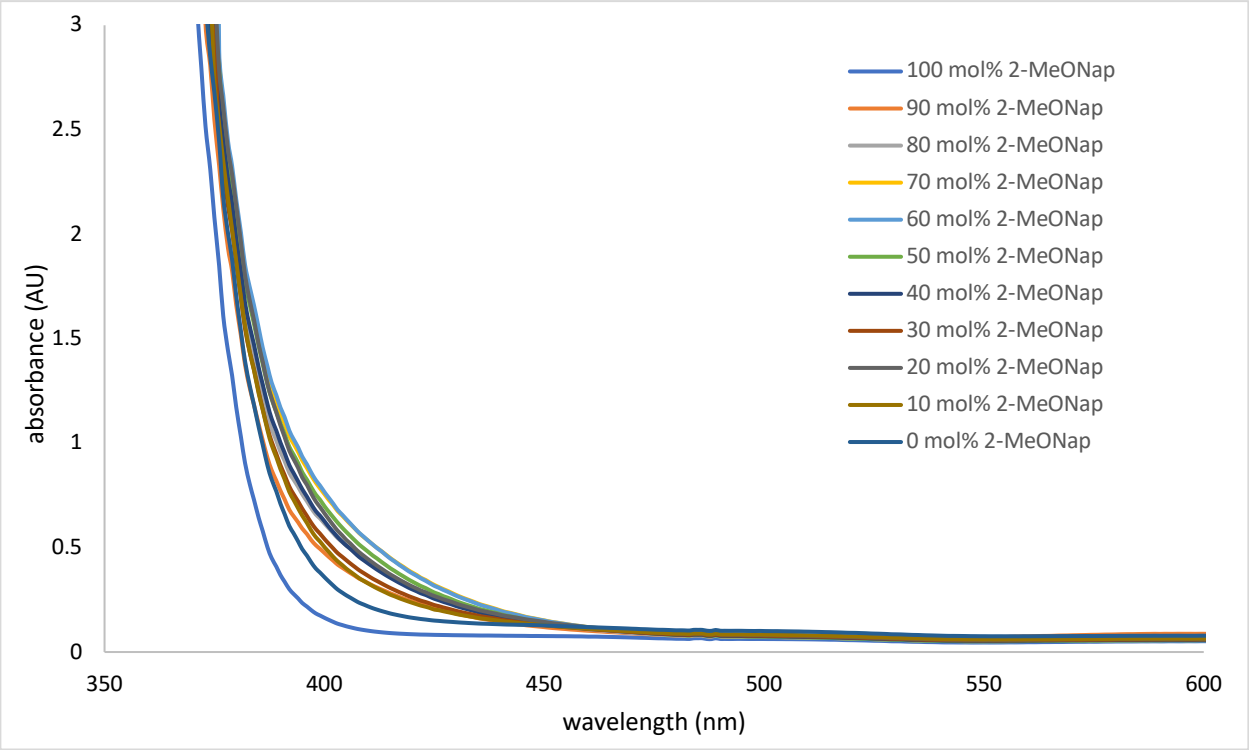

Figure S24. UV/vis EDA complex V at 0.2 M with continuous variation of 2-methoxynaphthalene and ethyl isonicotinate *N*-oxide components.

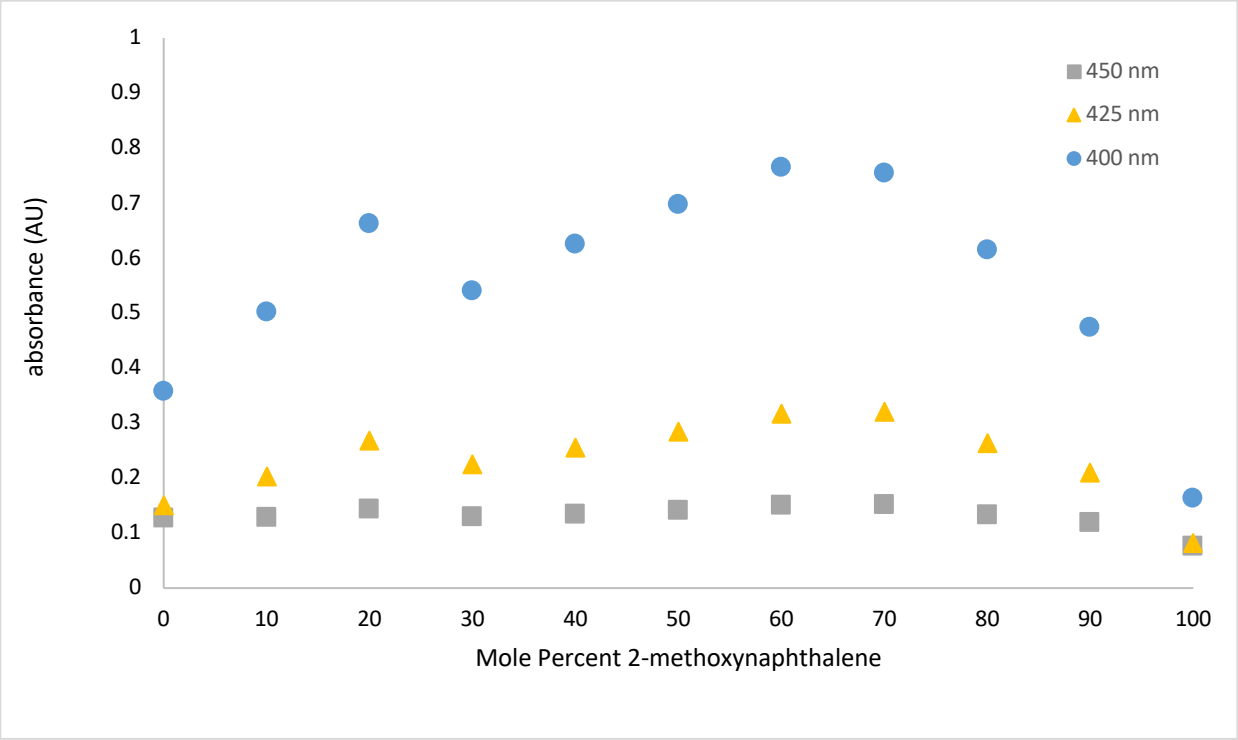

Figure S25. Job plot EDA complex V at 0.2 M concentration. (●) Plot of absorbance at 400 nm. (▲) Plot of absorbance at 425 nm. (■) Plot of absorbance at 450 nm.

Following obtaining UV-vis spectra for the Job plot of EDA complex V, it was discovered that the vials containing predominantly 2-methoxynaphthalene began to turn blue in color. This color persisted and became more intense with time (see below).

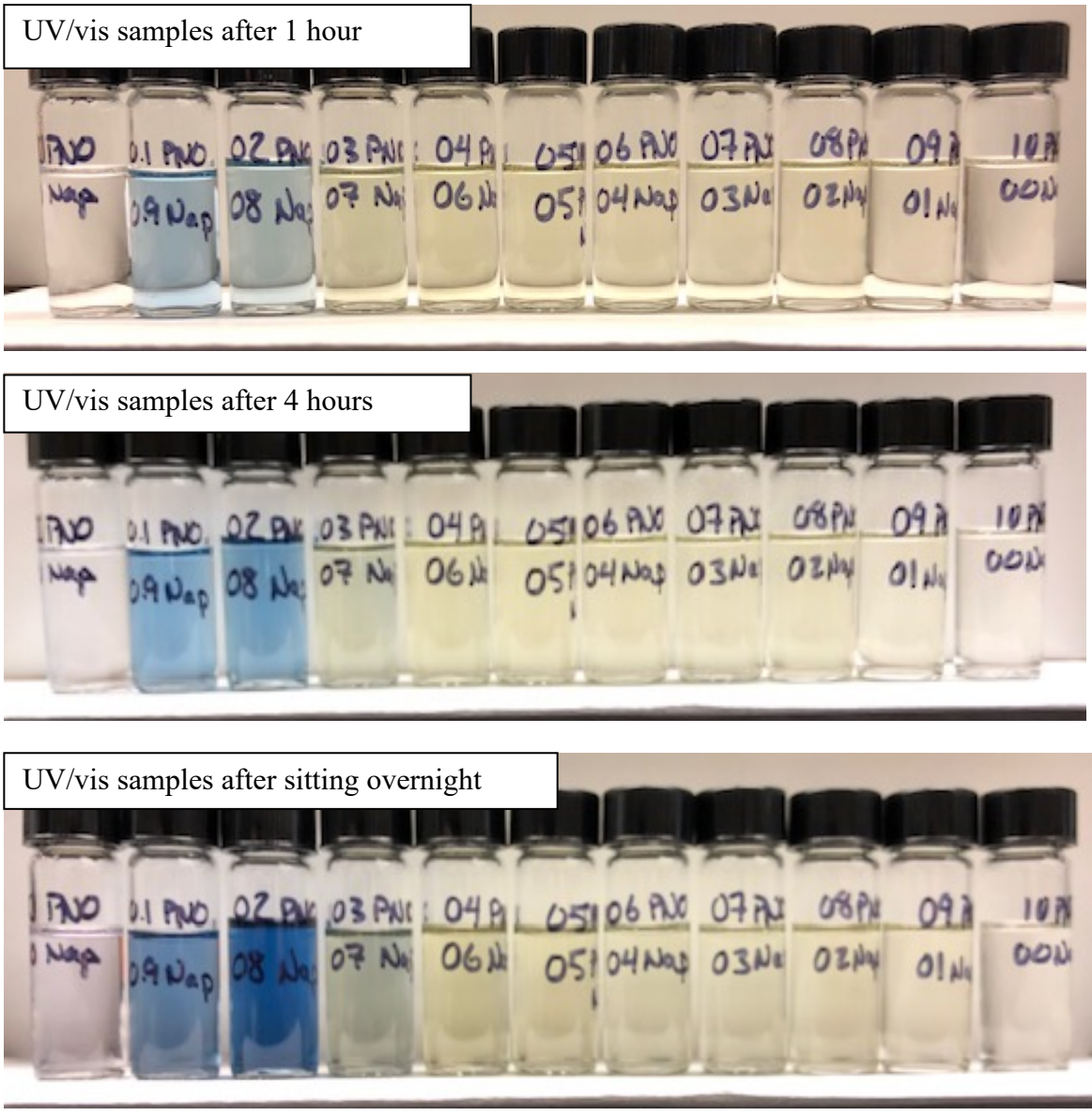

Figure S26. Images of samples of 2-methoxynaphthalene in $MeNO_2$ following obtaining UV/vis measurements for a Job plot.

Minimal to no coloration of the sample containing 100 mol% 2-methoxynaphthalene was observed. The blue complex shows a new broad absorbance feature from 470-720 nm (see below). We believe that the coloration is due to a slow oxidation of 2-methoxynaphthalene by the nitromethane solvent, followed by complexation. This phenomenon was not observed when employing TFAA as the acyl equivalent.

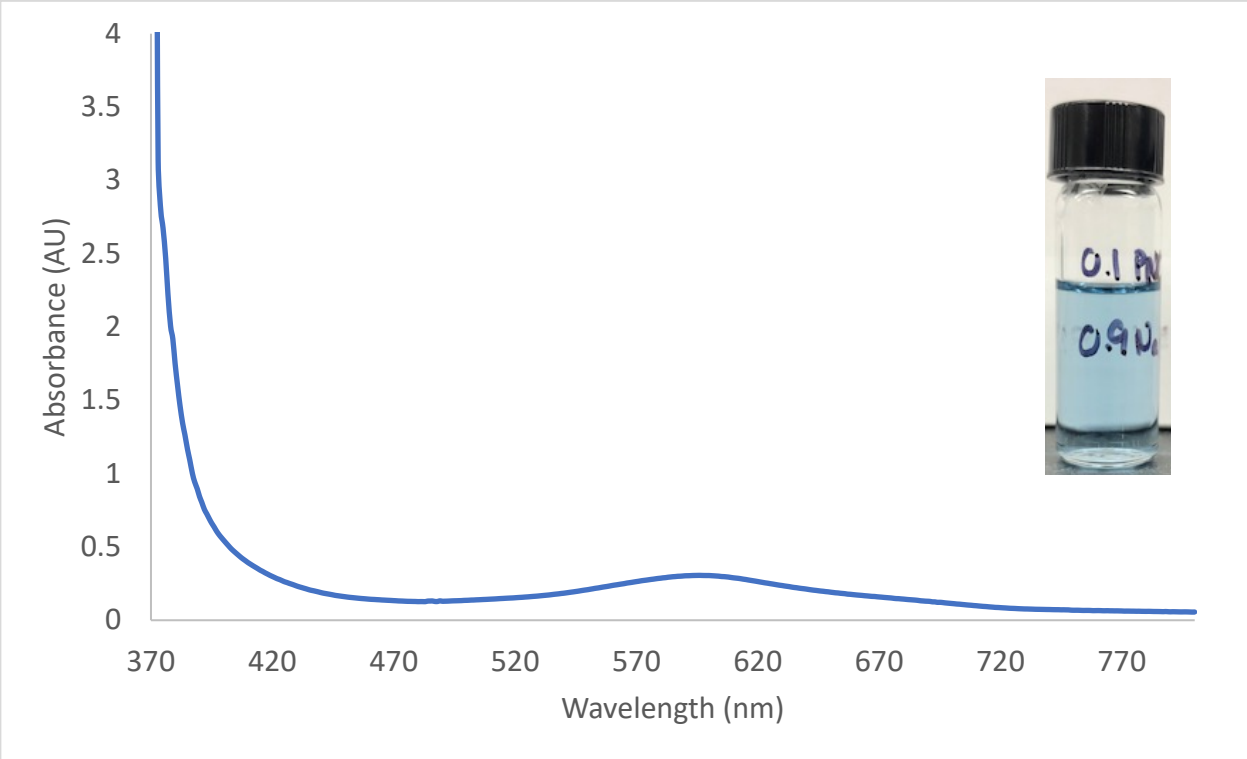

Figure S27. UV/vis spectra of the blue colored sample of 90 mol% 2-methoxynaphthalene with ethyl *N*-(heptafluorobutyroxy)pyridinium-4-carboxylate in $MeNO_2$.

Plot of TFAA volume with EDA complex I. In an effort to maximize the Absorbance values obtained from the EDA complex I, a plot of TFAA vs total volume was generated. For these solutions, the solid ethyl isonicotinate *N*-oxide was weighed out in combination with 2-

methoxynaphthalene flakes into each cuvette individually. The following masses were added: ethyl isonicotinate *N*-oxide (23.4 mg, 0.140 mmol), 2-Methoxynaphthalene (22.1 mg, 0.140 mmol)

A solution was created by solvating the solids in a combination of TFAA and $MeNO_2$ equivalent to 2 mL in volume.

Volume Fraction TFAA	Volume of TFAA (mL)	Volume of $MeNO_2$ (mL)	A_{450} of solution
0.00	0	2000	0
0.00*	0	2000	0.136231
0.10	200	1800	0.239014
0.20	400	1600	0.305786
0.30	600	1400	0.36084
0.50	1000	1000	0.41272
0.70	1400	600	0.367066
0.80	1600	400	0.257691
1.00	2000	0	0.029419

*40 µL (1 equiv) TFAA added to generate EDA complex

Job Plot 3: Constant Volumetric Variance in TFAA-MeNO2 mixture to maximize EDA complex absorption

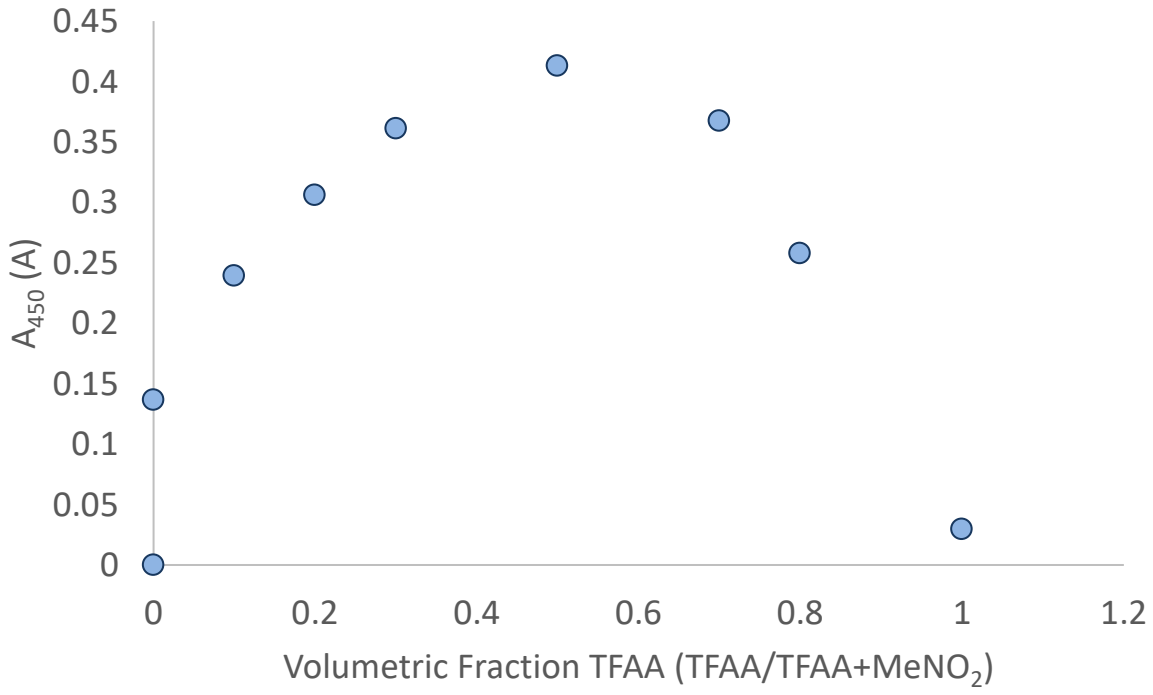

Figure S28. Job plot of EDA complex I absorbance as a function of volumetric ratio of TFAA.

Discussion:

Job Plot of EDA complex 1 does not center at 0.5, but rather, 0.6-0.8. This would suggest the optimal EDA binding stoichiometry is a 2:1 or 4:1 complex between acceptor and donor. But it cannot be ruled out that an equilibrium exists in solution, due to the presence of TFA counter ion, that distorts the Job plot.

To rule out the possibility of an equilibrium, a Job plot of EDA complex V was carried out. In this complex, replacement of TFA counter ion by chloride counter ion should remove the possibility

of an equilibrium existing. However, the Job plot still describes the formation of a complicated 2:1 or 3:2 EDA complex in solution. The true structure of the complex is further complicated as a new local absorbance maximum is observed at 20 mol% 2-methoxynaphthalene, suggesting that a 4:1 acceptor to donor complex may also be accessible under these conditions. It is hypothesized that the TFA counter ion may play a more important role in the absorbance of the complex than can be ascertained from these experiments.

Job plot (Job Plot 3) of the TFAA-$MeNO_2$ volumetric relationship. These data demonstrate that the EDA complex increasing in absorptivity, while remaining at the same concentration, until TFAA and $MeNO_2$ are in a 1:1 ratio. Biasing the ratio towards TFAA results in a lower absorbance of the EDA complex because the complex is sensitive to the polarity of the solution (see figure S28), despite a great amount of acylation reagent being present in the solution.

Section 7: Determination of molar absorptivity of EDA complex 1

To a flame dried 1-dram vial was weighed 2-methoxynaphthalene (0.1 equiv, 0.06 mmol) and ethyl isonicotinate *N*-oxide (1 equiv, 0.6 mmol, 50 mg). To the solids was added 3 mL of sparged acetonitrile and the mixture was sonicated for about 1 minute. To this mixture was added 2 equiv of TFAA, the vial was shaken vigorously, and then the solution was immediately transferred to a 3 mL quartz cuvette. A UV/vis spectrum of the sample was obtained. This procedure was repeated to produce samples at 0.44 M and 0.65 M concentrations. The data was processed using Microsoft excel. The absorbance was plotted against the concentration multiplied by path length (1 cm), and the slope of the line provides the molar absorptivity. For complexes of greater than 1:1

stoichiometry, the theoretical maximum centration of EDA complex in solution was used (i.e. if the complex is 4:1 donor to acceptor, then the theoretical max concentration of complex is 0.005 M for a solution that is 0.02 M in donor). A UV/vis spectra were obtained on a Varian Cary-50 spectrophotometer.

A more detailed investigation of the equilibrium states that may exist in solution and absorb light at or near 450 nm, contributing to the overall absorbance but distorting the apparent absorptivity of the EDA complex (I) is beyond the scope of this study.

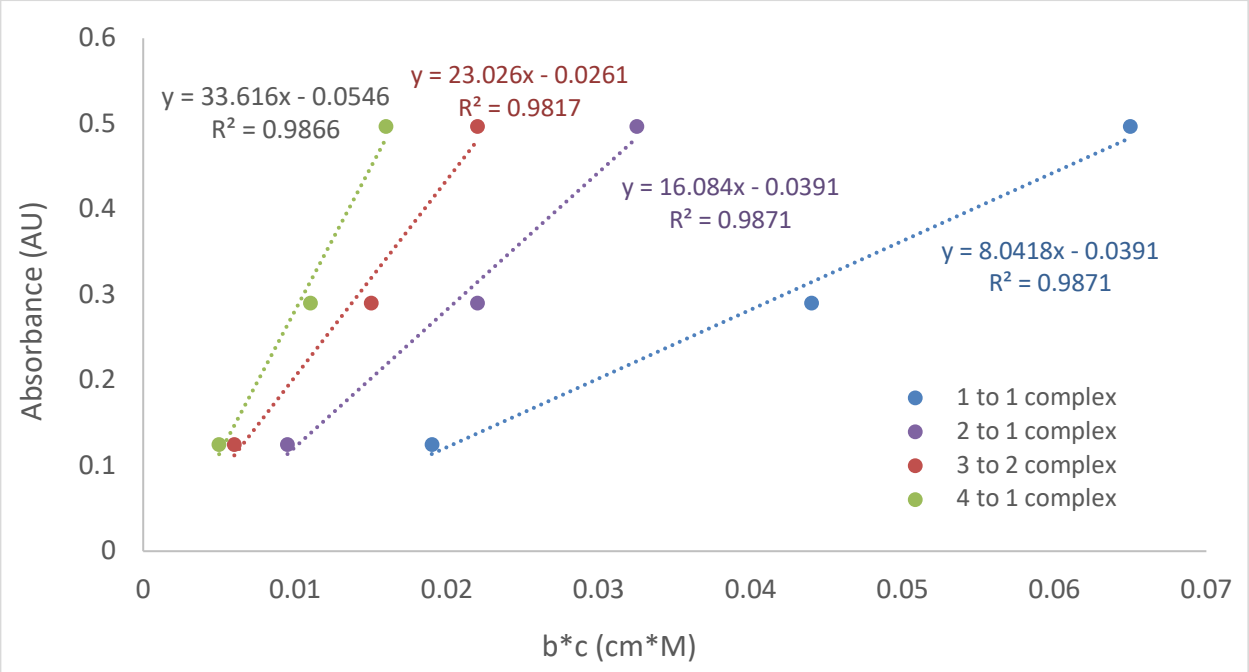

Figure S29. Determination of molar extinction coefficient at 450 nm according to Beer's law.

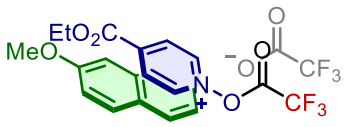

EDA complex

Molar Absorptivity
[8-34 $M^{-1}cm^{-1}$]

Section 8: K_{eq} Calculation

Experiment 1 – constant ethyl isonicotinate *N*-oxide and TFAA, variable 2-methoxynaphthalene

To a clean 3 mL (1 cm path length) cuvette, 175 µL of a 0.8 M solution of ethyl isonicotinate *N*-oxide in $MeNO_2$ was added. This was followed by 1.825 µL of $MeNO_2$ void volume. To generate the accepter, 40 µL of TFAA was added to the cuvette.

To increase the concentration of 2-methoxynaphthalene 14 mg were added in single portions prior to spectra collection.

UV/Vis spectra were recorded on a Shimadzu UV-1601 UV-VOS spectrometer with a Peltier temperature controller, set to 23°C. Prior to analyzing each sample, the cuvette was equilibrated in the temperature-controlled chamber for 3 minutes.

Absorbance data was analyzed in accordance to Benesi-Hildebrand as well as non-linear regression analysis using OriginPro software. These gave similar values.

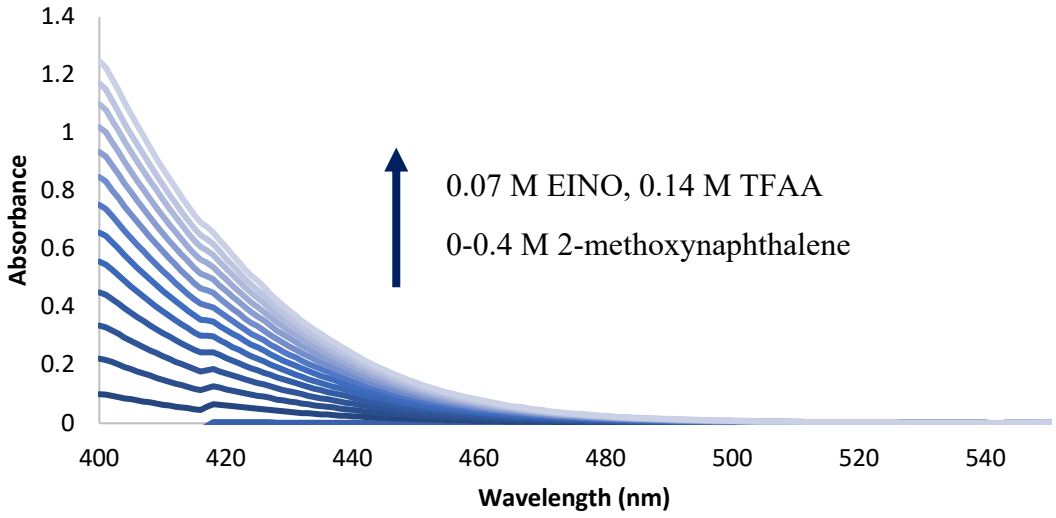

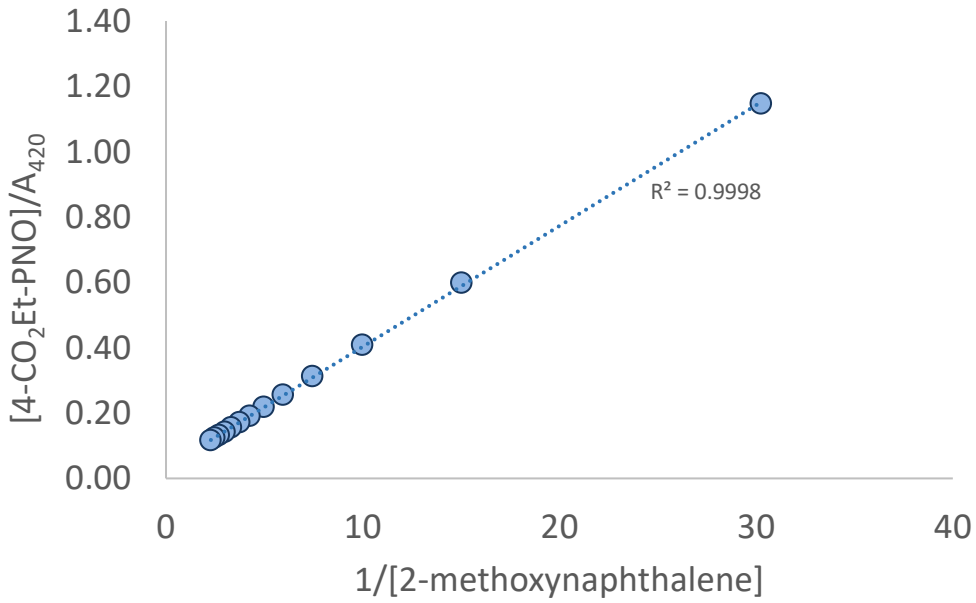

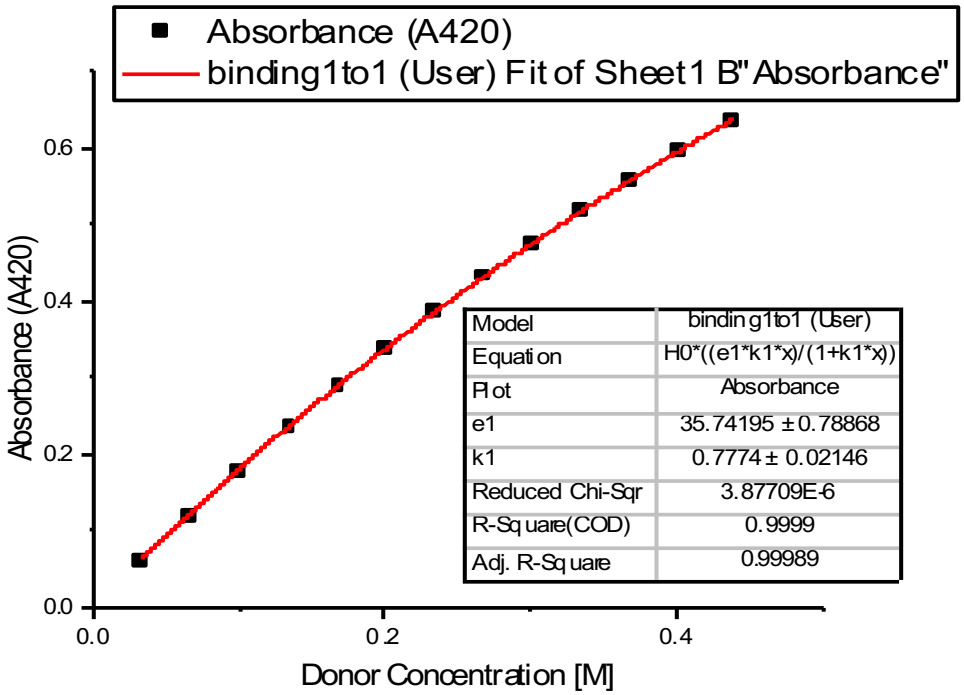

Analysis Method	K_{EDA} (M^{-1}) / λ = 420 nm	ε_{EDA} ($M^{-1}cm^{-1}$) / λ = 420 nm
Benesi-Hildebrand Linear Regression Model	0.912	29.7

Non-Linear Regression Model	0.777	35.7

Experiment 2 – Variable ethyl isonicotinate *N*-oxide, constant TFAA, constant 2-methoxynaphthalene.

To a clean 3 mL (1 cm path length) cuvette, 300 μL of a 0.2 M solution of 2-methoxynaphthalene in $MeNO_2$ was added. This was followed by 1.625 μL of $MeNO_2$ void volume. To generate the acceptor, 85 μL of TFAA was added to the cuvette.

To increase the concentration of ethyl isonicotinate *N*-oxide in solution, 5 mg of this *N*-oxide was added iteratively followed by spectra collection.

UV/Vis spectra were recorded on a Shimadzu UV-1601 UV/VOS spectrometer with a Peltier temperature controller, set to 23°C. Prior to analyzing each sample, the cuvette was equilibrated in the temperature-controlled chamber for 3 minutes.

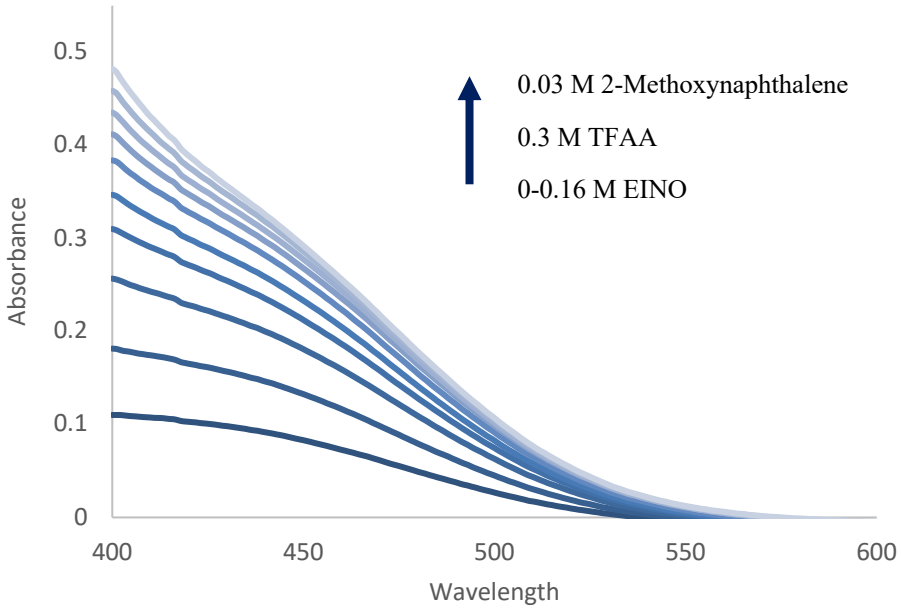

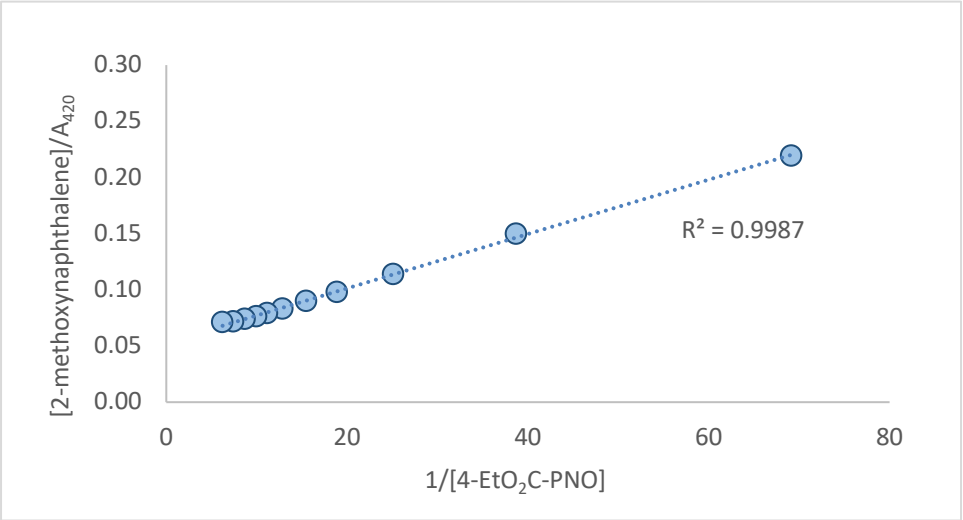

Analysis Method	K_{EDA} (M^{-1}) / λ = 420 nm	ε_{EDA} ($M^{-1}cm^{-1}$) / λ = 420 nm
Benesi-Hildebrand Linear Regression Model	21.8	18.8
Non-Linear Regression Model	18.5	23.2

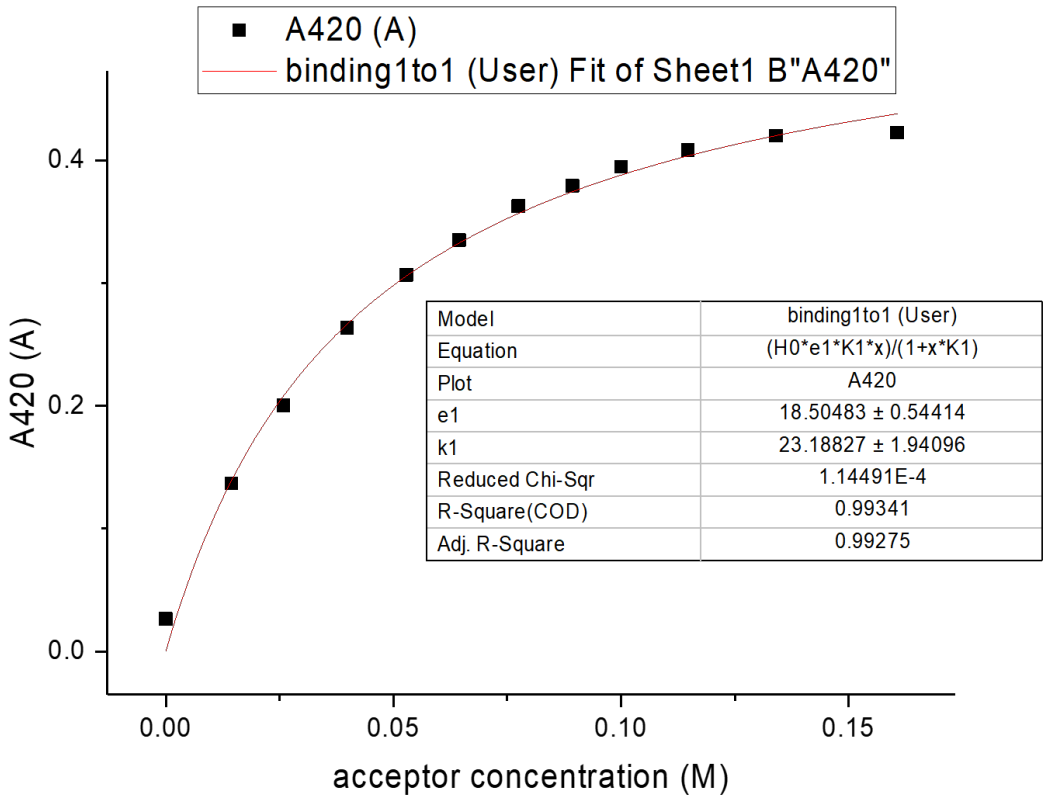

Section 9: Optical Profiles of LED and Laser irradiation sources.

The optical profiles were analyzed with an Ocean Optics USB4000 detector, with a standard multimode fiber optic available at ThorLabs. Absolute intensities were normalized to allow for wavelength comparisons across multiple devices.

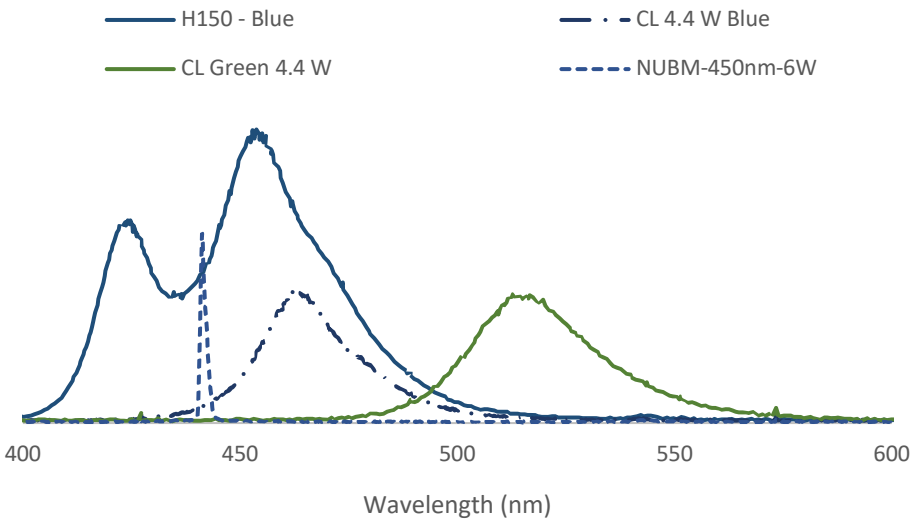

Irradiation Source	λ_{max} (nm)	Spectral Range (nm)
Kessil - H150 Blue	466	420-520
Creative Lighting 4.4 W Blue	423, 454	400-500
Creative Lighting 4.4 W Green	515	471-591
NUBM-450nm-6W	441	440-445

*approximate values given

Section 10: Isolation and Characterization of Products

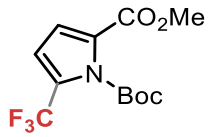

Following Reaction Procedure C, methyl N-Boc pyrrole-2-carboxylate (0.200 mmol, 45 mg, 1 equiv) was reacted with ethyl isonicotinate *N*-oxide (66.8 mg, 2 equiv), 2-methoxynaphthalene (3.16 mg, 0.1 equiv), TFAA (113 µL, 4 equiv) and $CaCl_2$ (22.2 mg, 1 equiv) in 250 µL of solvent for 1 hour at 1.70 A 450 nm laser irradiation. ^{19}F NMR analysis of the crude reaction mixture referenced to benzotrifluoroide revealed the volatile title compound methyl N-Boc-5-

(trifluoromethyl-pyrrole-2-carboxylate [^{19}F NMR ($CDCl_3$, 388 MHz): δ -59.6 (s, 3F, 55%)]. The isolation and characterization of this compound has been previously reported.

^{1}H NMR (400 MHz, $CDCl_3$): δ 6.80 (d, J = 3.9 Hz, 1H), 6.61 (d, J = 3.9 Hz, 1H), 3.87 (s, 3H), 1.61 (s, 9H) ppm.

^{19}F NMR (376 MHz, CDCl3): δ -59.6 ppm.

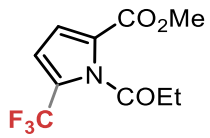

Following Reaction Procedure C, methyl N-(propionyl)-pyrrole-2-carboxylate (0.200 mmol, 36.2 mg, 1 equiv) was reacted with ethyl isonicotinate *N*-oxide (66.8 mg, 2 equiv), 2-methoxynaphthalene (3.16 mg, 0.1 equiv), TFAA (113 µL, 4 equiv) and $CaCl_2$ (22.2 mg, 1 equiv) in 250 µL of solvent for 1 hour at 1.70 A 450 nm laser irradiation. ^{19}F NMR analysis of the crude reaction mixture referenced to benzotrifluoroide revealed the volatile title compound methyl N-(propionyl)-5-(trifluoromethyl)-pyrrole-2-carboxylate [^{19}F NMR ($CDCl_3$, 376 MHz): δ -58.91 (s, 3F, 34%)].

The crude reaction material was taken up in to 10 mL of water and extracted with DCM (3 x 10 mL). The combined organic extracts were washed with sat. sodium bicarbonate (1 x 10 mL) and sat. NaCl solution (1 x 10 mL). The combined organic extracts were dried over sodium sulfate.

The crude material was concentrated to a small volume then carried on to chromatography. The crude material was purified by column chromatography with a gradient from 0-30% ethyl ether in pentane. The resultant pure fractions were carefully concentrated to a small volume *in vacou*. The solution was taken up in 1 ml of pentane and concentrated under a stream of nitrogen gas to give N-(propionyl)-5-(trifluoromethyl)-pyrrole-2-carboxylate was isolated as a colorless oil (7 mg, 14%).

^{1}H NMR (500 MHz, $CDCl_3$): δ 6.90 (d, *J* = 3.9 Hz, 1H), 6.64 (d, *J* = 3.9 Hz, 1H), 3.87 (s, 3H), 2.86 (q, *J* = 7.2 Hz, 2H), 1.30 (t, *J* = 7.2 Hz, 3H) ppm.

^{13}C NMR (126 MHz, CDCl3): δ 176.0, 160.5, 134.3, 128.6, 128.1, 126.4, 125.7 (q, *J* = 40.0 Hz), 124.2, 119.9 (q, *J* = 269.2 Hz), 116.4, 114.1, 112.3 (q, *J* = 3.5 Hz), 52.3, 35.0, 8.7 ppm.

^{19}F NMR (471 MHz, $CDCl_3$): δ -58.91 ppm.

IR (neat): 3144, 2997, 2959, 1774, 1715, 1550, 1437, 1406, 1371, 1251, 1192, 1177, 1116, 1077, 983, 934, 809, 758, 719 cm^{-1}.

HRMS (EI, positive): Predicted [M]+ = 249.0613. Found [M]+ = 249.0624.

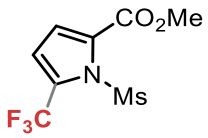

Following Reaction Procedure C, methyl N-(mesyl)-pyrrole-2-carboxylate (0.200 mmol, 36.2 mg, 1 equiv) was reacted with ethyl isonicotinate *N*-oxide (66.8 mg, 2 equiv), 2-methoxynaphthalene (3.16 mg, 0.1 equiv), TFAA (113 µL, 4 equiv) and $CaCl_2$ (22.2 mg, 1 equiv) in 250 µL of solvent for 1 hour at 1.70 A 450 nm laser irradiation. ^{19}F NMR analysis of the crude reaction mixture referenced to benzotrifluoroide revealed the volatile title compound methyl N-(mesyl)-5-(trifluoromethyl)-pyrrole-2-carboxylate [^{19}F NMR ($CDCl_3$, 388 MHz): δ -57.35 (s, 3F, 25%)]. The crude reaction material was taken up in to 10 mL of water and extracted with DCM (3 x 10 mL). The combined organic extracts were washed with sat. sodium bicarbonate (1 x 10 mL), and sat. NaCl solution (1 x 10 mL). The combined organic extracts were dried over sodium sulfate. The crude material was purified by column chromatography on a Biotage Selekt automatic column system, gradient from 0-10% ethyl acetate in hexanes. The product was concentrated to a small volume *in vacou*, and then was blown down from pentane under a stream of nitrogen. then N-(mesyl)-5-(trifluoromethyl)-pyrrole-2-carboxylate was isolated as a colorless solid (12 mg, 21%).

^1H NMR (500 MHz, $CDCl_3$): δ 6.83 (d, J = 3.9 Hz, 1H), 6.76 (d, J = 3.8 Hz, 1H), 3.91 (s, 3H), 3.73 (s, 3H) ppm.

^{13}C NMR (126 MHz, $CDCl_3$): δ 160.5, 131.3 (q, J = 2.2 Hz), 128.7 (q, J = 41.0 Hz), 125.3, 119.9 (q, J = 269.0 Hz), 118.3, 116.3 (q, J = 4.4 Hz), 109.3 (q, J = 3.95 Hz), 53.0, 43.5 ppm.

^{19}F NMR (471 MHz, $CDCl_3$): δ -57.35 ppm.

IR (neat): 3155.6, 3138.7, 3047.5, 3028.5, 2973.4, 2943.7, 2852.6, 1720.7, 1564.7, 1434.8, 1372.3, 1347.2, 1326.0, 1245.1, 1184.3, 1126.8, 1082.1, 1023.5, 971.8, 956.3, 915.8, 826.8, 809.1, 758.1, 742.7 cm^{-1}.

HRMS (EI, positive): Predicted [M+H]+ = 272.0199. Found [M+H]+ = 272.0204.

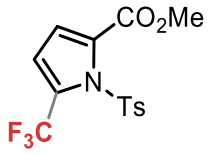

Following Reaction Procedure C, methyl N-tosylpyrrole-2-carboxylate (55.86 mg, 0.200 mmol, 1 equiv) was reacted with ethyl isonicotinate *N*-oxide (66.9 mg, 2 equiv), 2-methoxynaphthalene (3.2 mg, 0.1 equiv), TFAA (113 µL, 4 equiv) and $CaCl_2$ (22.2 mg, 1 equiv) in 250 µL of solvent for 1 hour at 1.70 A 450 nm laser irradiation. ^{19}F NMR analysis of the crude reaction mixture referenced to benzotrifluoroide revealed the title compound N-tosyl-5-(trifluoromethyl)pyrrole-2-carboxylate [^{19}F NMR ($CDCl_3$, 388 MHz): δ –56.89 (s, 3F, 14%)]. The material was purified by column chromatography 0-20% ethyl acetate in hexanes gradient. An additional pipette column of 50% pentanes in dichloromethane afforded N-(tosyl)-5-(trifluoromethyl)pyrrole-2-carboxylate as a clear and colorless oil (7.8 mg, 0.04 mmol, 11% yield).

The crude reaction material was taken up in to 10 mL of water and extracted with DCM (3 x 10 mL). The combined organic extracts were washed with sat. sodium bicarbonate (1 x 10 mL), and sat. NaCl solution (1 x 10 mL). The combined organic extracts were dried over sodium sulfate. The crude material was purified by column chromatography on a Biotage Selekt automatic column system, gradient from 0-10% ethyl acetate in hexanes. N-tosyl-5-(trifluoromethyl)pyrrole-2-carboxylate was isolated as a colorless solid (8 mg, 11%).

^{1}H NMR (500 MHz, $CDCl_3$): δ 8.06 (d, *J* = 7.55 Hz, 2H), 7.36 (d, *J* = 7.95 Hz, 2H), 6.76 (m, 2H), 3.87 (s, 3H), 3.07 (s, 3H) ppm.

^{13}C NMR (125.7 MHz, $CDCl_3$): δ 160.49 (s), 145.75 (s), 135.53 (s), 131.64 (d, *J* = 2.13 Hz), 129.57 (s), 128.52 (s), 127.90 (q, *J* = 41.48 Hz), 119.80 (q, *J* = 267.74 Hz), 116.92 (q, *J* = 5.03 Hz), 116.59 (s), 52.81 (s), 21.72 (s) ppm.

^{19}F NMR (470.4 MHz, $CDCl_3$): δ -55.9 (s) ppm.

IR (neat): 2956, 2928, 2854, 1740, 1595, 1439, 1385, 1341, 1315, 1240, 1181, 1122, 1088, 1025, 964, 915, 805, 758, 744, 701, 660 cm^{-1}.

HRMS (ESI, positive): Predicted [M+H]+ = 348.0512, Found [M+H]+ = 348.0511

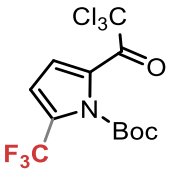

Following Reaction Procedure C, *tert*-butyl 2-(2,2,2-trichloroacetyl)pyrrole-1-carboxylate (93.8 mg, 0.300 mmol, 1 equiv) was reacted with ethyl isonicotinate *N*-oxide (100 mg, 2 equiv), 2-methoxynaphthalene (4.75 mg, 0.1 equiv), TFAA (169 µL, 4 equiv) and $CaCl_2$ (33 mg, 1 equiv) in 375 µL of solvent for 1 hour at 1.70 A 450 nm laser irradiation. ^{19}F NMR analysis of the crude reaction mixture referenced to benzotrifluoroide revealed the volatile title compound N-Boc 2-

(2,2,2-trichloroacetyl)-5-(trifluoromethyl)pyrrole [^{19}F NMR ($CDCl_3$, 388 MHz): δ –59.9 (s, 3F, 77%)].

The crude reaction material was taken up in to 10 mL of water and extracted with DCM (3 x 10 mL). The combined organic extracts were washed with sat. sodium bicarbonate (1 x 10 mL), and sat. NaCl solution (1 x 10 mL). The combined organic extracts were dried over sodium sulfate. The crude material was purified by column chromatography on a Biotage Isolera automatic column system, gradient from 0-10% ethyl acetate in hexanes (R_f = 0.6 in Hexanes). N-tosyl-5-(trifluoromethyl)pyrrole-2-carboxylate was isolated as a pale yellow oil (8 mg, 11%).

^{1}H NMR (700 MHz, $CDCl_3$) = δ 7.24 (d, *J* = 3.8 Hz, 2H), 6.71 (d, *J* = 3.8 Hz, 2H), 1.62 (s, 9H).

^{13}C NMR (175 MHz, $CDCl_3$) = δ 174.12 (s), 146.80 (s), 128.02 (q, *J* = 41.1 Hz), 119.57 (q, *J* = 269.2 Hz), 119.35 (s), 113.13 (d, *J* = 3.4 Hz), 94.43 (s), 87.95 (s), 27.14 (s).

^{19}F NMR (376 MHz, $CDCl_3$) = δ -59.9 ppm (s).

IR (neat): 2986.8, 2939.8, 1781.7, 1698.8, 1546.1, 1397.5, 1373.3, 1354.2, 1321.7, 1277.2, 1245.7, 1188.4, 1141.4, 1068.1, 907.0, 841.0, 819.6, 800.2, 781.9, 729.9, 667.1, 677.2, 650.0 cm^{-1}

Mass spectra of the N-Boc protected product could not be obtained because Boc deprotection occurred during data collection. We were able to collect HRMS data corresponding to the deprotected pyrrole. Molecular formula: C7H3Cl3F3NO.

HRMS (APCI, positive): Predicted [M+H]+ = 279.9305, Found [M+H]+ = 279.9311

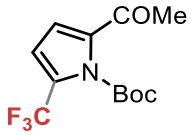

Following Reaction Procedure C, *tert*-butyl 2-acetyl-1H-pyrrole-1-carboxylate (0.100 mmol, 26.3, 1 equiv) was reacted with ethyl isonicotinate *N*-oxide (33.4 mg, 2 equiv), 2-methoxynaphthalene (1.58 mg, 0.1 equiv), TFAA (56.4 µL, 4 equiv) and $CaCl_2$ (11.1 mg, 1 equiv) in 125 µL of solvent for 1 hour at 1.70 A 450 nm laser irradiation. ^{19}F NMR analysis of the crude reaction mixture referenced to benzotrifluoroide revealed the volatile title compound *tert*-butyl 2-acetyl-5-(trifluoromethyl)-1H-pyrrole [^{19}F NMR ($CDCl_3$, 388 MHz): δ -59.8 (s, 3F, 66%)]. The isolation and characterization of these compounds has been previously reported.

^{1}H NMR (500 MHz, $CDCl_3$) = δ 6.80 (d, J = 3.9 Hz, 1H), 6.60 (d, J = 3.9 Hz, 1H), 2.48 (s, 3H), 1.61 (s, 9H) ppm.

^{13}C NMR (126 MHz, $CDCl_3$) = δ 188.0 (s), 151.1 (s), 147.9 (s), 135.3 (s), 126.7 (q, J = 39.8 Hz), 125.9 (s), 120.1 (q, J = 269.1 Hz), 120.0 (q, J = 3.0 Hz), 116.3 (s), 112.3 (s), 87.0 (s), 27.3 (s), 26.9 (s) ppm.

^{19}F NMR (376 MHz, $CDCl_3$) = δ -59.8 ppm (s).

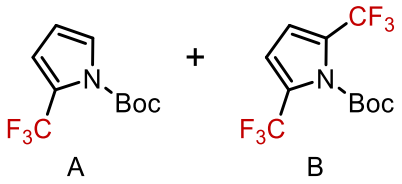

Following Reaction Procedure C, N-Boc-pyrrole (0.200 mmol, 33.4 mg, 1 equiv) was reacted with ethyl isonicotinate *N*-oxide (66.8 mg, 2 equiv), 2-methoxynaphthalene (3.16 mg, 0.1 equiv), TFAA (113 µL, 4 equiv) and $CaCl_2$ (22.2 mg, 1 equiv) in 250 µL of solvent for 1 hour at 1.70 A 450 nm laser irradiation. 1^9F NMR analysis of the crude reaction mixture referenced to benzotrifluoroide revealed the volatile title compound *tert*-butyl 2-(trifluoromethyl)-1H-pyrrole [^{19}F NMR ($CDCl_3$, 388 MHz): δ -58.31 (s, 3F, 62%)] and *tert*-butyl 2,5-bis(trifluoromethyl)-1H-pyrrole [^{19}F NMR ($CDCl_3$, 388 MHz): δ -58.38 (s, 3F, 14%)]. The isolation and characterization of these compounds has been previously reported.

A) N-Boc 2-(trifluoromethyl)pyrrole

^{1}H NMR (500 MHz, $CDCl_3$) = δ 7.44 (dd, *J* = 3.3, 2.0 Hz, 1H), 6.75-6.72 (m, 1H), 6.19 (t, *J* = 3.3 Hz, 1H), 1.61 (s, 9H) ppm.

^{19}F NMR (376 MHz, $CDCl_3$) = δ -58.31 ppm (s).

B) N-Boc 2,5-bis(trifluoromethyl)pyrrole

^{1}H NMR (500 MHz, $CDCl_3$) = δ 6.71 (s, 2H), 1.62 (s, 9H) ppm.

^{19}F NMR (376 MHz, $CDCl_3$) = δ -58.38 ppm (s).

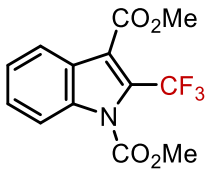

Following Reaction Procedure C, dimethyl N-(carboxylate)-indole-3-carboxylate (0.200 mmol, 46.6 mg, 1 equiv) was reacted with ethyl isonicotinate *N*-oxide (66.8 mg, 2 equiv), 2-methoxynaphthalene (3.16 mg, 0.1 equiv), TFAA (113 µL, 4 equiv) and $CaCl_2$ (22.2 mg, 1 equiv) in 250 µL of solvent for 1 hour at 1.70 A 450 nm laser irradiation. ^{19}F NMR analysis of the crude reaction mixture referenced to benzotrifluoroide revealed the title compounds dimethyl N-(carboxylate)-2-(trifluoromethyl)indole-3-carboxylate [^{19}F NMR ($CDCl_3$, 377 MHz): δ -57.31 (s, 3F, 30%)].

The crude reaction material was taken up in to 10 mL of water and extracted with DCM (3 x 10 mL). The combined organic extracts were washed with sat. sodium bicarbonate (1 x 10 mL), and sat. NaCl solution (1 x 10 mL). The combined organic extracts were dried over sodium sulfate. The crude material was purified by column chromatography on a Biotage Selekt automatic column system, gradient from 0-20% ethyl acetate in hexanes. N-(carboxylate)-2-(trifluoromethyl)indole-3-carboxylate was isolated as a colorless solid (20 mg, 32%).

^1H NMR (500 MHz, $CDCl_3$) = δ 8.11 (d, J = 8.5 Hz, 1H), 7.86 (d, J = 8.0, Hz, 1H), 7.51 (t, J = 7.9 Hz, 1H), 7.39 (t, J = 7.6 Hz, 1H), 4.10 (s, 3H), 4.00 (s, 3H) ppm.

^{13}C NMR(176 MHz, $CDCl_3$) δ 163.6 (s), 150.6 (s), 136.2 (s), 128.2 (s), 126.45 (q, J = 39.8 Hz), 125.4 (s), 124.8 (s), 121.9 (s), 120.3 (q, J = 250.2 Hz), 119.3 (q, J = 3.6 Hz), 117.0 (s), 115.1 (s), 55.1 (q, J = 5.5 Hz), 52.9 (q, J = 7.0 Hz) ppm.

^{19}F NMR (470 MHz, $CDCl_3$) = δ -57.31 ppm.

IR (neat): 2961.4, 2924.4, 2854.5, 1751.6, 1717.8, 1564.4, 1438.2, 1359.1, 1317.6, 1257.9, 1225.5, 1175.8, 1134.4, 1080.7, 1026.7, 960.8, 920.5, 766.4, 746.7, 682.2 cm^{-1}.

HRMS (ESI, positive): Predicted [M+H]+ = 302.0635, Found [M+H]+ = 302.0631

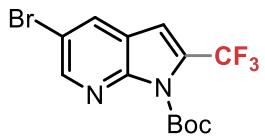

Following Reaction Procedure C, N-(boc)-5-Bromo-7-azaindole (0.100 mmol, 29.7 mg, 1 equiv) was reacted with ethyl isonicotinate *N*-oxide (33.4 mg, 2 equiv), 2-methoxynaphthalene (1.58 mg, 0.1 equiv), TFAA (56.4 µL, 4 equiv) and $CaCl_2$ (11.1 mg, 1 equiv) in 125 µL of solvent for 1 hour at 1.70 A 450 nm laser irradiation. ^{19}F NMR analysis of the crude reaction mixture referenced to benzotrifluoroide revealed the title compounds N-(boc)-2-(trifluoromethyl)-5-Bromo-7-azaindole [^{19}F NMR ($CDCl_3$, 388 MHz): δ -58.8 (s, 3F, 30%)]. The isolation and characterization of these compounds has been previously reported.

^{1}H NMR (500 MHz, $CDCl_3$) = δ 8.67 (s, 1H), 8.11 (s, 1H), 7.01 (s, 1H), 1.67 (s, 9H) ppm.

^{19}F NMR (470 MHz, $CDCl_3$) = δ -58.76 ppm.

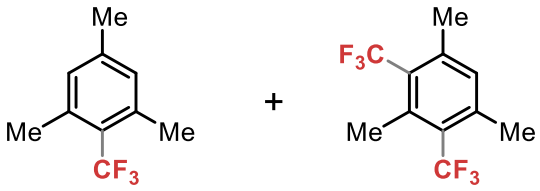

Following Reaction Procedure C, mesitylene (0.100 mmol, 13.9 µL, 1 equiv) was reacted with ethyl isonicotinate *N*-oxide (33.4 mg, 2 equiv), 2-methoxynaphthalene (1.58 mg, 0.1 equiv), TFAA (56.4 µL, 4 equiv) and $CaCl_2$ (11.1 mg, 1 equiv) in 125 µL of solvent for 1 hour at 1.70 A 450 nm laser irradiation. ^{19}F NMR analysis of the crude reaction mixture referenced to benzotrifluoroide revealed the volatile title compounds 1,3,5-trimethyl-2-(trifluoromethyl)benzene [^{19}F NMR ($CDCl_3$, 388 MHz): δ -54.7 (s, 3F, 49%)] and 1,3,5-trimethyl-2,4-bis(trifluoromethyl)benzene [^{19}F NMR (CDCl3, 388 MHz): δ -53.9 (s, 3F, 14%)]. The isolation and characterization of these compounds has been previously reported.

Mono-trifluoromethylated product

^{1}H NMR (500 MHz, $CDCl_3$) = δ 6.90 (s, 2H), 2.46-2.42 (m, 6H), 2.29 (s, 3H) ppm.

^{19}F NMR (376 MHz, $CDCl_3$) = δ -53.89 ppm (s).

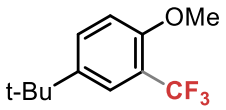

66%
66%*

Following Reaction Procedure C, 4-*tert*-butylanisole (0.100 mmol, 17.5 µL, 1 equiv) was reacted with ethyl isonicotinate *N*-oxide (33.4 mg, 2 equiv), 2-methoxynaphthalene (1.58 mg, 0.1 equiv), TFAA (56.4 µL, 4 equiv) and $CaCl_2$ (11.1 mg, 1 equiv) in 125 µL of solvent for 1 hour at 1.70 A 450 nm laser irradiation. ^{19}F NMR analysis of the crude reaction mixture referenced to benzotrifluoroide revealed the volatile title compound 4-(*tert*-butyl)-1-methoxy-2-(trifluoromethyl)benzene [^{19}F NMR ($CDCl_3$, 388 MHz): δ -63.12 (s, 3F, 66%)].

The procedure was repeated with the omission of 2-Methoxynaphthalene to obtain a yield of 66% signifying a competitive binding and reaction between the 4-*tert*-butylanisole and acylated PNO reagent, as compared to the 2-Methoxynaphthalene enabled reaction.

Following Reaction Procedure C, 4-*tert*-butylanisole (0.500 mmol, 87.6 µL, 1 equiv) was reacted with ethyl isonicotinate *N*-oxide (167.2 mg, 2 equiv), 2-methoxynaphthalene (7.9 mg, 0.1 equiv), TFAA (281.9 µL, 4 equiv) and $CaCl_2$ (55.5 mg, 1 equiv) in 0.625 mL of solvent for 1 hour at 1.70 A 450 nm laser irradiation. The compound was isolated by silica gel column chromatography to give a clear, colorless (60 mg, 0.26 mmol, 52%)

The isolation and characterization of these compounds has been previously reported.

^1H NMR (500 MHz, $CDCl_3$) = δ 7.56 (s, 1H), 7.50 (d, J = 12 Hz, 1H), 6.93 (d, J = 12 Hz, 1H), 3.89 (s, 3H), 1.31 (s, 9H).

^{19}F NMR (376 MHz, $CDCl_3$) = δ -62.17 ppm (s).

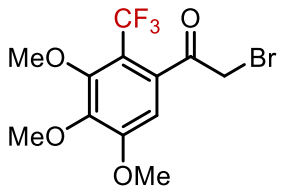

Following Reaction Procedure C, 3,4,5-(trimethoxy)-2'-bromo-acetophenone (0.200 mmol, 57.8 mg, 1 equiv) was reacted with ethyl isonicotinate *N*-oxide (66.8 mg, 2 equiv), 2-methoxynaphthalene (3.16 mg, 0.1 equiv), TFAA (113 µL, 4 equiv) and $CaCl_2$ (22.2 mg, 1 equiv) in 250 µL of solvent for 1 hour at 1.70 A 450 nm laser irradiation. ^{19}F NMR analysis of the crude reaction mixture referenced to benzotrifluoroide revealed the title compounds 2-(trifluoromethyl)-3,4,5-(trimethoxy)-2'-bromo-acetophenone [^{19}F NMR ($CDCl_3$, 388 MHz): δ -55.93 (s, 3F, 45%)]. The crude reaction material was taken up in to 10 mL of water and extracted with DCM (3 x 10 mL). The combined organic extracts were washed with sat. sodium bicarbonate (1 x 10 mL), and sat. NaCl solution (1 x 10 mL). The combined organic extracts were dried over sodium sulfate. The crude material was purified by column chromatography on a Biotage Selekt automatic column system, gradient from 0-20% ethyl acetate in hexanes (R_f = 0.54 in 20% EA/H). 2-(trifluoromethyl)-3,4,5-(trimethoxy)-2'-bromo-acetophenone was isolated as a yellow oil that solidified after a few hours (18 mg, 25%).

^1H NMR (400 MHz, $CDCl_3$) = δ 6.56 (s, 1H), 4.26 (s, 2H), 3.97 (s, 3H), 3.92 (s, 6H) ppm.

^{13}C NMR (126 MHz, $CDCl_3$) = δ 195.8 (s), 156.4 (s), 153.0 (q, J = 2.04 Hz), 144.3 (s), 133.4 (q, J = 2.6 Hz), 123.4 (q, J = 273.7 Hz), 113.7 (q, J = 30.9 Hz), 106.3 (s), 62.0 (s), 61.1 (s), 56.5 (s), 35.1 (q, J = 4.2), 29.86 (s) ppm.

^{19}F NMR (470 MHz, $CDCl_3$) = δ -55.93 (s) ppm.

IR (neat): 3022.8, 3006, 2946.3, 2854.2, 1729.0, 1575.7, 1504.0, 1454.0, 1405.5, 1337.0, 1307.2, 1292.3, 1267.9, 1197.4, 1161.6, 1126.9, 1086.8, 999.3, 939.1, 909.0, 852.8, 828.4, 716.8 cm^{-1}

HRMS (EI, positive): Predicted [M]+ = 355.9871 Found [M]+ 355.9874

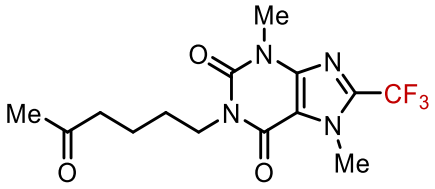

Following Reaction Procedure C, pentoxifylline (0.200 mmol, 54.8 mg, 1 equiv) was reacted with ethyl isonicotinate *N*-oxide (66.8 mg, 2 equiv), 2-methoxynaphthalene (3.16 mg, 0.1 equiv), TFAA (113 µL, 4 equiv) and $CaCl_2$ (22.2 mg, 1 equiv) in 250 µL of solvent for 1 hour at 1.70 A 450 nm laser irradiation. ^{19}F NMR analysis of the crude reaction mixture referenced to benzotrifluoroide revealed the title compounds 1-(5-oxohexyl)-3,7-dimethyl-6-(trifluoromethyl)-xanthine [^{19}F NMR ($CDCl_3$, 388 MHz): δ –63.4 (s, 3F, 20%)].

The crude reaction material was taken up in to 10 mL of water and extracted with DCM (3 x 10 mL). The combined organic extracts were washed with sat. sodium bicarbonate (1 x 10 mL), and sat. NaCl solution (1 x 10 mL). The combined organic extracts were dried over sodium sulfate.

The crude material was purified by column chromatography on a Biotage Selekt automatic column system, gradient from 0-20% ethyl acetate in hexanes. 1-(5-oxohexyl)-3,7-dimethyl-6-(trifluoromethyl)-xanthine was isolated as colorless solid (11 mg, 16%).

^{1}H NMR (700 MHz, $CDCl_3$) = δ 4.14 (s, 3H), 4.01 (t, *J* = 6.9 Hz, 2 H), 3.57 (s, 3H), 2.50 (t, *J* = 6.9 Hz, 2H), 2.14 (s, 3H), 1.68-1.61 (m, 4H) ppm.

^{13}C NMR (176 MHz, $CDCl_3$) δ 208.8 (s), 155.4 (s), 151.2 (s), 146.7 (s), 139.0 (q, *J* = 40.0 Hz), 118.3 (q, *J* = 271.3 Hz), 109.8 (s), 43.2 (s), 41.3 (s), 33.3 (q, *J* = 2.1 Hz), 30.1 (s), 30.0 (s), 27.4 (s), 21.0 (s) ppm.

^{19}F NMR (470 MHz, $CDCl_3$) = δ -63.4 (s) ppm.

IR (neat): 2957.8, 2921.6, 2856.3, 1704.5, 1661.8, 1609.6, 1545.5, 1514.7, 1462.41430.9, 1366.1, 1324.5, 1288.7, 1244.3, 1197.0, 1178.0,1140.6, 1108.9, 1062.9, 1008.2, 873.6, 764.6, 750.6, 724.3, 686.4 cm^{-1}

HRMS (ESI, negative): Predicted [M-H]- = 347.1336; Found [M-H]- = 347.1299

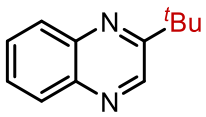

Following Reaction Procedure D. 2-phenyl-5-chloropyridazine (0.200 mmol, 26 mg, 1 equiv) was weighed into a 1 dram vial equipped with a stirbar. To this was added ethyl isonicotinate *N*-oxide

(66.8 mg, 2 equiv), 2-methoxynaphthalene (3.16 mg, 0.1 equiv), and $CaCl_2$ (22.2 mg, 1 equiv). The solids were evacuated and backfilled 5 times with nitrogen. Then 250 μL of $MeNO_2$ was added, followed by pivaloyl chloride (98 μL, 4 equiv). The vial was then sealed with electrical tape and parafilm, placed in front of a 456 nm Kessil lamp and irradiated for 12 hours ambient temperature. At the conclusion of the reaction period, the reaction mixture was taken up into 9 mL of water and extracted with 3 x 10 mL of DCM. The combined organic extracts were washed once with sodium bicarbonate (10 mL) and once with saturated brine solution (10 mL). The organic layer was then dried over sodium sulfate. A biotage column was run on the crude reaction mixture and yielded a mixture of t*ert*-butylated quinoxailine, mono-*tert*-butylated ethyl isonicotinate, and bis-*tert*-butylylated ethyl isonicotinate. The mixture of *tert*-butylated products was subjected to basic soaponification. The mixture was taken up in 1 mL of THF, and 1 mL of 6M KOH was added to create a biphasic mixture. The mixture was stirred vigorously (1000 rpm) and heated to 70 °C for 5 hours. Upon completion of the reaction, the TLC plate showed 1 major UV active spot (R_f 0.56 in 4:1 H:EA). Purification by flash chromatography on Biotage Isolera (0% to 20% EA) provided cyclohexane quinoxaline as the major product (21 mg). The isolation and characterization of these compounds has been previously reported.

^{1}H NMR (700 MHz, $CDCl_3$) = δ 8.99 (s, 1H), 8.10-8.02 (m, 2H), 7.77-7.66 (m, 2H), 1.52 (s, 9H) ppm.

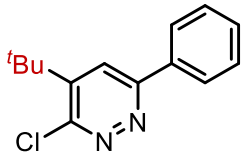

Following Reaction Procedure D. 2-phenyl-5-chloropyridazine (0.200 mmol, 26 mg, 1 equiv) was weighed into a 1 dram vial equipped with a stirbar. To this was added ethyl isonicotinate *N*-oxide (66.8 mg, 2 equiv), 2-methoxynaphthalene (3.16 mg, 0.1 equiv), and $CaCl_2$ (22.2 mg, 1 equiv). The solids were evacuated and backfilled 5 times with nitrogen. Then 250 µL of $MeNO_2$ and 250 µL of DCM was added, followed by pivaloyl chloride (98 µL, 4 equiv). The vial was then sealed with electrical tape and parafilm, placed in front of a 456 nm Kessil lamp and irradiated for 12 hours ambient temperature. At the conclusion of the reaction period, the reaction mixture was taken up into 9 mL of water and extracted with 3 x 10 mL of DCM. The combined organic extracts were washed once with sodium bicarbonate (10 mL) and once with saturated brine solution (10 mL). The organic layer was then dried over sodium sulfate. Purification by flash chromatography using a Biotage Isolera automatic column (0% to 20% EA) provided 2-phenyl-4-(*tert*-butyl)-5-chloropyridazine as the major product (11 mg).

^{1}H NMR (700 MHz, $CDCl_3$) = δ 8.06-8.01 (m, 2H), 7.81 (s, 1H), 7.55-7.50 (m, 3H), 1.55 (s, 9H) ppm.

^{13}C NMR(176 MHz, $CDCl_3$) δ 159.1, 155.7, 148.4, 135.8, 130.4, 129.2, 127.3, 123.8, 35.6, 28.6 ppm.

IR (neat): 2961, 2926, 2875, 1730, 1574, 1399, 1366, 1244, 1156, 1067, 771, 690, 660 cm^{-1}.

HRMS (ESI-TOF): Predicted [M+H]+ = 247.0997, Found [M+H]+ = 247.0995

1D NOSEY – Irradiation from 7.82-7.79 ppm produced two correlations. The first a signal at 8.06-8.01 ppm, the second at 1.55 ppm. The strength of these correlations demonstrated build-up when the mixing time was gradually changed from 150 ms to 500 ms.

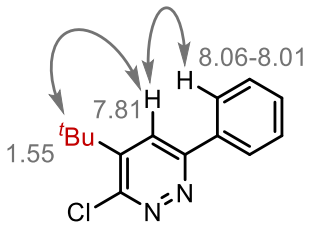

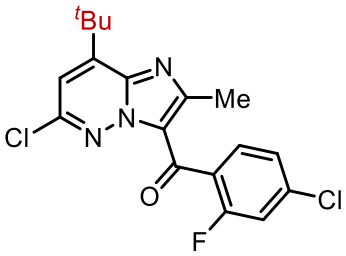

Following Reaction Procedure D. (4-chloro-2-fluorophenyl)(6-chloro-2-methylimidazo[1,2-*b*]pyridazin-3-yl)methanone (0.200 mmol, 65 mg, 1 equiv) was weighed into a 1 dram vial equipped with a stirbar. To this was added ethyl isonicotinate *N*-oxide (66.8 mg, 2 equiv), 2-methoxynaphthalene (3.16 mg, 0.1 equiv), and $CaCl_2$ (22.2 mg, 1 equiv). The solids were evacuated and backfilled 5 times with nitrogen. Then 250 µL of $MeNO_2$ and 250 µL of DCM was added, followed by pivaloyl chloride (98 µL, 4 equiv). The vial was then sealed with electrical tape and parafilm, placed in front of a 456 nm kessil lamp and irradiated for 12 hours ambient temperature. The reaction mixture was taken up into 9 mL of water and extracted with 3 x 10 mL of DCM. The combined organic extracts were washed once with sodium bicarbonate (10 mL) and once with saturated brine solution (10 mL). The organic layer was then dried over sodium sulfate.

Isolation by flash chromatography on a Biotage Isolera automatic column afforded (4-chloro-2-fluorophenyl)(8-(*tert*-butyl)-6-chloro-2-methylimidazo[1,2-*b*]pyridazin-3-yl)methanone as the sole product (20 mg). The isolation and characterization of these compounds has been previously reported.

^{1}H NMR (400 MHz, $CDCl_3$) = δ 7.60 (t, J = 8.0, 1H), 7.28 (dd, J = 8.3, 1.9 Hz, 1H), 7.10 (dd, J = 10.0, 1.9 Hz, 1H), 6.99 (s, 1H), 2.66 (s, 3H), 1.57 (s, 9H) ppm.

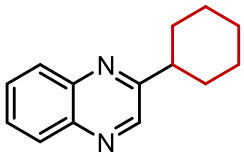

Following Reaction Procedure D. Quinoxaline (0.200 mmol, 26 mg, 1 equiv) was weighed into a 1 dram vial equipped with a stirbar. To this was added ethyl isonicotinate *N*-oxide (66.8 mg, 2 equiv), 2-methoxynaphthalene (3.16 mg, 0.1 equiv), and $CaCl_2$ (22.2 mg, 1 equiv). The solids were evacuated and backfilled 5 times with nitrogen. Then 250 µL of $MeNO_2$ was added, followed by cyclohexanecarbonyl chloride (108 µL, 4 equiv). The vial was then sealed with electrical tape and parafilm, placed in front of a 456 nm Kessil lamp and irradiated for 12 hours ambient temperature. The reaction mixture was taken up into 9 mL of water and extracted with 3 x 10 mL of DCM. The combined organic extracts were washed once with sodium bicarbonate (10 mL) and once with saturated brine solution (10 mL). The organic layer was then dried over sodium sulfate. A biotage column was run on the crude reaction mixture and yielded a mixture of cyclohexylated quinoxailine, mono-cyclohexylated ethyl isonicotinate, and bis-cyclohexylated ethyl isonicotinate. The mixture of cyclohexylated products was subjected to basic saponification. The mixture was taken up in 1 mL of THF, and 1 mL of 6M KOH was added to create a biphasic mixture. The

mixture was stirred vigorously (1000 rpm) and heated to 70 °C for 5 hours. Upon completion of the reaction, the TLC plate showed 1 major UV active spot (R_f ~0.5 in 9:1 H:EA). Purification on the biotage (0% to 20% EA) provided 2-cyclohexylquinoxaline as the major product (17 mg). The isolation and characterization of these compounds has been previously reported.

^{1}H NMR (500 MHz, $CDCl_3$) = δ 8.77 (s, 1H), 8.09-8.02 (m, 2H), 7.73 (ddd, *J* = 8.2, 6.8, 1.7 Hz, 1H), 7.69 (ddd, *J* = 8.3, 7.0, 1.6 Hz, 1H), 2.97 (tt, *J* = 12.0, 3.5 Hz, 1H), 2.09-1.99 (m, 2H), 1.96-1.88 (m, 2H), 1.84-1.77 (m, 2H), 1.71 (qd, *J* = 12.6, 3.4 Hz, 2H), 1.48 (qt, *J* = 12.8, 3.4 Hz, 2H), 1.37 (tt, *J* = 12.8, 3.4 Hz, 1H) ppm.

^{13}C NMR (126 MHz, $CDCl_3$) = δ 161.2, 145.1, 142.3, 141.5, 129.9, 129.2, 129.1, 129.0, 45.2, 32.5, 26.5, 26.0 ppm.

HRMS (ESI-TOF): Predicted [M+H]+ = 213.1386, Found [M+H]+ = 213.1396

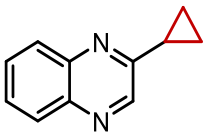

Cyclopropanecarbonyl chloride was distilled under vacuum at 55 °C immediately prior to use. Following Reaction Procedure D. Quinoxaline (0.200 mmol, 26 mg, 1 equiv) was weighed into a 1 dram vial equipped with a stirbar. To this was added ethyl isonicotinate *N*-oxide (66.8 mg, 2 equiv), 2-methoxynaphthalene (3.16 mg, 0.1 equiv), and $CaCl_2$ (22.2 mg, 1 equiv). The solids were evacuated and backfilled 5 times with nitrogen. Then 250 µL of $MeNO_2$ was added, followed by cyclopropanecarbonyl chloride (63 µL, 4 equiv). The vial was then sealed with electrical tape and

parafilm, placed in front of a 456 nm Kessil lamp and irradiated for 12 hours ambient temperature. At the conclusion of the reaction period, the reaction mixture was a dark violet in color. The reaction mixture was taken up into 9 mL of water and extracted with 3 x 10 mL of DCM. The combined organic extracts were washed once with sodium bicarbonate (10 mL) and once with saturated brine solution (10 mL). The organic layer was then dried over sodium sulfate. A biotage column was run on the crude reaction mixture and yielded a mixture of cyclopropylated quinoxailine, mono-cyclopropylated ethyl isonicotinate, and bis-cyclopropylated ethyl isonicotinate. The mixture of cyclopropylated products was subjected to basic saponification. The mixture was taken up in 1 mL of THF, and 1 mL of 6M KOH was added to create a biphasic mixture. The mixture was stirred vigorously (1000 rpm) and heated to 70 °C for 5 hours. Upon completion of the reaction, the TLC plate showed 1 major UV active spot (R_f ~0.4 in 4:1 H:EA). Purification on the biotage (0% to 20% EA) provided 2-cyclopropylquinoxaline as the major product (4 mg). The isolation and characterization of these compounds has been previously reported. The isolation and characterization of these compounds has been previously reported.

^{1}H NMR (400 MHz, $CDCl_3$) = δ 8.73 (s, 1H), 8.04 (dd, *J* = 8.4, 1.7 Hz, 1H), 7.94 (dd, *J* = 8.5, 1.6 Hz,1H), 7.70 (ddd, *J* = 8.4, 6.9, 1.7 Hz, 1H), 7.70 (ddd, *J* = 8.4, 6.9, 1.6 Hz, 1H), 2.28 (tt, *J* = 8.1, 4.8 Hz, 1H), 1.30-1.26 (m, 2H), 1.20-1.14 (m, 2H) ppm.

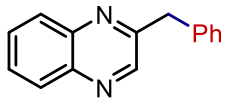

Phenylacetyl chloride was distilled under high vac at 95 °C prior to use. Following Reaction Procedure D. Quinoxaline (0.200 mmol, 26 mg, 1 equiv) was weighed into a 1dram vial equipped with a stirbar. To this was added ethyl isonicotinate *N*-oxide (66.8 mg, 2 equiv), 2-

methoxynaphthalene (3.16 mg, 0.1 equiv), and $CaCl_2$ (22.2 mg, 1 equiv). The solids were evacuated and backfilled 5 times with nitrogen. Then 250 μL of $MeNO_2$ was added, followed by phenylacetyl chloride (106 μL, 4 equiv). Note: Upon the addition of phenylacetyl chloride the reaction underwent a rapid change in color from clear to yellow (consistent with EDA complex appearance) to red that became more intense with time. The vial was then sealed with electrical tape and parafilm, placed in front of a 456 nm Kessil lamp and irradiated for 12 hours ambient temperature. At the conclusion of the reaction period, the reaction mixture was a dark red in color. The reaction mixture was taken up into 9 mL of water and extracted with 3 x 10 mL of DCM. The combined organic extracts were washed once with sodium bicarbonate (10 mL) and once with saturated brine solution (10 mL). The organic layer was then dried over sodium sulfate. A biotage column was run on the crude reaction mixture and yielded a mixture of benzylated quinoxailine, mono-benzylated ethyl isonicotinate, and bis-benzylated ethyl isonicotinate. The mixture of benzylated products was subjected to basic saponification. The mixture was taken up in 1 mL of THF, and 1 mL of 6M KOH was added to create a biphasic mixture. The mixture was stirred vigorously (1000 rpm) and heated to 70 °C for 5 hours. Upon completion of the reaction, the TLC plate showed 1 major UV active spot (R_f ~0.5 in 9:1 H:EA). Purification on the biotage (0% to 20% EA) provided 2-benzylquinoxaline as the major product (6 mg). The isolation and characterization of these compounds has been previously reported.

^{1}H NMR (400 MHz, $CDCl_3$) = δ 8.65 (s, 1H), 8.05-7.96 (m, 2H), 7.73-7.62 (m, 2H), 7.28-7.21 (m, 3H), 7.21-7.14 (m, 2H), 4.32 (s, 2H) ppm.

^{13}C NMR (126 MHz, $CDCl_3$) = δ 155.8, 146.1, 142.0, 141.3, 137.9, 130.3, 129.5, 129.31, 129.27, 129.1, 129.0, 127.1, 43.1 ppm.

3.5 References

1. Turro, N. J.; Ramamurthy, V.; Scaiano, J. C. Supramolecular Organic Photochemistry: The Control of Organic Photochemistry and Photophysics Through Intermolecular Interactions. *Modern Molecular Photochemistry of Organic Molecules*; University Science Books, 2010.

2. Hilinski, E. F.; Masnovi, J. M.; Amatore, C.; Kochi, J. K.; Rentzepis, P. M. Charge-Transfer Excitation of Electron DonorAcceptor Complexes. Direct Observation of Ion Pairs by Time Resolved (Picosecond) Spectroscopy. *J. Am. Chem. Soc.* **1983,** *105,* 6167−6168.

3. Lee, K. Y.; Kochi, J. K. Charge-Transfer Structures of Aromatic EDA Complexes with N-Heteroatom-Substituted Pyridinium Cations. *J. Chem. Soc., Perkin Trans. 2* **1992,** 1011−1017.

4. Crisenza, G. E. M.; Mazzarella, D.; Melchiorre, P. Synthetic Methods Driven by the Photoactivity of Electron Donor−Acceptor Complexes. *J. Am. Chem. Soc.* **2020,** *142,* 5461−5476.

5. Liu, B.; Lim, C.-H.; Miyake, G. M. Visible-Light-Promoted C−S Cross-Coupling via Intermolecular Charge Transfer. *J. Am. Chem. Soc.* **2017,** *139,* 13616−13619.

6. Börgel, J.; Tanwar, L.; Berger, F.; Ritter, T. Late-Stage Aromatic C−H Oxygenation. *J. Am. Chem. Soc.* **2018,** *140,* 16026−16031.

7. Yang, M.; Cao, T.; Xu, T.; Liao, S. Visible-Light-Induced Deaminative Thioesterification of Amino Acid Derived Katritzky Salts via Electron Donor-Acceptor Complex Formation. *Org. Lett.* **2019,** *21,* 8673−8678.

8. Lübbesmeyer, M.; Mackay, E. G.; Raycroft, M. A. R.; Elfert, J.; Pratt, D. A.; Studer, A. Base-Promoted C−C Bond Activation Enables Radical Allylation with Homoallylic Alcohols. *J. Am. Chem. Soc.* **2020,** *142,* 2609−2616.

9. Bockman, T. M.; Lee, K. Y.; Kochi, J. K. Time-Resolved Spectroscopy and Charge-Transfer Photochemistry of Aromatic EDA Complexes with X-Pyridinium Cations. *J. Chem. Soc., Perkin Trans. 2* **1992,** 1581−1594.

10. Kim, E. K.; Bockman, T. M.; Kochi, J. K. Electron Transfer Mechanism for Aromatic Nitration via the Photoactivation of EDA (Electron Donor Acceptor) Complexes. Direct Relationship to Electrophilic Aromatic Substitution. *J. Am. Chem. Soc.* **1993,** *115,* 3091−3104.

11. Arceo, E.; Jurberg, I. D.; Álvarez-Fernandez, A.; Melchiorre, P. Photochemical Activity of a Key Donor−Acceptor Complex Can Drive Stereoselective Catalytic α-Alkylation of Aldehydes. *Nat. Chem.* **2013,** *5,* 750−756.

12. Wozniak,́ Ł.; Murphy, J. J.; Melchiorre, P. Photoorganocatalytic Enantioselective Perfluoroalkylation of β-Ketoesters. *J. Am. Chem. Soc.* **2015,** *137,* 5678−5681.

13. Bahamonde, A.; Melchiorre, P. Mechanism of the Stereoselective α-Alkylation of Aldehydes Driven by the Photochemical Activity of Enamines. *J. Am. Chem. Soc.* **2016,** *138,* 8019−8030.

14. Cao, Z.-Y.; Ghosh, T.; Melchiorre, P. Enantioselective Radical Conjugate Additions Driven by a Photoactive Intramolecular Iminium-Ion-Based EDA Complex. *Nat. Commun.* **2018,** *9,* 3274.

15. Morack, T.; Mück-Lichtenfeld, C.; Gilmour, R. Bioinspired Radical Stetter Reaction: Radical Umpolung Enabled by Ion-Pair Photocatalysis. *Angew. Chem., Int. Ed.* **2019,** *58,* 1208−1212.

16. Fu, M.-C.; Shang, R.; Zhao, B.; Wang, B.; Fu, Y. Photocatalytic Decarboxylative Alkylations Mediated by Triphenylphosphine and Sodium Iodide. *Science* **2019,** *363,* 1429–1434.

17. Wang, Y.-T.; Fu, M.-C.; Zhao, B.; Shang, R.; Fu, Y. Photocatalytic decarboxylative alkenylation of α-amino and α-hydroxy acid-derived redox active esters by NaI/PPh3 catalysis. *Chem. Commun.* **2020,** *56,* 2495−2498.

18. Fu, M.-C.; Wang, J. X.; Shang, R. Triphenylphosphine-Catalyzed Alkylative Iododecarboxylation with Lithium Iodide under Visible Light. *Org. Lett.* **2020,** *22,* 8572–8577.

19. Bosque, I.; Bach, T. 3-Acetoxyquinuclidine as Catalyst in Electron Donor−Acceptor Complex-Mediated Reactions Triggered by Visible Light. *ACS Catal.* **2019,** *9,* 9103−9109.

20. Beatty, J. W.; Douglas, J. J.; Cole, K. P.; Stephenson, C. R. J. A Scalable and Operationally Simple Radical Trifluoromethylation. *Nat. Commun.* **2015,** *6,* 7919.

21. Beatty, J. W.; Douglas, J. J.; Miller, R.; McAtee, R. C.; Cole, K. P.; Stephenson, C. R. J. Photochemical Perfluoroalkylation with Pyridine *N*-Oxides: Mechanistic Insights and Performance on a Kilogram Scale. *Chem* **2016,** *1,* 456−472.

22. Nappi, M.; Bergonzini, G.; Melchiorre, P. Metal-Free Photochemical Aromatic Perfluoroalkylation of α-Cyano Arylacetates. *Angew. Chem., Int. Ed*. **2014,** *53,* 4921−4925.

23. Wang, Y.; Wang, J.; Li, G.-X.; He, G.; Chen, G. Halogen-Bond-Promoted Photoactivation of Perfluoroalkyl Iodides: A Photochemical Protocol for Perfluoroalkylation Reactions. *Org. Lett.* **2017,** *19,* 1442−1445.

24. Li, Y.; Rao, M.; Fan, Z.; Nian, B.; Yuan, Y.; Cheng, J. A visible-light-irradiated electron donor-acceptor complex-promoted radical reaction system for the CH perfluoroalkylation of quinolin-4-ols. *Tetrahedron Lett.* **2019,** *60,* 151046.

25. Liu, Y.; Chen, X. L.; Sun, K.; Li, X.-Y.; Zeng, F.-L.; Liu, X.-C.; Qu, L.-B.; Zhao, Y.-F.; Yu, B. Visible-Light Induced Radical Perfluoroalkylation/Cyclization Strategy To Access 2 Perfluoroalkylbenzothiazoles/Benzoselenazoles by EDA Complex. *Org. Lett.* **2019,** *21,* 4019−4024.

26. Guo, Q.; Wang, M.; Liu, H.; Wang, R.; Xu, Z. Visible-Light-Promoted Dearomative Fluoroalkylation of β-Naphthols through Intermolecular Charge Transfer. *Angew. Chem., Int. Ed.* **2018,** *57,* 4747−4751.

27. Fukuzumi, S.; Wong, C. L.; Kochi, J. K. Unified View of Marcus Electron Transfer and Mulliken Charge Transfer Theories in Organometallic Chemistry. Steric Effects in Alkylmetals as

Quantitative Probes for Outer-Sphere and Inner-Sphere Mechanisms. *J. Am. Chem. Soc.* **1980,** *102,* 2928−2939.

28. Nagakura, S. Mulliken's Charge-Transfer Theory and its Application to Chemical Reactions. *Mol. Cryst. Liq. Cryst.* **1985,** *126,* 9−18.

29. Renny, J. S.; Tomasevich, L. L.; Tallmadge, E. H.; Collum, D. B. Method of Continuous Variations: Applications of Job Plots to the Study of Molecular Associations in Organometallic Chemistry. *Angew. Chem., Int. Ed.* **2013,** *52,* 11998−12013.

30. Nizhnik, Y. P.; Lu, J.; Rosokha, S. V.; Kochi, J. K. Lewis Acid Effects on Donor−Acceptor Associations and Redox Reactions: Ternary Complexes of Heteroaromatic *N*-oxides with Boron Trifluoride and Organic Donors. *New J. Chem.* **2009,** *33,* 2317−2325.

31. For a review of EDA complex promoted perfluoroalkylation see: Postigo, A. Electron Donor-Acceptor Complexes in Perfluoroalkylation Reactions. *Eur. J. Org. Chem.* **2018,** 6391−6404.

32. Douglas, J.J.; Albright, H.; Sevrin, M.J.; Cole, K.P.; Stephenson, C.R.J. A Visible-Light-Mediated Radical Smiles Rearrangement and its Application to the Synthesis of a Difluoro-Substituted Spirocyclic ORL-1 Antagonist. *Angew. Chem. Int. Ed.* **2015,** *54,* 14898-14902.

33. Alpers, D.; Cole, K. P.; Stephenson, C. R. J. Visible Light Mediated Aryl Migration by Homolytic C−N Cleavage of Aryl Amines. *Angew. Chem. Int. Ed.* **2018,** *57,* 12167-2170.

34. Monos, T. M.; McAtee, R. C.; Stephenson, C. R. J. Arylsulfonylacetamides as bifunctional reagents for alkene aminoarylation. *Science* **2018,** *361,* 1369–1373.

35. Li, L.; Gu, Q.-S.; Wang, N.; Song, P.; Li, Z.-L.; Li, X.-H.; Wang, F.-L.; Liu, X.-L. 1,2-Difunctionalization-type (hetero)arylation of unactivated alkenes triggered by radical addition/remote (hetero)aryl migration. *Chem. Commun.* **2017,** *53,* 4038-4041.

36. Gerleve, C.; Studer, A. Transition-Metal-Free Oxidative Cross-Coupling of Tetraarylborates to Biaryls Using Organic Oxidants. *Angew. Chem. Int. Ed.* **2020,** *59,* 15468-15473.

Chapter 4 **Designed Dissociative Excited State Enables Photoinduced Radical Generation**

*Portions of this chapter have been published in E. J. McClain, A. K. Wortman, C. R. J. Stephenson, Photoinduced Radical Generation Enabled by the Strategic Design of a Dissociative Excited State. *J. Am. Chem. Soc.* **2021,** Submitted.

4.1 Photochemistry of Heteroaromatic *N*-oxides

The photochemistry of heteroaromatic *N*-oxides has been a point of interest for photochemical studies since the early 1960s and provides a wealth of complex reactivity promoted by near UV/visible light.[1,2] Early studies of the photochemical reactivity of quinoline *N*-oxide by Buchardt, among others, demonstrated that photolysis of quinoline *N*-oxides in aqueous media led to complex mixtures of 2-quinolones, benzo[1,3]oxazipines, and 3-acylindole rearrangement products.[3] From these early studies it was determined that the rearrangement products arose from a fast reaction on the singlet surface to generate a highly strained oxaziridine intermediate, which proceed to form the observed products through thermal ring opening/contraction reactions.[4] Subsequent studies by Hata and coworkers revealed that heteroaromatic *N*-oxide in the presence of boron trifluoride underwent an efficient deoxygenation upon irradiation.[5] It was proposed that the deoxygenation reaction arose from the excited triplet state of the *N*-oxide. Informed by these reports, several groups have studied the photochemical deoxygenation of heteroaromatic *N*-oxides, demonstrating that suitable oxygen accepting reagents led to efficient deoxygenation upon irradiation.[6-8] In 2001, Tokumura and Masushita spectroscopically studied the efficient deoxygenation of 6-cyanophenantridine N-oxide in ethanol in the presence of a triplet sensitizer. In this study, Tokumura and Masushita experimentally probed the mechanistic proposal that

deoxygenation arose from the triplet excited state. by employing the selective excitation of known triplet sensitizer proflavine at 460 nm, Tokumura and Masushita were able to spectroscopically observe conversion to the deoxygenation product, 6-cyanophenanthridine.

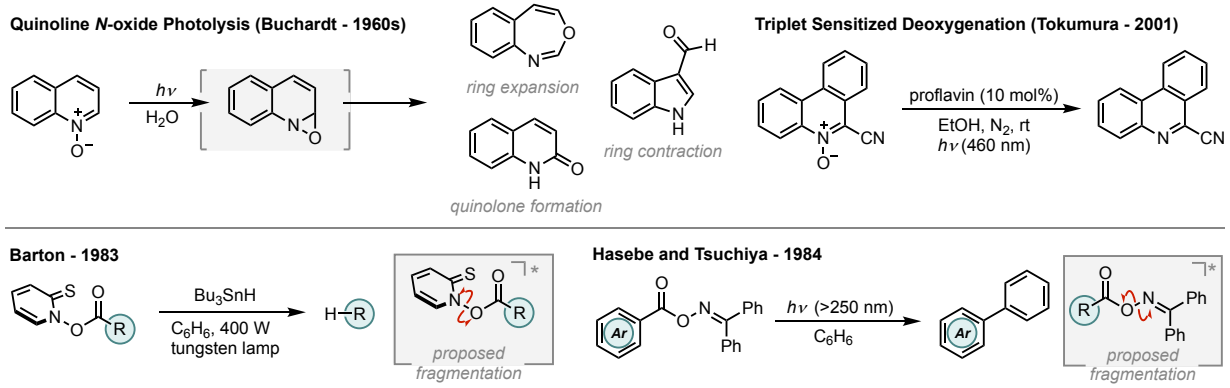

Figure 27. Deoxygenation of Heteroaromatic N-oxides, background.

Although the photochemical reactivity of heteroaromatic *N*-oxides has been studied since the early 1960s, the excited state deoxygenation has seldom been leveraged to facilitate radical generation. An early study from Hasebe and Tsuchiya demonstrated that benzophenone oxime esters could be efficiently employed for decarboxylative radical generation upon irradiation with UV light (>250 nm).[9] In analogy to heteroaromatic *N*-oxides, the benzophenone oxime esters were suggested to undergo efficient N–O bond homolysis from the triplet excited state, leading to efficient radical generation. Pioneering studies by Sir Derek Barton and coworkers demonstrated that thiohydroxamate esters underwent efficient radical generation upon irradiation with 400 W tungsten lamp.[10] The efficient photochemical radical generation could be leveraged for Hunsdiecker reaction, radical reduction, and rearrangement to pyridyl sulfide products.[11,12]

Inspired by the studies of Barton, Hasebe and Tsuchiya, and informed by early studies of photochemical reactivity of heteroaromatic *N*-oxides; we sought to design a photolabile activator based on the quinoline *N*-oxide core structure that could be leveraged for efficient decarboxylative radical generation under visible light irradiation. Importantly, the designed activator would be

derived from simple, easily obtained heteroaromatic *N*-oxide core structure and electrophilic carboxylic acid equivalents. Providing access to a broad array of radical precursors.

4.2 Results and Discussion

At the outset of our study, we established several requirements to be satisfied by potential photocleavable auxiliaries (Figure 2A): 1) the pyridine *N*-oxide core structure needed to be preserved, 2) the heteroaromatic core would need to have blocking substituents at the sites of alkylation to slow deleterious functionalization of the ester (*i.e.* 2–, 4–, and 6–substituted pyridine *N*-oxide derivatives), 3) the heteroaromatic *N*-oxide core would need to maintain its nucleophilic character, 4) the heteroaromatic backbone would need to deliver a sterically accessible *N*-oxide functionality. Additionally, it was recognized that pyridine *N*-oxide derivatives bearing alkyl substituents with benzylic C–H bonds were not suitable photoactive esters, as a deleterious Boekelheide reaction occurred upon acylation of the *N*-oxide functionality. Ultimately, 2,4,6-triphenyl pyridine *N*-oxide (TPPNO), methyl 2-phenylquinoline-4-carboxylate *N*-oxide (PQCNO), and methyl acridine-9-carboxylate *N*-oxide (ACNO) were identified as potential photoactive esters that met all aforementioned requirements.

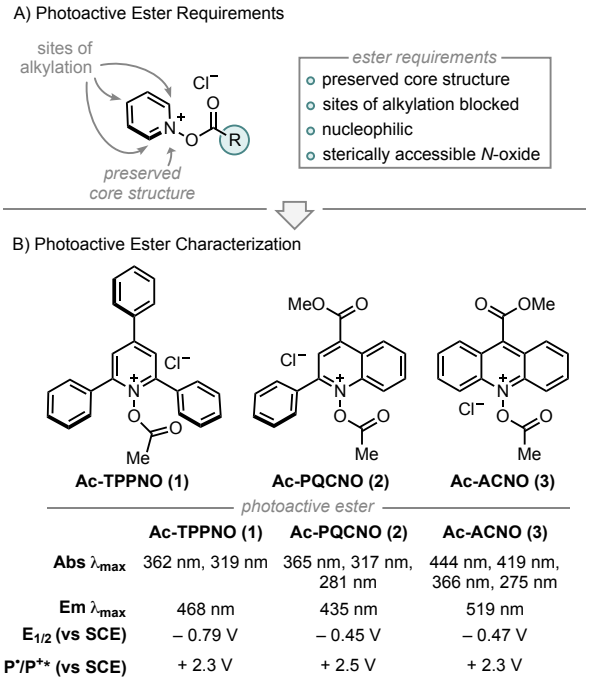

	Ac-TPPNO (1)	Ac-PQCNO (2)	Ac-ACNO (3)
Abs λ_{max}	362 nm, 319 nm	365 nm, 317 nm, 281 nm	444 nm, 419 nm, 366 nm, 275 nm
Em λ_{max}	468 nm	435 nm	519 nm
$E_{1/2}$ (vs SCE)	– 0.79 V	– 0.45 V	– 0.47 V
P^*/P^{+*} (vs SCE)	+ 2.3 V	+ 2.5 V	+ 2.3 V

Figure 28. A) Overview of photoactive ester design principles. B) Characterization of Ac-TPPNO, Ac-PQCNO, and Ac-ACNO.

Initial investigations focused on the photophysical characterization of the three heteroaromatic *N*-oxides (Figure 2B). UV/vis spectroscopy in acetonitrile revealed TPPNO to have two maximum absorbances at 319 nm and 365 nm, with the latter absorbance tailing off beyond 400 nm. PQCNO and ACNO also displayed a strong absorbance feature at 365 nm, however, for ACNO two additional lower energy absorbance features at 418 nm and 444 nm were observed. Addition of acetyl chloride to TPPNO and PQCNO resulted in an increase of intensity for the absorbance features, with no apparent shift in the absorbance maxima. Acylation of the ACNO auxiliary with acetyl chloride caused the maximum at 274 nm to diverge into two distinct sharp absorbance features with maxima at 264 nm and 275 nm. Additionally, the absorbance feature at 364 nm both increased in intensity and became more structured upon acylation, revealing an apparent shoulder at 352 nm. Measurement of the fluorescence spectra for the heteroaromatic *N*-oxides (excitation at 361 nm) revealed that Ac-TPPNO, Ac-PQCNO, and Ac-ACNO to have emission maxima at 435 nm, 468 nm and 519 nm, respectively (Figure 3A). In the absence of an

acyl equivalent, no emission was observed for the heteroaromatic *N*-oxides. This finding is consistent with previous reports that pyridine *N*-oxides and quinoline *N*-oxides possess non-emissive excited states under basic conditions due to a propensity to undergo a fast rearrangement on the singlet surface.[3]

Investigation of the photoinduced N–O bond cleavage of Ac-PQCNO revealed that upon successive fluorescence scans (excitation at 335 nm), Ac-PQCNO is observed to decompose steadily with the concomitant appearance of the fluorescence signal corresponding to the generation of deoxygenated quinoline (Figure 3B). Interrogation of the decomposition by UV/vis spectroscopy revealed that after 60 s of irradiation of Ac-PQCNO with a 427 nm Kessil lamp, a decrease in the absorbance feature at 365 nm was observed. Extending irradiation time out to 30 mins, significant degradation of the Ac-PQCNO was observed.

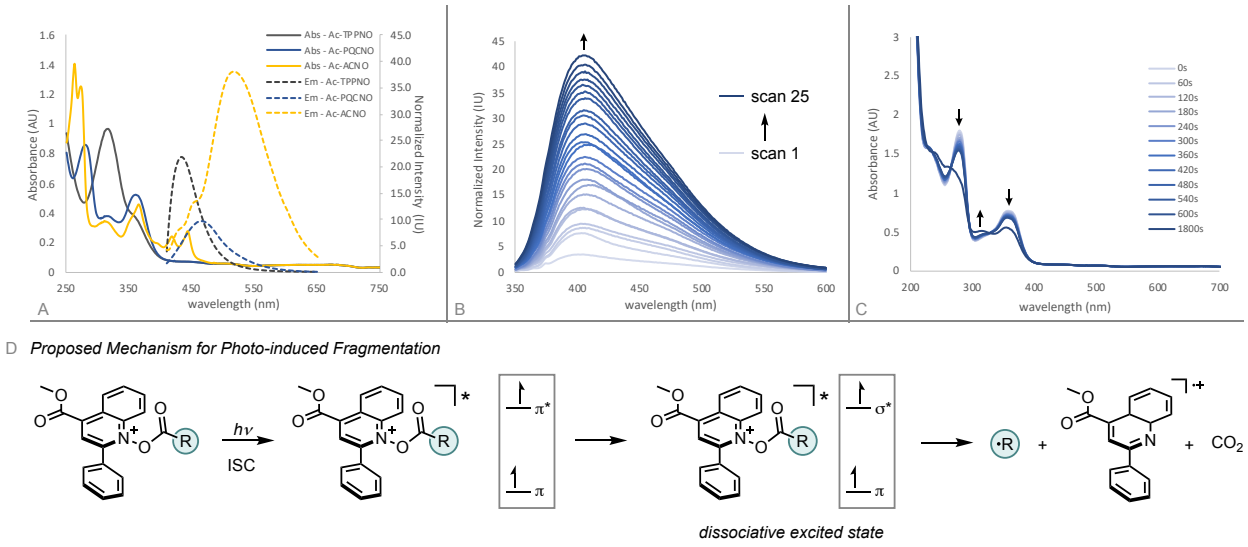

Figure 29. A) Absorbance and Emission spectra for Ac-TPPNO, Ac-PQCNO, and Ac-ACNO. Emission recorded upon irradiation at 361 nm. B) Fluorescence spectra of Ac-PQCNO monitored over 25 successive scans (excitation 335 nm). C) Decomposition of Ac-PQCNO upon irradiation by a 427 nm Kessil lamp, monitored by UV/vis. D) Proposed mechanism for photochemical decomposition of Ac-PQCNO.

Together, the photophysical characterization shows the photoactive esters possess conserved absorption features at 365 nm. Consistent with previous studies on quinoline *N*-oxide photochemistry, the absorption feature at 365 nm is thought to be π,π* in character and responsible

for the observed deoxygenation reactivity.[5] The deoxygenation of the aromatic *N*-oxides is hypothesized to arise from crossing over of the π,π* excited state to a dissociative π, σ* state.[13]

Interrogation of the thermal reactivity of Ac-PQCNO revealed there was no deoxygenation of the heteroaromatic *N*-oxide after heating to 90 °C for 3 hours. This demonstrates that the remarkable reactivity of Ac-PQCNO is due to dissociation of the N–O bond from a low energy photoexcited state.

Electrochemical analysis of the heteroaromatic *N*-oxide photoactive eaters using cyclic voltammetry in acetonitrile revealed the Ac-TPPNO, Ac-PQCNO, and Ac-ACNO to have a low energy reduction waves, with measured $E_{1/2}$ of –0.79 V vs SCE, – 0.45 V vs SCE, and –0.47 V vs SCE. Applying information gathered from absorbance and emission spectroscopy, as well as the electrochemical data, the standard potential for oxidation of Ac-TPPNO, Ac-PQCNO and Ac-ACNO in the excited state was estimated to be +2.30 V [$E^{\circ}(T^{+}*/T\bullet)$], +2.57 V [$E^{\circ}(P^{+}*/P\bullet)$], and +2.32 V [$E^{\circ}(A^{+}*/A\bullet)$] vs SCE according to the Rehm-Weller approximation (Figure 2B).[14]

Due to the mild photolytic conditions for decarboxylative radical generation and characteristics as excited state oxidants, we sought assess the reactivity of the photocleavable esters towards the development of an intermolecular Minisci alkylation (Figure 4). Initial studies focused on the addition of the *tert*-butyl radical to 4-chloroquinoline in acetonitrile. Assessment of reactivity revealed TPPNO and PQCNO to perform identically under unoptimized conditions delivering 27% of the desired 2-(*tert*-butyl)-4-chloroquinoline product, while ACNO produced less than 5% of the desired product. Due to the low cost of the parent quinoline and high yielding *N*-oxidation for preparation, we elected to focus our investigations on the application of PQCNO as a photocleavable auxiliary. Degassing the reaction resulted in a substantial increase in yield,

providing 90% isolated yield of the desired product. Further investigation of the solvents and additives did not result in increased reactivity.

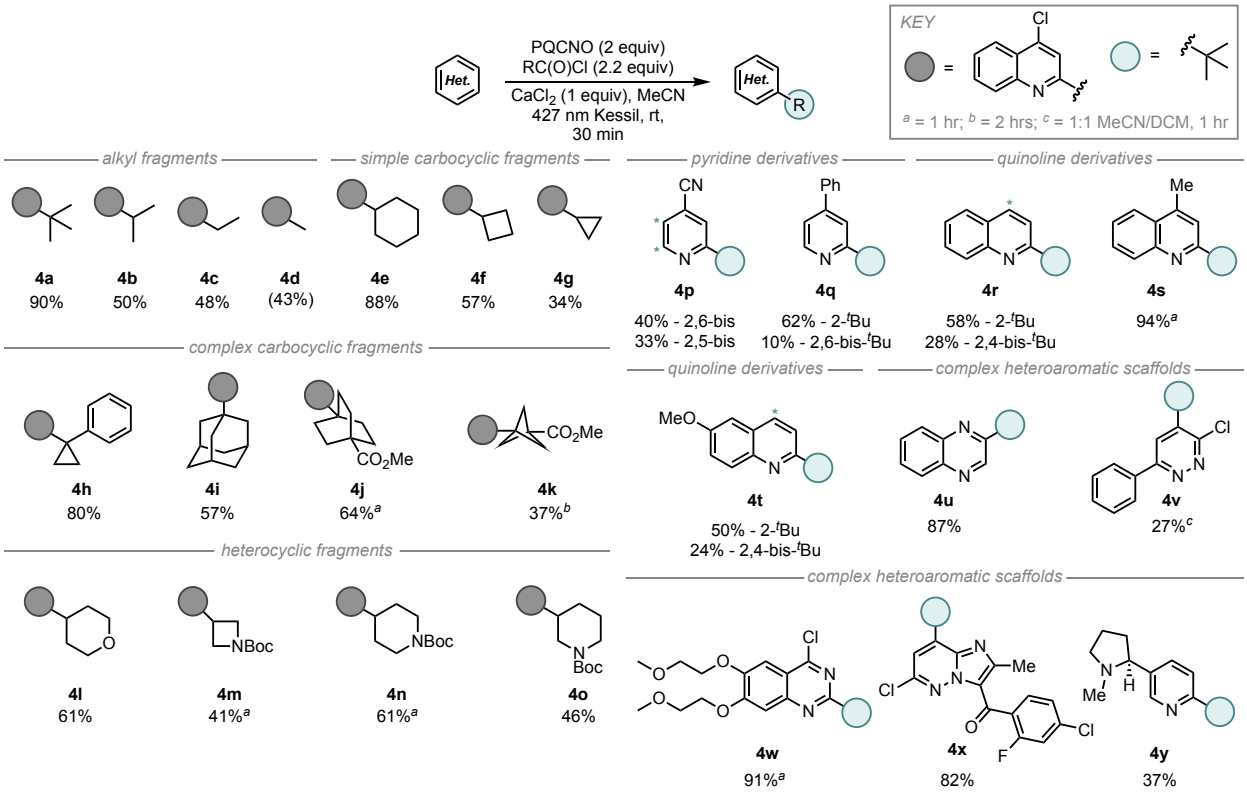

Figure 30. Scope of intermolecular Minisci alkylation. Isolated yields unless otherwise noted. [b]Reaction run for 2 hours. [c] Reaction run for 1 hour with a 1:1 mixture of MeCN to DCM as solvent. ()-NMR yield with methyl tert-butylether as internal standard.

Assessment of the scope for the intermolecular Minisci alkylation revealed the *tert*-butyl radical addition was the most efficient of the simple alkyl fragments (90%, 4a), followed by isopropyl addition (50%, 4b), ethyl addition (48%, 4c), and finally methyl addition (43%, 4d) (Figure 4). Simple carbocyclic radical fragments such as cyclohexyl (4e), cyclobutyl (4f), and cyclopropyl (4g) provided the corresponding alkylation products in 88%, 57%, and 34% yield, respectively. Interestingly, Minisci alkylation products from more complex carbocyclic radical fragments were also accessible under developed reaction conditions as 1-phenylcyclopropyl (4h), adamantyl (4i), 4-(methoxycarbonyl)-[2.2.2]-bicycloctyl (4j), and 3-(methoxycarbonyl)-[1.1.1]-bicyclopentyl (4k) fragments gave the corresponding radical addition products in 37-80% yield.

Application of tetrahydropyran-4-carbonyl chloride (4l), N-Boc azetidine 3-carbonyl chloride (4m), N-Boc piperidine 4-carbonyl chloride (4n), and N-Boc piperidine 3-carbonyl chloride (4o) provided the desired coupling products in 41-61% yield, respectively.

Assessment of heterocycle coupling partners revealed that substituted pyridine and quinoline derivatives performed well in the Minisci alkylation, however, over-alkylation of the heteroarene was often observed (4p-4t). Notably, 4-cyanopyridine (4p) and lepidine (4s) performed well under the developed intermolecular reaction conditions; these substrates were either low yielding or inaccessible under our previously reported fragment coupling conditions.[15] Modestly complex heteroaromatic scaffolds such as quinoxaline (4u), and 3-chloro-6-phenylpyridazine (4v) also performed well under the *tert*-butylation reaction conditions. Biologically active scaffolds such as the 4-chloroquinazoline core of Erlotinib (4w) and the imidazopyrazine core structure of Gandotinib (4x) each provided the single regio-isomers of the *tert*-butyl addition product in high yield. Finally, nicotine (4y) was observed to undergo *tert*-butyl addition in 37% yield with retention of the configuration for the benzylic stereocenter.

During the exploration of the Minisci alkylation reaction, it was realized that the deoxygenated quinoline can be recovered in high yields (87% recovery). Resubjecting the recovered quinoline to oxidation conditions, PQCNO could be re-generated in 71% yield. Regenerated PQCNO was observed to show no decrease in reactivity when recycled through three consecutive reactions (Figure 28).

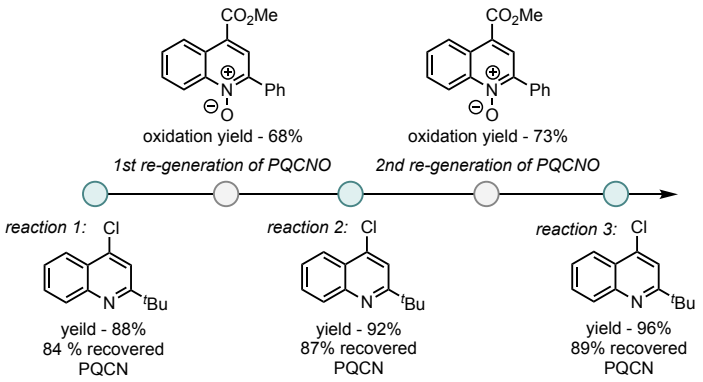

Figure 31. Recycling of methyl 2-phenylquinoline-4-carboxylate.

To probe the mechanism of the photoinduced Minisci alkylation reaction, we monitored the reaction by employing an *in-situ* LED NMR device equipped with a 430 nm LED source. Preliminary investigations demonstrated that the rate of deoxygenation of Piv-PQCNO increased in the presence of 4-chloroquinoline substrate (Figure 5A). We hypothesize that the change in rate for deoxygenation is indicative of a propagative reaction mechanism, in which electron transfer from the radical addition product (III) to acylated PQCNO (I) leads to formation of the final C–H alkylated product as well as generating a second equivalent of R• through a reductive decarboxylation of acylated PQCNO (I). Further support for the proposed propagation step was found when subjecting 2-phenylpropionyl chloride to the reaction conditions in the absence of a heteroaromatic substrate, 1-chloro-1-phenylethane was observed (See SI), demonstrating the ability of acyl PQCNO to oxidize stabilized radical intermediates.

On the basis of these findings, we propose the following mechanism (Figure 5B). Initiation of the Minisci alkylation occurs by the photoinduced decomposition of acyl-PQCNO (I) to generate an equivalent of a reactive radical intermediate (R•). Addition of R• to an equivalent of the heteroaromatic substrate provides intermediate (II). Deprotonation of (II) generates radical anion intermediate (III) that is in turn oxidized by a second equivalent of acyl-PQCNO (I),

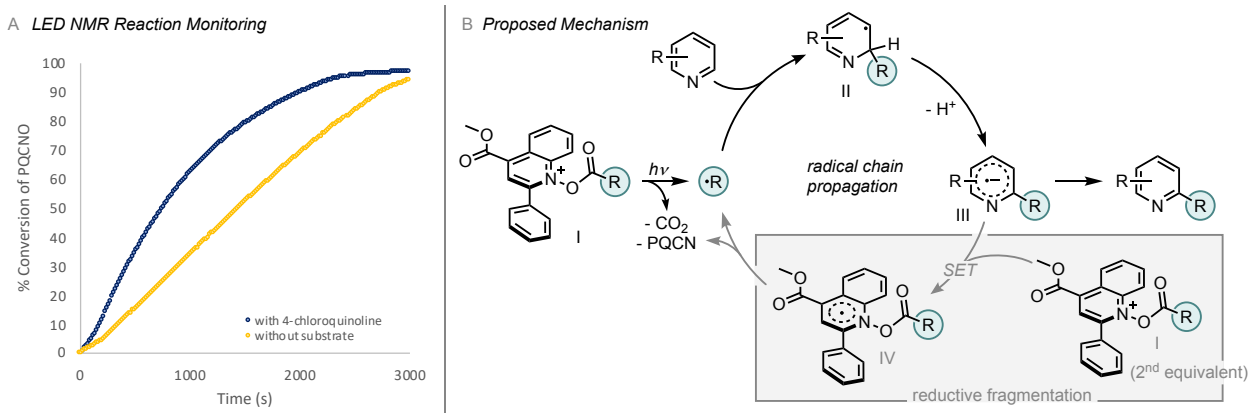

Figure 32. A) Reaction profile in the presence (blue) and absence (yellow) of substrate, monitored using 430 nm LED NMR apparatus. B) Proposed mechanism for photo-mediated Minisci reaction.

providing the desired C–H alkylated product while generating a second equivalent of R• through the decomposition of reduced acyl-PQCNO (IV), thereby propagating the reaction.

Finally, we sought to explore alternate radical based transformations that can be promoted by the PQCNO based ester (Figure 30). Lactonization of 2-phenylbenzoyl chloride was carried out, providing moderate yield for the 3,4-benzocoumarin product.[16] Employing trifluoroacetic anhydride (TFAA) as an acyl equivalent, in the presence of *tert*-butyl anisole, radical trifluoromethylation of the electron rich arene was achieved in moderate yields.[18] Further assessments of reactivity are currently on going within our laboratory.

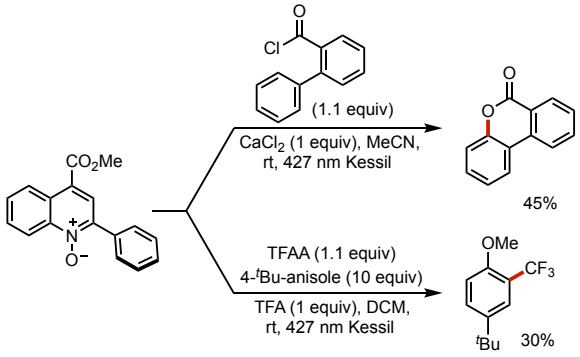

Figure 33. Alternate radical transformations enabled by PQCNO.

In conclusion, we have developed a photoactive ester based upon the quinoline *N*-oxide core which delivers a strong oxidant in its excited state. The designed photocleavable auxiliary

enabled the development of a photochemical Minisci alkylation, providing a reaction platform that leveraged both the photochemical dissociation and oxidant characteristics of the photoactive esters. Photochemical reactivity of the PQCNO auxiliary was also demonstrated to effect radical lactonization and trifluoromethylation reactions.

4.3 Outlook and Future Directions

With the successful development of the PQCNO based photocleavable ester, future studies can be directed at extending the approach to access new, challenging transformations.

Copper Cross-Coupling. Cross-coupling has become a focal point of contemporary organic methods development, providing the opportunity for regio-selective incorporation of new substituents into aromatic, drug-like scaffolds. In this regard, the development of new methods merging the photochemical reactivity of the PQCNO auxiliary with copper-based cross-coupling could provide access to selective alkyl and perfluoroalkyl cross-coupling reactivity. In this reactivity paradigm the oxidant and radical precursor properties of PQCNO based esters could be leveraged to facilitate reactivity. In addition, the development of cross-coupling method would provide a complementary approach to those developed by Sanford, MacMillan, Larionov, and others.[17-22]

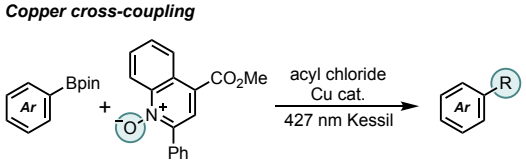

Figure 34. Copper catalyzed cross-coupling.

Allylic Oxidation. Upon photoexcitation, heteroaromatic *N*-oxides are proposed rearrange through a highly reactive oxaziridine intermediate.[2] Although a short-lived intermediate that is responsible for the generation of rearrangement products, literature reports indicate that in

the presence of suitable substrates the oxaziridine intermediate may be leveraged for oxygen transfer reactions.[5-8] In particular, Xu and coworkers reported in 1989 that aciridine *N*-oxide was observed to promote the efficient allylic C–H oxidation of cyclohexene when irradiated with visible light (>400 nm).[24] While a fascinating spectroscopic investigation of the physical organic principles for oxygen atom transfer reactivity, the potential utility of the C–H oxidation was never explored, and this reactivity was not developed into a useful synthetic protocol. Allylic oxidation promoted by the photochemical reactivity of heteroaromatic *N*-oxides should be further investigated.

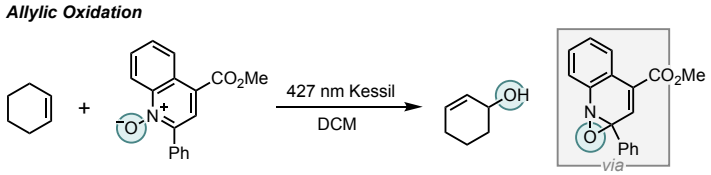

Figure 35. PQCNO enabled allylic oxidation.

Nitrogen Centered Radicals. In addition to heteroaromatic *N*-oxides, the reactivity of *N*-amino pyridinium and *N*-amino pyridinium ylides have been thoroughly studied.[25-27] *N*-amino pyridinium reagents have been leveraged as N-centered radical precursors.[28] In conjunction with photoredox catalysis, it has been demonstrated that single electron reduction of *N*-amino pyridinium reagents results in an N–N bond cleavage, giving rise to a reactive N-centered radical that can be engaged in downstream reactivity.[28-31] In this vein, preparation of the N-amino quinolinium (PQCNN) may provide access to complementary reactivity without need for an external light harvesting catalyst to drive reactivity. Preparation of PQCNN can be achieved by subjecting the parent quinoline to electrophilic nitrogen source *O*-(mesitylsulfonyl)hydroxylamine (MSH).[32,33] Differential protection of the amine using sulfonyl chlorides and/or acyl chlorides can provide access to an array of PQCNN derivatives with varying reactivity profiles.

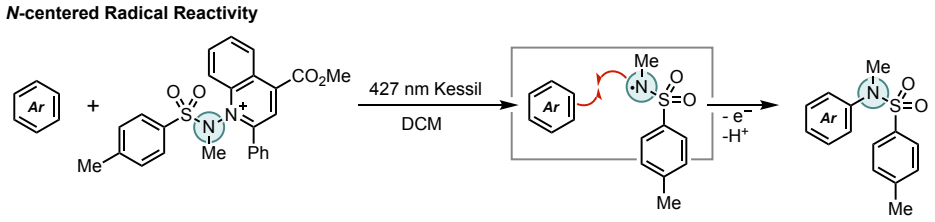

Figure 36. Arene amination enabled by PQCNN

Diaziridine Reactivity. In analogy to heteroaromatic *N*-oxides, *N*-amino pyridinium ylides are suggested to undergo a fast rearrangement on the singlet surface to diaziridine intermediated upon photoexcitation.[26,27] Studies from the 1960s indicate that the diaziridine intermediates generated upon irradiation may be intercepted with suitable substrates, providing access to C–H amination and aziridination products.[34] Similar to the oxidation chemistry proposed above, the development of the novel reactivity *N*-amino quinolinium ylides could provide low cost, easily handled reagents for photochemical nitrogen insertion and aziridination reactivity.

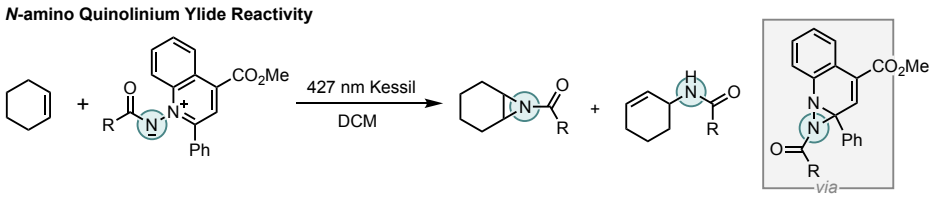

Figure 37. Proposed N-Quinolinium Ylide Reactivity

Mechanistic Studies of PQCNO Reactivity. Intimate study of the mechanistic underpinnings for photoinduced radical alkylation from pyridine *N*-oxide derivatives will provide a fruitful future direction. However, deciphering photochemical reactivity from background thermal, propagative reactions represents a significant challenge to understanding the mechanism.

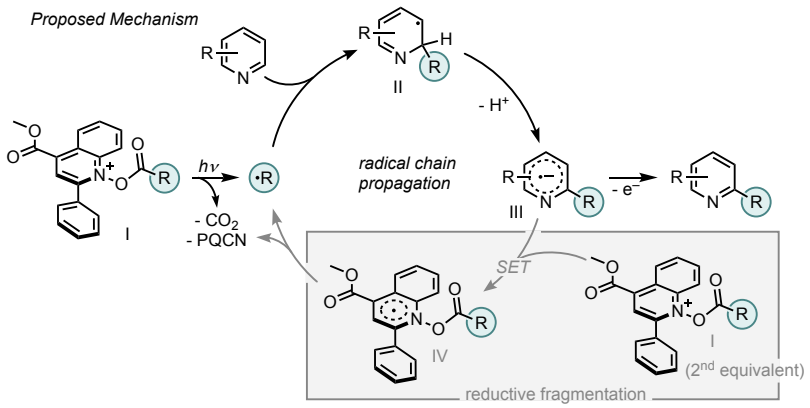

Figure 38. Proposed mechanism for photoinduced Minisci alkylation.

Initial studies of the mechanism should focus on the photochemical decomposition of the *N*-(acyloxy)pyridinium derivative. With little background alkylation (~10% with *tert*-butyl radical) and well documented unimolecular photochemical decomposition, PQCNO should serve as an ideal model system. Employing LED NMR reaction monitoring, initial rates studies can be used to determine the observed rate of N–O bond fragmentation in an excess of photon equivalents.[35,36] In analogy to mechanistic studies from Barton and coworkers, it is likely that carrying out the photochemical decomposition of PQCNO at low temperatures (≤ 0 °C) will suppress background alkylation of the auxiliary, eliminating any propagative electron transfer reactions that may skew kinetic measurements of decomposition.[37] Next, the quantum yield for N–O bond fragmentation from PQCNO can be determined, shedding light on the photon dependence of PQCNO for decarboxylative radical generation.[38] These studies can be carried out with a fluorimeter or the LED NMR reaction monitoring apparatus, but the photon flux of the light source must be determined (likely using ferrioxalate as a chemical actinometer) prior to reaction quantum yield measurements. Exploration of the excited state that leads to N–O bond fragmentation by means of transient absorption spectroscopy may provide an interesting caveat but is not necessary to provide a full kinetic analysis of the reaction. The preliminary studies of *N*-

oxide decomposition can then be extrapolated to gain a more in-depth understanding of the photoinduced Minisci alkylation reaction.

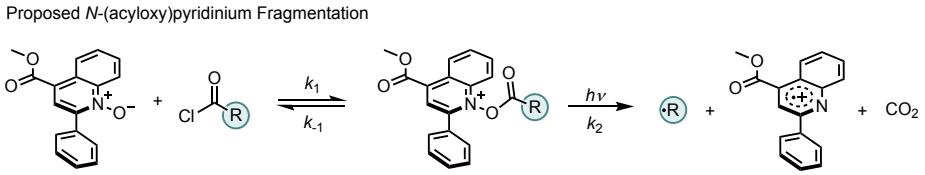

Figure 39. Photoinduced N-(acyloxy)pyridinium fragmentation

With an understanding of the kinetics for the photochemical decomposition of PQCNO, attention may be turned to understanding the mechanism for the photoinduced Minisci alkylation reaction. The looming challenging when studying the mechanism for the alkylation reaction is characterizing the chain processes that lead to the background propagative, thermal reactivity. Mechanistic studies by Minisci have determined that the addition of a carbon centered radical to the heteroarene substrate is often reversible, but the deprotonation/oxidation of the radical addition adduct is the rate limiting step for the reaction.[39,40] In the context of the pyridine *N*-oxide mediated reaction, chain carrying process likely arises from electron transfer from the deprotonated radical addition intermediate to the *N*-(acyloxy)pyridinium radical precursor, inducing a fast N–O bond fragmentation and decarboxylative radical generation.[41,42] Assessment of the thermodynamic and kinetic constraints of the chain carrying process can be studied by monitoring the decomposition of Ac-PQCNO when subjected to authentic standards of reduced radical addition adducts via NMR or UV/vis spectroscopy. Pyridinium salts form isolable reduced adducts, thus several variants may be prepared by chemical or electrochemical reduction of the corresponding pyridinium reagents (N–Me).[43,44] With an intimate understanding of the background electron transfer kinetics, a complete picture for the mechanism of the photoinduced Minisci alkylation may be constructed by study of the kinetics of the reaction via LED NMR reaction monitoring.

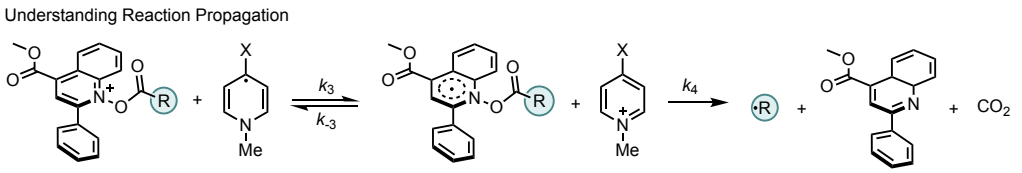

Figure 40. Study of background propagation reaction

The construction of a full kinetic profile for the photoinduced Minisci alkylation will not only help to build the understanding of current reaction outcome observations but will allow for the expansion of the scope of accessible reactivity. Study of the PQCNO model system will provide simplified reaction kinetics that can be extrapolated to the fragment coupling approach to the Minisci alkylation, which is likely more attractive reaction manifold to the pharmaceutical industry, facilitating the application of the photoinduced reaction into drug development. Additionally, the determination of the quantum yield for PQCNO decomposition can allow for PQCNO to be developed as a soluble, visible-light actinometer. This would represent a significant advance, as the development of a soluble chemical actinometer will allow for the facile determination of photon flux in flow reactors, a significant limitation of current known chemical actinometers.[45]

4.4 Experimental Procedures, Compound Characterization and Spectral Data

General Information

All chemicals were used as received unless otherwise noted. Reactions were monitored by TLC and visualized with a dual short wave/long wave UV lamp. Column flash chromatography was performed using 230-400 mesh silica gel or via automated column chromatography using Biotage Selekt or Biotage Isolera purification systems. Basic alumina was stored in an oven at 150° C until use. Preparative TLC purifications were run on silica plates of 1000 μm thickness. NMR spectra were recorded on Varian MR400, Varian Inova 500, Varian Vnmrs 600, Varian Vnmrs 500, or Varian Vnmrs 700 spectrometers. Chemical shifts for ^{1}H NMR were reported as δ, parts per million, relative to the signal of $CHCl_3$ at 7.26 ppm. Chemical shifts for ^{13}C NMR were reported as δ, parts per million, relative to the center line signal of the $CDCl_3$ triplet at 77.16 ppm. Chemical shifts for ^{19}F NMR were reported as δ, parts per million, relative to the signal of a trifluorotoluene internal standard at -63.72 ppm. The abbreviations s, br. s, d, dd, br. d, ddd, t, q, br. q, qi, m, and br. m stand for the resonance multiplicity singlet, broad singlet, doublet, doublet of doublets, broad doublet, doublet of doublet of doublets, triplet, quartet, broad quartet, quintet, multiplet and broad multiplet, respectively. IR spectra were recorded on a PerkinElmer Frontier FT-IR spectrometer with a universal ATR accessory. Mass Spectra were recorded with an Agilent 1290 Infinity II UPLC with a TOF 6230B Dual AJS Ion source, as well as at the Mass Spectrometry Facility at the Department of Chemistry of the University of Michigan in Ann Arbor, MI on an Agilent Q-TOF HPCL-MS with ESI high resolution mass spectrometer. Fluorescence measurements were performed with a Horiba Qunatamaster 8000 fluorimeter equipped with a Xe arc lamp. UV/VIS measurements were obtained on a Varian Cary-50 spectrophotometer. NMR reaction monitoring was carried out using an LED NMR ser-up that consisted of a Prizmatix High Power Microscope

LED Head (430 nm), Prizmatix Low Noise Benchtop Mic-LED Current-Controller, and Prizmatix Fiber Coupling Adaptor. Irradiation of reactions was carried out using Kessil PR-160 lamps (390 nm, 427 nm, and 456 nm). Solvents were purified on a SciMatCo solvent purification system under a constant flow of argon prior to use.

Experimental Procedures

General Procedure A: Minisci Alkylation with PQCNO

To a flame dried 1-dram vial equipped with a magnetic stirbar was weighed substrate (0.2 mmol, 1 equiv), PQCNO (112 mg, 0.4 mmol, 2 equiv), acyl chloride (if solid) (0.44 mmol, 2.2 equiv) and calcium chloride (22.2 mg, 0.2 mmol, 1 equiv). The reaction vial was then sealed with a screw cap with a teflon lined septa top. The solids were evacuated and back filled with nitrogen 5 times. To the vial was then added 0.5 mL of MeCN, followed by acyl chloride (if liquid) (0.44 mmol, 2.2 equiv). The needle was removed from the septa cap and the cap sealed with a piece of electrical tape, followed by parafilm. The reaction mixture was then affixed to the stir plate by a piece of double-sided tape at a distance of 5-7 cm from the Kessil lamp. The reaction mixtures were irradiated for 30 mins at 100% power.

At the conclusion of the reaction, the reaction was taken up into 10 mL of saturated sodium bicarbonate. The aqueous mixture was extracted with 3 x 10 mL of DCM, the combined organic extracts were then washed with 1 x 10 mL of saturated sodium chloride and dried over sodium sulfate, filtered and concentrated in vacou. The crude organic material was purified by flash chromatography. Best results were obtained when running a column with 10-20% ethyl acetate in hexanes followed by a second column using 2-5% acetone in dichloromethane.

General Procedure B: Oxidation of Heteroaromatic *N*-oxides

To a round bottom flask equipped with a magnetic stir bar was added methyl 2-phenylquinoline-4-carboxylate (1 equiv). The solid was then taken up into DCM (0.2M) and the solution was cooled to 0 °C in an ice bath. To the cold solution was added *m*-CPBA in small batches over the course of 5 mins. The reaction was then sealed with a septa, transferred to a heating mantle and heated at 50 °C for 8-15 hours. [CAUTION!] The reaction builds up pressure during the heating process, the reaction should be removed from heat and vented prior to removing the septa. The cooled reaction mixture was then taken up into 50 mL of DCM and extracted 3 x 50 mL with saturated sodium bicarbonate. The combined aqueous layers were then extracted 3 times with 50 mL portions of DCM. The combined organic extracts were washed with 50 mL of saturated sodium chloride and dried over sodium sulfate. The combined organic layers were concentrated *in vacou* to give a crude golden oil. Heteroaromatic *N*-oxides were purified by flash chromatorgraphy on silica.

General Procedure C: Preparation of Acid Chlorides

To a flame dried 100 mL round bottom flask equipped with a stir bar was added carboxylic acid (1 equiv.), and DCM (0.2 M). The flask was then equipped with a septa and a vent needle. To this was added oxalyl chloride (1.1 equiv), followed by DMF (0.1 equiv, a few drops). At this point, the reaction mixture will begin to bubble vigorously. The reaction was allowed to stir at room temperature for 30 mins to 1 hour. At the conclusion of the reaction (when bubbling ceased), the crude reaction was concentrated in vacou to a small volume, and then run through a plug of basic

alumina oxide (approx. 1 in L x 1 cm D). The organic layer was then concentrated in vacou and used without further purification. A crude 1H NMR was acquired for each sample.

UV/Vis Analysis of Aromatic *N*-oxides

To a flame dried 1-dram vial was weighed heteroaromatic *N*-oxide (0.011 mmol), and this was taken up into 3 mL of MeCN. For measurements of acylated heteroaromatic *N*-oxides, acyl chloride (1.1 equiv) was added and the mixture was shaken vigorously, the solution was a clear and colorless. A 30 μM solution of heteroaromatic *N*-oxide was prepared by diluting 25 μL to a volume of 3 mL, and the mixture was shaken vigorously to ensure mixing. The final solution was then transferred to a quartz cuvette with a 1 cm path length. Measurements were taken using a Varian Cary-50 spectrophotometer. Data was exported as a .csv file and processed using Microsoft Excel.

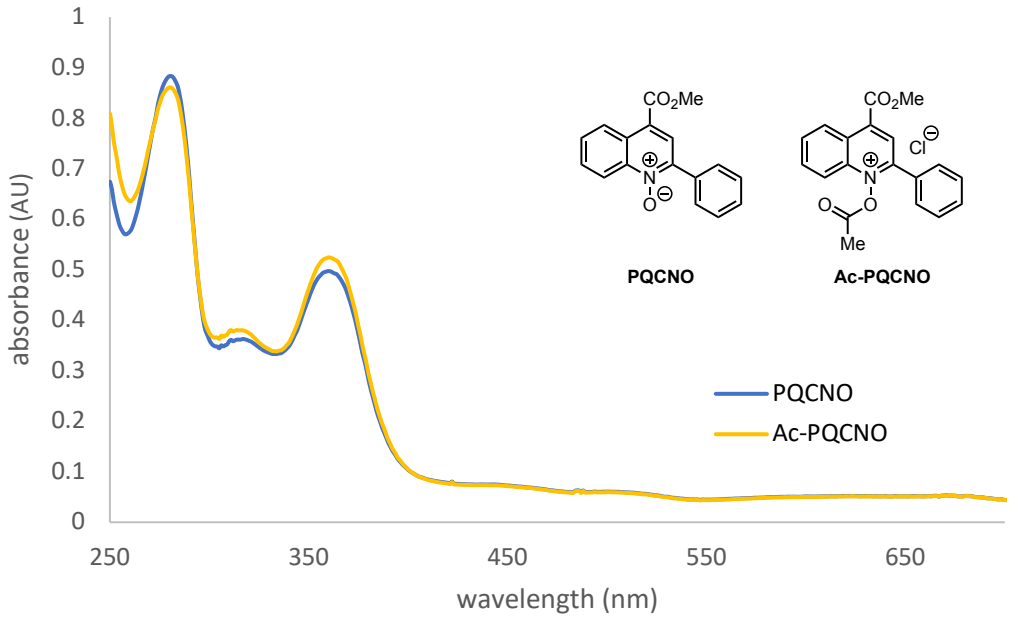

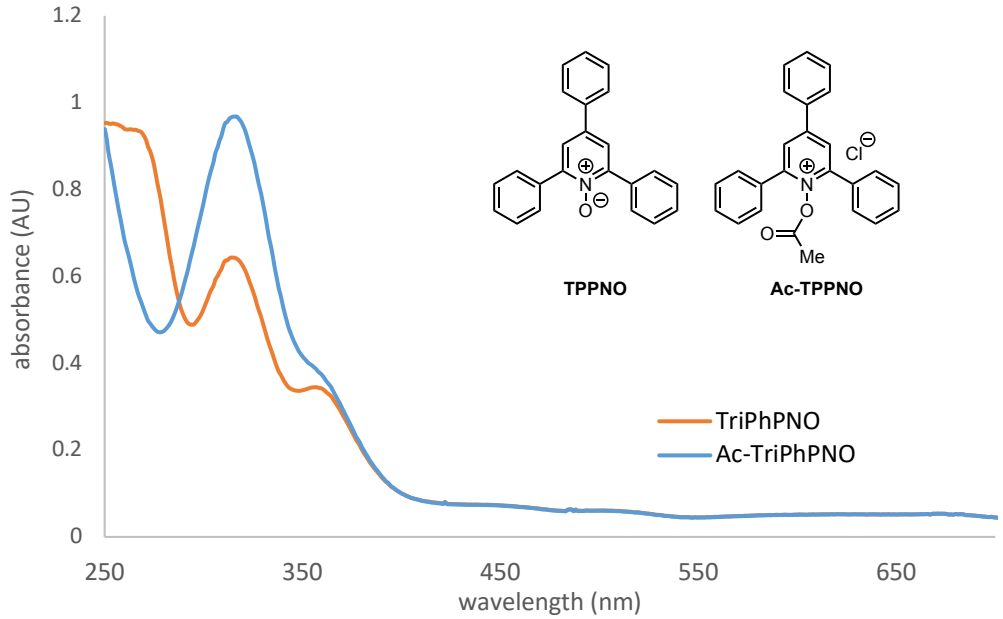

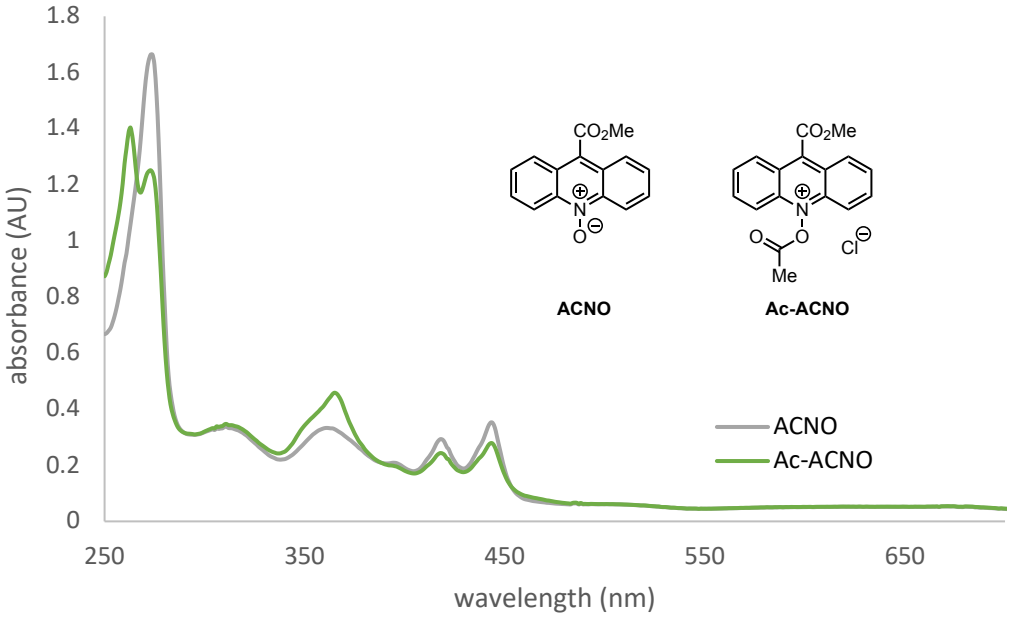

Cyclic Voltammetry of heteroaromatic *N*-oxides

Prior to cyclic voltammetry experiments, MeCN was sparged with an argon balloon for 15 mins.

To a flame dried 4-dram vial was weighed 1.2 mmol (930 mg) of tetra-butylammonium hexafluorophosphate (Bu_4NPF_6), and this was taken up in to 12 mL of dry, sparged MeCN. This solution was then used to prepare the heteroaromatic *N*-oxide samples for CV experiments.

To a flame dried 1-dram vial was weighed heteroaromatic *N*-oxide (0.3 mmol). The solid was then dissolved in 3 mL of the Bu_4NPF_6/MeCN electrolyte solution. The solution was transferred to 4-neck e-chem cell (pictured below) and equipped with a working (glassy carbon), counter (platinum), and reference (0.1 M $Ag/AgNO_3$) electrodes. The solution was sparged with nitrogen for 5 mins, then a CV experiment was run and data collected. Following collection of data for the free heteroaromatic *N*-oxide, 4.3 μL of acetyl chloride was added to the solution, and the solution was sparged for an additional 5 mins. A CV experiment was then run and data collected. Data was processed and plotted in Microsoft excel. Raw current was converted to current density.

2,4,6-triphenylpyridine *N*-oxide (TPPNO)

Experimental parameters for TPPNO: Init E (V) = 0; High E (V) = 1.6; Low E (V) = -2.5; Final E (V) = 0; Init P/N = N; Scan; Rate (V/s) = 0.1; Segment = 3; Sample Interval (V) = 0.001; Quiet Time (sec) = 2; Sensitivity (A/V) = 1e-4

Experimental parameters for Ac-TPPNO: Init E (V) = 0; High E (V) = 1.5; Low E (V) = -1.5; Final E (V) = 0; Init P/N = P; Scan Rate (V/s) = 0.1; Segment = 3; Sample Interval (V) = 0.001; Quiet Time (sec) = 2; Sensitivity (A/V) = 1e-4

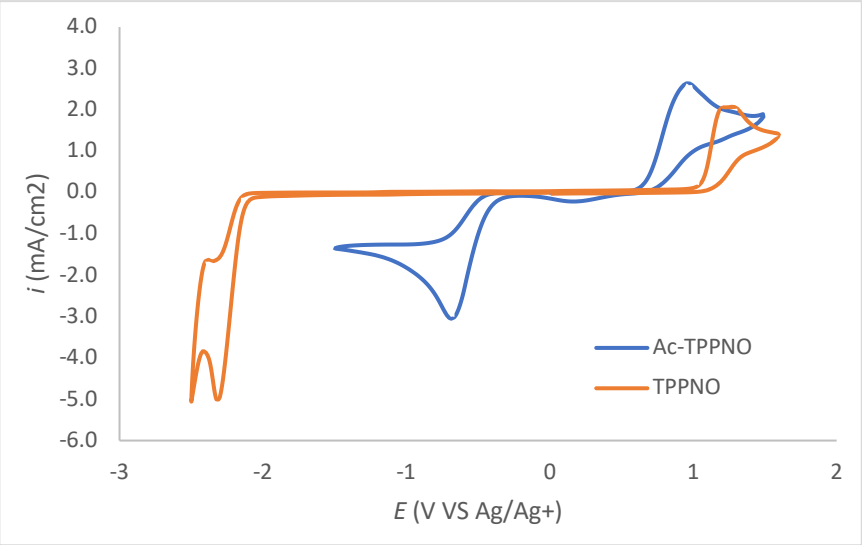

Methyl 2-phenylquinoline-4-carboxylate *N*-oxide (PQCNO)

Experimental parameters for PQCNO: Init E (V) = 0; High E (V) = 1.6; Low E (V) = -2; Init P/N = N; Scan Rate (V/s) = 0.1; Segment = 3; Sample Interval (V) = 0.001; Quiet Time (sec) = 2; Sensitivity (A/V) = 1e-4

Experimental parameters for Ac-PQCNO: Init E (V) = 0; High E (V) = 2; Low E (V) = -2; Final E (V) = 0; Init P/N = N; Scan Rate (V/s) = 0.1; Segment = 3; Sample Interval (V) = 0.001; Quiet Time (sec) = 2; Sensitivity (A/V) = 1e-4

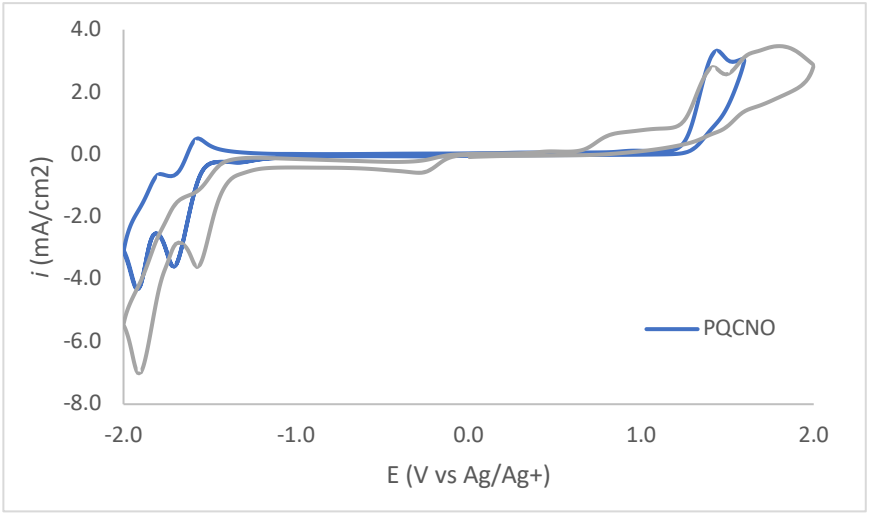

Methyl acridine-9-carboxylate *N*-oxide (ACNO)

Experimental parameters for ACNO: Init E (V) = 0; High E (V) = 1.5; Low E (V) = -1.6; Final E (V) = 0; Init P/N = N; Scan Rate (V/s) = 0.1; Segment = 3; Sample Interval (V) = 0.001; Quiet Time (sec) = 2; Sensitivity (A/V) = 1e-4

Experimental parameters for Ac-ACNO: Init E (V) = 0; High E (V) = 2; Low E (V) = -2; Final E (V) = 0; Init P/N = P; Scan Rate (V/s) = 0.1; Segment = 3; Sample Interval (V) = 0.001; Quiet Time (sec) = 2; Sensitivity (A/V) = 1e-4

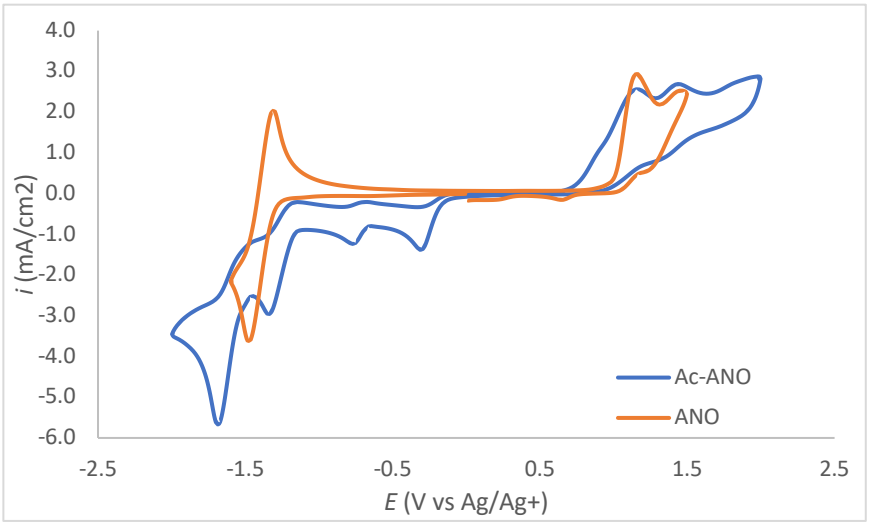

Determination of Molar Absorptivity of Ac-PQCNO

To a flame dried 1-dram vial was weighed heteroaromatic N-oxide (3 mg, 0.011 mmol), and this was taken up into 3 mL of MeCN. For measurements of acylated heteroaromatic N-oxides, acyl chloride (2 μL) was added and the mixture was shaken vigorously, the solution was a clear and colorless. Solutions of heteroaromatic N-oxide were prepared by diluting the stock solution to a volume of 3 mL, and the mixture was shaken vigorously to ensure mixing. The final solution was then transferred to a quartz cuvette with a 1 cm path length. Measurement were taken using a Varian Cary-50 spectrophotometer. Data was exported as a .csv file and processed using Microsoft Excel.

The molar absorptivity of Ac-PQCNO was determined by UV/vis spectroscopy. Measurements were taken at 10 μM, 30 μM, 50 μM, 70 μM, 100 μM, 500 μM, 1 mM, 10 mM, and 100 mM.

The following solutions were prepared by diluting the stock solution to a final volume of 3 mL.

10 μM - 8 μL of the stock solution was diluted to 3 mL

30 μM - 25 μL of the stock solution was diluted to 3 mL

50 μM - 42 μL of the stock solution was diluted to 3 mL

70 μM - 58 μL of the stock solution was diluted to 3 mL

100 μM - 83 μL of the stock solution was diluted to 3 mL

500 μM – 417 μL of the stock solution was diluted to 3 mL

1 mM – 833 μL of the stock solution was diluted to 3 mL

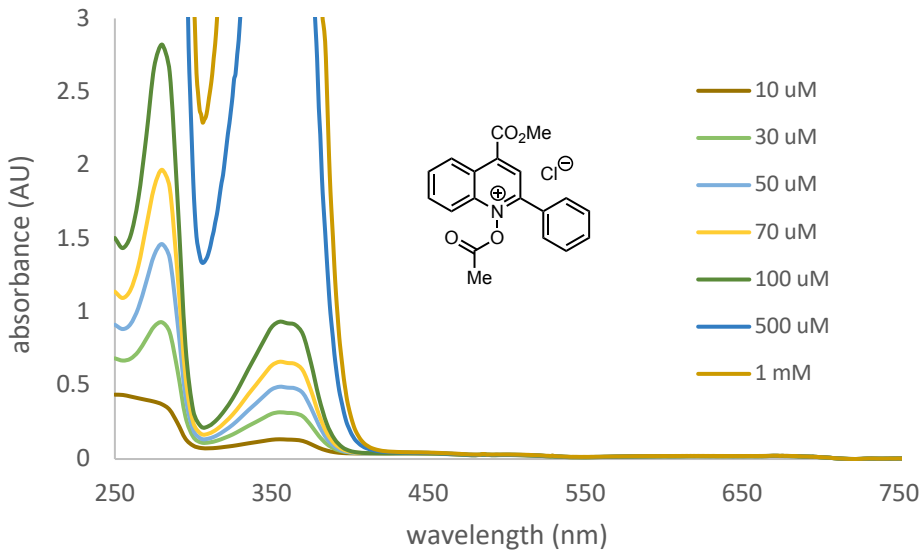

The molar absorptivity of the electronic transition at 365 nm was determined according to Beer's law:

Beer's Law: A= εlc

Where A = absorbance; e = molar absorptivity; l = path length (1 cm); c = concentration. Plotting the absorbance vs concentration(c)•path length (l) gives a line with a slope that equals the molar absorptivity of the electronic transition. (ε= A/(l•c))

Molar absorptivity of Ac-PQCNO at 365 nm was determined to be 8,543 $M^{-1}cm^{-1}$

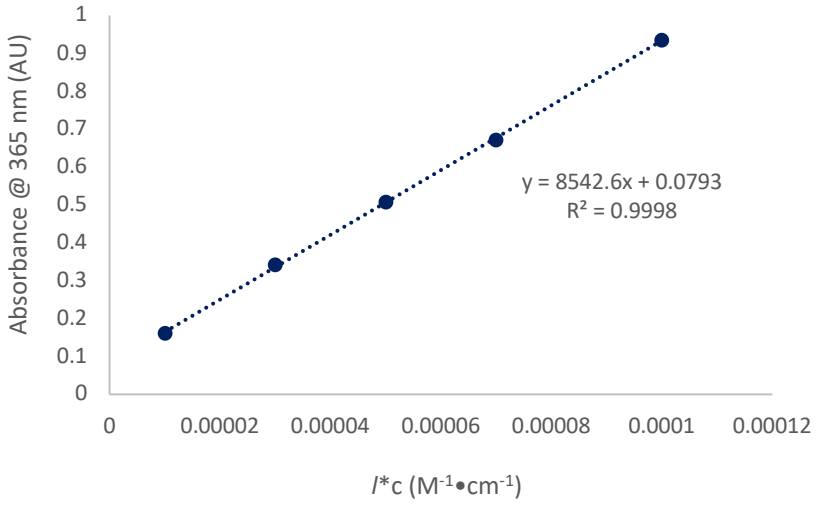

By this method, the molar absorptivity at 427 nm was determined to be 14 M^{-1} cm^{-1}.

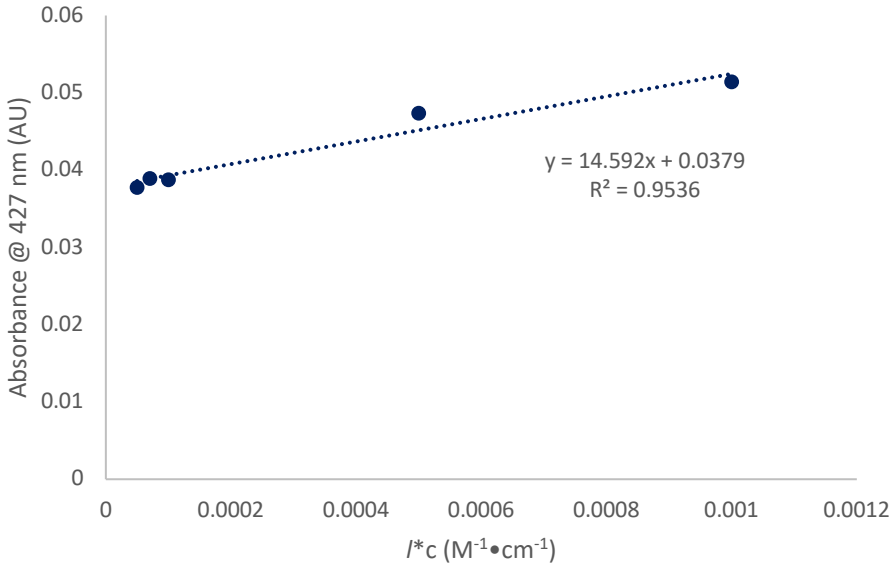

UV/vis Titration of PQCNO with Acetyl Chloride

To a flame dried 1-dram vial was weighed heteroaromatic *N*-oxide (3 mg, 0.011 mmol), and this was taken up into 3 mL of MeCN. A 30 µM solution of PQCNO was prepared by diluting 25 µL to a volume of 3 mL, and the mixture was shaken vigorously to ensure mixing. The final solution was then transferred to a quartz cuvette with a 1 cm path length. Measurements were taken using

a Varian Cary-50 spectrophotometer. Data was exported as a .csv file and processed using Microsoft Excel.

For measurements, 1 mL of acetyl chloride was added to the *N*-oxide sample, and the sample was shaken 5 times to ensure mixing. A UV/vis of the sample was then obtained. This process was repeated for additions of 1-15 µL of acetyl chloride.

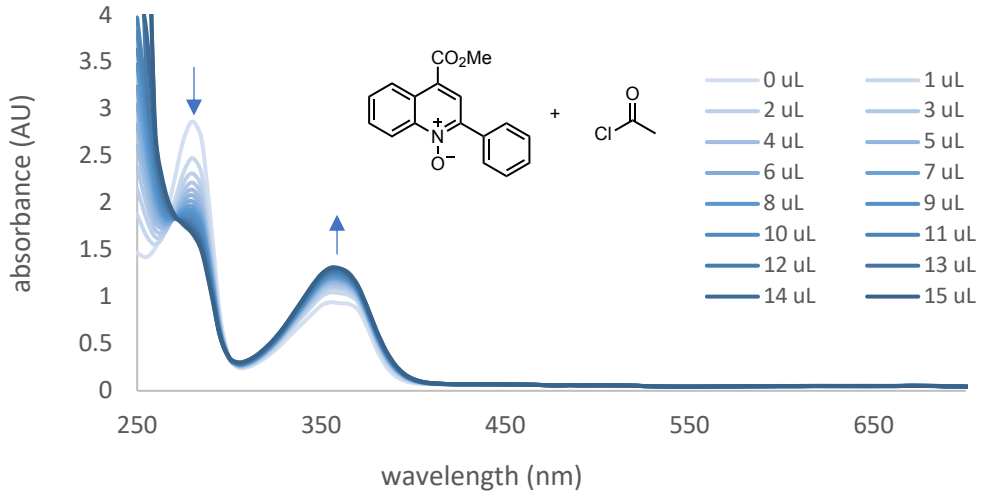

UV/Vis Monitoring of Photochemical Decomposition of Ac-PQCNO

To a flame dried 1-dram vial was weighed PQCNO (3 mg, 0.011 mmol), and this was taken up into 3 mL of MeCN. For measurements of acylated PQCNO, acyl chloride (1.1 equiv) was added and the mixture was shaken vigorously, the solution was a clear and colorless. A 100 µM solution of PQCNO was prepared by diluting 83 µL to a volume of 3 mL, and the mixture was shaken vigorously to ensure mixing. The final solution was then transferred to a quartz cuvette with a 1 cm path length. UV/vis of the AcPQCNO material was obtained, then the sample was irradiated with a 427 nm Kessil lamp from 5 cm for 60 s, and a second UV/vis was obtained. This process was repeated for 10 times. The sample was then irradiated for 20 additional minutes, and a final

UV/vis measurement was obtained. Measurement were taken using a Varian Cary-50 spectrophotometer. Data was exported as a .csv file and processed using Microsoft Excel.

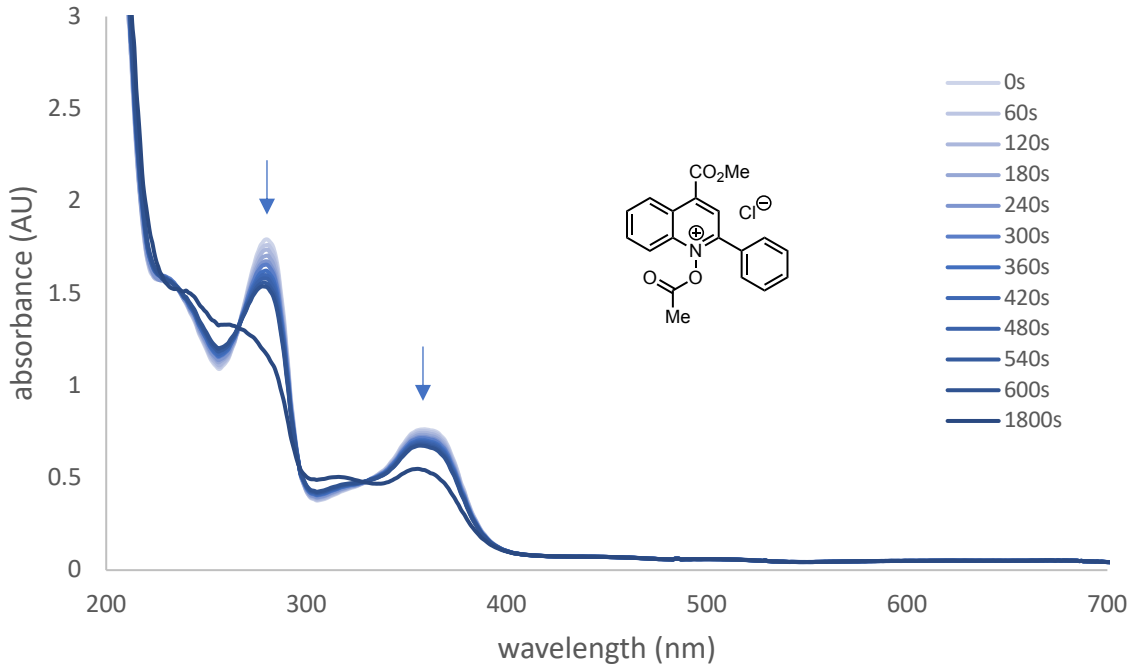

Discussion – The above experiment supports the hypothesis that the decomposition of Ac-PQCNO species is a photo-induced reaction, as degradation could be observed by UV/vis after as little as 60s of irradiation from a 427 nm Kessil lamp. In the design of this study, we sought to observe PQCN derived fragmentation products with unique electronic structures (such as radical cation intermediates), however, no such products were observed.

Fluorescence Spectroscopy

To a flame dried 1-dram vial was weighed heteroaromatic *N*-oxide, and this was taken up into 3 mL of sparged MeCN. A 100 μM solution of heteroaromatic *N*-oxide was prepared by diluting 83 μL to a volume of 3 mL, and the mixture was shaken vigorously to ensure mixing. The final

solution was then transferred to a quartz cuvette with a 1 cm path length. For measurements of acylated heteroaromatic *N*-oxides, acyl chloride (1.1 equiv) was added to the cuvette and the mixture was shaken vigorously, the solution remained clear and colorless. Measurements were taken using a Horiba Quantamaster 8000 Fluorimeter. Data was exported as a .csv file and processed using Microsoft Excel.

Decomposition of PQCNO Monitored by Fluorescence Spectroscopy

To a flame dried 1-dram vial was weighed PQCNO (3 mg, 0.011 mmol), and this was taken up into 3 mL of sparged MeCN. Acetyl chloride (1.1 equiv) was added, and the mixture was shaken vigorously, the solution was a clear and colorless. A 100 μM solution of Ac-PQCNO was prepared by diluting 83 μL to a volume of 3 mL, and the mixture was inverted 15 times to ensure mixing. The final solution was then transferred to a quartz cuvette with a 1 cm path length. Fluorescence measurements were carried out in the dark. A fluorescence experiment was run, shaken with a gentle wrist flick 5 times and returned to the sample holder and a subsequent fluorescence measurement was taken. This was process was repeated 25 times. After the 25th experiment, 39 μL of a 0.0038 M (0.15 mmol, 0.5 equiv with respect to PQCNO) solution of methyl 2-phenylquinoline-4-carboxylate was added to the fluorescence sample, and the cuvette was vigorously shaken to ensure mixing. Five more fluorescence measurements were carried out.

Measurement were taken using a Horiba Quantamaster 8000 Fluorimeter. Data was exported as a .csv file and processed using Microsoft Excel. Excitation beam was set to 335 nm to minimize spectral distortions from Raman scattering of the acetonitrile solvent. Excitation 335 nm, slit width 3 nm. Emission was scanned from 350 nm to 500 nm, slit width of 5 nm.

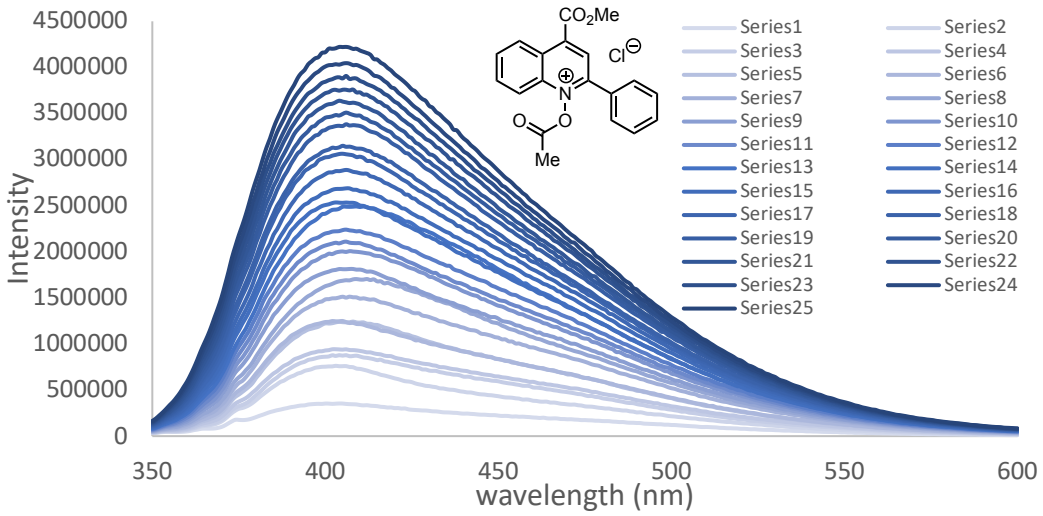

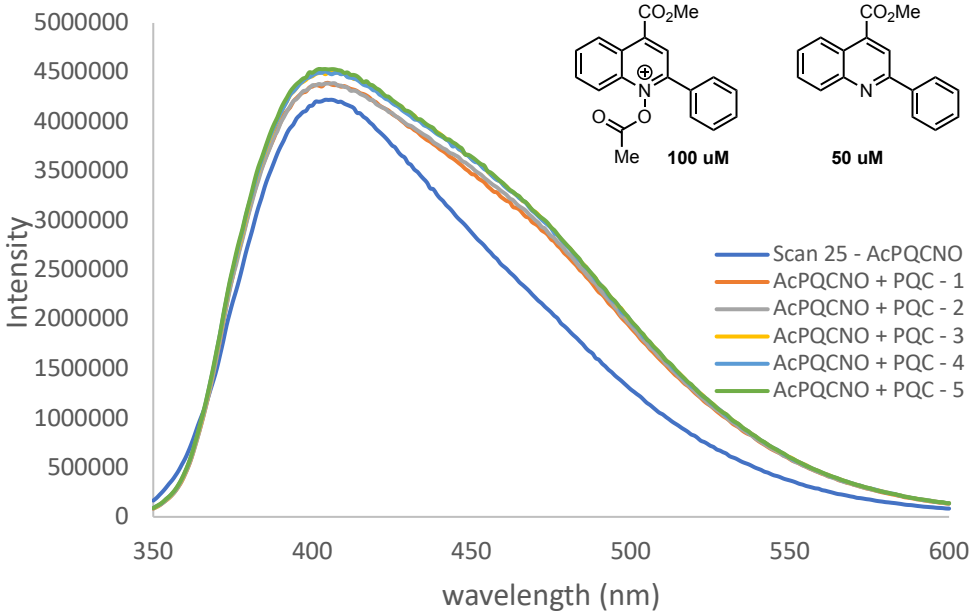

Discussion –Ac-PQCNO is observed to have an increase in fluorescence upon successive fluorescence experiments with an excitation at 335 nm. Addition of free quinoline (PQCN), which is the primary fragmentation product, to the sample results in an increase in the fluorescence maximum, with no change to the wavelength of maximum fluorescence. Together, this data supports the hypothesis that excitation of Ac-PQCNO results in a fast N–O bond homolysis, leading to decarboxylation and liberating an equivalent of PQCN. As successive fluorescence measurements are taken, PQCN builds up and becomes the primary fluorophore. Because

fluorescence is the primary process that occurs upon excitation of the PQCN, it washes out fluorescence due to Ac-PQCNO. Additionally, the weak initial fluorescence that is attributed to Ac-PQCNO demonstrates that there is an excited state reaction pathway that competes with fluorescence upon excitation.

Investigation of Thermal Reactivity

To a flame dried vial equipped with a stir bar was weighed 112 mg (1 equiv) PQCNO, and 22.2 mg (1 equiv) calcium chloride. The vial was capped with a septa cap, and the solids were evacuated and backfilled 5 times with nitrogen. 0.5 mL of acetonitrile followed by 35 μL of acetyl chloride were added and the vial was sealed under nitrogen with electrical tape and parafilm. The vial was then wrapped with aluminum foil and placed in the center of a stir plate. Aliquots of the reaction were taken after stirring for 1 h at room temperature, 50 °C for 15 hours, and 90 °C for 3 hours. No reactivity was observed, however, at elevated temperatures acetyl chloride was boiled off of the reaction solution.

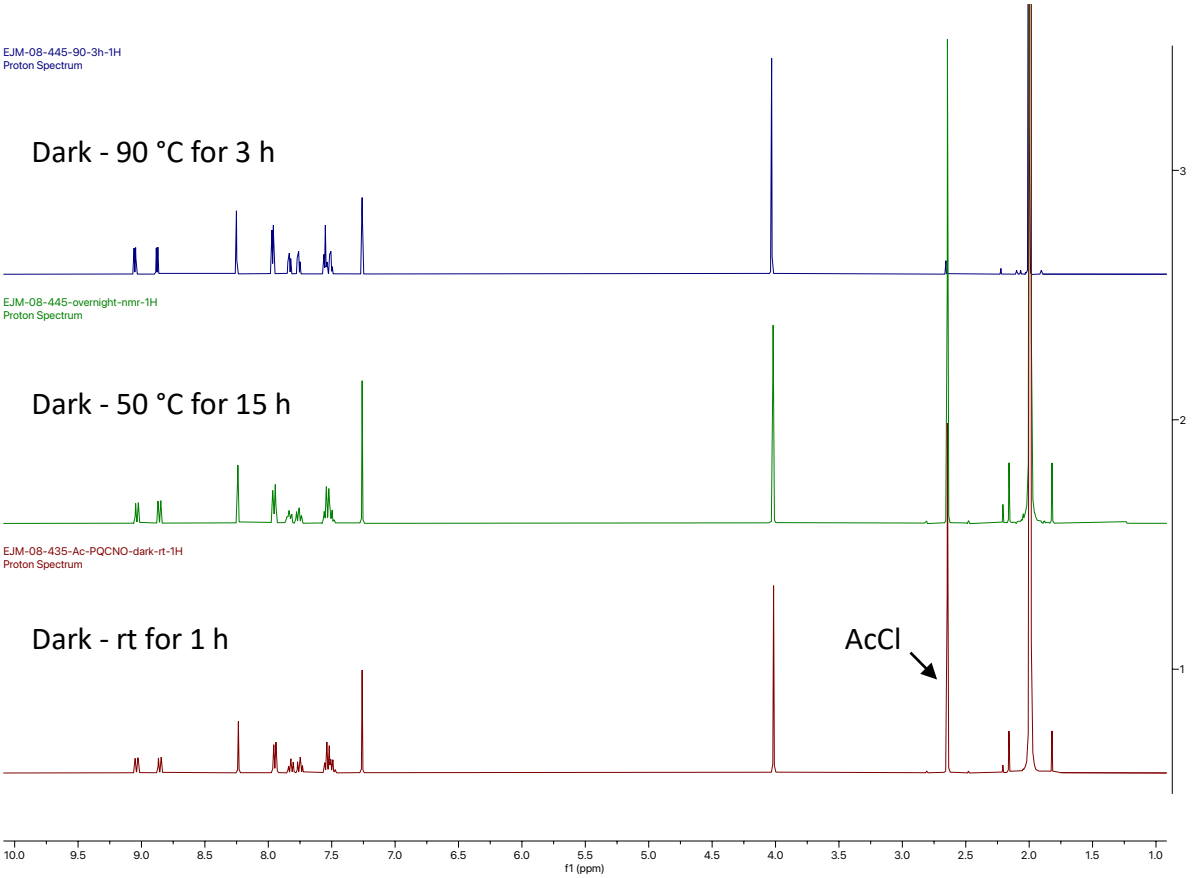

Discussion – The above experiment demonstrates the thermal stability of PQCNO and Ac-PQCNO, as no thermal reactivity was observed upon heating the sample to 90 °C for 3 hours. Because the temperature and time far exceed that of the standard reaction (35-45 °C, 30 min to 1 h), we believe that this result demonstrates the observed decomposition of Ac-PQCNO is due to photochemical reactivity.

Investigation of PQCN Alkylation

A reaction was carried out according to General Procedure A in the absence of a substrate. The non-volatile organic products of the reaction were assessed. Methyl 3-(*tert*-butyl)-2-

phenylquinoline-4-carboxylate was isolated as a minor product in 13% yield. No other functionalization products of PQCN were observed.

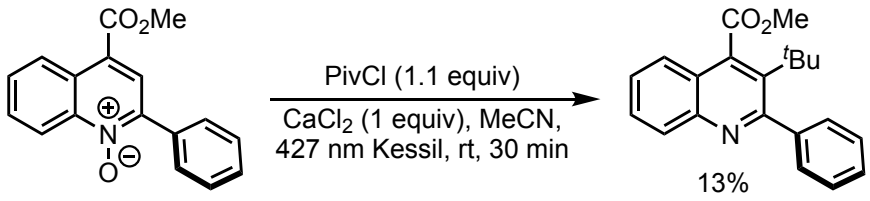

Discussion – The results of this reaction demonstrate that in the absence of substrates, alkylation of PQCN is still very slow and only occurs to a minor extent.

Recycling of PQCNO

To demonstrate the utility of PQCNO photo-active ester, a recycling experiment was performed in which the parent quinoline (PQCN) following the Minisci alkylation was recovered, re-oxidized to regenerate PQCNO, and re-subjected to Minisci alkylation reaction conditions. This process was carried for 3 consecutive Minisci alkylation reactions. Each of the Minisci alkylation reactions were carried out according to General Procedure A with the only alteration being to the scale of the reaction. Oxidation reactions were carried out according to General Procedure B.

1st Minisci alkylation was carried out on 1 mmol scale, reaction was run for 30 mins. 2-(*tert*-butyl)-4-chloroquinoline was isolated in 88% yield. 84% of deoxygenated PQCN was recovered.

2nd Minisci alkylation was carried out on 0.5 mmol scale, reaction was run for 30 mins. 2-(*tert*-butyl)-4-chloroquinoline was isolated in 92% yield. 87% of deoxygenated PQCN was recovered.

3rd Minisci alkylation was carried out on 0.29 mmol scale, reaction was run for 30 mins. 2-(*tert*-butyl)-4-chloroquinoline was isolated in 96% yield. 89% of deoxygenated PQCN was recovered.

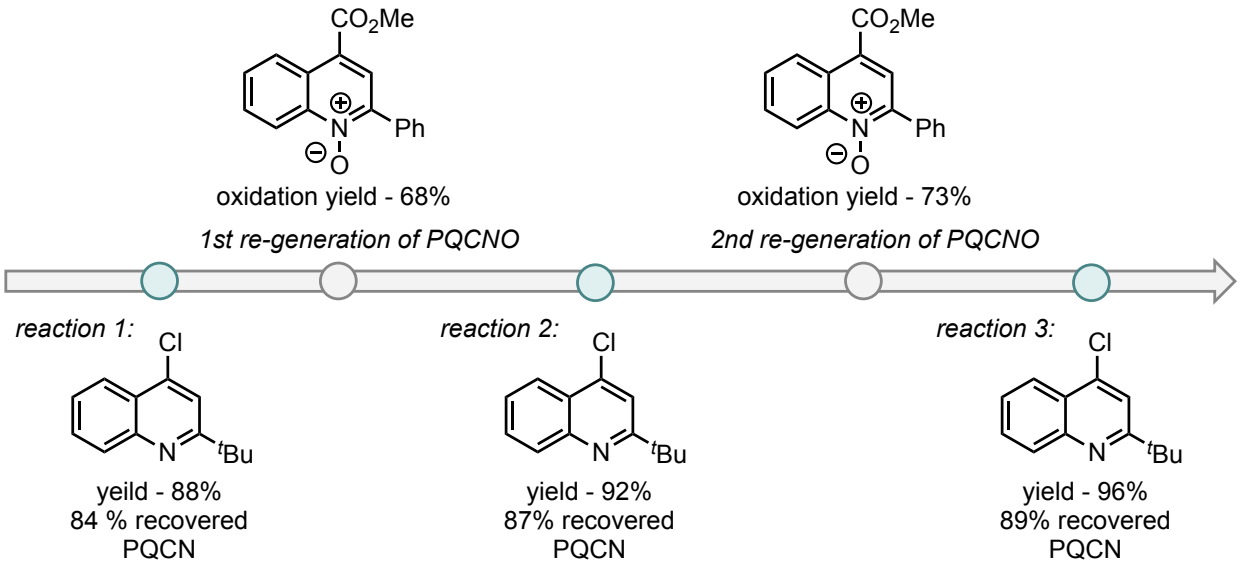

Discussion – These experiments demonstrate the potential applicability of PQCNO derived photo-active esters towards large scale synthesis. Importantly, our findings demonstrate that the deoxygenated quinoline material (PQCN) can be recovered and PQCNO regenerated in high yields with no loss of efficiency under Minisci alkylation conditions.

LED NMR Reaction Monitoring

To a flame dried vial equipped with a stir bar was weighed out PQCNO (56 mg, 0.2 mmol, 1 equiv) and 4-chloroquinoline (16.4 mg, 0.1 mmol, 0.5 equiv). The vial was capped with a septa cap, and the solids were evacuated and backfilled 5 times with nitrogen. The mixture of solids was then taken up into 0.5 mL of MeCN, and 27 μL of PivCl followed by the addition of 16 μL of TFA. The reaction mixture was then sealed under nitrogen atmosphere with electrical tape and parafilm, and allowed to stir for 10 to 15 mins, or until the PQCNO had completely dissolved. A thin-walled NMR tube that was purged with argon for 15 mins, at which point, the reaction solution was transferred to the NMR tube via a 1 mL syringe. The co-axial insert was added immediately, and

the NMR tube was sealed with parafilm. The fiber optic cable was inserted to the co-axial insert and secured with a small piece of parafilm prior to the NMR experiment. The NMR sample was inserted and at least one experiment was collected prior to starting irradiation with a 430 nm LED light source. Data was processed in MestraNova using the reaction monitoring plugin, the methyl ester signal corresponding to PQCNO and deoxygenated PQCNO was monitored to assess the conversion. In the presence of TFA, two equilibria states of PQCNO exist (free PQCNO and PQCNOH+), the two integrals were summed to give an integration that was assumed to equal 100%. Data was plotted in Microsoft Excel.

NMR parameters: Relaxation delay of 0.5 s, 45 ° pulse angle, acquisition time of 2.83 s, 2 steady state scans prior to each experiment, 4 scans per experiment, for a total of 16.98 s per experiment (.fid file). 200 experiments were collected for a total time of 57 mins.

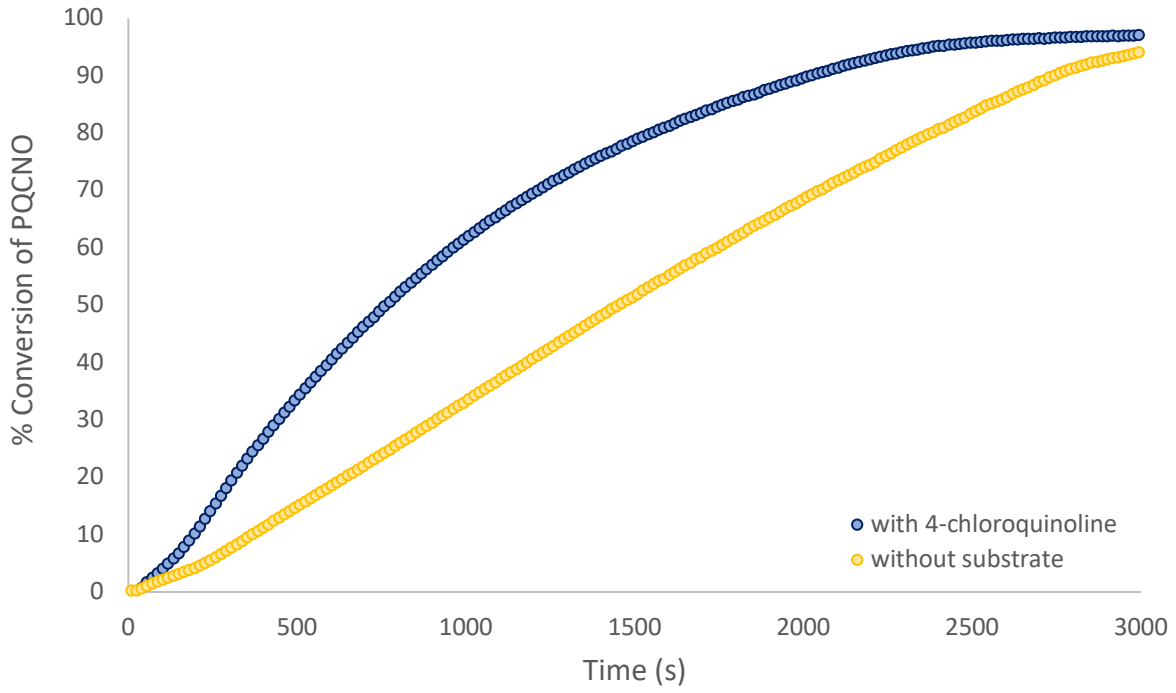

In the absence of 4-chloroquinoline

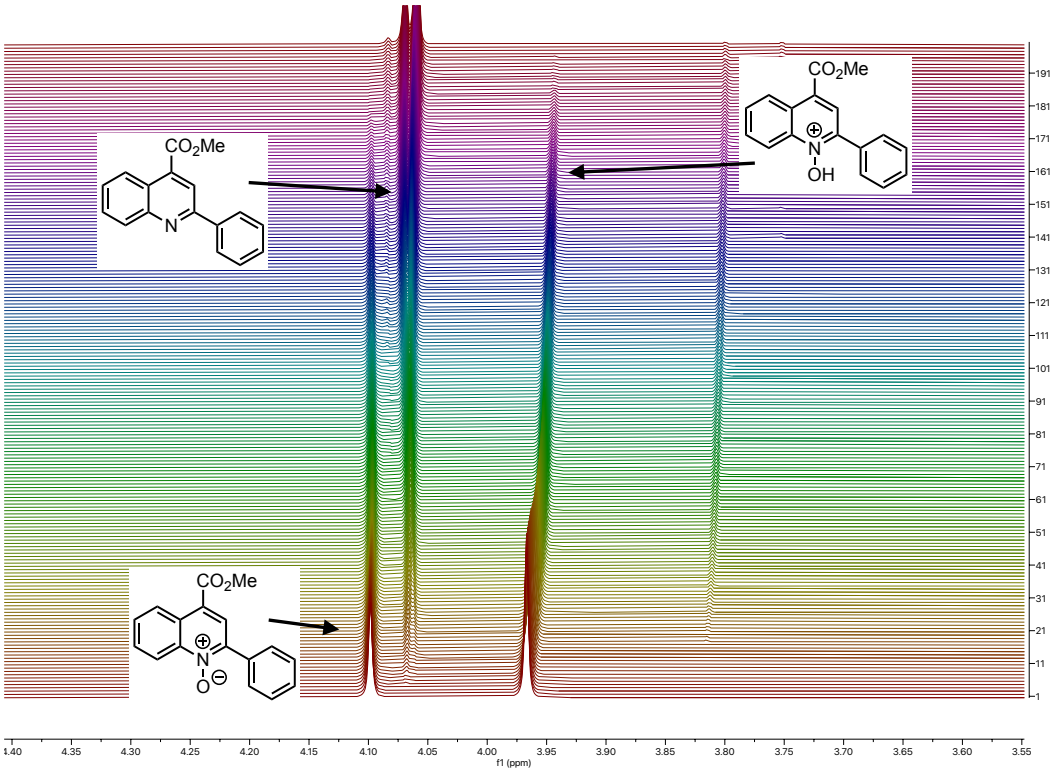

In the presence of 4-chloroquinoline

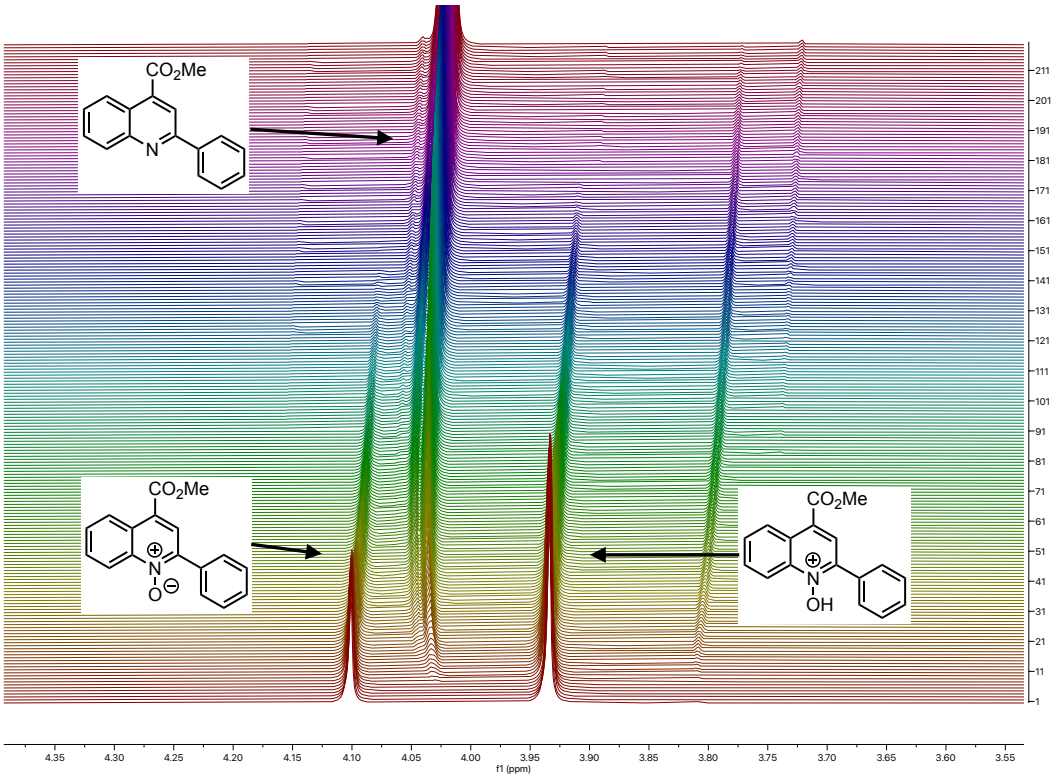

Discussion – The results of this experiment show that there is a change in the overall kinetics of the deoxygenation reaction in the presence/absence of a substrate. We believe that the observed change in the kinetic profile of the reaction is due to a background electron transfer from the substrate following radical addition to an equivalent of Piv-PQCNO, resulting in propagation of the reaction.

Reaction with 2-phenylpropionyl chloride

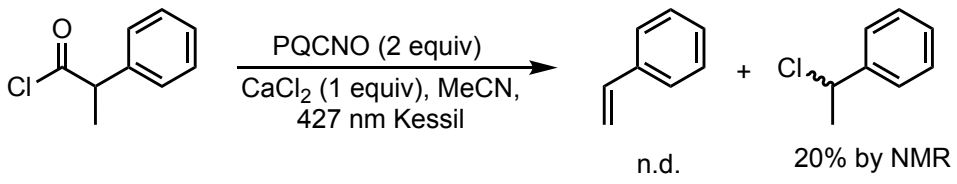

To a flame dried 1-dram vial equipped with a Teflon stir bar was weighed PQCNO (112 mg, 0.4 mmol, 1 equiv) and calcium chloride (0.5 equiv, 22.2 mg). The solids were evacuated and backfilled 5 times with nitrogen. To the vial was added 0.5 mL MeCN, followed by the addition of 2-phenylpropionyl chloride (1.1 equiv, 0.44 mmol, 74.2 mg). The vial was then sealed with a piece of electrical tape and parafilm, and then irradiated with a 427 nm Kessil lamp for 30 min. At the conclusion of the reaction, 24 uL of MTBE was added as an internal standard and NMR was obtained in chloroform. Crude analysis showed the appearance of 1-chloro-1-phenylethane in 20% yield.

Discussion: We believe that this result demonstrates the ability of acylated-PQCNO to oxidize stabilized carbon centered radicals.

Compound Isolation and Characterization Data

2,4,6-triphenylpyridine *N*-oxide (TPPNO)

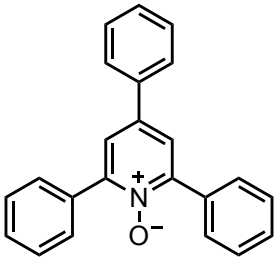

2,4,6-triphenylpyridine N-oxide was prepared according to Buchardt, *et al. Acta Chem. Scand.* **1970,** *24,* 3435-3443.

2,4,6-triphenylpyridine *N*-oxide was isolated as an off-white amorphous solid.

^{1}H NMR (600 MHz, $CDCl_3$) δ 7.93 – 7.88 (m, 4H), 7.67 (d, *J* = 7.8 Hz, 4H), 7.53 – 7.42 (m, 9H) ppm.

^{13}C NMR (151 MHz, $CDCl_3$) δ 150.04, 136.85, 133.46, 129.75, 129.56, 129.38, 129.03, 128.32, 128.24, 126.57, 123.96 ppm.

IR(neat): 3057, 1620, 1577, 1549, 1495, 1452, 1402, 1341, 1304, 1254, 1182, 1163, 1075, 1028, 1015, 1001, 983, 878, 867, 838, 764, 728, 689 cm^{-1}.

HRMS: Calculated [M+H]+: 324.1383; Found [M+H]+: 324.1380.

Methyl 2-phenylquinoline-4-carboxylate *N*-oxide (PQCNO)

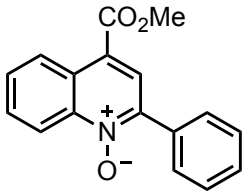

Preparation of PQCNO was carried out according to General Procedure B, using methyl 2-phenylquinoline-4-carboxylate as the starting material. PQCNO was isolated as an off-white amorphous solid.

^{1}H NMR (500 MHz, $CDCl_3$) δ 9.06 (dt, *J* = 8.6, 1.7 Hz, 1H), 8.87 (d, *J* = 8.8 Hz, 1H), 8.24 (d, *J* = 1.1 Hz, 1H), 7.99 – 7.93 (m, 2H), 7.81 (ddd, *J* = 8.5, 7.1, 1.5 Hz, 1H), 7.75 (ddd, *J* = 8.8, 6.9, 1.8 Hz, 1H), 7.58 – 7.46 (m, 3H), 4.02 (s, 3H) ppm.

^{13}C NMR (126 MHz, $CDCl_3$) δ 165.50, 144.31, 143.20, 132.86, 130.75, 130.03, 129.86, 129.65, 128.59, 127.44, 126.89, 126.78, 122.63, 120.46, 52.77 ppm.

IR(neat): 3054, 2990, 2947, 1715, 1579, 1553, 1506, 1495, 1454, 1428, 1373, 1334, 1308, 1248, 1228, 1192, 1139, 1065, 1033, 1024, 929, 913, 862, 784, 765, 736, 723, 695, 678 cm-1.

HRMS: Calculated [M+H]+: 280.0968; Found [M+H]+: 280.0963.

Methyl acridine-9-carboxylate *N*-oxide (ACNO)

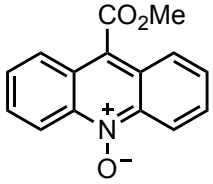

Preparation of PQCNO was carried out according to General Procedure B, using methyl acridine-9-carboxylate as the starting material. Methyl acridine-9-carboxylate *N*-oxide was isolated as a vibrant yellow amorphous solid.

^{1}H NMR (600 MHz, $CDCl_3$) δ 8.90 (d, *J* = 9.0 Hz, 3H), 8.12 (d, *J* = 8.7 Hz, 3H), 7.79 (ddd, *J* = 9.1, 6.6, 1.3 Hz, 3H), 7.64 (ddd, *J* = 8.8, 6.6, 1.2 Hz, 3H), 4.19 (d, *J* = 0.9 Hz, 5H) ppm.

^{13}C NMR (151 MHz, $CDCl_3$) δ 167.33, 139.51, 130.94, 128.58, 126.15, 124.98, 124.37, 120.13, 53.21 ppm.

IR(neat): 2958, 1721, 1622, 1571, 1536, 1482, 1429, 1376, 1292, 1272, 1221, 1202, 1162, 1110, 926, 902, 842, 812, 783, 762, 743 cm^{-1}.

HRMS: Calculated [M+H]+: 254.0812; Found [M+H]+: 254.0809.

Methyl acridine-9-carboxylate

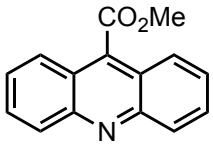

To a flame dried round bottom flask equipped with a magnetic stir bar was weighed acridine-9-carboxylate (1 equiv., 4.5 mmol, 1 g, pale yellow powder). The solid was taken up into 50 mL of DCM. Note: At this point the material was insoluble and the mixture was stirred as yellow solid floated on top of DCM. The round bottom flask was equipped with a septum with a vent needle, and oxalyl chloride (1.2 equiv., 5.4 mmol, 685 mg, 463 mL) was added. To the mixture was added DMF (0.1 equiv., ~5 drops), the acridine-9-carboxylate immediately went into solution and the reaction began to bubble vigorously. The reaction was allowed to stir for about 3 hours (when bubbling ceased), at which point methanol (5 mL) and sodium methoxide (2 equiv., 9 mmol, 486 mg) were added and the reaction mixture was allowed to stir for an additional 3 hours. Upon conclusion of the reaction, the mixture was taken up into saturated sodium bicarbonate (20 mL) and extracted with 3 portions of 20 mL DCM. [Note: An emulsion forms at this point. The reaction mixture is a dark orange in color at this point and both aqueous and organic layers will become colored. On several occasions, a solid yellow precipitate was observed to crash out of solution, this was collected with the DCM layers]. The combined organic extracts were washed with 20 mL saturated sodium chloride [Note: emulsion forms], and dried over sodium sulfate. The crude organic material was purified by column chromatography using DCM/Acetone as a mobile phase.

2-(tert-butyl)-4-chloroquinoline

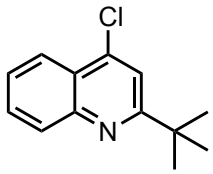

Reaction run according to General Procedure A. 2-(*tert*-butyl)-4-chloroquinoline was isolated as a colorless oil.

^{1}H NMR (600 MHz, $CDCl_3$) δ 8.18 (dd, *J* = 8.3, 1.3 Hz, 1H), 8.09 (dt, *J* = 8.3, 0.9 Hz, 1H), 7.72 (ddd, *J* = 8.4, 6.8, 1.5 Hz, 1H), 7.62 (s, 1H), 7.57 (ddd, *J* = 8.3, 6.9, 1.3 Hz, 1H), 1.47 (s, 9H) ppm.

^{13}C NMR (151 MHz, $CDCl_3$) δ 169.49, 148.47, 142.41, 130.05, 129.89, 126.74, 124.80, 123.84, 118.59, 38.39, 31.43, 31.26, 30.33, 30.13 ppm.

IR(neat): 3064, 2961, 2907, 2868, 1617, 1589, 1552, 1492, 1462, 1397, 1364, 1303, 1262, 1218, 1204, 1147, 1105, 1023, 977, 897, 868, 840, 757, 713 cm^{-1}.

HRMS – Calculated [M+H]+: 220.0888; Found [M+H]+: 220.0880.

2-(*iso*-propyl)-4-chloroquinoline

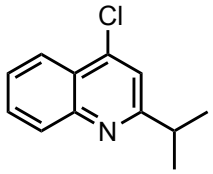

Reaction run according to General Procedure A. 2-*iso*propyl-4-chloroquinoline was isolated as a colorless oil. Characterization data is consistent with previously reported literature (Chen *et al. Chem. Sci.* **2016,** *7,* 6407–6412.).

^{1}H NMR (700 MHz, $CDCl_3$) δ 8.18 (dd, *J* = 8.3, 1.4 Hz, 1H), 8.06 (d, *J* = 8.4 Hz, 1H), 7.73 (ddd, *J* = 8.4, 6.8, 1.4 Hz, 1H), 7.57 (td, *J* = 7.5, 6.8, 1.2 Hz, 1H), 7.43 (s, 1H), 3.23 (p, *J* = 7.0 Hz, 1H), 1.39 (d, *J* = 6.9 Hz, 7H) ppm.

HRMS: Calculated [M+H]+: 206.0731; Found [M+H]+: 206.0733.

2-ethyl-4-chloroquinoline

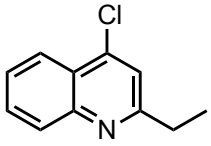

Reaction run according to General Procedure A. 2-ethyl-4-chloroquinoline was isolated as a colorless oil. Characterization data is consistent with previously reported literature (Chen *et al. Chem. Sci.* **2016,** *7,* 6407–6412.).

^{1}H NMR (500 MHz, $CDCl_3$) δ 8.18 (d, *J* = 8.4 Hz, 1H), 8.05 (d, *J* = 8.5 Hz, 1H), 7.73 (t, *J* = 8.5 Hz, 1H), 7.58 (t, *J* = 8.5 Hz, 1H), 7.41 (s, 1H), 2.98 (q, *J* = 7.7 Hz, 2H), 1.40 (t, *J* = 7.6 Hz, 3H) ppm.

HRMS: Calculated [M+H]+: 192.0575; Found [M+H]+: 192.0576

2-methyl-4-chloroquinoline

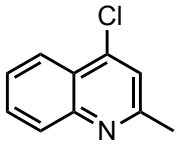

Reaction run according to General Procedure A, run for 1 hour. 2-methyl-4-chloroquinoline was isolated as a 1:2.5 inseparable mixture with 4-chloroquinoline. Characterization data is consistent with previously reported literature (Chen *et al. Chem. Sci.* **2016,** *7,* 6407–6412.).

^{1}H NMR (401 MHz, $CDCl_3$) δ 8.18 (d, *J* = 8.4 Hz, 1H), 8.05 (d, *J* = 8.4 Hz, 1H), 7.74 (t, *J* = 8.0 Hz, 1H), 7.58 (t, *J* = 8.0 Hz, 1H), 7.41 (s, 1H), 2.73 (s, 3 H) ppm.

HRMS: Calculated [M+H]+: 178.0418; Found [M+H]+: 178.0412.

2-(cyclohexyl)-4-chloroquinoline

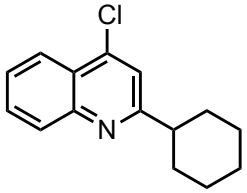

Reaction run according to General Procedure A. 2-cyclohexyl-4-chloroquinoline was isolated as a colorless amorphous solid. Characterization data is consistent with previously reported literature (Chen *et al. Chem. Sci.* **2016,** *7,* 6407–6412.).

^{1}H NMR (500 MHz, $CDCl_3$) δ 8.18 (dd, *J* = 8.4, 1.4 Hz, 1H), 8.06 (d, *J* = 8.5 Hz, 1H), 7.73 (ddd, *J* = 8.4, 6.9, 1.4 Hz, 1H), 7.57 (ddd, *J* = 8.2, 6.8, 1.2 Hz, 1H), 7.43 (s, 1H), 2.90 (tt, *J* = 12.0, 3.5 Hz, 1H), 2.03 (ddq, *J* = 11.9, 3.6, 1.9 Hz, 2H), 1.90 (dt, *J* = 13.0, 3.4 Hz, 2H), 1.79 (dtt, *J* = 11.5, 3.3, 1.6 Hz, 1H), 1.61 (qd, *J* = 12.6, 3.3 Hz, 2H), 1.46 (qt, *J* = 12.8, 3.4 Hz, 2H), 1.39 – 1.24 (m, 1H) ppm.

HRMS: Calculated [M+H]+: 246.1044; Found [M+H]+: 246.1051

2-(cyclobutyl)-4-chloroquinoline

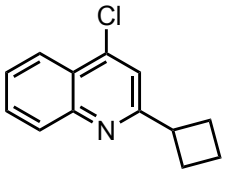

Reaction run according to General Procedure A. 2-cyclobutyl-4-chloroquinoline was isolated as a pale-yellow oil. Characterization data is consistent with previously reported literature (Chen *et al. Chem. Sci*. **2016,** *7,* 6407–6412.).

^{1}H NMR (500 MHz, $CDCl_3$) δ 8.17 (dd, *J* = 8.3, 1.4 Hz, 1H), 8.08 (d, *J* = 8.4 Hz, 1H), 7.72 (ddd, *J* = 8.4, 6.9, 1.4 Hz, 1H), 7.56 (ddd, *J* = 8.2, 6.9, 1.2 Hz, 1H), 7.43 (s, 1H), 3.88 – 3.78 (m, 1H), 2.45 (td, *J* = 9.0, 6.0 Hz, 4H), 2.13 (dq, *J* = 10.9, 9.0 Hz, 1H), 2.00 – 1.91 (m, 1H) ppm.

HRMS – Calculated [M+H]+: 218.0731; Found [M+H]+: 218.0731.

2-(cyclopropyl)-4-chloroquinoline

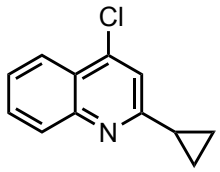

Reaction run according to General Procedure A. 2-cyclobutyl-4-chloroquinoline was isolated as a pale-yellow oil. Characterization data is consistent with previously reported literature (Chen *et al. Chem. Sci.* **2016,** *7,* 6407–6412.).

^{1}H NMR (700 MHz, $CDCl_3$) δ 8.14 (d, *J* = 8.3 Hz, 1H), 7.98 (d, *J* = 8.5 Hz, 1H), 7.70 (t, *J* = 7.7 Hz, 1H), 7.52 (t, *J* = 7.6 Hz, 1H), 7.29 (s, 1H), 2.21 (s, 1H), 1.17 (dq, *J* = 5.4, 3.7, 2.7 Hz, 2H), 1.15 – 1.09 (m, 2H) ppm.

HRMS – Calculated [M+H]+: 204.0575; Found [M+H]+: 204.0579.

2-(1-phenylcyclopropyl)-4-chloroquinoline

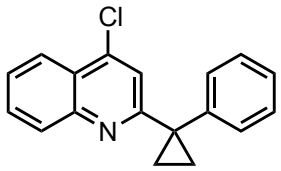

Reaction run according to General Procedure A. 2-(1-phenylcyclopropyl)-4-chloroquinoline was isolated as a pale-yellow amorphous solid.

^{1}H NMR (700 MHz, $CDCl_3$) δ 8.12 (d, *J* = 8.3 Hz, 1H), 8.04 (d, *J* = 8.5 Hz, 1H), 7.72 (t, *J* = 7.7 Hz, 1H), 7.54 (t, *J* = 7.6 Hz, 1H), 7.44 (d, *J* = 8.0 Hz, 2H), 7.39 (t, *J* = 7.6 Hz, 2H), 7.34 – 7.30 (m, 1H), 7.16 (s, 1H), 1.87 (q, *J* = 3.9 Hz, 2H), 1.41 (q, *J* = 3.9 Hz, 2H) ppm.

^{13}C NMR (176 MHz, $CDCl_3$) δ 164.61, 142.92, 130.61, 130.33, 129.47, 128.91, 127.24, 126.60, 124.73, 124.00, 121.17, 32.31, 18.11 ppm.

IR(neat): 3061, 2923, 2867, 1719, 1584, 1549, 1492, 1446, 1406, 1322, 1244, 1205, 1172, 1145, 1090, 1076, 1059, 1025, 979, 937, 907, 860, 842, 753, 697 cm^{-1}.

HRMS: Calculated [M+H]+: 280.0888; Found [M+H]+: 280.0892.

2-(1-adamantyl)-4-chloroquinoline

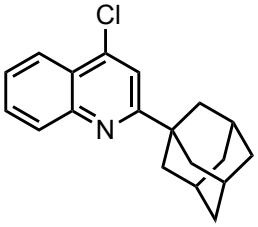

Reaction run according to General Procedure A. 2-(1-adamantyl)-4-chloroquinoline was isolated as a colorless amorphous solid.

^{1}H NMR (401 MHz, $CDCl_3$) δ 8.17 (dd, *J* = 8.4, 1.4 Hz, 1H), 8.07 (d, *J* = 8.4 Hz, 1H), 7.71 (ddd, *J* = 8.4, 6.9, 1.5 Hz, 1H), 7.57 (s, 1H), 7.56 (ddd, *J* = 8.3, 6.9, 1.2 Hz, 1H), 2.19 – 2.13 (m, 4H), 2.10 (d, *J* = 2.9 Hz, 7H), 1.83 (t, *J* = 3.0 Hz, 7H) ppm.

^{13}C NMR (176 MHz, CDCl3) δ 169.30, 148.71, 142.48, 130.00, 129.87, 126.70, 124.96, 123.90, 118.33, 41.88, 40.03, 36.91, 28.89 ppm.

IR(neat): 2903, 2848, 1617, 1584, 1548, 1494, 1449, 1410, 1344, 1323, 1293, 1255, 1228, 1191, 1149, 1103, 1000, 970, 904, 868, 841, 756, 707, 662 cm^{-1}.

HRMS: Calculated [M+H]+: 298.1357; Found [M+H]+: 298.1359.

2-(methyl 4-[2.2.2]-bicyclooctyl-1-carboxylate)-4-chloroquinoline

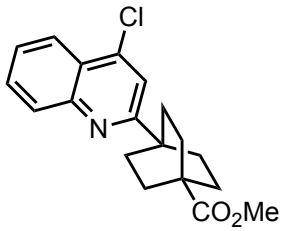

Reaction run according to General Procedure A. 2-(methyl 4-[2.2.2]-bicyclooctyl-1-carboxylate)-4-chloroquinoline was isolated as a colorless amorphous solid.

^{1}H NMR (500 MHz, $CDCl_3$) δ 8.15 (dd, *J* = 8.4, 1.4 Hz, 1H), 8.04 (d, *J* = 8.5 Hz, 1H), 7.71 (ddd, *J* = 8.4, 6.8, 1.4 Hz, 1H), 7.56 (ddd, *J* = 8.3, 6.8, 1.2 Hz, 1H), 7.51 (s, 1H), 3.69 (s, 3H), 2.04 (dd, *J* = 10.3, 5.2 Hz, 6H), 1.96 (dd, *J* = 10.4, 5.1 Hz, 6H) ppm.

^{13}C NMR (126 MHz, $CDCl_3$) δ 178.36, 167.74, 148.49, 142.51, 130.17, 129.75, 126.86, 124.89, 123.88, 118.72, 51.83, 39.47, 38.56, 30.57, 28.67 ppm.

IR(neat): 2945, 2920, 2868, 1718, 1615, 1586, 1551, 1493, 1455, 1437, 1414, 1402, 1300, 1254, 1237, 1218, 1192, 1170, 1075, 1006, 967, 922, 866, 841, 765, 704, 666 cm^{-1}.

HRMS – Calculated [M+H]+: 330.1255; Found [M+H]+: 330.1267.

2-(methyl 3-[1.1.1]-bicyclopentyl-1-carboxylate)-4-chloroquinoline

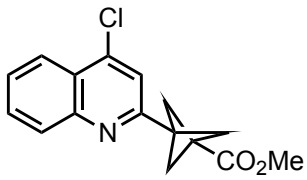

Reaction run according to General Procedure A. 2-(methyl 3-[1.1.1]-bicyclopentyl-1-carboxylate)-4-chloroquinoline was isolated as a colorless amorphous solid.

^{1}H NMR (600 MHz, $CDCl_3$) δ 8.17 (d, *J* = 8.4 Hz, 1H), 8.09 (d, *J* = 8.5 Hz, 1H), 7.76 – 7.71 (m, 1H), 7.61 – 7.56 (m, 1H), 7.42 (s, 1H), 3.74 (s, 3H), 2.51 (s, 6H) ppm.

^{13}C NMR (151 MHz, $CDCl_3$) δ 170.54, 158.69, 148.84, 142.99, 130.62, 129.66, 127.34, 125.38, 124.05, 119.08, 53.48, 51.92, 42.80, 37.42 ppm.

IR(neat): 2996, 2958, 2925, 1723, 1590, 1550, 1492, 1442, 1404, 1372, 1326, 1304, 1208, 1187, 1136, 1111, 1027, 976, 946, 871, 824, 790, 769, 718, 695 cm^{-1}.

HRMS – Calculated [M+H]+: 288.0786; Found [M+H]+: 288.0786.

2-(tetrahydro-*2H*-pyran-4-yl)-4-chloroquinoline

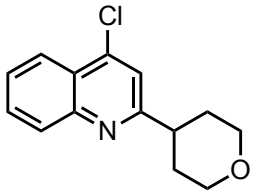

Reaction run according to General Procedure A. 2-(tetrahydro-*2H*-pyran-4-yl)-4-chloroquinoline was isolated as a colorless amorphous solid.

^{1}H NMR (600 MHz, $CDCl_3$) δ 8.17 (dd, *J* = 8.4, 1.4 Hz, 1H), 8.07 – 8.02 (m, 1H), 7.72 (ddd, *J* = 8.4, 6.9, 1.4 Hz, 1H), 7.57 (ddd, *J* = 8.2, 6.9, 1.2 Hz, 1H), 7.41 (s, 1H), 4.16 – 4.08 (m, 2H), 3.57 (td, *J* = 11.7, 2.2 Hz, 2H), 3.12 (tt, *J* = 11.9, 4.0 Hz, 1H), 2.00 (dtd, *J* = 13.3, 11.8, 4.4 Hz, 2H), 1.92 (ddd, *J* = 13.2, 4.2, 2.1 Hz, 2H) ppm.

^{13}C NMR (151 MHz, $CDCl_3$) δ 164.59, 148.76, 143.02, 130.46, 129.48, 127.00, 125.30, 124.02, 119.63, 68.05, 44.23, 32.20 ppm.

IR(neat): 3064, 2953, 2842, 1730, 1615, 1589, 1553, 1494, 1465, 1443, 1411, 1386, 1298, 1237, 1212, 1150, 1128, 1085, 1011, 981, 939, 913, 869, 841, 820, 758, 730, 695, 672 cm^{-1} .

HRMS - Calculated [M+H]+: 248.0837; Found [M+H]+: 248.0838.

tert-butyl 3-(4-chloroquinolin-2-yl)azetidine-1-carboxylate

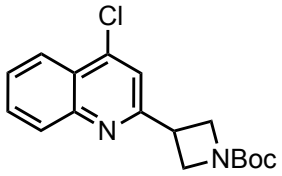

Reaction run according to General Procedure A. *tert*-butyl 3-(4-chloroquinolin-2-yl)azetidine-1-carboxylate was isolated as a pale yellow oil.

^{1}H NMR (600 MHz, $CDCl_3$) δ 8.21 (dd, *J* = 8.3, 1.3 Hz, 1H), 8.08 (d, *J* = 8.4 Hz, 1H), 7.77 (ddd, *J* = 8.5, 6.9, 1.4 Hz, 1H), 7.62 (ddd, *J* = 8.2, 6.9, 1.2 Hz, 1H), 7.51 (s, 1H), 4.39 (t, *J* = 8.7 Hz, 2H), 4.28 (dd, *J* = 8.7, 5.9 Hz, 2H), 4.03 (dq, *J* = 12.8, 4.4, 3.0 Hz, 1H), 1.48 (s, 10H) ppm.

^{13}C NMR (151 MHz, $CDCl_3$) δ 161.28, 156.64, 148.66, 143.50, 130.81, 129.60, 127.46, 125.43, 124.12, 119.79, 79.83, 54.62, 35.78, 29.84, 28.57 ppm.

IR(neat): 3062, 2976, 2887, 1695, 1616, 1589, 1554, 1495, 1479, 1455, 1391, 1365, 1300, 1252, 1216, 1162, 1132, 1027, 971, 927, 863, 838, 760, 734 cm^{-1}.

HRMS – During MS analysis of with ESI source in positive mode, we observed Boc deprotection of the product.

Molecular Formula: C12H11ClN2; Calculated [M+H]+: 219.0684; Found [M+H]+: 219.0688.

***tert*-butyl 4-(4-chloroquinolin-2-yl)piperidine-1-carboxylate**

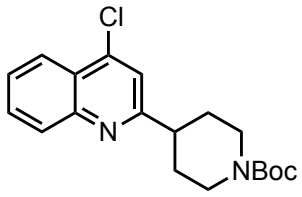

Reaction run according to General Procedure A. *tert*-butyl 4-(4-chloroquinolin-2-yl)piperidine-1-carboxylate was isolated as a pale yellow oil. Characterization data is consistent with previously reported literature (Wang *et al. J. Org. Chem.* **2019,** *84,* 7532–7540.).

^{1}H NMR (600 MHz, $CDCl_3$) δ 8.17 (dt, *J* = 8.4, 1.8 Hz, 1H), 8.03 (d, *J* = 8.5 Hz, 1H), 7.73 (ddd, *J* = 8.4, 6.8, 1.6 Hz, 1H), 7.57 (ddd, *J* = 8.2, 7.0, 1.3 Hz, 1H), 7.39 (d, *J* = 1.8 Hz, 1H), 4.28 (s, 2H), 3.02 (td, *J* = 11.6, 5.8 Hz, 1H), 2.87 (s, 2H), 1.98 (d, *J* = 13.1 Hz, 2H), 1.82 (qd, *J* = 12.5, 4.4 Hz, 2H), 1.48 (s, 9H) ppm.

HRMS – During MS analysis of with ESI source in positive mode, we observed Boc deprotection of the product.

Molecular Formula: C14H15ClN2; Calculated [M+H]+: 247.0997; Found [M+H]+: 247.1002.

***tert*-butyl 3-(4-chloroquinolin-2-yl)piperidine-1-carboxylate**

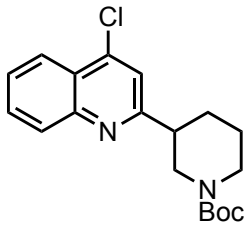

Reaction run according to General Procedure A. *tert*-butyl 3-(4-chloroquinolin-2-yl)piperidine-1-carboxylate was isolated as a pale yellow oil.

^{1}H NMR (700 MHz, $CDCl_3$) δ 8.17 (d, *J* = 8.3 Hz, 1H), 8.05 (d, *J* = 8.5 Hz, 1H), 7.73 (t, *J* = 7.7 Hz, 1H), 7.58 (t, *J* = 7.6 Hz, 1H), 7.42 (s, 1H), 4.60-4.20 (m, 1H), 4.13 (bs, 1H), 3.42-3.03 (m, 1H), 3.04-2.95 (m, 1H), 2.85 (t, *J* = 12.8 Hz, 1H), 2.13 (d, *J* =13.2 Hz, 1H), 1.95-1.84 (m, 1H), 1.80 (d, *J* = 13.5 Hz, 1H), 1.68-1.57 (m, 1H), 1.47 (s, 9H) ppm.

^{13}C NMR (176 MHz, $CDCl_3$) δ 163.03, 154.96, 148.87, 142.78, 130.42, 129.60, 127.06, 125.34, 124.04, 120.62, 79.69, 48.83, 44.84, 43.76, 30.82, 29.82, 28.59, 25.21ppm.

IR(neat): 2976, 2931, 2856, 1687, 1616, 1589, 1494, 1411, 1365, 1301, 1256, 1162, 1146, 1136, 1024, 977, 938, 864, 839, 759, 736, 702 cm^{-1}.

HRMS – During MS analysis of with ESI source in positive mode, we observed Boc deprotection of the product.

Molecular Formula: C14H15ClN2; Calculated [M+H]+: 247.0997; Found [M+H]+: 247.1005.

2,6-di-*tert*-butylisonicotinonitrile

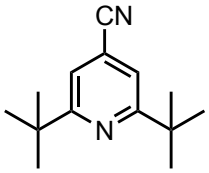

Reaction run according to General Procedure A. 2,6-bis(tert-butyl)-4-cyanopyridine was isolated as a colorless oil.

^{1}H NMR (500 MHz, $CDCl_3$) δ 7.31 (s, 2H), 1.35 (s, 18H) ppm.

^{13}C NMR (151 MHz, $CDCl_3$) δ 169.76, 120.67, 118.28, 117.78, 38.38, 30.17 ppm.

HRMS – Calculated [M+H]+: 217.1699; Found [M+H]+: 217.1709.

2,5-di-*tert*-butylisonicotinonitrile

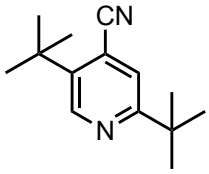

Reaction run according to General Procedure A. 2,5-bis(*tert*-butyl)-4-cyanopyridine was isolated as a 1:1 mixture with 2,6- bis(*tert*-butyl)-4-cyanopyridine.

^{1}H NMR (400 MHz, $CDCl_3$) δ 8.77 (s, 1H), 7.54 (s, 1H), 1.54 (s, 9H), 1.37 (s, 9H) ppm.

^{13}C NMR (126 MHz, $CDCl_3$) δ 207.06, 169.55, 147.27, 123.74, 37.38, 34.43, 31.07, 29.98, 29.97 ppm.

2-(*tert*-butyl)-4-phenylpyridine

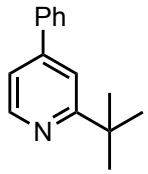

Reaction run according to General Procedure A. 2-(tert-butyl)-4-phenylpyridine was isolated as a colorless oil. Characterization data is consistent with previously reported literature (Stephenson *et al. Org. Lett.* **2018,** *20,* 3487–3490.).

^{1}H NMR (401 MHz, $CDCl_3$) δ 8.62 (d, *J* = 5.1 Hz, 1H), 7.63 (dt, *J* = 8.1, 1.2 Hz, 2H), 7.54 (s, 1H), 7.52 – 7.43 (m, 3H), 7.31 (d, *J* = 4.9 Hz, 1H), 1.43 (d, *J* = 1.0 Hz, 9H) ppm.

HRMS – Calculated [M+H]+: 212.1434; Found [M+H]+: 212.1442.

2-(*tert*-butyl)quinoline

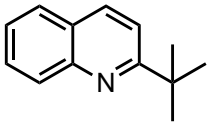

Reaction run according to General Procedure A. A mixture of 2-(*tert*-butyl)quinoline and 2,4-bis(*tert*-butyl)quinoline was isolated as a colorless oil. Characterization data is consistent with previously reported literature (Stephenson *et al. Org. Lett.* **2018,** *20,* 3487–3490.).

^{1}H NMR (600 MHz, $CDCl_3$) δ 8.07 (dd, *J* = 8.6, 2.3 Hz, 2H), 7.77 (dd, *J* = 8.1, 1.5 Hz, 1H), 7.67 (ddd, *J* = 8.4, 6.8, 1.5 Hz, 1H), 7.53 (d, *J* = 8.6 Hz, 1H), 7.48 – 7.42 (m, 1H, distorted by 2,4-bis(*tert*-butyl)quinoline), 1.48 (s, 18H, distorted by 2,4-bis(*tert*-butyl)quinoline) ppm.

HRMS – Calculated [M+H]+: 186.1277; Found [M+H]+: 186.1284.

2,4-bis(*tert*-butyl)quinoline

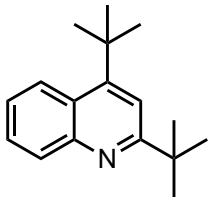

Characterization data is consistent with previously reported literature (Stephenson *et al. Org. Lett.* **2018,** *20,* 3487–3490.). 2,4-bis(*tert*-butyl)quinoline was isolated as a colorless oil.

^{1}H NMR (600 MHz, $CDCl_3$) δ 8.34 (dd, *J* = 8.7, 1.4 Hz, 1H), 8.09 (dd, *J* = 8.4, 1.5 Hz, 1H), 7.60 (ddd, *J* = 8.3, 6.7, 1.4 Hz, 1H), 7.48 (s, 1H), 7.44 (ddd, *J* = 8.4, 6.7, 1.4 Hz, 1H), 1.62 (s, 10H), 1.47 (s, 11H) ppm.

HRMS – Calculated [M+H]+: 242.1903; Found [M+H]+: 242.1910.

2-(*tert*-butyl)-6-methoxyquinoline

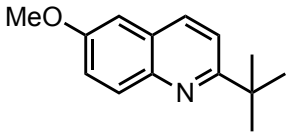

Reaction run according to General Procedure A. A mixture of 2-(*tert*-butyl)-6-methoxyquinoline and 2,4-bis(*tert*-butyl)-6-methoxyquinoline was isolated as a colorless oil. Characterization data is consistent with previously reported literature (Wojciechowski *et al. Syn. Lett.* **2012,** *23,* 2682–2686.).

^{1}H NMR (401 MHz, $CDCl_3$) δ 7.97 (d, *J* = 9.1Hz, 1H), 7.95 (d, *J* = 8.5 Hz, 1H) 7.48 (d, *J* = 8.7 Hz, 1H), 7.32 (dd, *J* = 9.2, 2.8 Hz, 1H), 7.04 (d, *J* = 2.8 Hz, 1H), 3.94 (s, 2H), 3.92 (s, 3H), 1.46 (s, 14H) ppm.

HRMS – Calculated [M+H]+: 216.1383; Found [M+H]+: 216.1389.

2,4-bis(*tert*-butyl)-6-methoxyquinoline

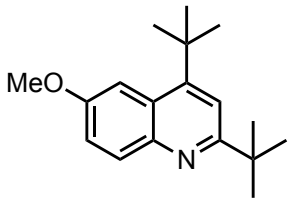

^{1}H NMR (401 MHz, $CDCl_3$) δ 8.01 (d, *J* = 9.2 Hz, 1H), 7.63 (d, *J* = 2.8 Hz, 1H), 7.45 (s, 1H), 7.29 (d, *J* = 2.6 Hz, 1H), 3.94 (s, 3H), 1.62 (s, 10H), 1.46 (s, 9H) ppm.

HRMS – Calculated [M+H]+: 272.2009; Found [M+H]+: 272.2017.

2-(*tert*-butyl)-4-methylquinoline

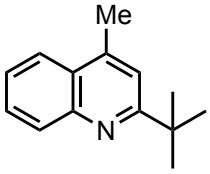

Reaction run according to General Procedure A. 2-(*tert*-butyl)-4-methylquinoline was isolated as a colorless oil. Characterization data is consistent with previously reported literature (Stephenson *et al. Org. Lett.* **2018,** *20,* 3487–3490.).

^{1}H NMR (401 MHz, $CDCl_3$) δ 8.06 (d, *J* = 8.4 Hz, 1H), 7.94 (dd, *J* = 8.3, 1.5 Hz, 1H), 7.66 (ddd, *J* = 8.4, 6.8, 1.4 Hz, 1H), 7.49 (ddd, *J* = 8.2, 6.8, 1.3 Hz, 1H), 7.35 (d, *J* = 1.2 Hz, 1H), 2.69 (d, *J* = 1.0 Hz, 3H), 1.46 (s, 9H) ppm.

HRMS – Calculated [M+H]+: 200.1434; Found [M+H]+: 200.1437.

2-(*tert*-butyl)quinoxaline

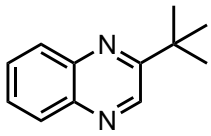

Reaction run according to General Procedure A. 2-(*tert*-butyl)-quinoxaline was isolated as a colorless oil. Characterization data is consistent with previously reported literature (Stephenson *et al. Org. Lett.* **2018,** *20,* 3487–3490.).

^{1}H NMR (600 MHz, $CDCl_3$) δ 8.99 (s, 1H), 8.09 – 8.03 (m, 2H), 7.71 (dddd, *J* = 19.8, 8.3, 6.9, 1.6 Hz, 2H), 1.52 (s, 9H) ppm.

HRMS: Calculated [M+H]+: 187.1230; Found [M+H]+: 187.1234.

4-(*tert*-butyl)-3-chloro-6-phenylpyridazine

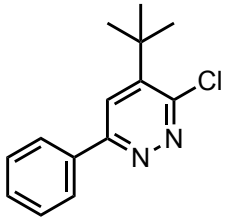

Reaction run according to General Procedure A. 4-(tert-butyl)-3-chloro-6-phenylpyridazine was isolated as a colorless, amorphous solid. Characterization data is consistent with previously reported literature (Stephenson *et al. ACS Catal.* **2020,** *10,* 12636–12641.).

^{1}H NMR (600 MHz, $CDCl_3$) δ 8.19 (dd, *J* = 8.3, 1.4 Hz, 1H), 8.10 (d, *J* = 8.5 Hz, 1H), 7.75 (ddd, *J* = 8.4, 6.9, 1.4 Hz, 1H), 7.61 (ddd, *J* = 8.3, 6.9, 1.2 Hz, 1H), 7.42 (s, 1H), 3.75 (s, 3H), 2.51 (s, 6H).

HRMS – Calculated [M+H]+: 288.0786; Found [M+H]+: 288.0786.

2-(*tert*-butyl)-4-chloro-6,7-bis(2-methoxyethoxy)quinazoline

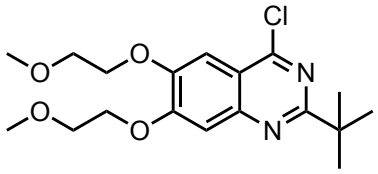

Reaction run according to General Procedure A. 2-(*tert*-butyl)-4-chloro-6,7-bis(2-methoxyethoxy)quinazoline was isolated as a colorless, amorphous solid.

^{1}H NMR (600 MHz, $CDCl_3$) δ 7.39 (s, 1H), 7.27 (s, 1H), 4.31 (dt, *J* = 9.7, 4.7 Hz, 4H), 3.89 – 3.85 (m, 4H), 3.49 (s, 2H), 3.48 (s, 1H), 1.45 (s, 9H) ppm.

^{13}C NMR (151 MHz, $CDCl_3$) δ 171.76, 159.12, 156.04, 150.17, 149.22, 117.15, 107.99, 104.58, 70.79, 70.56, 68.94, 68.79, 59.54, 59.53, 39.46, 29.69 ppm.

IR(neat): 2958, 2928, 2896, 2821, 1617, 1571, 1497, 1452, 1416, 1350, 1235, 1219, 1175, 1125, 1098, 1053, 1032, 993, 933, 911, 868, 807, 731, 687 cm^{-1}.

HRMS – Calculated [M+H]+: 369.1576; Found [M+H]+: 369.1578.

(8-(*tert*-butyl)-6-chloro-2-methylimidazo[1,2-*b*]pyridazin-3-yl)(4-chloro-2-fluorophenyl)methanone

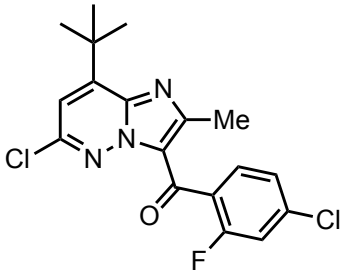

Reaction run according to General Procedure A. (8-(*tert*-butyl)-6-chloro-2-methylimidazo[1,2-*b*]pyridazin-3-yl)(4-chloro-2-fluorophenyl)methanone was isolated as a colorless, amorphous solid. Characterization data is consistent with previously reported literature (Stephenson *et al. Org. Lett.* **2018,** *20,* 3487–3490.).

^{1}H NMR (500 MHz, $CDCl_3$) δ 7.60 (dd, *J* = 8.2, 7.5 Hz, 1H), 7.29 (dd, *J* = 8.3, 1.9 Hz, 1H), 7.12 (dd, *J* = 9.9, 1.9 Hz, 1H), 6.98 (s, 1H), 2.67 (s, 3H), 1.58 (s, 9H) ppm.

HRMS – Calculated [M+H]+: 380.0727; Found [M+H]+: 380.0729.

(*S*)-2-(*tert*-butyl)-5-(1-methylpyrrolidin-2-yl)pyridine

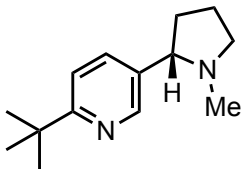

Reaction run according to General Procedure A. (S)-2-(tert-butyl)-5-(1-methylpyrrolidin-2-yl)pyridine was isolated as a pale-yellow oil.

^{1}H NMR (600 MHz, C_6D_6) δ 8.71 (d, *J* = 2.4 Hz, 1H), 7.61 – 7.57 (m, 1H), 7.13 (dd, *J* = 8.2, 0.8 Hz, 1H), 3.03 (td, *J* = 8.5, 2.2 Hz, 1H), 2.78 (t, *J* = 8.3 Hz, 1H), 2.03-1.97 (m, 4H), 1.84 (dddd, *J* = 14.6, 9.6, 6.0, 3.8 Hz, 1H), 1.77 – 1.65 (m, 1H), 1.61 – 1.51 (m, 1H), 1.48-1.41 (m, 10H) ppm.

^{13}C NMR (151 MHz, C_6D_6) δ 168.12, 148.59, 134.55, 118.51, 68.27, 56.56, 39.93, 37.15, 35.41, 30.14, 22.43 ppm.

IR(neat): 2959, 2872, 2839, 2774, 1737, 1599, 1567, 1485, 1460, 1397, 1362, 1332, 1284, 1225, 1126, 1088, 1045, 1026, 904, 839, 733 cm^{-1}.

HRMS – Calculated [M+H]+: 219.1856; Found [M+H]+: 219.1857.

HPLC trace for chiral separation of 2-(*tert*-butyl)nicotine.

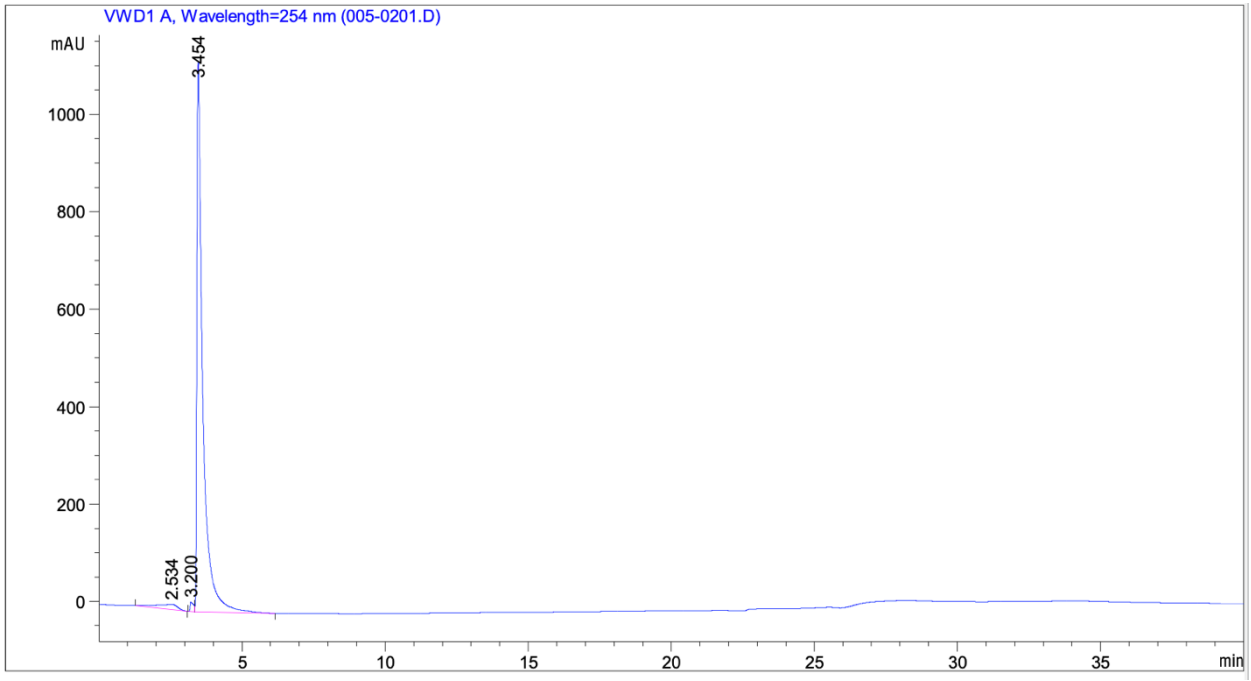

4.5 References

1. Spence, G. G.; Taylor, E. C.; Buchardt, O. Photochemical reactions of azoxy compounds, nitrones, and aromatic amine *N*-oxides. *Chem. Rev.* **1970,** *70,* 231–265.

2. Albini, A.; Alpegiani, M. The photochemistry of the *N*-oxide function. *Chem. Rev.* **1984,** *84,* 43–71.

3. Ole Buchardt. The Photorearrangement of Quinoline *N*-oxide. *Acta Chem. Scand.* **1963,** *17,* 1461-1462.

4. Buchardt, O.; Kumler, P. L.; Lohse, C. XVI. Photolysis of Phenylquinoline *N*-oxides in Solution. A Novel Light Induced Reaction. Solvent Influence on the Product Distribution. *Acta Chem. Scand.* **1969,** *23,* 2149-2157.

5. Hata, N.; Ono, I.; Kawasaki, M. The Photoinduced Deoxygenation Reaction of Heterocyclic *N*-oxides. *Chem. Lett.* **1975**, *4*, 25-28.

6. Kaneko, C.; Yamamori, M.; Yamamoto, A.; Hayashi, R. Irradiation of aromatic amine oxides in dichloromethane in presence of triphenylphosphine: A facile deoxygenation procedure of aromatic amine *N*-oxides. *Tetrahedron Lett.* **1978,** *19,* 2799-2802.

7. Pietra, S.; Bettinetti, G. F.; Albini, A.; Fasani, E.; Oberti, R. Photoreaction of 2-nitrophenazine 10-oxide with amines. *J. Chem. Soc., Perkin Trans. 2.* **1978,** 185-189.

8. Albini, A.; Fasani, E.; Frattini, V. Medium and substituent effects on the photochemistry of phenanthridine N-oxides. Is an intermediate of diradical character involved in the photorearrangement of heterocyclic *N*-oxides? *J. Chem. Soc., Perkin Trans. 2* **1988,** 235-240.

9. Hasebe, M.; Kogawa, K.; Tsuchiya, T. Photochemical arylation by oxime esters in benzene and pyridine: simple synthesis of biaryl compounds. *Tet. Lett.* **1984,** *25,* 3887-3890.

10. Barton, D. H. R.; Crich, D.; Motherwell, W. B. New and improved methods for the radical decarboxylation of acids. *J. Chem. Soc., Chem. Commun.* **1983,** 939-941.

11. Barton, D. H. R.; Crich, D.; Motherwell, W. B. A practical alternative to the hunsdiecker reaction. *Tet. Lett.* **1983,** *24,* 4979–4982.

12. Barton, D. H. R.; Crich, D.; Motherwell, W. B. The invention of new radical chain reactions. Part VIII. Radical chemistry of thiohydroxamic esters; A new method for the generation of carbon radicals from carboxylic acids. *Tetrahedron* **1985,** *41,* 3901–3924.

13. Fukuda, R.; Ehara, M. Electronic Excitation and Ionization Behavior of *N*-hydroxypyridine-2(*1H*)-thione and its Deprotonated Anion in a Polarizable Medium Studied Using Quantum Chemical Computations. *Theor. Chem. Acc.* **2016,** *135,* 105.

14. Rehm, D.; Weller, A. Kinetics of Fluorescence Quenching by Electron and H-Atom Transfer. *Isr. J. Chem.* **1970,** *8,* 259−271.

15. Sun, A. C.; McClain, E. J.; Beatty, J. W.; Stephenson, C. R. J. Visible Light-Mediated Decarboxylative Alkylation of Pharmaceutically Relevant Heterocycles. *Org. Lett.* **2018,** *20*, 3487-3490.

16. Ramirez, N. P.; Bosque, I.; Gonzalez-Gomez, J. C. Photocatalytic Dehydrogenative Lactonization of 2-Arylbenzoic Acids. *Org. Lett.* **2015,** *17,* 4550-4553.

17. Ye, Y.; Sanford, M. S. Merging Visible-Light Photocatalysis and Transition-Metal Catalysis in the Copper-Catalyzed Trifluoromethylation of Boronic Acids with CF_3I. *J. Am. Chem. Soc.* **2012,** *134,* 9034–9037.

18. Le, C.; Chen, T. Q.; Liang, T.; Zhang, P.; MacMillan, D. W. C. A radical approach to the copper oxidative addition problem: Trifluoromethylation of bromoarenes. *Science* **2018,** *360,* 1010–1014.

19. Liang, Y.; Zhang, X.; MacMillan, D.W.C. Decarboxylative sp3 C–N coupling via dual copper and photoredox catalysis. *Nature* **2018,** *559,* 83–88.

20. Kornfilt, D. J. P.; MacMillan, D. W. C. Copper-Catalyzed Trifluoromethylation of Alkyl Bromides. *J. Am. Chem. Soc.* **2019,** *141,* 6853−6858.

21. Zhao, X.; MacMillan, D. W. C. Metallaphotoredox Perfluoroalkylation of Organobromides. *J. Am. Chem. Soc.* **2020**, *142*, 19480-19486.

22. Nguyen, V. T.; Nguyen, V. D.; Haug, G. C.; Vuong, N. T. H.; Dang, H. T.; Arman, H. D.; Larionov, O. V. *Angew. Chem. Int. Ed.* **2020,** *59,* 7921-7927.

23. Zhang, H.; Zhang, P.; Jiang, M.; Yang, H.; Fu, H. Merging Photoredox with Copper Catalysis: Decarboxylative Alkynylation of α-Amino Acid Derivatives. *Org. Lett.* **2017,** *19,* 1016–1019.

24. Xu, H. J.; Lin, S. Q.; Shen, S. Y.; Li, L.; Chen, D. W.; Xu, G. Z. Radical mechanism in the photoinduced oxygen transfer from acridine N-oxides to cyclohexene. *J. Photochem. Photobiol. A* **1989,** *48,* 53-59.

25. Feygelman, V. M.; Tymyanskii, Y. R.; Makarova, N. I.; Knyazhanskii, M. I.; Druzhinin, S. I.; Uzhinov, B. M. Photochemistry of pyridinium salts 1. Intramolecular charge transfer in *N*-amino-substituted pyridinium cations. *J. Phys. Org. Chem.* **1990,** *3,* 200-204.

26. Jacques Streith. THE PHOTOCHEMISTRY OF AROMATIC-N-YLIDES. REARRANGEMENT AND FRAGMENTATION PATTERNS. *Photochemistry-6* **1977,** 305-315.

27. Jacques Streith. The Photochemistry of *N*-Iminopyridinium Ylides in Retrospect. From a Simple Concept to Some Applications. *Chimia* **1991**, *45,* 65-76.

28. Markus D. Kärkäs. Photochemical Generation of Nitrogen-Centered Amidyl, Hydrazonyl, and Imidyl Radicals: Methodology Developments and Catalytic Applications. *ACS Catal.* **2017,** *7,* 4999–5022.

29. Greulich, T. W.; Daniliuc, C. G.; Studer, A. *N*-Aminopyridinium Salts as Precursors for N-Centered Radicals – Direct Amidation of Arenes and Heteroarenes. *Org. Lett.* **2015,** *17,* 254–257.

30. Yu, W.-L.; Chen, J.-Q.; Wei, Y.-L.; Wanga, Z.-Y.; Xu, P.-F. Alkene functionalization for the stereospecific synthesis of substituted aziridines by visible-light photoredox catalysis. *Chem. Commun.* **2018,** *54,* 1948-1951.

31. Moon, Y.; Park, B.; Kim, I.; Kang, G.; Shin, S.; Kang, D.; Baik, M.-H.; Hong, S. Visible light induced alkene aminopyridylation using *N*-aminopyridinium salts as bifunctional reagents. *Nat. Commun.* **2019,** *10,* 4117.

32. Mendiola, J.; Rincón, J. A.; Mateos, C.; Soriano, J. F.; de Frutos, Ó.; Niemeier, J. K.; Davis, E. M. Preparation, Use, and Safety of *O*-Mesitylenesulfonylhydroxylamine. *Org. Process Res. Dev.* **2009,** *13,* 263–267.

33. Gösl, R.; Meuwsen, A. 1-Aaminopyridinium Iodide. *Org. Synth.* **1963,** *43,* 1.

34. Nastasi, M.; Strub, H.; Streith, J. Formation d'un nitrene triplet par photolyse d'un ylure de N-aminopyridinium. *Tet. Lett.* **1976,** *17,* 4719-472.

35. Ji, Y.; DiRocco, D. A.; Kind, J.; Thiele, C. M.; Gschwind, R. M.; Reibarkh, M. LED-Illuminated NMR Spectroscopy: A Practical Tool for Mechanistic Studies of Photochemical Reactions. *ChemPhotoChem* **2019,** *3*, 984-992.

36. Skubi, K. L.; Swords, W. B.; Hofstetter, H.; Yoon, T. P. LED-NMR Monitoring of an Enantioselective Catalytic [2+2] Photocycloaddition. *ChemPhotoChem* **2020,** *4,* 685-690.

37. Barton, D. H. R.; Bridon, D.; Fernandaz-Picot, I.; Zard, S. Z. The invention of radical reactions: Part XV. Some mechanistic aspects of the decarboxylative rearrangement of thiohydroxamic esters. *Tetrahedron* **1987,** *43,* 2733-2740.

38. Buzzetti, L.; Crisenza, G. E. M.; Melchiorre, P. Mechanistic Studies in Photocatalysis. *Angew. Chem. Int. Ed.* **2019,** *58,* 3730-3747.

39. Citterio, A.; Minisci, F.; Franchi, V. Nucleophilic character of the alkyl radicals. 19. Absolute rate constants in the homolytic alkylation of protonated heteroaromatic bases by *n*-butyl and *tert*-butyl radicals. *J. Org. Chem.* **1980,** *45,* 4752–4757.

40. Minisci, F.; Vismara, E.; Fontana F. Recent Developments of Free-Radical Substitutions of Heteroaromatic Bases. *Heterocycles* **1989,** *28,* 489-517.

41. Lorance, E. D.; Kramer, W. H.; Gould, I. R. Barrierless Electron Transfer Bond Fragmentation Reactions. *J. Am. Chem. Soc.* **2004,** *126,* 14071–14078.

42. Lorance, E. D.; Kramer, W. H.; Gould, I. R. Kinetics of Reductive N−O Bond Fragmentation: The Role of a Conical Intersection. *J. Am. Chem. Soc.* **2002,** *124,* 15225–15238.

43. Gaudiello, J. G.; Larkin, D.; Rawn, J. D.; Sosnowski, J. J.; Bancroft, E. E.; Blount, H. N. On the mechanism of the electrochemical reduction of *N*-methylpyridinium ion. *J. Electroanal. Chem. Interf. Electrochem.* **1982,** *131,* 203-214.

44. Leventis, N.; Rawaswdeh, A.-M. M.; Zhang, G.; Elder, I. A.; Sotiriou-Leventis, C. Tuning the Redox Chemistry of 4-Benzoyl-*N*-methylpyridinium Cations through Para Substitution. Hammett Linear Free Energy Relationships and the Relative Aptitude of the Two-Electron Reduced Forms for H-Bonding. *J. Org. Chem.* **2002,** *67,* 7501–7510.

45. Aillet, T.; Loubiere, K.; Dechy-Cabaret, O.; Prat, L. Accurate Measurement of the Photon Flux Received Inside Two Continuous Flow Microphotoreactors by Actinometry. *Int. J. Chem. React. Eng.* **2014,** *12,* 257-269.